Synthesis, Properties, and Coordination Chemistry of *t*-Bu-Xantphos Ligands

by

Melanie Ruth Maria Nelson

A thesis
submitted to the Victoria University of Wellington
in fulfilment of the
requirements for the degree of
Doctor of Philosophy
in Chemistry.

Victoria University of Wellington
2015

Abstract

This thesis provides an account of research into a group of diphosphine ligands with a rigid xanthene backbone and *tert*-butyl substituents on the phosphorus atoms. The three ligands have different groups in the bridgehead position of the backbone (CMe_2, $SiMe_2$, or S) which change the natural (calculated) bite-angle of the ligand. The coordination chemistry of these *t*-Bu-xantphos ligands with late-transition metals has been investigated with a focus on metal complexes that may form in catalytic reactions.

The three *t*-Bu-xantphos ligands were synthesised by lithiation of the backbone using *sec*-butyllithium/TMEDA and treatment with P^tBu_2Cl. The natural bite-angles of the Ph-xantphos (111.89–114.18°) and *t*-Bu-xantphos (126.80–127.56°) ligands were calculated using DFT. The bite-angle of the *t*-Bu-xantphos ligands is larger due to the increased steric bulk of the *tert*-butyl substituents. The electronic properties of the *t*-Bu-xantphos ligands were also investigated by synthesis of their phosphine selenides. The values of $^1J_{PSe}$ (689.1–698.5 Hz) indicate that the *t*-Bu-xantphos ligands have a higher basicity than Ph-xantphos between PPh_2Me and PMe_3.

The silver complexes, [Ag(*t*-Bu-xantphos)Cl] and [Ag(*t*-Bu-xantphos)]BF_4 were synthesised with the *t*-Bu-xantphos ligands. In contrast to systems with phenyl phosphines, all species were monomeric. [Rh(*t*-Bu-xantphos)Cl] complexes were synthesised, which reacted with H_2, forming [Rh(*t*-Bu-xantphos-κ*P,O,P'*)Cl$(H)_2$] complexes, and with CO, forming [Rh(*t*-Bu-xantphos)$(CO)_2$Cl] complexes. The [Rh(*t*-Bu-xantphos)Cl] species are air-sensitive readily forming [Rh(*t*-Bu-xantphos)Cl(η^2-O_2)] complexes. The crystal structure of [Rh(*t*-Bu-xantphos)Cl(η^2-O_2)], contained 15% of the dioxygen sites replaced with an oxo ligand. This is the first crystallographic evidence of a rhodium(III) oxo complex, and only the third rhodium oxo species reported.

The coordination chemistry of the ligands with platinum(0) and palladium(0) showed some differences. [Pt(*t*-Bu-xantphos)(C_2H_4)] complexes were synthe-

sised for all three ligands. However, reaction with [Pt(nb)$_3$] produced a mixture of [Pt(*t*-Bu-xantphos)] and [Pt(*t*-Bu-xantphos)(nb)] for *t*-Bu-sixantphos and *t*-Bu-thixantphos. Although few examples of isolable [Pt(PP)] complexes with diphosphines have been reported [Pt(*t*-Bu-thixantphos)] was isolated by removal of the norbornene. *t*-Bu-Xantphos formed small amounts of [Pt(*t*-Bu-xantphos)] initially, which progressed to [Pt(*t*-Bu-xantphos)H]X. The analogous reactions with [Pd(nb)$_3$] gave [Pd(*t*-Bu-xantphos)] and [Pd(*t*-Bu-xantphos)(nb)] complexes in all cases. [Pt(*t*-Bu-thixantphos)(C_2H_4)] and [M(*t*-Bu-thixantphos)] (M = Pd, Pt) react with oxygen forming [Pt(*t*-Bu-thixantphos)(η^2-O_2)], which reacts with CO to give [Pt(*t*-Bu-thixantphos-H-κ-*C,P,P'*)OH] through a series of intermediates.

[M(*t*-Bu-xantphos)Cl_2] (M = Pd, Pt) complexes were synthesised, showing exclusive *trans* coordination of the diphosphine ligands. The X-ray crystal structure of [Pt(*t*-Bu-thixantphos)Cl_2] has a bite-angle of 151.722(15)°. This is the first [$PtCl_2$(PP)] complex with a bite-angle between 114 and 171°. In polar solvents a chloride ligand dissociates from the [Pt(*t*-Bu-xantphos)Cl_2] complexes producing [Pt(*t*-Bu-xantphos-κ*P,O,P'*)Cl]$^+$. The analogous [Pd(*t*-Bu-xantphos-κ*P,O,P'*)Cl]$^+$ complexes were formed by reaction of the dichlorides complexes with NH_4PF_6. The [Pt(*t*-Bu-xantphos-κ*P,O,P'*)Me]$^+$ pincer complexes were the only product from reaction with [Pt(C_6H_{10})ClMe], with the stronger *trans* influence of the methyl ligand promoting loss of the chloride. The formation of the pincer complexes was further explored using DFT.

The values of J_{PtC} for the methyl carbons in the [Pt(*t*-Bu-xantphos-κ*P,O,P'*)Me]$^+$ complexes, and J_{RhH} for the hydride *trans* to the oxygen atom in the [Rh(*t*-Bu-xantphos-κ*P,O,P'*)Cl($H)_2$] complexes were largest for *t*-Bu-sixantphos, then *t*-Bu-thixantphos, then *t*-Bu-xantphos. The *trans* influence of the *t*-Bu-xantphos oxygen donor follows the trend *t*-Bu-sixantphos $<$ *t*-Bu-thixantphos $<$ *t*-Bu-xantphos.

Acknowledgements

As always there are numerous people that have helped me over the years. My supervisor, Prof. John Spencer, thank you for your guidance, advice and support, even coming in to University after a major earthquake to rescue our reaction. Dr. Matthias Lein, thank you for being an excellent supervisor while John was on research and study leave and for all of your assistance with DFT. Thanks to both of you for reading through various sections while on holiday.

The past and present members of the JLS research group: Almas, Brad, Chris, David, Kathryn, Lia, Rosie, Sarah and Teresa. Thank you for getting excited with me over the minutiae of NMR spectra, and for all of the good times and commiserations that we've shared. The other postgraduate students in SCPS, particularly my office mates in AM204, thanks for your friendship over the years.

The general staff of SCPS are amazingly supportive towards the research in the school and many things would be impossible without them. Particular thanks to the lab technicians Teresa, Jamie-Ann and Jackie, for letting me borrow glassware and other equipment. Thanks to Peter Northcote, Ian Vorster and John Ryan for helping with NMR. I am grateful to Rob Keyzers and Yinrong Lu for help with mass spectrometry and to Jan Wikaira, Christ Fitchett and Matt Polson at the University of Canterbury for X-ray crystallography.

Thank you to the members of Disarray, and all of my non-chemistry friends for giving me something else to think about when I just needed a break. My family have been extremely supportive and caring, as they always are. Finally to my husband, Stephen, these last 10 years have been wonderful, thank you for all of your love and understanding especially over these last few months.

I would also like to acknowledge Victoria University of Wellington for funding through the PhD, submission, and Curtis-Gordon scholarships.

Contents

Contents **v**

List of Figures **ix**

List of Schemes **x**

List of Tables **xiii**

Acronyms **xv**

1 Introduction **1**
1.1 Tertiary Phosphine Ligands 1
1.1.1 Electronic and Steric Properties 2
1.1.2 Diphosphine Ligands 3
1.1.3 Wide Bite-Angle Diphosphine Ligands 6
1.2 Pincer Ligands 6
1.3 Xantphos 9
1.3.1 Alkyl-Substituted Xantphos Ligands 12
1.3.2 *t*-Bu-Xantphos 16
1.4 Research Objectives 20

2 Ligand Synthesis and Properties **23**
2.1 Ligand Synthesis 24
2.2 Bite-Angle Calculations 29
2.3 Basicity 33
2.4 Selenides 38
2.5 Summary 45

3 Coordination Complexes with Silver **47**

3.1 Silver Chloride Complexes . . . 49
3.2 Reactions with Silver Tetrafluoroborate . . . 56
3.2.1 Reactions with LiCCPh . . . 60
3.3 Summary . . . 61

4 Coordination Complexes with Rhodium 63
4.1 Synthesis of [Rh(κ*P,O,P'*)Cl] Complexes . . . 65
4.2 Reaction with Hydrogen . . . 71
4.3 Rhodium Carbonyl Complexes . . . 78
4.4 Dioxygen and Oxo Complexes . . . 87
4.5 Summary . . . 98

5 Coordination Complexes with Platinum(0) and Palladium(0) 101
5.1 Reactions of Ph-thixantphos with Platinum(0) Precursors . . . 103
5.2 Reaction of *t*-Bu-xantphos Ligands with [Pt(nb)$_3$] . . . 112
5.3 Reaction of *t*-Bu-thixantphos with [Pt(cod)$_2$] . . . 116
5.4 Reaction of *t*-Bu-xantphos Ligands and [Pt(C_2H_4)$_3$] . . . 116
5.5 Formation of Platinum Dioxygen Complexes . . . 119
5.6 Reactions of [Pt(*t*-Bu-thixantphos)(η^2-O_2)] . . . 125
5.7 Reactions with Palladium(0) Precursors . . . 130
5.7.1 Reaction of [Pd(*t*-Bu-thixantphos)] with Oxygen . . . 132
5.8 Computational Results . . . 133
5.9 Summary . . . 135

6 Coordination Complexes with Platinum(II) and Palladium(II) 141
6.1 Reactions with Platinum Dichloride Starting Materials . . . 144
6.1.1 Reactions with [PtCl$_2$(hex)] . . . 155
6.2 Reactions with [Pd(cod)Cl$_2$] . . . 161
6.2.1 Formation of [Pd(*t*-Bu-xantphos-κ*P,O,P'*)Cl]PF_6 Complexes 163
6.3 Computational Results . . . 164
6.4 Reactions with Platinum Dimethyl Starting Materials . . . 166
6.5 Reactions with [PtCl(hex)Me] . . . 168
6.5.1 Computational Results . . . 174
6.6 Summary . . . 178

7 Conclusion 181

8 Experimental **185**
8.1 General Procedures 185
8.2 Ligands and Non-Transition Metal Derivatives 186
8.3 Silver Complexes 192
8.4 Rhodium Complexes 196
8.5 Platinum Complexes 204
8.6 Palladium Complexes 221

Bibliography **227**

List of Figures

1.1 Selection of diphosphine ligands 4
1.2 The bite angle 5
1.3 Wide bite-angle diphosphine ligands 6
1.4 Trans-spanning diphosphine ligands 7
1.5 Naming of pincer ligands 7
1.6 First reported pincer ligands 8
1.7 General representation of pincer complexes 8
1.8 Selection of xantphos derivatives 10

2.1 Comparison of the natural and crystallographic bite-angles 30
2.2 ^{1}H NMR spectra for the [(*t*-Bu-xantphos)H]$^{+}$ ions 35
2.3 VT-NMR for [(*t*-Bu-thixantphos)H]$^{+}$ 37
2.4 VT ^{1}H-coupled ^{31}P NMR for [(*t*-Bu-thixantphos)H]$^{+}$ 38
2.5 X-ray crystal structure of [(*t*-Bu-thixantphos)H]CPh$(SO_2CF_3)_2$ . . . 39

3.1 1:1 silver diphosphine complexes 48
3.2 Silver Ph-xantphos complexes 48
3.3 X-ray crystal structure of AgBr(Ph-xantphos) 49
3.4 X-ray crystal structure of Ag(Ph-xantphos)(HpyS)Br 50
3.5 NMR spectra for [Ag(*t*-Bu-sixantphos)Cl] 51
3.6 X-ray crystal structure of [Ag(*t*-Bu-thixantphos)Cl] 53
3.7 X-ray crystal structure of [Ag(*t*-Bu-thixantphos)Cl], side view . . . 54
3.8 Silver complexes with free coordination sites and BF_4^- counterions 57
3.9 NMR spectra for [Ag(*t*-Bu-sixantphos)]BF_4 58

4.1 Chiral phosphine ligands used in asymmetric catalysis 64
4.2 Complexes from $[Rh(coe)_2Cl]_2$ and phosphine ligands 67
4.3 ^{31}P and ^{1}H NMR spectra for [Rh(*t*-Bu-xantphos)Cl] 68

4.4 X-ray crystal structure of [Rh(*t*-Bu-xantphos-κ*P,O,P'*)Cl] 69
4.5 NMR spectra for [Rh(*t*-Bu-thixantphos)Cl(H_2)] 75
4.6 NMR spectra of [Rh(*t*-Bu-sixantphos)Cl] with CO 81
4.7 Possible products from reaction of [Rh(*t*-Bu-xantphos-κ*P,O,P'*)Cl] complexes with CO 83
4.8 X-ray crystal structure of [Rh(*t*-Bu-xantphos)Cl(η^2-O_2)] 90
4.9 X-ray crystal structure of [Rh(*t*-Bu-xantphos-κ*P,O,P'*)Cl(O) 92
4.10 Rhodium dioxygen complexes with shorter Rh-O bonds than [Rh(*t*-Bu-xantphos-κ*P,O,P'*)(η^2-O_2)Cl] 93
4.11 A rhodium oxo crystal structure 95
4.12 Previously reported late transition metal oxo complexes 96

5.1 X-ray crystal structure of [Pt(Ph-thixantphos)$_2$] 105
5.2 X-ray crystal structure of [Pt(Ph-thixantphos)$_2$] 105
5.3 X-ray crystal structures of [Pt(Et-xantphos)$_2$] and [Pd(Ph-xantphos)$_2$] 108
5.4 Low temperature ^{31}P NMR spectra of [Pt(Ph-thixantphos)$_2$] 109
5.5 Low temperature ^{1}H NMR spectra of [Pt(Ph-thixantphos)$_2$] 110
5.6 X-ray crystal structure of [Pt(*t*-Bu-thixantphos)(η^2-O_2)] · 2 C_6D_6 . . 122
5.7 X-ray crystal structure of [Pt(*t*-Bu-thixantphos)(η^2-O_2)] · 2 C_6D_6 side view 123

6.1 X-ray crystal structure of [Pd(*t*-Bu-xantphos)Cl_2] 143
6.2 Previously reported palladium complex of *t*-Bu-xantphos and Ph-xantphos 143
6.3 X-ray crystal structure of [Pt(*t*-Bu-thixantphos)Cl_2] 146
6.4 X-ray crystal structure of [Pt(*t*-Bu-thixantphos)Cl_2], side view . . . 146
6.5 Distribution of the P-Pt-P angles in [$PtCl_2(P_2)$] complexes 149
6.6 X-ray crystal structures of dichloridoplatinum complexes with *trans*-spanning diphosphine ligands 150
6.7 X-ray crystal structures of complexes of the type [$PtCl_2$(xantphos)] 151
6.8 Side-on view of X-ray crystal structures of complexes of the type [$PtCl_2$(xantphos)] 153
6.9 Energy change for conversion from [M(*t*-Bu-xantphos)Cl_2] to [M(*t*-Bu-xantphos)Cl]Cl (M = Pd, Pt) 165
6.10 X-ray crystal structures of [PtMe(P^iPr_3)$_2$]$^+$ and [PdMe(P^tBu_3)$_2$]$^+$ . . . 173

List of Schemes

1.1 Chloride abstraction from [PdClMe(xantphos)] 13
1.2 Reactions of [Rh(*i*-Pr-xantphos)] 15
1.3 Reactions of [Ir(*i*-Pr-xantphos)] 15
1.4 Reactions of Rh and Ir *i*-Pr-xantphos complexes with silanes 17

2.1 Literature synthesis of *t*-Bu-xantphos 24
2.2 Ligand synthesis 25
2.3 Reaction of *n*-butyllithium with diethyl ether 26
2.4 Influence of methyl groups on the synthesis of *t*-Bu-thixantphos . . 27
2.5 Protonation of the ligands using a strong acid 34
2.6 Selenation of *t*-Bu-xantphos ligands 42

3.1 Synthesis of [Ag(*t*-Bu-xantphos)Cl] complexes 52
3.2 Inversion of the xantphos backbone in [Ag(*t*-Bu-xantphos)Cl] . . . 56
3.3 Synthesis of [Ag(*t*-Bu-xantphos)]BF_4 complexes 59

4.1 Asymmetric catalytic hydrogenation developed by Knowles 64
4.2 Reaction of $[Rh(coe)_2Cl]_2$ and *t*-Bu-xantphos ligands 68
4.3 Catalytic cycle for homogeneous hydrogenation 72
4.4 Catalytic cycle for homogeneous hydroformylation 73
4.5 Reaction of [Rh(*t*-Bu-xantphos)Cl] with hydrogen 74
4.6 Reaction of [Rh(*t*-Bu-xantphos)Cl] with carbon monoxide 86
4.7 Reaction of [Rh(*t*-Bu-xantphos)Cl] complexes with oxygen 89
4.8 Reaction of [Rh(*t*-Bu-xantphos)Cl] with trimethylamine oxide . . . 98
4.9 Reaction of [Rh(*t*-Bu-xantphos)Cl(O)] with DCl 98

5.1 Reaction of Ph-thixantphos with tris(norbornene)platinum 104
5.2 Reaction between tBu-thixantphos and $[Pt(nb)_3]$ 113
5.3 Reaction between *t*-Bu-xantphos and $[Pt(nb)_3]$ 114

5.4 Reaction between *t*-Bu-thixantphos and [Pt(C_2H_4)$_3$] 117
5.5 Reaction of [Pt(alkene)(*t*-Bu-thixantphos)] and [Pt(*t*-Bu-thixantphos)] with air 119
5.6 Reaction between Pt(*t*-Bu-thixantphos)(η^2-O_2)] and CO 129
5.7 Synthesis of [Pd(*t*-Bu-xantphos)] 132

6.1 Synthesis of [Pt(*t*-Bu-thixantphos)Cl_2] 145
6.2 Equilibrium between [Pt(*t*-Bu-thixantphos)Cl_2] and Pt(*t*-Bu-thixantphos)Cl]Cl 155
6.3 Synthesis of [Pd(*t*-Bu-xantphos)Cl_2] 161
6.4 Synthesis of [Pd(*t*-Bu-xantphos-κ*P,O,P′*)Cl]PF_6 163
6.5 Attempted reaction of [Pt(hex)Me_2] and *t*-Bu-thixantphos 167
6.6 Proposed reaction between [Pt(hex)Me_2] and a diphosphine ligand 168
6.7 Reaction between [PtCl(hex)Me] and *t*-Bu-xantphos ligands 169
6.8 Equilibrium between [Pt(*t*-Bu-xantphos)Me] and [Pt(*t*-Bu-xantphos-κ*P,O,P′*)Me] 174

List of Tables

2.1 Selected NMR data for *t*-Bu-xantphos ligands 28
2.2 Crystallographic and natural bite-angles for diphosphine ligands . 31
2.3 Natural bite-angles of xantphos ligands 32
2.4 Selected NMR data for [(*t*-Bu-xantphos)H]CH(SO_2CF_3)$_2$ 34
2.5 Selected bond distances (Å) and angles (°) of 2[(*t*-Bu-thixantphos)H] CPh(SO_2CF_3)$_2$· C_6D_6 40
2.6 Crystallographic data of 2[*t*-Bu-thixantphos(H)]CPh(SO_2CF_3)$_2$·C_6D_6 41
2.7 Selected ^{31}P NMR data for *t*-Bu-xantphos selenides 44

3.1 Selected NMR data of [Ag(*t*-Bu-xantphos)Cl] complexes 52
3.2 Selected bond distances and angles of [Ag(*t*-Bu-thixantphos)Cl] . . 54
3.3 Crystallographic data for [Ag(*t*-Bu-thixantphos)Cl] 55
3.4 Selected NMR data of [Ag(*t*-Bu-xantphos)]BF_4 complexes 59

4.1 Selected NMR data of [Rh(*t*-Bu-xantphos)Cl] complexes 69
4.2 Chemical shift and coupling of the *O-ipso* carbon in the free ligand, [Ag(*t*-Bu-xantphos)Cl] and [Rh(*t*-Bu-xantphos)Cl] complexes 70
4.3 Hydride ^{1}H NMR data for [Rh(*t*-Bu-xantphos-κ*P,O,P'*)Cl$(H)_2$] . . . 76
4.4 Selected NMR data of [Rh(*t*-Bu-xantphos)$(CO)_2$Cl] complexes . . . 80
4.5 Chemical shift and coupling for the *O-ipso* carbon in *t*-Bu-xantphos, [Rh(*t*-Bu-xantphos-κ*P,O,P'*)Cl] and carbonyl complexes . . . 84
4.6 Selected NMR data for [Rh(*t*-Bu-xantphos-κ*P,O,P'*)Cl(η^2-O_2)] . . . 88
4.7 Crystallographic data and structure refinement of [Rh(*t*-Bu-xantphos)Cl(η^2-O_2)] 91
4.8 Selected bond distances (Å) and angles (°) of [Rh(tBu-xantphos)Cl(η^2-O_2)] 92

5.1 Selected bond distances (Å) and angles (°) of [Pt(Ph-thixantphos)$_2$] 106

5.2 Crystallographic data and refinement of [Pt(Ph-thixantphos)$_2$] . . . 107
5.3 ^{31}P NMR data for [Pt(*t*-Bu-xantphos)] complexes 115
5.4 ^{31}P NMR data for [Pt(*t*-Bu-xantphos)(C_2H_4)] complexes 118
5.5 Selected bond distances (Å) and angles (°) of [Pt(*t*-Bu-thixantphos)(η^2-O_2)] · 2 C_6D_6 120
5.6 Crystallographic data and structure refinement of [Pt(*t*-Bu-thixantphos)(η^2-O_2)] · 2 C_6D_6 121
5.7 Selected bond distances and angles of [Pt(PP)(η^2-O_2)] 124
5.8 Calculated bond lengths and angles for [M(*t*-Bu-xantphos)] 134
5.9 Calculated bond lengths and angles for [M(*t*-Bu-xantphos)(nb)] . . 134
5.10 Calculated bond lengths and angles for M(*t*-Bu-xantphos)(η^2-O_2) . 134
5.11 Gibbs free energies calculated for the formation of [M(*t*-Bu-xantphos)(nb)] 136
5.12 Gibbs free energies calculated for the formation of [M(*t*-Bu-xantphos)(η^2-O_2)] 137

6.1 Bond distances (Å) and angles (°) of [Pt(*t*-Bu-thixantphos)Cl_2] . . . 145
6.2 Crystallographic data and structure refinement of [Pt(*t*-Bu-thixantphos)Cl_2] 147
6.3 Selected NMR data for [Pt(xantphos)Cl_2] complexes 158
6.4 Selected NMR data for [Pt(*t*-Bu-xantphos)Cl_2] and [Pt(*t*-Bu-xantphos)Cl]Cl 159
6.5 Selected NMR data for [Pt(*t*-Bu-xantphos)Cl]X complexes 160
6.6 Selected NMR data for [Pd(*t*-Bu-xantphos)Cl_2] complexes 162
6.7 Selected NMR data for [Pd(*t*-Bu-sixantphos)Cl_2] 162
6.8 Selected NMR data for [Pd(*t*-Bu-xantphos)Cl]PF_6 complexes 164
6.9 Selected NMR Data for [Pt(*t*-Bu-xantphos)Me]Cl complexes. 171
6.10 Selected bond lengths and angles for [Pt(*t*-Bu-xantphos)Me]$^+$ 175
6.11 Selected bond lengths and angles for [Pt(*t*-Bu-xantphos-κ*P,O,P'*)Me]$^+$ 175
6.12 Gibbs free energies calculated for agostic and pincer [Pt(*t*-Bu-xantphos)Me]$^+$ 176
6.13 Energy change for the conversion of the [Pt(*t*-Bu-xantphos)ClMe] to the pincer complex 177
6.14 Energy change for the conversion of the [Pt(*t*-Bu-xantphos)ClMe] to the agostic complex 177

Acronyms

BINAP 2,2′-bis(diphenylphosphino)-1,1′-binaphthyl

BISBI 1,1′-bis(diphenylphosphinomethyl)-2,2′-biphenyl

cod 1,5-cyclooctadiene

coe cyclooctene

CSD Cambridge Structural Database

Cyp cyclopentyl

dba dibenzylideneacetone

dbpx α,α'-bis(di-*t*-butylphosphino)-*o*-xylene

dcype 1,2-bis(dicyclohexylphosphino)ethane

depp 1,2-bis(diethylphosphino)propane

depPE bis(2-diethylphosphinophenyl)ether

depx α,α'-bis(diethylphosphino)-*o*-xylene

DFT density functional theory

diop *O*-isopropylidene-2,3-dihydroxy-1,4-bis(diphenylphosphino)butane

DPEphos bis(2-diphenylphosphinophenyl)ether

dppb 1,2-bis(diphenylphosphino)butane

dppe 1,2-bis(diphenylphosphino)ethane

dppf 1,1′-bis(diphenylphosphino)ferrocene

dppp 1,2-bis(diphenylphosphino)propane

esd estimated standard deviation

HMDA hexamethylene-1,6-diamine

IR infrared

nb norbornene, bicyclo[2.2.1]hept-2-ene

NMR nuclear magnetic resonance

pta 1,3,5-triaza-7-phosphaadamantane

py 2-pyridyl

SEGphos 4,4′-Bi-1,3-benzodioxole-5,5′-diylbis(diphenylphosphane)

tht tetrahydrothiophene

TMEDA *N,N,N′,N′*-tetramethyl-ethane-1,2-diamine

TOF turnover frequency

TON turnover number

xantphos 4,5-bis(diphenylphosphino)-9,9-dimethylxanthene

Chapter 1

Introduction

This thesis provides an account of research into a group of diphosphine ligands with a rigid xanthene backbone and *tert*-butyl substituents on the phosphorus atoms. The three ligands have different groups in the bridgehead position of the backbone (CMe_2, $SiMe_2$, or S) which changes the natural bite-angle of the ligand. The coordination chemistry of these *t*-Bu-xantphos ligands with late-transition metals has been investigated with a focus on metal complexes that may form in catalytic reactions.

1.1 Tertiary Phosphine Ligands

Transition metal complexes have a number of different applications, from use as homogeneous catalysts, chemotherapeutics, or organic light emitting diodes.[1–3] Tertiary phosphine ligands are some of the most ubiquitous in coordination chemistry. Phosphines coordinate to transition metals by donation of the lone pair of electrons on the phosphorus atom forming a σ-bond and π-back-donation into the P-C anti-bonding σ^* orbitals which have π symmetry.[4] This combination forms stable coordination complexes with a range of different transition metals and oxidation states. A large array of different phosphine ligands are known with a range of different steric and electronic properties. These allow the phosphines to impart different physical environments and electron densities on the metal centre, which can result in different reactivities of the complexes. Due to this, phosphine ligands are frequently used as ancillary ligands in a wide range of different

catalytic systems including industrial-scale processes.[5–7]

1.1.1 Electronic and Steric Properties

As the chemical properties of the metal in a coordination complex are controlled largely by the coordinated ligands, several studies have quantified the electronic and steric properties of phosphine ligands.[8–14]

Investigations of electronic properties of ligands involve the measurement of the C≡O stretching frequency in a metal carbonyl complex such as $[Ni(CO)_3L]$, $[Mo(CO)_5L]$ or $[Rh(CO)ClL_2]$.*[8,9,11,14] If a metal with a spin active isotope such as rhodium or platinum is used, then the value of the one-bond metal-phosphorus coupling constant can also offer insight into the electronic properties of the phosphine ligand.[9,11,12,16] The value of the one-bond phosphorus-selenium coupling constant in a phosphinoselenide has been used as a way to study the electronic properties of phosphines.[17,18] The phosphinoselenides are readily synthesised, air-stable solids which avoids the need for transition metals or the use of toxic gases. A comparison of the different techniques used to measure the electronic properties has shown good correlation between the various series.[9]

The steric properties of different ligands have also been examined from a quantitative perspective. The Tolman cone angle is the angle formed at the apex of a cone centred at a metal positioned 2.28 Å from the phosphorus atom where the outer edges of the cone lie at the van der Waals radii of the outer most atom of the ligand.[14] The Tolman cone angle has some limitations: it was originally determined using physical molecular models with idealised bond lengths and van der Waals radii while actual molecules may vary from these values. In addition, the Tolman cone angle is a maximum cone angle which works well for approximately symmetrical spherical substituents such as PMe_3 or P^tBu_3, however when planar rings, such as phenyl substituents, are present these can rotate readily, resulting in much larger changes to the cone angle than a trialkyl phosphine would exhibit. The Tolman cone angles for aryl systems tends to be larger than the crystallographically determined cone angle.

An alternative quantification of the steric properties of phosphine ligands is the

*The nomenclature used in this thesis is in accordance with the Nomenclature of Inorganic Chemistry - IUPAC Recommendations 2005.[15]

percentage buried volume which is defined as the percentage of a sphere that is occupied by a given ligand.[19] This sphere has a metal atom at the centre and a defined radius to allow for comparison across different ligands. The percent buried volume for a phosphine ligand is calculated using parameters obtained from the crystal structure of that ligand with hydrogen atoms omitted. The resulting values generally correlate well with the values of the Tolman cone angle (R^2 = 0.959).[20] However, the values of percentage buried volume for phosphite ligands do not fit the trend, with the correlation giving calculated cone angles of 128 and 155° for $P(OMe)_3$ and $P(OPh)_3$ respectively instead of the values from Tolman's work of 128 and 155°.[14]

1.1.2 Diphosphine Ligands

Diphosphine ligands consist of two tertiary phosphines linked by a backbone. A selection of diphosphine ligands are shown in Figure 1.1. Most commonly, the backbone has a carbon skeleton such as an ethane, propane, or xylene group as found in dppe, dppp, or dbpx. Larger groups can also be used as backbones, such as the binapthyl ligand BINAP, or the BISBI system. The backbones can also include heteroatoms such as diop or DPEphos, or transition metals as in the ferrocene moiety found in dppf. The backbone can also be used to produce chiral ligands including BINAP, diop or SEGphos, which can be used for asymmetric catalysis.[5,21,22] Diphosphine ligands typically chelate to transition metals, resulting in enhanced stability through the chelate effect. The chelate effect is an entropic effect, where a complex with a bidentate ligand is observed to have increased thermodynamic stability compared to an analogous complex with similar monodentate ligands.[23] In monophosphine complexes, the monophosphine must compete with the other components in the reaction mixture as there is no entropic driver for a second molecule of the monophosphine to coordinate over any other ligands in the system. Hence the increased thermodynamic stability of complexes with bidentate chelating ligands compared to the analogous complex with related monodentate ligands.

The electronic and steric properties of diphosphine ligands can be described using the techniques developed for monophosphines.[8–14] The bite-angle, defined as the P-M-P angle in a transition-metal complex (Figure 1.2), can also be used to quantify and compare different diphosphine ligands. The natural bite-angle is

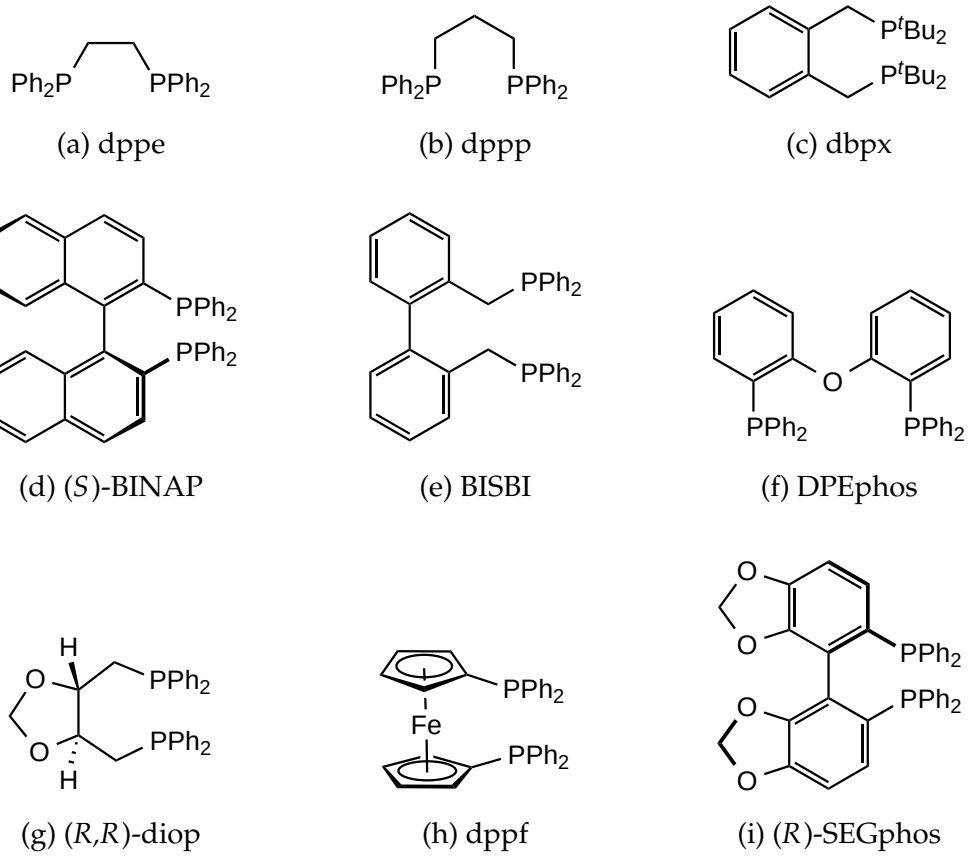

(a) dppe (b) dppp (c) dbpx

(d) (*S*)-BINAP (e) BISBI (f) DPEphos

(g) (*R*,*R*)-diop (h) dppf (i) (*R*)-SEGphos

Figure 1.1: Selection of diphosphine ligands.

defined as the P-Rh-P angle calculated by molecular modelling using a rhodium atom with fixed Rh-P distances of 2.315 Å.[24] The bite-angle for a given complex can also be measured from an X-ray crystal structure. The original development of the natural bite-angle parameter included a comparison of the natural and crystallographic bite-angles for seven different complexes, showing good correlation between the natural and crystallographic bite-angles.[24] A further study in 1999 showed that, for a range of different diphosphine ligands, the crystallographic bite-angles occur within a very narrow range which correlate well with the natural bite-angles.[25]

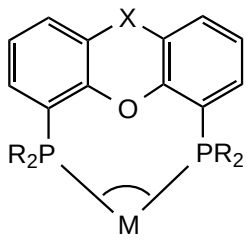

Figure 1.2: The bite angle

When used as ancillary ligands in transition metal catalysts, diphosphines can produce different product distributions compared with the analogous monophosphines. The catalytic reaction of ethene and carbon monoxide, in a methanol solution, produced short chain oligomers when $[Pd(MeCN)_4](BF_4)_2$ was used as the precatalyst with an excess of a monophosphine ligand such as triphenylphosphine.[26] Changing to a stoichiometric amount of a chelating diphosphine with $[Pd(OAc)_2]$ ($OAc = CH_3COO^-$), resulted in the co-polymerisation of carbon monoxide and ethene giving polyketone, indicating that the rate of chain termination is faster for monophosphine complexes than in the diphosphine complexes.[27] The bite-angle of the diphosphine was shown to have a significant impact on the rate of the reaction. When the $Ph_2P(CH_2)_nPPh_2$ (n = 1 - 6) series of ligands was studied, the highest reaction rate was observed for 1,2-bis(diphenylphosphino)propane (dppp) (n = 3) with the rate decreasing as the chain length was increased or decreased.[27] The steric bulk of the ligands is also important, changing the phenyl substituents on dppp for *tert*-butyl groups resulted in high selectivity for the mono-insertion product methyl propionate.[28] Introducing further rigidity to the system by changing to the xylene backbone ligand α,α'-bis(di-*t*-butylphosphino)-*o*-xylene (dbpx) resulted in methyl propionate exclusively.[29]

1.1.3 Wide Bite-Angle Diphosphine Ligands

The bite-angle of diphosphine ligands impacts the types of coordination complexes that will form upon reaction with an appropriate metal precursor. Ligands with bite-angles around 90° will typically coordinate in a *cis* geometry in square-planar and octahedral complexes and occupy axial-equatorial positions in trigonal bipyramidal complexes. Ligands with natural bite-angles closer to 120° can coordinate in a bis-equatorial arrangement in the trigonal bipyramidal complexes.[30] Two of the most important catalytic steps are oxidative addition and reductive elimination, which result in changes to the coordination number and geometry of the metal centres.[31] Altering the bite-angles of the ancillary ligands can have a significant impact on the selectivity and reactivity of these reactions, typically with larger bite-angle ligands favouring reductive elimination steps.[32] The strain on ligands to coordinate with bite-angles significantly different to their natural bite-angle, can result in destabilisation of particular intermediates in catalytic cycles leading to increased selectivity.[32] A wide-range of diphosphine ligands with large bite-angles have been reported, including dbpx, BISBI, DBFphos and Ph-xantphos (Figures, 1.1c, 1.1e, 1.3). Diphosphines with extremely large bite-angles, designed to coordinate in an exclusively *trans* geometry in square-planar complexes have been reported, such as TRANSphos, SPANphos, and norphos (Figure 1.4).[25,33,34]

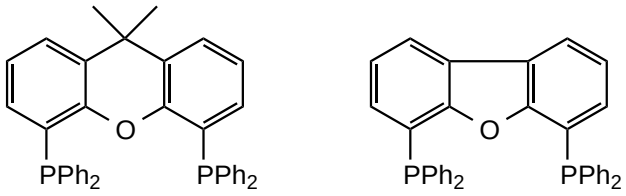

(a) Ph-xantphos (b) DBFphos

Figure 1.3: Wide bite-angle diphosphine ligands.

1.2 Pincer Ligands

Diphosphine ligands such as Ph-xantphos with wide bite-angles and a heteroatom in the centre of the backbone have the potential to act as pincer ligands. Pincer ligands have attracted research attention due to the unique balance of stability and

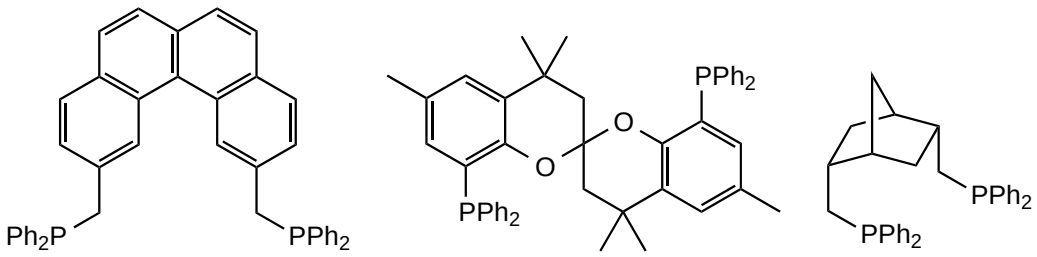

(a) TRANSphos (b) SPANphos (c) norphos

Figure 1.4: Selected trans-spanning diphosphine ligands.

reactivity that they impart on transition metal complexes.[35] Pincer ligands are tridentate ligands that coordinate to transition metals preferentially in a meridional fashion.[36] The ligands are typically named according to their donor atoms, such as PCP, POP or NCN (Figure 1.5). If the groups between the donor atoms contain heteroatoms then these may be included in the naming also, for example POCOP. The pincer ligands may be anionic (as with PCP ligands) or neutral (PNP and POP).[37,38] Although phosphines are the most common donor groups, amines,[39] imines,[40] thioethers[41] and N-heterocyclic carbenes[42] have all been reported.

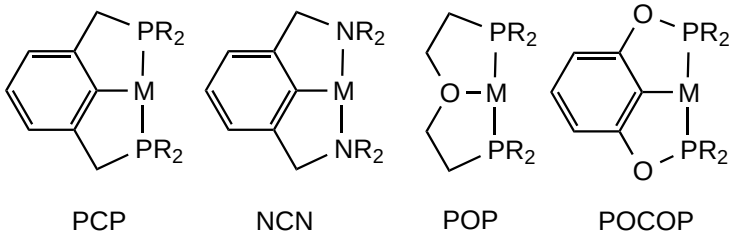

Figure 1.5: Naming of pincer ligands.

Pincer ligands were first reported in 1976 by Shaw[43] and Alcock.[44] Shaw reported a *tert*-butyl PCP ligand (Figure 1.6a) and introduced the naming scheme that has become commonplace for pincer ligands. When reacted with an appropriate metal precursor, complexes of the tridentate ligand formed with nickel, palladium, platinum, rhodium, and iridium with chloride, nitrile, hydride, and carbon monoxide ligands.[43] Alcock reported the first POP pincer ligands together with their rhodium carbonyl complexes, characterised by X-ray crystallography (Figure 1.6b).[44]

The different components of pincer ligands have a significant influence on the steric and electronic properties and hence their reactivity.[39] Altering the central

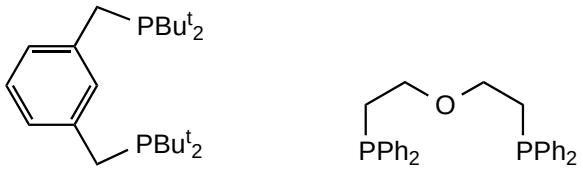

(a) (b)

Figure 1.6: First reported pincer ligands.

donor group, X (Figure 1.7), can lead to changes in electronic effects mostly through the *trans*-influence.[36] For example, a carbon donor ligand has a greater *trans*-influence than an oxygen donor. Thus ligands *trans* to X in PXP complexes will be bound more strongly when X = O than X = C.[45] The donor group Y controls the steric environment around the metal centre and the electron density. Changing the backbone and other remote groups gives control over the electron density on the metal and can be used to improve solubility properties.[36] The tridentate coordination of pincer ligands, typically forming two five-membered metallacycles, imparts significant stability to metal complexes with pincer ligands.

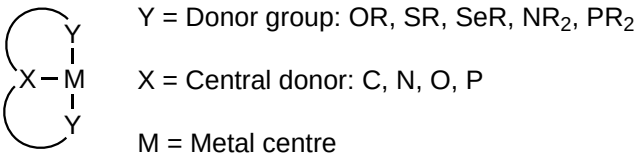

Figure 1.7: General representation of pincer complexes.

Coordination complexes of pincer ligands have a large number of applications. Platinum complexes of an NCN pincer ligand have been utilised as sensors for the detection of sulfur dioxide.[46–48] Palladium and nickel complexes of a number of pincer ligands have shown activity in cross-coupling reactions.[41,42,49–51] Theoretical studies have shown potential uses for pincer ligands in water-splitting[52] and nitrogen fixation.[53] However, one of the most prominent uses of pincer ligands is the activation of C-H bonds, typically as dehydrogenation catalysts.[36,48,54]

1.3 Xantphos

First reported in 1995 by van Leeuwen et al., the xantphos[†] class of diphosphine ligands were designed to investigate the influence of the bite-angle on catalytic reactions, in particular rhodium catalysed hydroformylation.[30] The general structure and a selection of different xantphos derivatives are given in Figure 1.8. The first paper on xantphos included derivatives where the CMe_2 group in the backbone of Ph-xantphos (Figure 1.8d) was replaced by a S (Ph-thixantphos, Figure 1.8f), $SiMe_2$ (Ph-sixantphos, Figure 1.8e), a direct bond between the atoms (DBFphos, Figure 1.8c), or removed entirely (DPEphos, Figure 1.8b). Since then a vast array of derivatives have been reported. The most common position for derivatisation is the bridgehead position (occupied by a CMe_2 group in Ph-xantphos). Changes to this position can create changes in the natural bite-angles of the ligands. Another site for derivatisation is the substituents on the phosphorus atoms which have been changed for cyclic groups, chiral derivatives or alkyl chains including methyl, ethyl, isopropyl and *tert*-butyl groups. The phosphorus donors have also been replaced with a range of different groups including phosphonites, amines, imines, arsines, and thioethers.[55–58] The third site for derivatisation is the position *meta* to the phosphorus atoms on the backbone phenyl rings. In Ph-xantphos this position is occupied by hydrogen atoms, while in Ph-thixantphos methyl groups are present. Derivatives with *tert*-butyl or sulfate groups have also been reported.[59–61‡] These alterations all result in changes to the bite-angle of the ligand.

The influence of the bite-angle of diphosphine ligands on the selectivity and activity of their transition metal complexes in various catalytic process has been investigated using the xantphos ligands. The hydroformylation of alkenes to give branched and linear aldehydes is an industrially important reaction with the lin-

[†]The term xantphos is used in the literature to mean either the general class of ligands or the specific ligand 9,9-dimethyl-4,6-bis(diphenylphosphino)xanthene. For the purposes of this thesis the specific ligand will be referred to as Ph-xantphos and the term xantphos will be used to represent a generic ligand from this class.

[‡]In the literature two different structures are commonly referred to as *t*-Bu-xantphos, one with *tert*-butyl substituents on the aromatic backbone and one with *tert*-butyl groups on the phosphorus atoms. For the purpose of this thesis the structure with the *tert*-butyl substituents on the phosphorus will be named *t*-Bu-xantphos and the structure with the *tert*-butyl groups on the aromatic backbone will be named *t*-Bu-(Ph-xantphos).

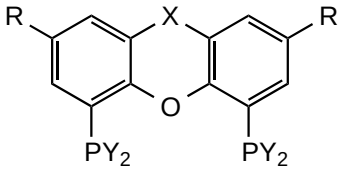

(a) General structure

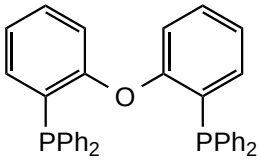

(b) DPEphos, 102°

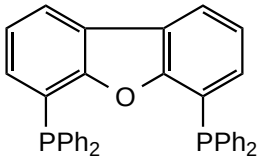

(c) DBFphos, 131°

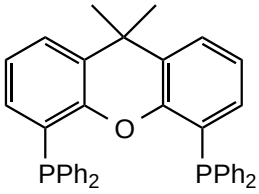

(d) Ph-xantphos, 111°

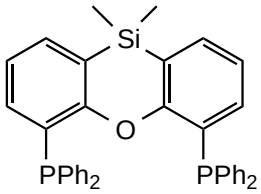

(e) Ph-sixantphos, 108°

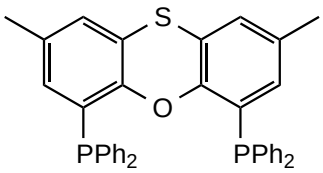

(f) Ph-thixantphos, 110°

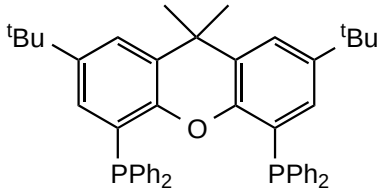

(g) *t*-Bu-(Ph-xantphos), 110°

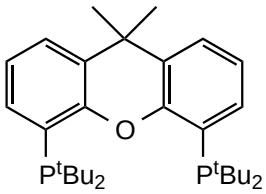

(h) *t*-Bu-xantphos, 140°

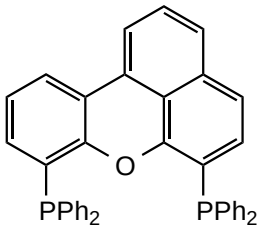

(i) Benzoxantphos, 120.6°

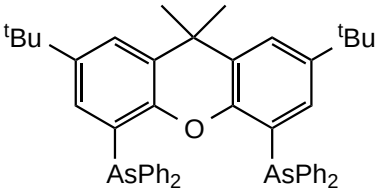

(j) Xantarsine, 113°

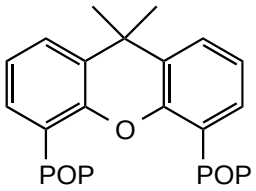

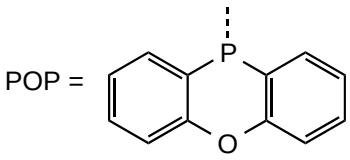

(k) POP-xantphos, 123°

Figure 1.8: Selection of xantphos derivatives with their natural bite-angles.[25,55,61,62]

ear aldehydes typically of higher industrial importance.[28] In the hydroformylation of 1-octene using various xantphos ligands, a linear correlation was observed between the natural bite-angle of the diphosphine and the percentage of linear aldehyde product.[30] From this and other kinetics studies, the bite-angle has been determined to have both a steric and electronic component.[63,64] In hydroformylation the hydride-migration step determines the regioselectivity of the reaction. In this case additional steric crowding of the metal centre, resulting from a larger bite-angle, can lead to a favouring of the less sterically demanding transition state - that which produces the linear aldehyde.[32] Carrying out the hydroformylation of styrene or 1-octene with a series of thixantphos complexes where the phenyl substituents on the phosphorus atoms were substituted in the *para*-position with various electron donating or electron withdrawing substituents, showed differences in the turnover frequency (TOF) of each reaction.[63] This is thought to be related to changes in the metal hybridisation, changing the reactivity of the metal towards reductive elimination.[32,65]

The xantphos ligands were the first tertiary phosphine ligands to form active hydrocyanation catalysts on nickel.[66] Using styrene as a substrate, diphosphines with alkyl backbones, such as 1,2-bis(diphenylphosphino)ethane (dppe), dppp and 1,2-bis(diphenylphosphino)butane (dppb) gave poor yields (<10%) whereas the xantphos ligands gave yields ranging from 27-95%, with the highest yield for Ph-sixantphos. Ligands with bite-angles close to 105° resulted in higher yields and selectivities whilst decreasing the bite-angle to 101° or increasing to 110° led to a much lower activity. The bite-angle can influence the selectivity of the reaction by stabilising preferred reaction intermediates and destabilising inactive species. In the hydrocyanation reaction a bite-angle close to 109° destabilises square-planar Ni(II) species and stabilises the tetrahedral Ni(0) species, enhancing the reductive elimination step and resulting in a faster reaction.[57] The increased reactivity of xantphos complexes compared to other diphosphines including, dppp, BINAP, dppf, and DPEphos has also been observed in a range of different cross-coupling reactions.[67]

A search of the Cambridge Structural Database (CSD) indicates that of the crystallographically determined structures, most complexes with xantphos derivatives involve bidentate $\kappa P,P'$ coordination.[68] Four complexes with a 2-coordinate metal centre have been reported, all coordinated to gold. Ten 3-coordinate structures have been published. With 4-coordinate metals, tetrahedral complexes are

the most common (31 structures), followed by pseudo-*trans* square-planar complexes (26), then *cis* square-planar geometries (20). This is particularly interesting as the natural bite-angle of Ph-xantphos ligands is closer to a 90° than to 180°. On pentacoordinate metals 10 complexes have been reported with one square-pyramidal structure, three axial-equatorial, and six bis-equatorial trigonal bipyramidal complexes found. Six different octahedral complexes have been reported, all with the xantphos ligand displaying a *cis*-geometry. The xantphos ligands can also coordinate in a κ*P,O,P'* geometry in addition to the bidentate κ*P,P'* mode. This κ*P,O,P'* coordination is more common than the κ*P,P'* in octahedral complexes with 24 reported. However, it is much less common in five coordinate complexes with only four κ*P,O,P'* complexes and 10 κ*P,O,P'* four-coordinate complexes. A monodentate κ*P* bonding mode is also possible, though it is very rare, with only one crystal structure reported to date.[69]

Given the possibility of κ*P,O,P'* and κ*P,P'* coordination the xantphos ligands also have the potential for hemilability of the central donor group whereby the oxygen can bind reversibly to the metal centre in order to stabilise catalytic intermediates. This has been utilised in the hydroacylation of alkenes and alkynes using a rhodium pincer complex, where the oxygen can bind in order to stabilise important intermediates and prevent the competing decarbonylation reactions from occurring.[70–72] A range of rhodium complexes with Ph-xantphos or bis(2-diphenylphosphinophenyl)ether (DPEphos) as ancillary diphosphine ligands were tested for the hydroacylation reaction.[70] The DPEphos complexes were more active than the dppe complex used for comparison, achieving conversions of 100% after 30 and 90 minutes respectively. However, the Ph-xantphos complex was completely inactive. The lower reactivity is thought to be a result of the increased rigidity of the Ph-xantphos backbone compared to that of DPEphos.[72]

1.3.1 Alkyl-Substituted Xantphos Ligands

Despite the large number of xantphos derivatives few examples of xantphos ligands with alkyl substituents on the phosphorus atoms have been reported. The synthesis and some coordination chemistry of xantphos ligands with methyl, ethyl, isopropyl, and *tert*-butyl substituents has been studied. Me-xantphos was reported in 2002 and investigated for reactivity with [Pd(cod)ClMe] (cod = 1,5-cyclooctadiene), to produce *cis*-[PdClMe(Me-xantphos)].[73] The *cis* isomer was

also formed using Ph-sixantphos. However, using the larger bite-angle ligands Ph-thixantphos and Ph-xantphos *cis-trans* isomerism was observed at room temperature. Reaction of the four chloridomethyl complexes with $AgSO_3CF_3$ yielded the pincer complexes [PdMe(xantphos-κ*P,O,P'*)][SO_3CF_3] (Scheme 1.1).

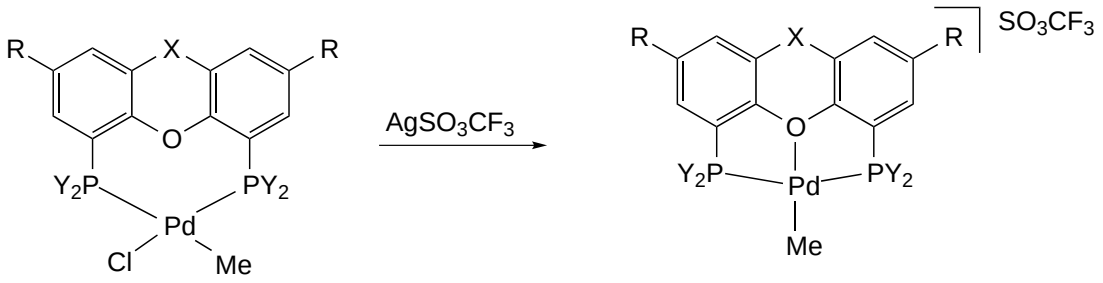

Scheme 1.1: Chloride abstraction from [PdClMe(xantphos)] xantphos = Ph-sixantphos, Ph-thixantphos, Ph-xantphos, and Me-xantphos.

A variant of xantphos with ethyl groups on the phosphorus atoms (Et-xantphos) was reported in 2004.[74,75] Palladium and platinum complexes, [M(Et-xantphos)$_2$], [M(Et-xantphos)$_2$]$^{2+}$ and platinum complexes [Pt(Et-xantphos)$_2$H]PF_6 and [Pt(Et-xantphos)$_2$(H)$_2$]$^{2+}$ have been studied for their electrochemical properties. The X-ray crystal structures of [M(Et-xantphos)$_2$] (M = Pd, Pt) were obtained and have a tetrahedral geometry, with average bite-angles of 108.3° for both metals. The palladium(II) complex had two molecules in the asymmetric unit, one closer to a square-planar geometry (average bite-angle = 139.7°) and the other closer to a tetrahedral geometry (average bite-angle = 95.8°). The pseudo-square planar [Pd(Et-xantphos)$_2$](BF_4)$_2$ complex was also crystallised, and had much larger bite-angles than any of the other ethyl substituted diphosphines included in the study (1,2-bis(diethylphosphino)propane (depp), α,α'-bis(diethylphosphino)-*o*-xylene (depx) and bis(2-diethylphosphinophenyl)ether (depPE)) indicating the ability of the xantphos ligands to support metals in unusual geometries.

A xantphos ligand with isopropyl substituents on the phosphorus atoms, *i*-Pr-xantphos, was first reported in 2010, together with the osmium complex [$OsCl_3$(*i*-Pr-xantphos-κ*P,O,P'*)], showing the κ*P,O,P'* coordination which is common for xantphos ligands in octahedral complexes.[76] The same group, has since reported the synthesis and reactivity of [MCl_2(DMSO-κ*S*)(*i*-Pr-xantphos-κ*P,O,P'*)] (M = Os, Ru) producing a number of different osmium and ruthenium complexes including various polyhydrides and bis(alkynyl)vinylidene complexes.[77,78]

A study of the reactivity of *i*-Pr-xantphos towards palladium shows differences to the Ph-xantphos ligand.[79] The [Pd(CF_3)Ph(Ph-xantphos)] complex exists in a *cis* geometry in the solid state, and as *cis* and *trans* isomers in solution, whereas the analogous *i*-Pr-xantphos complex shows only a *trans* configuration. The *i*-Pr-xantphos complex was synthesised in a different manner as the Ph-xantphos ligand was readily displaced by CF_3^- from CF_3SiMe_3/F^- while the *i*-Pr-xantphos ligand was not, indicating the different chemistry of the two ligands. The difference in the coordination geometries also meant that the $PhCF_3$ was more readily lost from the *cis*-[Pd(CF_3)Ph(Ph-xantphos)] than the *trans*-[Pd(CF_3)Ph(*i*-Pr-xantphos)]. A related study investigated nickel complexes of *i*-Pr-xantphos for the trifluoromethylation of aryl halides.[80] The [NiF(1-naphthyl)(*i*-Pr-xantphos)] complex reacted with CF_3SiMe_3 forming [Ni(CF_3)(1-naphthyl)(*i*-Pr-xantphos)]. Both of these complexes were found to have *trans*-geometries through X-ray crystallography, and showed slow decomposition at 140 °C and 120 °C respectively, giving rise to a range of products, with no C-F compounds or 1-trifluoromethylnaphthyl formed.

The chemistry of rhodium and iridium complexes with *i*-Pr-xantphos ligands has also been studied. Reaction of *i*-Pr-xantphos with $[Rh(coe)_2(\eta^2\text{-Cl})]_2$ (coe = cyclooctene) generated the [RhCl(*i*-Pr-xantphos-κ*P,O,P'*)] complex cleanly.[81] However, reaction with the iridium analogue resulted in cyclometallation of one of the isopropyl groups forming [IrClH(*i*-Pr-xantphos-κ-*C,P,O,P'*]. The chloride ligand in [RhCl(*i*-Pr-xantphos-κ*P,O,P'*)], was replaced with a hydride, *via* reaction with KO^iPr, producing KCl and acetone as by-products. The trihydride [$Ir(H)_3$(*i*-Pr-xantphos-κ*P,O,P'*)] was produced by reaction of the metallated iridium complex with KOH and ^{i}PrOH. The rhodium chloride complex undergoes oxidative addition of H_2 to form [RhCl$(H)_2$(*i*-Pr-xantphos-κ*P,O,P'*)]. The analogous iridium complex was synthesised by reaction of the metallated complex with *n*-octane at 90 °C. Recent research has shown that the chloride can be removed from [RhCl$(H)_2$(*i*-Pr-xantphos-κ*P,O,P'*)] by reaction with $Li[B(C_6F_5)_4]OEt_2$ forming [$Rh(H)_2$(*i*-Pr-xantphos-κ*P,O,P'*)]$^+$.[82] Reacting triflic acid with [RhCl(*i*-Pr-xantphos-κ*P,O,P'*)] or [IrClH(*i*-Pr-xantphos-κ-*C,P,O,P'*] results in [MCl(H)(OTf)(*i*-Pr-xantphos-κ*P,O,P'*)] (M = Rh, Ir).[81] The reactivity of the *i*-Pr-xantphos complexes is summarised in Figure 1.2 and 1.3 for rhodium and iridium respectively.

The reactivity of the rhodium and iridium complexes towards silyl compounds has also been investigated with the results summarised in Scheme 1.4.[83] Reac-

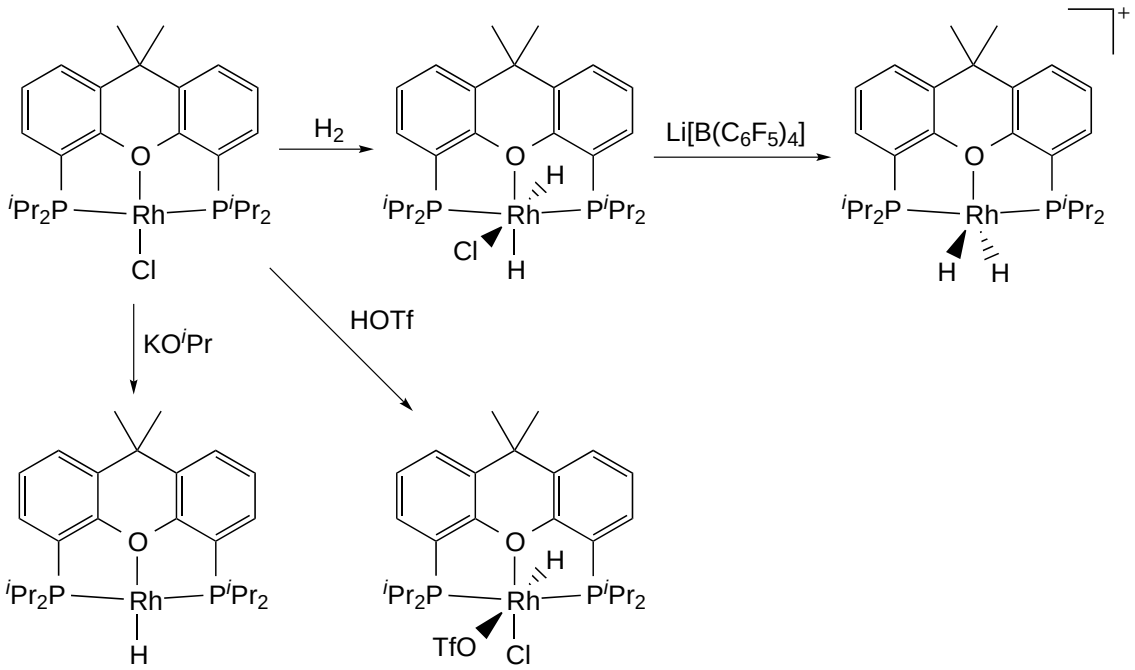

Scheme 1.2: Reactions of [Rh(*i*-Pr-xantphos)].

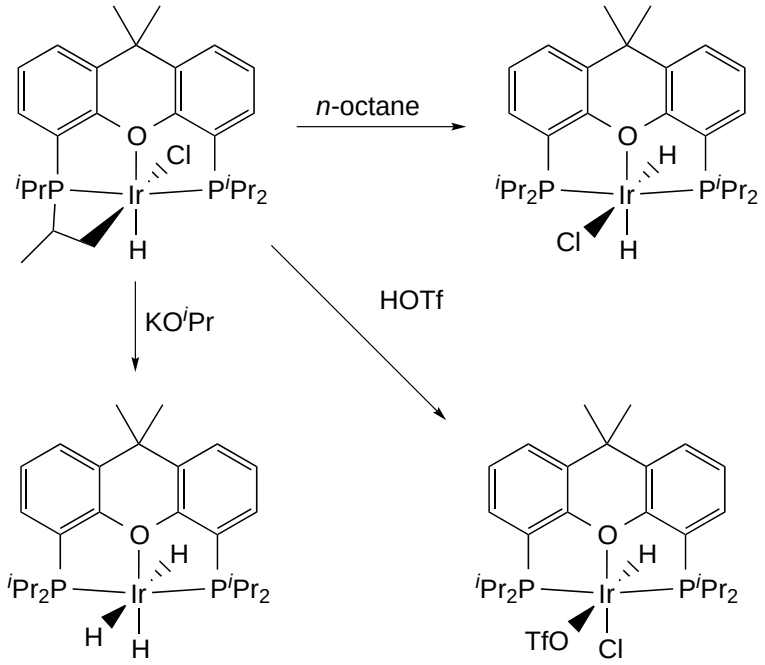

Scheme 1.3: Reactions of [Ir(*i*-Pr-xantphos)].

tion of [RhCl(*i*-Pr-xantphos-κ*P,O,P'*)] or [IrClH(*i*-Pr-xantphos-κ-*C,P,O,P'*] with SiH_2Ph_2 or $SiHEt_3$ resulted in [MCl(H)(*i*-Pr-xantphos-κ*P,O,P'*)(SiR_3)] (M = Rh, Ir, SiR_3 = $SiHPh_2$, $SiEt_3$). The diphenylsilane complexes were unstable in solution converting to [Rh($SiClPh_2$)(*i*-Pr-xantphos-κ*P,O,P'*)] *via* loss of molecular hydrogen and *trans*-[Ir($SiClPh_2$)$(H)_2$(*i*-Pr-xantphos-κ*P,O,P'*)]. The rhodium complex [RhH(*i*-Pr-xantphos)] also underwent reaction with $SiHEt_3$ and $SiHPh_3$ initially forming the dihydride [Rh$(H)_2$(*i*-Pr-xantphos-κ*P,O,P'*)(SiR_3)] (R = Et, Ph) which loses molecular hydrogen to form [Rh(*i*-Pr-xantphos-κ*P,O,P'*)(SiR_3)]. Reaction of [Rh($SiClPh_2$)(*i*-Pr-xantphos-κ*P,O,P'*)] with Na[BAr^F_4] in the presence of water produced [Rh(H)(*i*-Pr-xantphos-κ*P,O,P'*)($SiOHPh_2$)] which was tested as a catalyst for the alcoholysis of SiH_2Ph_2 with various alcohols in toluene at 32 °C, forming $ROSiHPh_2$ in isolated yields of 71 - 92% with TOFs of 4000 to 76500 h^{-1}.

1.3.2 *t*-Bu-Xantphos

This thesis covers an investigation into the coordination chemistry of three different xantphos ligands with *tert*-butyl substituents on the phosphorus atoms. The three ligands differ in the bridgehead position: *t*-Bu-xantphos has CMe_2, *t*-Bu-sixantphos has $SiMe_2$ and *t*-Bu-thixantphos has a thioether bridge. The first mention of *t*-Bu-xantphos was in 2002 with the unsuccessful attempts to synthesise *t*-Bu-xantphos from either 4,5-dilithio-9,9-(dimethyl)xanthene or 9,9-dimethyl-4,5-bis(dichlorophosphino)xanthene, the researchers postulated that steric crowding was the reason for the lack of reactivity.[73] A successful synthesis of *t*-Bu-xantphos from the dilithiated backbone was reported in 2005 using heptane as a solvent and heating the reaction mixture to 60 °C.[84] *t*-Bu-Xantphos has subsequently been studied for use as an ancillary ligand in the palladium catalysed cross-coupling of thiols and aryl bromides or triflates, the iron catalysed sp^3-sp^3 cross-coupling of alkyl halides with alkyl Grignard reagents, the platinum catalysed amination of allylic alcohols and the N-arylation of heterocyclic diamines, all with poor yields, while higher yields were observed when Ph-xantphos was used.[84–87] These studies have focussed on the addition of *t*-Bu-xantphos as a component of the catalytic system. Few complexes of *t*-Bu-xantphos have been characterised, although the difference in the catalytic results suggest differences in the coordination chemistry of Ph-xantphos and *t*-Bu-xantphos.

Prior to the start of this research, the only isolated coordination complexes of

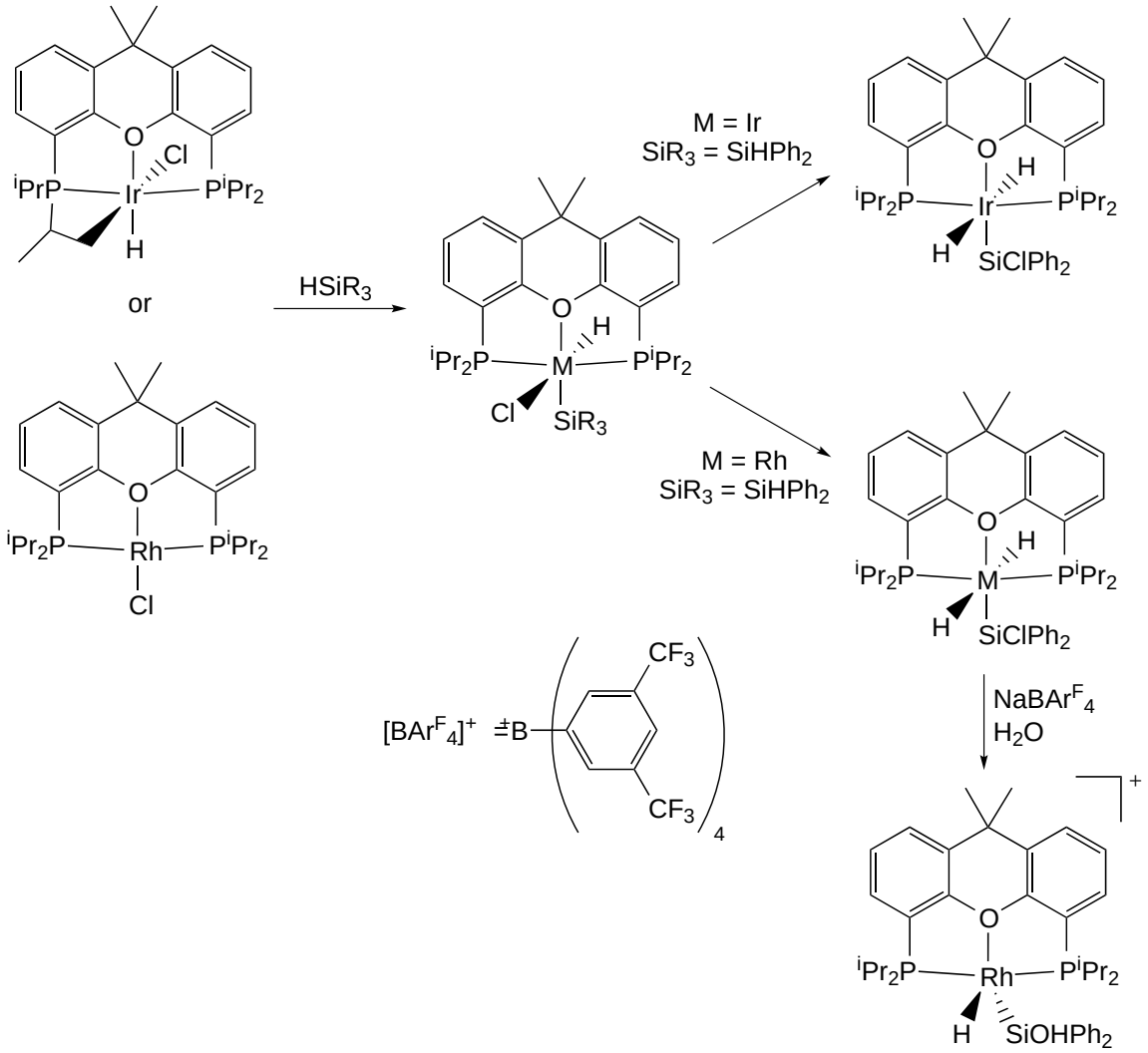

Scheme 1.4: Reactions of Rh and Ir *i*-Pr-xantphos complexes with silanes. SiR_3 = $SiHPh_2$, $SiEt_3$.

t-Bu-xantphos were [Au(*t*-Bu-xantphos)][AuX_2] (X = Cl, Br, I), formed by reaction of [AuCl(tht)] (tht = tetrahydrothiophene) with *t*-Bu-xantphos and subsequent reaction with KBr or KI.[88] The analogous reaction using Ph-xantphos gave [$(AuX)_2$(Ph-xantphos)] (X = Cl, Br, I) with each phosphorus atom coordinated to a separate gold centre with a Au-Au interaction.[88,89] Subsequent investigations into the catalytic activity of gold xantphos complexes towards the C-F bond activation of perfluoroarenes showed turnover numbers (TONs) of 200 for [AuCl(Ph-xantphos)] and 1000 for [Au(*t*-Bu-xantphos)][$AuCl_2$].[90] Mechanistic studies into the reaction showed that [Au(xantphos)]$^+$ was an important intermediate and is in equilibrium with the inactive [Au$(xantphos)_2$]. Due to the size of *t*-Bu-xantphos the equilibrium favours the two-coordinate species while for Ph-xantphos the four-coordinate complex is preferred, resulting in lower activity.[90] This clearly shows the difference between the two xantphos ligands and suggests that a difference in the coordination chemistry may be the cause of the observed differences in catalytic reactivity.

Subsequent to the start of the research presented in this thesis *t*-Bu-xantphos has gained increasing attention, likely as a result of the ligand becoming commercially available. In the six years from the first successful synthesis in 2005 to the start of this research in mid-2011, only the four papers discussed above were published investigating *t*-Bu-xantphos.[§] However, the following three years showed increasing attention with 9 papers published[82,90,93–99] and 10 patent applications.[100–109]

Further investigations into the catalytic properties of *t*-Bu-xantphos have been reported, without investigation into the coordination chemistry. These include the palladium-catalysed cross-coupling of 2-(4-bromophenyl)-5-chloropyrazine with a benzimidazole boronic ester and hydroesterification of methyl oleate.[97,98] In both cases little conversion was observed when *t*-Bu-xantphos was used, though the Ph-xantphos systems showed significant reactivity. The aminocarbonylation of aryl bromides was performed with each of Ph-xantphos and *t*-Bu-xantphos in an unusual monodentate coordination mode.[93] Little reactivity was observed with *t*-Bu-xantphos, while the Ph-xantphos system gave the product in 92% isolated yield. In the rhodium catalysed reductive amination of aldehydes *t*-Bu-xantphos showed a 59% total conversion with only 19% selectivity for the desired

[§]Two papers investigating the use of the dioxidised *t*-Bu-xantphos as a ligand on europium and samarium were also published in 2011 and 2012.[91,92]

product, while Ph-xantphos had an 84% conversion and 93% selectivity.[96]

In some cases the *t*-Bu-xantphos system is more active than the Ph-xantphos system, such as the palladium catalysed N-alkylation of aniline with benzyl alcohol.[94] The *t*-Bu-xantphos system gave near quantitative conversion at 100 °C while the Ph-xantphos system showed only 63% conversion at 110 °C. Improved activity with *t*-Bu-xantphos compared to Ph-xantphos was also observed in the palladium catalysed methylation of alkynyl C-H bonds with dimethyl sulfonium ylides.[95] Under the same conditions a yield of 46% was obtained with *t*-Bu-xantphos while only 15% was produced using Ph-xantphos. *t*-Bu-Xantphos and Ph-xantphos can also have similar results, such as in the rhodium catalysed hydroamidomethylation of 1-pentene with acetamide, Ph-xantphos and *t*-Bu-xantphos showed conversions of 83 and 80% respectively with greater than 99% linearity in both cases.[99]

Despite the increased interest in *t*-Bu-xantphos in the last four years, research has focussed on its use as an ancillary ligand for catalytic reactions, mostly with the catalyst formed *in situ*. A crystal structure of *trans*-[Pd(*t*-Bu-xantphos)Cl_2], was reported *via* communication to the CSD in 2011 (CSD-XARXAR), no further publication of this complex has followed.[68] One paper has reported the coordination behaviour of the *t*-Bu-xantphos ligand with rhodium.[82] Similarly to the work with *i*-Pr-xantphos, the *t*-Bu-xantphos ligand reacts with [Rh(coe)(η^2-Cl)]$_2$ (coe = cyclooctene) to give [Rh(*t*-Bu-xantphos-κ*P,O,P'*)Cl]. This Rh(I) chloride readily undergoes oxidative addition of hydrogen to form a [Rh(*t*-Bu-xantphos-κ*P,O,P'*)Cl$(H)_2$] complex. The structures of [Rh(*t*-Bu-xantphos-κ*P,O,P'*)Cl] and [Rh(*t*-Bu-xantphos-κ*P,O,P'*)Cl$(H)_2$] have been confirmed by X-ray crystallography. Chloride abstraction from [Rh(*t*-Bu-xantphos-κ*P,O,P'*)Cl$(H)_2$] using $AgBF_4$ or $AgSbF_6$, generates the trigonal bipyramidal complex [Rh(*t*-Bu-xantphos-κ*P,O,P'*)$(H)_2$], with the *t*-Bu-xantphos ligand retaining the meridional coordination typical of pincer ligands. This dihydride was found to react with ethene to give ethane and [Rh(*t*-Bu-xantphos-κ*P,O,P'*)(C_2H_4)], however no reaction with the commonly used hydrogen acceptors, *t*-butylethylene or norbornene, or with terminal alkenes was observed. [Rh(*t*-Bu-xantphos-κ*P,O,P'*)Cl$(H)_2$] reacts with KO^tBu resulting [Rh(*t*-Bu-xantphos-κ*P,O,P'*)H]. Addition of ethene to [Rh(*t*-Bu-xantphos)H] resulted in the reversible formation of an ethyl complex. The [Rh(*t*-Bu-xantphos)H] complex also showed reactivity in the isomerisation of 1-hexene with a TON of 2000 after 16 hours.

The previous work exploring *t*-Bu-xantphos and Ph-xantphos as ancillary ligands for catalytic processes has shown significant differences in the yields of the reactions in most cases, though in one case similar activity was reported. Although a number of palladium catalysed reactions have been studied, only two palladium complexes have been reported (one being only a crystal structure). The only research into the coordination chemistry of the *t*-Bu-xantphos ligands is on gold and rhodium.[82,88] The original study into the xantphos ligands focussed on changing the bridging groups of Ph-xantphos showing the impact that subtle changes in the bite-angle can have on the catalytic activity of the transition metal complexes.[30] Given the number of studies investigating the catalytic activity of *t*-Bu-xantphos without investigating the coordination chemistry, an examination of the coordination chemistry of a range of subtly different *t*-Bu-xantphos ligands with late-transition metals is of particular interest.

1.4 Research Objectives

The xantphos class of ligands has been the subject of a number of studies, with interesting and varied results. The initial research with Ph-xantphos investigated the influence of changes in the bite-angle resulting from changing the group in the bridging position from the CMe_2 group found in Ph-xantphos.[30,34,110] These studies have shown that small changes in the bite-angle can have a significant impact on the catalytic reactivity and selectivity of the system. Recently a large amount of research has focussed on the development of xantphos derivatives with alkyl substituents on the phosphorus atoms, particularly the *i*-Pr-xantphos and *t*-Bu-xantphos ligands. Prior to the start of this research only one report investigating the coordination behaviour of *t*-Bu-xantphos had been published.[88] The other studies all showed much lower activity in catalytic systems than with the Ph-xantphos ligand.[84–86] Together this suggested that the coordination behaviour of the *t*-Bu-xantphos and Ph-xantphos ligands is different and deserved further attention. The papers published since the inception of this research have only sought to solidify the objectives, as these have reported several examples of studies into the use of *t*-Bu-xantphos in catalytic systems with only one further study into the coordination behaviour on rhodium, despite the majority of the catalytic studies being performed on palladium. Furthermore, despite the

much larger bite-angle and the electronic differences of *t*-Bu-xantphos compared to Ph-xantphos, and the impact small bite-angle changes have on the activity of Ph-xantphos only two xantphos ligands with *tert*-butyl substituents on the phosphines and CMe_2 or $C{=}CMe_2$ in the bridgehead position have been published, and no comparative investigation has been reported.

The over-arching goal of this research is to investigate the synthesis, properties and coordination chemistry of *t*-Bu-xantphos and two derivatives in the bridgehead position (S and $SiMe_2$). The first stage aimed to synthesise the *t*-Bu-thixantphos and *t*-Bu-sixantphos ligands, and investigate the steric and electronic properties of all three *t*-Bu-xantphos ligands by the calculation of their natural bite-angles and synthesis of non-transition metal derivatives.

Silver is a particularly interesting metal for the synthesis of coordination complexes, showing a distinct propensity to form dimers, trimers, or higher order structures, with differences dependent upon the steric bulk and flexibility of the diphosphine ligands used.[111] Hence, the initial coordination chemistry of the three *t*-Bu-xantphos ligands towards silver was investigated in order to gain an understanding of their coordination chemistry and gauge the impact of their large bite-angles on the coordination chemistry, and to allow comparison to the gold *t*-Bu-xantphos complexes previously published.

The remainder of the research focussed on transition metals which are commonly used in homogeneous catalysis. The xantphos class of ligands have been well-studied for their roles as ancillary ligands in hydroformylation.[30,63,112–116] The aim of this research was not to investigate the catalytic properties of the three *t*-Bu-xantphos ligands, but to produce discrete transition metal complexes to gain insight into the catalytic studies that have already been performed. Hence the coordination chemistry with rhodium focussed on the synthesis of a simple rhodium(I) complex and established the reactivity towards small molecules, including hydrogen and carbon monoxide, which are the foundation for a number of different catalytic processes.

The coordination chemistry of the three *t*-Bu-xantphos ligands towards palladium and platinum in both the 0 and +2 oxidation states was also studied, in order to gain insight into the differences in the catalytic activity of systems with *t*-Bu-xantphos and Ph-xantphos. Palladium is one of the most widely used metals for homogeneous catalysis and catalytic cycles frequently involve interconver-

sion between the two oxidation states.[31] Platinum complexes were synthesised prior to the palladium investigation as the presence of an NMR active isotope (^{195}Pt) coupled with the high stability of platinum complexes was beneficial to the identification and characterisation of the complexes produced. Although the coordination chemistry of Ph-xantphos with palladium is well-known, few coordination complexes of Ph-xantphos, and particularly Ph-thixantphos and Ph-sixantphos with platinum have been reported. This work began with a brief investigation into the coordination chemistry of Ph-thixantphos with platinum to assist in identifying any differences in the coordination chemistry that resulted from changing the phenyl substituents to *tert*-butyl groups. The coordination chemistry of the three *t*-Bu-xantphos ligands with palladium and platinum in the 0 and +2 oxidation states was subsequently investigated.

Throughout this research nuclear magnetic resonance (NMR) spectroscopy was used extensively to characterise the products of the reactions and aid in the identification of any intermediates or dynamic processes that were present. X-ray crystallography was also an important tool, particularly to compare the bite-angles and coordination geometries of the *t*-Bu-xantphos complexes produced with those previously reported for the Ph-xantphos. Theoretical chemistry using density functional theory (DFT) was used to gain further insight into reactions or processes when this was of benefit.

Chapter 2

Ligand Synthesis and Properties

The *t*-Bu-xantphos ligand was first reported in 2005.[84] The original paper and several since then, have tested *t*-Bu-xantphos for use as an ancillary ligand in a range of different catalytic systems with mixed results.[82,85–87,90,93–99] Despite the catalytic attention towards the *t*-Bu-xantphos ligand very little is known about the coordination chemistry or reasons for the very different catalytic activity compared to Ph-xantphos. Only one study comparing the coordination chemistry of the two ligands has been published.[88] This study found that *t*-Bu-xantphos formed [Au(*t*-Bu-xantphos)][AuX_2] (X = Cl^-, Br^-, and I^-) complexes whereas Ph-xantphos formed [$(AuX)_2$(Ph-xantphos)]. A *trans*-[Pd(*t*-Bu-xantphos)Cl_2] complex has been reported to the CSD (CSD-XARXAR), while the analogous complex with Ph-xantphos is *cis*, indicating a difference in the coordination chemistry of the two ligands.[68] A series of rhodium complexes with *t*-Bu-xantphos has been published,[82] though the analogous Ph-xantphos complexes have not been investigated.

The original study into the Ph-xantphos ligands investigated the effect of changing the bridging group in the backbone between CMe_2, $SiMe_2$, and S.[30] Changing this group subtly changes the natural bite-angle of the ligand and has been shown to impact the catalytic activity.[67] One derivative of *t*-Bu-xantphos in this position has been previously published with the CMe_2 replaced by a $C{=}CMe_2$.[117] Given the much larger bite-angle of the *t*-Bu-xantphos ligands the impact of small changes may be very different to those observed with the Ph-xantphos ligands. This chapter presents a study into the synthesis of *t*-Bu-sixantphos and *t*-Bu-thixantphos, and an alternative synthesis of *t*-Bu-xantphos, followed by calculation of their

natural bite-angles and the synthesis of some non-transition metal derivatives including phosphonium salts and phosphine selenides. The goal of this chapter is to investigate the steric and electronic properties of the three *t*-Bu-xantphos ligands to form the foundation of knowledge necessary to understand their coordination chemistry, which will be presented in later chapters.

2.1 Ligand Synthesis

In 2002 van Leeuwen *et al.* reported their unsuccessful attempts to synthesise *t*-Bu-xantphos from either the dilithiated xanthene backbone or starting with 9,9-dimethyl-4,5-bis(dichlorophosphino)xanthene, suggesting that steric crowding from the presence of two *tert*-butyl groups on a single phosphorus atom prevented the successful coupling.[73] However, in 2005 a synthesis of *t*-Bu-xantphos from 4,5-dilithio-9,9-(dimethyl)xanthene was reported.[84] This synthesis involves lithiation of the xanthene backbone using *n*-butyllithium and *N,N,N′,N′*-tetramethyl-ethane-1,2-diamine (TMEDA) in heptane, followed by addition of ClP^tBu_2 and heating at 60 °C for 24 hours, generating the product in 38% isolated yield (Scheme 2.1).

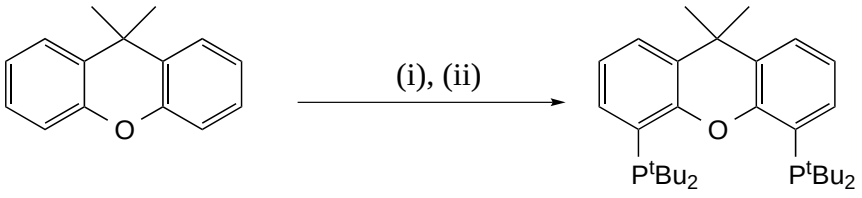

Scheme 2.1: Literature synthesis of *t*-Bu-xantphos in heptane.[84] *Reagents and conditions:* (i) *n*-BuLi, TMEDA, 15 h, heptane. (ii): ClP^tBu_2, 60 °C, 24 h.

Attempts to utilise the literature method for the synthesis of *t*-Bu-xantphos[84] to synthesise *t*-Bu-thixantphos resulted in a number of unidentifiable products. An alternative method using a potassium *tert*-butoxide/*n*-butyllithium "superbase" formed a mixture of products from which separation attempts were unsuccessful. This superbase mixture forms significant amounts of organopotassium compounds, which are more active metallating agents than their organolithium counterparts. However, organopotassium compounds are also more active in cleavage

of ethers.[118] Hence the mixture of products may result from cleavage of the ether or thioether bridges resulting in undesired compounds.

The syntheses of *t*-Bu-thixantphos, *t*-Bu-sixantphos and *t*-Bu-xantphos were successfully achieved by adaptation of the reported synthesis of the Ph-xantphos ligands.[30] This method involves the dilithiation of the backbone using *sec*-butyllithium and TMEDA, followed by reaction with chlorodi-*tert*-butyl phosphine (Scheme 2.2). Unlike the Ph-xantphos synthesis which is complete in 16 hours, the synthesis of the *tert*-butyl ligands required extended periods. The reactions were allowed to proceed until no further change was determined by NMR spectroscopy (typically seven days). NMR analysis of the crude reaction mixture showed the presence of both the mono and diphosphine. The diphosphine was isolated as white crystals by recrystallisation from *n*-propanol with yields of 14, 85 and 37% for *t*-Bu-sixantphos, *t*-Bu-thixantphos and *t*-Bu-xantphos respectively. The remaining *n*-propanol solution of the monophosphine could be reduced to dryness and then reused for a second lithiation and reaction with chlorodi-*tert*-butyl phosphine to produce more of the desired diphosphine.

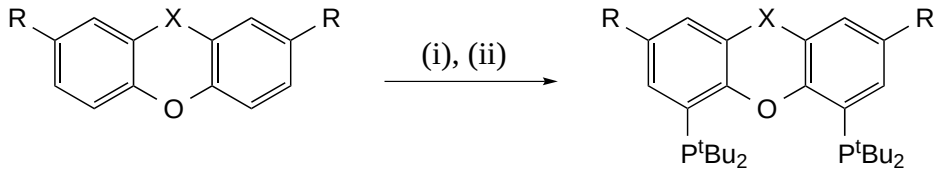

Scheme 2.2: Synthesis of *t*-Bu-xantphos (X = CMe_2, R = H), *t*-Bu-thixantphos (X = S, R = Me) and *t*-Bu-sixantphos (X = $SiMe_2$, R = H). *Reagents and conditions:* (i) *sec*-BuLi, Et_2O -78 °C → RT, 24 hours (ii) ClP^tBu_2, -78 °C → RT, 7 days.

The size of the *tert*-butyl groups leads to difficulties in the synthesis of the *t*-Bu-xantphos ligands. Reaction with one equivalent of chlorodi-*tert*-butyl phosphine to form the monophosphine is clean and rapid, occurring overnight. However, the steric hindrance of the monophosphine results in a much slower second addition, requiring extended reaction times to achieve significant conversion. When the reaction is allowed to proceed for longer than one week, no additional conversion is observed. This is likely due to degradation of either the lithiated monophosphine or the *sec*-butyllithium before the second lithiation can occur. Over extended periods organolithium reagents cleave diethyl ether resulting in

alkanes, alkenes, and lithium ethoxide (Scheme 2.3).[118,119] *sec*-Butyllithium has been shown to completely react with diethyl ether in one day.[119] Although the reaction between diethyl ether and phenyllithium is slower (half-time of 100 hours), the extended reaction periods required for the second phosphine addition mean that this degradation pathway may limit the yield of the diphosphine.

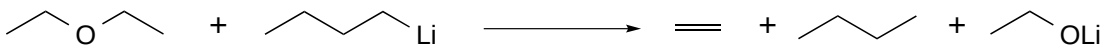

Scheme 2.3: Reaction of *n*-butyllithium with diethyl ether

In order to promote the dilithiation, three equivalents of a pre-formed *sec*-butyllithium/TMEDA complex was added to a solution of the backbone. An initial colour change to yellow (*t*-Bu-thixantphos and *t*-Bu-sixantphos) or green (*t*-Bu-xantphos) was observed, indicative of monolithiation. After stirring overnight this changed to red or yellow respectively. This colour change gives a clear indication of successful dilithiation. In order to favour the diphosphine over the monophosphine, the lithiated backbone was then added slowly to an ethereal solution of chloro-di-*t*-butylphosphine. Although a mixture of the mono and diphosphine was always obtained, this order of addition was found to be more successful, resulting in increased yields.

The synthesis of these ligands utilises directed *ortho* metallation as first described independently by Gilman and Wittig in 1939 and 1940 respectively.[120,121] Directed *ortho* metallation uses a heteroatom that can coordinate to the organolithium reagent, thereby directing it to the *ortho* sites. In the synthesis of the *t*-Bu-xantphos ligands the ether linkage can act as a director for the lithiation. Once lithiated, the electron density on the oxygen stabilises the lithiated site against degradation. For *t*-Bu-xantphos and *t*-Bu-sixantphos the oxygen is the only atom present with lone pairs of electrons and thus the lithiation occurs exclusively in the desired positions *ortho* to the oxygen. However, the precursor to *t*-Bu-thixantphos, phenoxathiin, contains both an ether and a thioether group, both of which can act as *ortho*-directors.[122] Previous research has shown that in the presence of both ether and thioether groups the lithiation will occur *ortho* to the oxygen.[123] Once the first lithiation has taken place the oxygen is less likely to contribute significantly to the second lithiation. For *t*-Bu-xantphos and *t*-Bu-sixantphos the influence of the oxygen is still sufficient for the second lithiation to occur

in the other *ortho* position. However, for phenoxathiin the thioether acts as a second directing group and the lithiation occurs *ortho* to the sulfur (Scheme 2.4). The addition of methyl groups in the positions *meta* to the thioether prevents the sulfur atom from acting as a director, resulting in the desired *t*-Bu-thixantphos ligand.

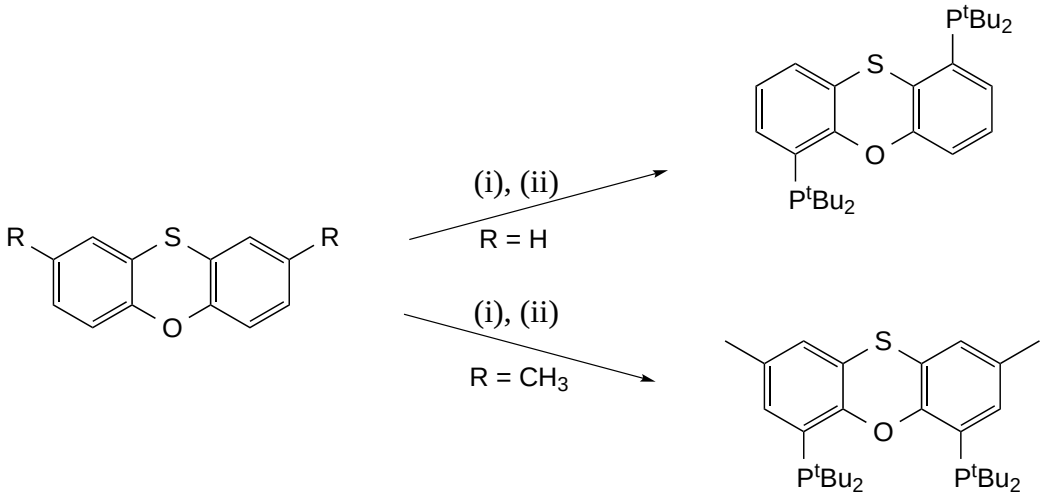

Scheme 2.4: Influence of methyl groups on the synthesis of *t*-Bu-thixantphos. *Reagents and conditions:* (i) *sec*-BuLi, Et_2O, 24 hours, (ii) ClP^tBu_2, 24 hours.

The *t*-Bu-xantphos ligand obtained using *sec*-butyllithium/TMEDA in diethyl ether had ^1H and ^{13}C NMR spectra consistent with the literature (Table 2.1).[84] However, the ^{31}P chemical shift differed by 2.2 ppm (10.2 ppm in this study compared to 12.4 ppm). The NMR spectra for the reported and the synthesised samples were both obtained in $CDCl_3$ and referenced to an external 85% H_3PO_4 standard. Hence the reason for this difference is unclear. However, as the remainder of the NMR and other characterisation data is consistent, it is likely that the two compounds are identical and a typographical error or otherwise was made in the preparation of the earlier paper.

The NMR data of the newly reported *t*-Bu-thixantphos and *t*-Bu-sixantphos ligands are consistent with expectations (Table 2.1). In both cases a plane of symmetry reduces the number of signals, showing a single peak in the ^{31}P NMR. The ^{31}P NMR chemical shifts for the *t*-Bu-sixantphos and *t*-Bu-thixantphos ligands are observed as singlets at 8.4 and 9.5 ppm respectively. The ^1H NMR signals for the

aromatic system are as expected, with two singlets present for *t*-Bu-thixantphos, and a doublet, a doublet of doublets and a virtual triplet observed for *t*-Bu-sixantphos and *t*-Bu-xantphos. The chemical shift of the backbone methyl substituents differs for each ligand, as expected. In *t*-Bu-sixantphos the dimethylsilyl group appears at 0.46 ppm, close to the tetramethylsilane reference. In *t*-Bu-xantphos the bridgehead methyls appear at 1.57 ppm, within the typical range for organic methyl groups. The methyl groups in *t*-Bu-thixantphos are evident at 2.25 ppm, consistent with methyl substituents attached to aryl rings.

Table 2.1: Selected NMR data for *t*-Bu-xantphos ligands in $CDCl_3$

	^{31}P	^{1}H				
Diphosphine	δ/**ppm**	δ ^{t}**Bu**/**ppm**	δ **Me**/**ppm**	δ **Ar**/**ppm**		
t-Bu-Xantphos[84]	12.4	1.21–1.26	1.57	7.02	7.38	7.60
t-Bu-Xantphos (this work)	10.2	1.21–1.25	1.57	7.03	7.38	7.60
t-Bu-Thixantphos	9.5	1.22–1.24	2.25	6.88	7.29	
t-Bu-Sixantphos	8.4	1.29	0.46	7.12	7.53	7.87

The ^{1}H NMR data for the *t*-Bu-xantphos ligands show a complex XAA'X' spin system for the *tert*-butyl protons. In a system where the two A atoms (in this case the phosphorus atoms) are strongly coupled, this leads to interaction between the three-bond and five-bond couplings (e.g. when the phosphorus atoms are in a *trans* configuration in a metal complex) resulting in a virtual triplet.[124] In the *t*-Bu-xantphos ligands there is no atom between the phosphorus atoms so we would expect a three-bond and a nine-bond coupling. A nine-bond coupling is an extremely remote coupling which we would expect to be negligible. Based on previous reports,[124,125] this peak shape with two sharp outer lines and a broad inner peak occurs when the difference between the short- and long-range couplings is very small but not zero. For this to occur the phosphines must have some degree of through-space spin-spin coupling through their lone pairs of electrons (for a review of non-bonded spin-spin coupling see Hierso[126]). This is further supported by the difference in the ^{1}H NMR spectra of the three ligands; the central peak is sharpest for *t*-Bu-sixantphos followed by *t*-Bu-thixantphos. For *t*-Bu-xantphos some further detail can be seen indicating that this has the weakest through-space coupling. This trend is consistent with the expected changes in the

distance between the phosphines upon varying the backbone, which will impact the degree of through-space coupling that can occur, and therefore the difference in the short and long-range coupling constants.

2.2 Bite-Angle Calculations

The steric and electronic properties of diphosphine ligands determine their complexation behaviour with transition metals and can influence the reactivity of the complexes, particularly impacting the activity and selectivity in catalytic transformations.[32,67] The xantphos class of ligands were initially investigated for their consistent electronic properties and steric bulk meaning that the impact of the bite-angle on rhodium catalysed hydroformylation could be studied exclusively.[30] Consequently, a number of studies have investigated the bite-angle impact on a variety of catalytic conversions (for examples see[66,67,127–129]). However, it has since been determined that the bite-angle is a result of both the steric and electronic properties of the ligand.[32]

The natural bite-angle (β_n) was first described by Casey and Whiteker[24] as a theoretically determined parameter to indicate the preferred chelation angle of diphosphine ligands irrespective of the metal they are coordinating to. These are determined computationally by optimising the geometry of a complex with a rhodium atom at 2.315 Å and measuring the resulting P-Rh-P angle. The crystallographic bite-angle for a given complex can be measured from the crystal structure. The original development of the natural bite-angle parameter included a comparison of the natural bite-angle for seven different ligands and crystallographic bite-angles for one transition metal complex of each ligand. The two bite-angles were found to be correlated in accordance with the equation $\Theta_{exp} = 0.98\beta_n + 2.13$ (R = 0.92).[24] Another study in 2009 showed that for a range of diphosphines the crystallographically determined bite-angles have a narrow range, which is close to the calculated natural bite-angle.[25] This study did not however, determine a correlation between the two.

Despite the ubiquity of the natural bite-angle within diphosphine chemistry, only two studies have investigated whether the natural bite-angle has proven to be an apt predictor of the crystallographically determined bite-angle.[24,25] One of these only used one complex for each ligand and the other did not calculate the math-

ematical relationship between the two. A large number of new crystal structures have also been reported since the studies were published in the 1990's.[68] In order to establish whether the natural bite-angle is still an apt predictor of the crystallographic bite-angle, almost 25 years after the original publication, the relationship between the two was investigated using data from the 2014 CSD.[68] The results are summarised in Table 2.2 and Figure 2.1. The median crystallographic bite-angle was used to decrease the influence of outliers on the results. The natural and experimental bite-angles show a good correlation described by the equation Θ_{exp} = 1.10 β_n- 5.70 (R^2 = 0.92). Some of the experimental and natural bite-angles that are most relevant to this work show significant differences (for example *t*-Bu-xantphos β_n = 140°, experimental = 153.317°, and Ph-sixantphos β_n = 109°, experimental = 99.165°). This may be due to the low numbers of structures available for these ligands (four and five respectively) at which point the metals used will have a significant impact.

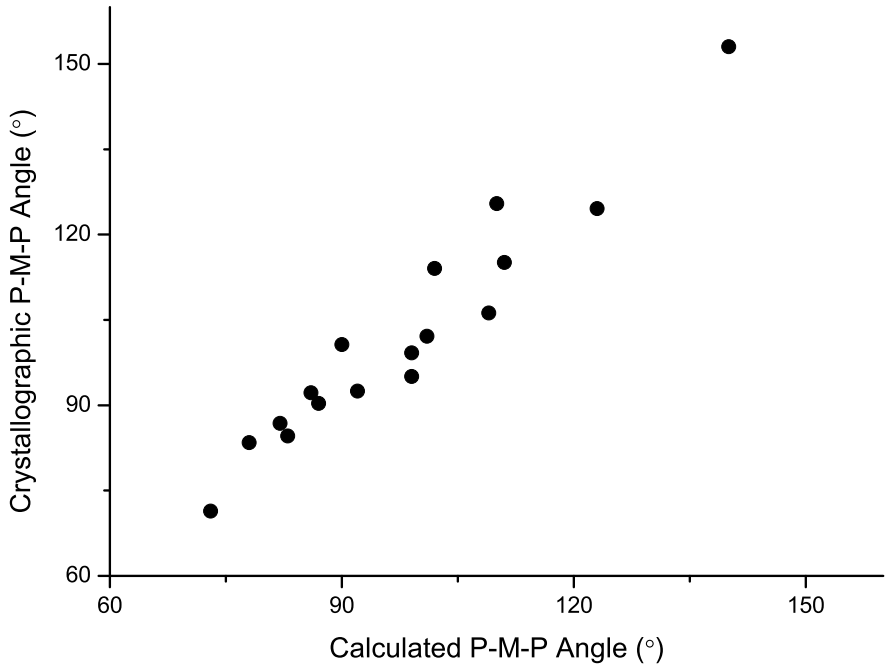

Figure 2.1: Comparison of the natural and crystallographic bite-angles. Trendline Θ_{exp} = 1.10 β_n- 5.70 (R^2 = 0.92).

Table 2.2: Crystallographic[68] and natural bite-angles[25,64,67,130] for diphosphine ligands.

Diphosphine	**Structures**	**P-P** /Å	**Range** /°	**Bite-Angle** /°	β_n /°
dppm	384	2.718	62.757–77.706	71.062	73
dppe	1939	3.095	71.073–92.926	83.818	78
dppp	3237	3.308	83.333–105.420	92.181	86
BINAP	146	3.296	85.9820–115.666	91.925	92
dppb	127	3.391	89.447–111.491	94.240	99
DPEphos	101	3.844	96.094–158.531	112.691	102
Ph-Xantphos	65	3.908	98.829–153.134	108.535	111
BISBI	4	4.079	103.533–151.951	124.789	123
Ph-Sixantphos	5	3.691	95.250–152.149	99.165	109
Ph-Thixantphos	3	4.021	109.528–155.050	111.724	110
t-Bu-xantphos	4	4.527	152.302–153.456	153.317	140
dpp-benzene	116	3.101	74.380–92.499	84.900	83
dppn	25	3.176	79.867–93.270	86.864	82
dppx	19	3.569	90.045–106.186	102.636	90
dbpe	109	3.200	83.989–95.949	90.369	87
dbpp	12	3.503	94.556–104.857	99.175	99
dbpx	10	3.634	98.758–107.255	101.881	101

In order to determine the potential differences between the *t*-Bu-xantphos and Ph-xantphos ligands, the natural bite-angles of the three *t*-Bu-xantphos ligands were calculated. Previously the *t*-Bu-xantphos bite-angle was calculated using molecular mechanics, however molecular mechanics has previously been reported as overestimating the bite-angles for diphosphines with bulky alkyl substituents, like the *tert*-butyl groups in the *t*-Bu-xantphos ligands.[25] As the bite-angles of the *t*-Bu-xantphos ligands are an integral part of the current study, DFT was utilised to reduce the likelihood of overestimation. The angles for the Ph-xantphos ligands were also calculated to allow for a comparison between the DFT and molecular mechanics methods. The structures were optimised using the B3LYP functional,[131–134] with the def2-TZVP basis set.[135,136] using a Rh-P distance of 2.315 Å. The resulting bite-angles along with those published using molecular mechanics are given in Table 2.3. The values calculated using DFT and molecular mechanics

are slightly larger for the Ph-xantphos ligands. The trend is consistent and molecular mechanics techniques can overestimate the impact of π-stacking in molecules with phenyl rings. The value for *t*-Bu-xantphos using DFT is much smaller than the literature value calculated with molecular mechanics. However, molecular mechanics is known to overestimate the bite-angles of bulky diphosphines which may account for this difference.[25]

Table 2.3: Natural bite-angles of xantphos ligands. Molecular mechanics values taken from the literature.[30]

Diphosphine	**Molecular Mechanics (°)**	**DFT (°)**
Ph-Sixantphos	108.7	111.89
Ph-Thixantphos	109.4	112.65
Ph-Xantphos	111.7	114.18
t-Bu-Sixantphos		126.80
t-Bu-Thixantphos		126.98
t-Bu-Xantphos	140	127.56

The natural bite-angles for the *t*-Bu-xantphos series of ligands are much larger than for the Ph-xantphos ligands. Given that the remainder of the ligands are unchanged, this effect is due to the impact of the *tert*-butyl groups. *Tert*-butyl groups are more electron-donating than the phenyl groups so the phosphorus atoms will have more electron density resulting in an electrostatic repulsion of the two phosphorus atoms. The *tert*-butyl groups also have a larger steric impact than the planar phenyl rings. This would result in a larger bite-angle as the steric bulk of the *tert*-butyl substituents pushes the two phosphorus atoms further apart. The trend between the two groups is the same with the CMe_2 bridged ligands having the largest bite-angles and the $SiMe_2$ bridged having the smallest. However, the range for the *t*-Bu-xantphos ligands (0.76°) is much smaller than for the Ph-xantphos ligands (2.3°). This suggests that the *tert*-butyl substituents are the main contributing factor to the bite-angle and the small changes in the bridging group have a smaller effect because the sterics of the *tert*-butyl groups dominates.

The bite-angles of the *t*-Bu-xantphos ligands are likely to have a significant impact on their coordination chemistry. The phenyl ligands form a range of com-

plexes favouring *cis*-chelation in square-planar and octahedral complexes, although *trans* square planar complexes have been reported.[115] With bite-angles of 126.8–127.6° the *t*-Bu-xantphos ligands may prefer bis-equatorial positions in trigonal bipyramidal complexes with angles close to 120°. However, the bite-angles are halfway between the *cis*- and *trans*-coordination angles for square-planar complexes, which may result in mixtures of products. Mixtures of *cis* and *trans* isomers have been reported for palladium Ph-xantphos complexes, so the ratio between the two geometries may favour *trans*-coordination for the *t*-Bu-xantphos ligands.[73,115] Diphosphine ligands that exhibit exclusive *trans*-chelation have been described in a review as "elusive".[137]

2.3 Basicity

Spectroscopic analysis of the *t*-Bu-xantphos ligands in $CDCl_3$ showed a small amount of an impurity, characterised by a new peak in the ^{31}P NMR spectra and an unusual spin system downfield of the aromatic signals in the ^{1}H NMR spectra. The amount of the impurity increased over time, suggesting that the ligands were reacting with the solvent. Chloroform is known to undergo slow degradation forming hydrochloric acid.[138] Tertiary phosphines can act as Brønsted bases, forming phosphonium ions that can be used as components in catalytic reactions.[139] Hence, the identity of these compounds as phosphonium salts seemed likely.

The three *t*-Bu-xantphos ligands react with the strong acids $HCPh(SO_2CF_3)_2$ (pK_a = 2.0 in DMSO) or $H_2C(SO_2CF_3)_2$ (pK_a = 2.4 in DMSO),[140] resulting in immediate formation of a phosphonium salt (Scheme 2.5). These acids are useful as they are non-hygroscopic solids allowing for accurate stoichiometry. Addition of excess acid results in the same product; no evidence for an additional protonation was observed. The NMR data is consistent with the data for the impurity observed in the synthesis of the *t*-Bu-xantphos ligands, indicating that the impurity is [(*t*-Bu-xantphos)H]$^+$.

Selected NMR data for the phosphonium salts [(*t*-Bu-xantphos)H]$CH(SO_2CF_3)_2$ with the three ligands is given in Table 2.4. A broad singlet is present in the ^{31}P NMR spectra for the three phosphonium ions, shifted slightly downfield from the

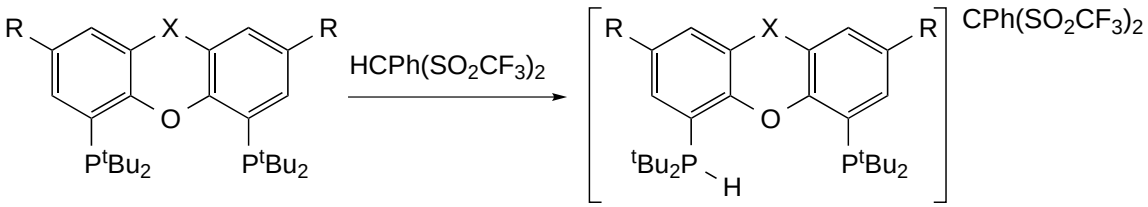

Scheme 2.5: Protonation of the ligands using a strong acid, in C_6D_6.

free ligand. The ^{1}H and ^{13}C NMR spectra show half the expected number of aromatic signals, and only one signal for the *tert*-butyl protons and the quaternary and terminal carbons. This indicates that although the expected complex is asymmetric the system is undergoing a dynamic process such that the two halves of the molecule are equivalent on the NMR timescale. The most likely process is the exchange of the proton between the two phosphorus atoms. The ^{1}H NMR spectra all show a complex spin system of the type XAA'X' for the phosphonium proton, which is further evidence for the dynamic exchange of the proton between the two phosphorus atoms.

Table 2.4: Selected NMR data for the [(*t*-Bu-xantphos)H]CH(SO$_2$CF$_3$)$_2$ compounds in $CDCl_3$ ($\Delta\delta = \delta_{[(\text{diphosphine})H]^+} - \delta_{\text{diphosphine}}$).

	^{31}P		^{1}H
Diphosphine	δ/**ppm**	$\Delta\delta$/**ppm**	**H$^+$**δ/**ppm**
t-Bu-Sixantphos	14.3	5.9	9.57
t-Bu-Thixantphos	15.8	6.3	8.99
t-Bu-Xantphos	17.4	7.2	8.57

The difference in the rate of exchange of the proton in the three compounds is clearly shown by their ^{31}P and ^{1}H NMR spectra. The ^{31}P NMR signal is sharpest for *t*-Bu-sixantphos followed by *t*-Bu-thixantphos while *t*-Bu-xantphos has a very broad signal. This indicates that the exchange is fastest for *t*-Bu-sixantphos and slowest for *t*-Bu-xantphos. The ^{1}H NMR spectra (Figure 2.2) show an XAA'X' spin system for the phosphonium proton. The signal appears most like a virtual triplet for *t*-Bu-sixantphos, implying very little difference in the coupling constants of the proton with each phosphorus. For *t*-Bu-thixantphos the central peak

has broadened slightly, while in *t*-Bu-xantphos the central peak is very broad, indicating that the difference in the two coupling constants is increasing. The chemical shift of the phosphonium proton is different for the three systems (*t*-Bu-sixantphos = 9.57, *t*-Bu-thixantphos = 8.99 and *t*-Bu-xantphos = 8.57 ppm). This indicates that the *t*-Bu-sixantphos proton is less shielded and thus has a faster rate of exchange, while the *t*-Bu-xantphos proton is the most shielded and has the slowest rate of exchange. This trend is consistent with the bite-angles of the ligands. *t*-Bu-Sixantphos has the smallest bite-angle, so the two phosphorus atoms are closer resulting in a lower barrier to exchange, whilst *t*-Bu-xantphos has the largest bite-angle and thus the slowest exchange.

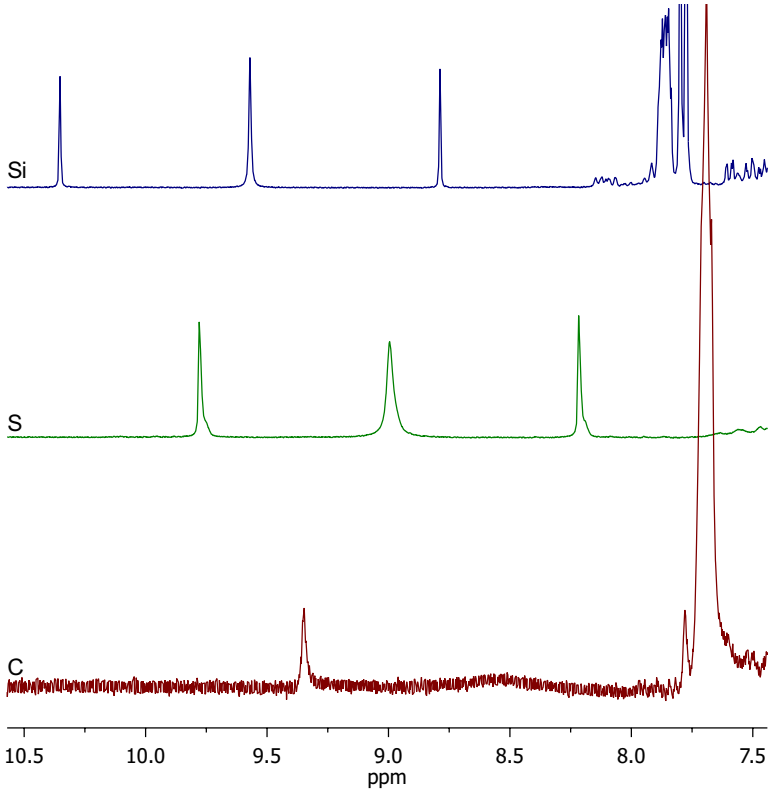

Figure 2.2: ^{1}H NMR spectra in $CDCl_3$ at 20 °C for [(*t*-Bu-sixantphos)H]$^+$, [(*t*-Bu-thixantphos)H]$^+$, and [(*t*-Bu-xantphos)H]$^+$ (Si, S and C respectively) showing the P-H region

The dynamic behaviour of the phosphonium ions was further investigated using variable temperature ^{31}P and ^{1}H NMR experiments on [(*t*-Bu-thixantphos)H]CH-$(SO_2CF_3)_2$ (Figure 2.3). At room temperature a single peak is present in the ^{31}P

NMR spectrum. When heated this peak shifts slightly to higher ppm and becomes sharper. This single peak indicates that the exchange of the proton between the two phosphorus atoms is occurring rapidly enough that the two phosphorus atoms appear to have the same environment on the NMR timescale. Cooling below room temperature causes the singlet to broaden significantly, with coalescence occurring around -40 °C. At -60 °C two broad signals are present. One of these signals resolves into a doublet at -80 °C, however the other peak is still very broad ranging from 11–23 ppm. Given that the protonation results in a downfield shift at room temperature, it is likely that the sharp doublet belongs to the unprotonated phosphorus and the broad peak is the protonated phosphorus.

The variable temperature ^{1}H NMR data for [(*t*-Bu-thixantphos)H]CH(SO_2CF_3)$_2$ (Figure 2.3) shows similar changes to the ^{31}P NMR spectra. At low temperature the proton is static on a single phosphorus atom so we observe a large doublet due to coupling with the phosphorus. As the temperature increases to -20 °C, a broad signal begins to appear in the centre of the doublet as exchange begins to occur and the signal changes from a simple doublet to a XAA'X' spin system. The intensity of the central peak increases and at 20 °C all three peaks begin to broaden again with coalescence at 50 °C. This broadening may be the result of the proton no longer being isolated on a single molecule but delocalised across the entire system.

Typically ^{31}P NMR spectra are proton decoupled. However, with very strongly coupled systems such as phosphonium ions the decoupler is not able to fully decouple the spin system, resulting in broadening and side bands. To further investigate the [(*t*-Bu-thixantphos)H]CH(SO_2CF_3)$_2$ system, proton-coupled phosphorus NMR spectra were obtained at room temperature and -80 °C (Figure 2.4). At room temperature a simple doublet appears, indicating rapid movement of the proton between the two phosphorus atoms thus coupling with both. When cooled to -80 °C, the ^{31}P$\{^{1}$H$\}$ spectrum showed a doublet and a broad singlet. In the proton-coupled phosphorus spectrum, the doublet is retained with a phosphorus-phosphorus coupling constant of 136.9 Hz confirming that this signal is for the non-protonated phosphorus which couples to the protonated phosphorus atom. The broad singlet resolves into a doublet of doublets with coupling constants of 481.5 and 136.9 Hz consistent with coupling to the proton and the other phosphorus. This further confirms that no exchange of the proton is occurring at

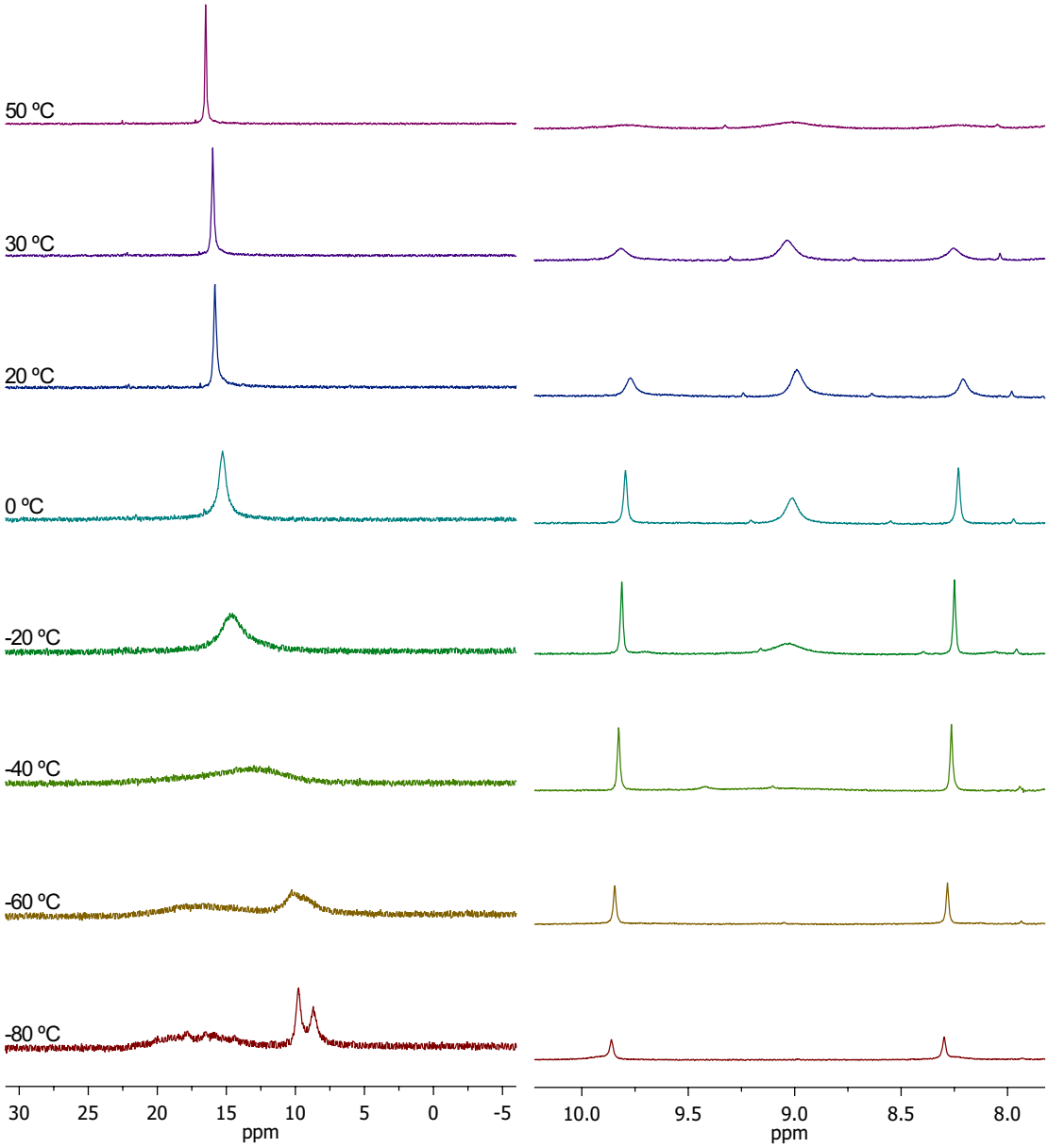

Figure 2.3: Variable temperature ^{31}P (left) and ^{1}H (right) NMR data for [(*t*-Bu-thixantphos)H]CH$(SO_2CF_3)_2$ in CD_2Cl_2.

low temperature.

Single colourless crystals of [*t*-Bu-thixantphos(H)]CPh$(SO_2CF_3)_2$ suitable for X-ray diffraction were grown from the reaction mixture in benzene. The compound crystallised with a benzene solvate, as 2[*t*-Bu-thixantphos(H)]CPh$(SO_2CF_3)_2 \cdot C_6D_6$ in the monoclinic space group $P2_1/n$. Selected bond lengths and angles are summarised in Table 2.5, and crystallographic data is given in Table 2.6. Although

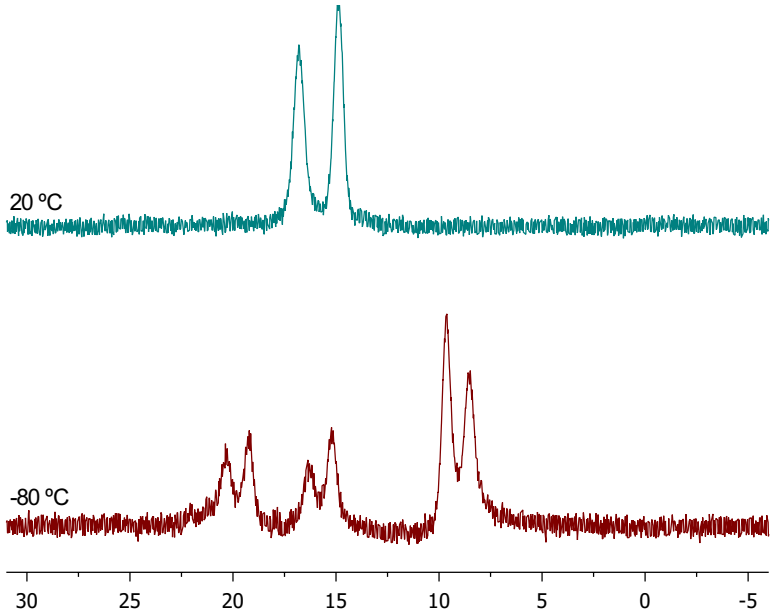

Figure 2.4: Variable-temperature proton coupled ^{31}P NMR data for [(*t*-Bu-thixantphos)H]$^+$ in CD_2Cl_2.

the cationic portion was well refined, one of the counterions is disordered with two positions for the SO_2CF_3 groups. The proton on the phosphonium ion is exclusively located on a single phosphorus atom. As a result the estimated standard deviation (esd) on the bond lengths and angles involving this proton are relatively high. The distances from the proton to the other phosphorus or to the oxygen atom are both too long to indicate any degree of interaction. The crystal structure was collected at 284.87 K, and based on the variable temperature NMR data significant exchange of the proton is expected at this temperature. However, this is not apparent in the X-ray structure suggesting that the exchange does not occur in the solid state.

2.4 Selenides

The electronic properties of phosphine ligands can be investigated in a number of different ways. The most well-known quantification is the Tolman electronic parameter.[14] This involves the measurement of the carbonyl stretching frequency in a $[Ni(CO)_3L]$ complex. Related approaches use $[Mo(CO)_5L]$ or $[Rh(CO)ClL_2]$

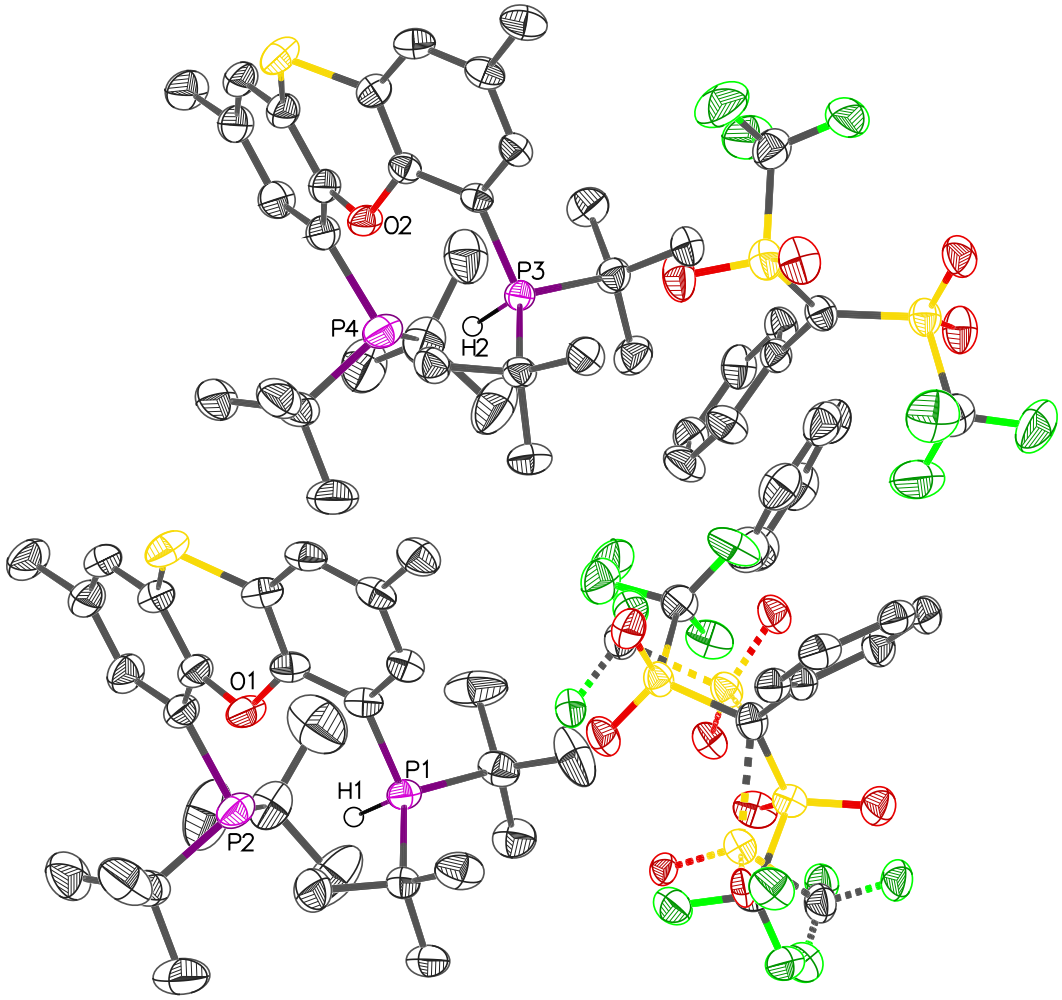

Figure 2.5: X-ray crystal structure of 2[(*t*-Bu-thixantphos)H]CPh(SO_2CF_3)$_2$· C_6D_6 (50% probability thermal ellipsoids). Selected hydrogen atoms omitted for clarity.

Table 2.5: Selected bond distances (Å) and angles (°) of 2[(*t*-Bu-thixantphos)-H]CPh$(SO_2CF_3)_2 \cdot C_6D_6$.

Bond distances (Å)		**Bond angles (°)**	
P1-H1	1.22(3)	P1-H1...P2	160(2)
P2...H1	2.96(3)	P1...O1...P2	89.19(6)
P1...P2	4.1290(11)	P3-H2...P4	154(2)
O1...H1	2.44(3)	P3...O2...P4	86.40(5)
P3-H2	1.22(3)	Ring 1...Ring 2	18.28(10)
P4...H2	2.91(3)	Ring 3...Ring 4	26.67(10)
P3...P4	4.0372(11)		
O2...H2	2.43(3)		

complexes.[9,11] The value of the phosphorus-metal coupling constants in platinum or rhodium complexes have also been used to quantify the electronic properties of phosphine ligands.[9,11,12,16] The values of the carbonyl stretching frequency and the phosphorus-metal coupling constants are dependent on the geometries of the metal complexes and these can be influenced significantly by steric properties, such as those imposed by large diphosphine ligands. The $^1J_{PSe}$ spin-spin coupling constants of phosphine selenides are a convenient and accurate measure of the electronic properties of tertiary phosphines.[17,141,142] In this case the more electron donating the phosphorus substituents are, the lower the resulting $^1J_{PSe}$.

The phosphine selenides are air-stable solids that are generally relatively straightforward to synthesise by reaction of the phosphine with either elemental selenium or potassium selenocyanide (with or without heating).[17,143] The value of $^1J_{PSe}$, as with all coupling constants, is governed by interactions between the s-orbitals. According to Bent's rule "atomic s-character concentrates in orbitals directed towards electropositive substituents".[144] Thus the greater the value of $^1J_{PSe}$ the more s-character is present in the P-Se bond, indicating a greater degree of electronegative substituents, and thus the less electron donating the phosphine ligand will be.

In addition to the use of $^1J_{PSe}$ as a measure of the electronic influence of a phosphine, it can also be used to measure the Brønsted basicity of a given phosphine.

Table 2.6: Crystallographic data and structure refinement of 2[*t*-Bu-thixantphos(H)]CPh(SO_2CF_3)$_2$·C_6D_6

Empirical formula	**$C_{84}H_{110}F_{12}O_{10}P_4S_6$**
Formula weight	1823.95
Temperature/K	284.87(10)
Crystal system	monoclinic
Space group	$P2_1/n$
a/Å	14.19615(12)
b/Å	39.4563(3)
c/Å	16.35832(15)
$\alpha/^\circ$	90
$\beta/^\circ$	100.1751(8)
$\gamma/^\circ$	90
Volume/Å^3	9018.64(13)
Z	4
ρ_{calc} mg/mm^3	1.343
µ/mm	2.749
F(000)	3832.0
Crystal size/mm	0.49 x 0.16 x 0.14
Radiation	CuKα (λ = 1.54184)
2θ range for data collection	5.928 to 147.832°
Index ranges	-17 $\leq$ h $\leq$ 17, -48 $\leq$ k $\leq$ 48, -20 $\leq$ l $\leq$ 20
Reflections collected	69203
Independent reflections	17960 [R_{int} = 0.0261, R_{sigma} = 0.0219]
Data/restraints/parameters	17960/291/1221
Goodness-of-fit on F^2	1.068
Final R indexes [I>=2σ (I)]	R_1 = 0.0549, wR_2 = 0.1473
Final R indexes [all data]	R_1 = 0.0623, wR_2 = 0.1531
Largest diff. peak/hole / e Å^{-3}	1.11/-0.56

A correlation between the experimentally measured pK_b and the $^1J_{PSe}$ value has been reported with linear regression: $^1J_{PSe}$ = 7.60 × pK_b + 646 (R^2 = 0.9492).[17] As such, determining the value of $^1J_{PSe}$ allows for calculation of the pK_b and has shown good agreement with the experimentally determined data. One limitation of this method is the impact that sterically bulky groups can have. For P^tBu_3 the correlation suggests a pK_b value of 6.0 however the experimentally determined value is 2.60.[17] This is the result of the *tert*-butyl groups increasing the C-P-C angles, thus decreasing the s-character of the lone pair of electrons.

The *t*-Bu-xantphos ligands showed significant resistance to selenation. Reaction directly with elemental selenium has been reported as preferable to potassium selenocyanide as the latter reacts slowly and gives lower yields.[17] The previously reported Ph-xantphos diselenide was synthesised by refluxing Ph-xantphos and red selenium in toluene overnight resulting in diselenation.[145] Attempting this method with the *t*-Bu-xantphos ligands reported here showed little reaction. Attempts were also made using KSeCN similar to those previously reported,[143] however these were also unsuccessful. Successful monoselenation was obtained by refluxing the ligands with a large excess of grey selenium in toluene for three days (Scheme 2.6). Extending the reaction period did not result in the formation of any diselenide. This is likely due to the steric restraints of these ligands.

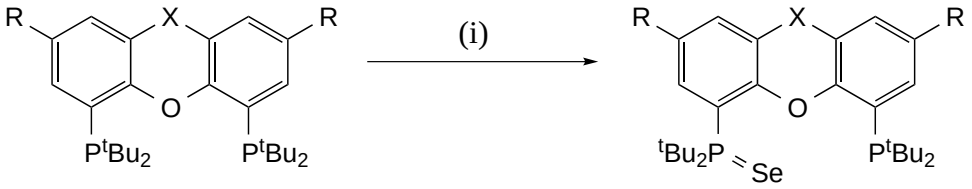

Scheme 2.6: Selenation of *t*-Bu-xantphos ligands, (X = CMe_2, R = H), *t*-Bu-thixantphos (X = S, R = Me) and *t*-Bu-sixantphos (X = $SiMe_2$, R = H). *Reagents and conditions:* (i) Se, reflux, toluene, 3 days.

The cleanest reaction was observed between *t*-Bu-xantphos and selenium, with a single asymmetric product observed. For *t*-Bu-thixantphos and *t*-Bu-sixantphos a single major product was observed, also consistent with monoselenation. Selected NMR data for the selenides is given in Table 2.7. The ^{31}P NMR spectra each show two peaks in a 1:1 ratio. One peak is shifted only slightly (0.4–7.5 ppm) from the starting material while the other peak is shifted significantly (91.7–

94.3 ppm) upfield. The asymmetry and the change in chemical shift of only one of the ^{31}P NMR signals indicates the formation of the monoselenide. The $^{1}J_{PSe}$ values are similar for the three ligands with a range of 12 Hz. The monoselenated *t*-Bu-thixantphos derivative was found to have $^{1}J_{PSe}$ = 698.5 Hz, while the monoselenated *t*-Bu-xantphos has $^{1}J_{PSe}$ = 696.3 Hz. These are much lower than that reported for Ph-xantphos selenide (749 Hz).[145] This lower coupling constant is expected as *tert*-butyl groups are more electron donating than phenyl substituents.

Using the correlation reported by Beckmann *et al.,* it is possible to convert the values of $^{1}J_{PSe}$ for the *t*-Bu-xantphos selenides and the previously reported Ph-xantphos diselenide into pK_b values.[145] The pK_b values for the *t*-Bu-xantphos ligands range between 5.67 and 6.90 which fall between the $PPhMe_2$ and PMe_3.[17] This is consistent with expectations as *tert*-butyl groups are more electron donating than methyl groups while the phenyl still results in a higher pK_b than those for the trialkyl phosphines. The pK_b value for Ph-xantphos is 13.55, indicating that the *t*-Bu-xantphos ligands are significantly more basic. This significant difference is expected as tert-butyl groups are strongly electron donating whilst phenyl substituents are electron withdrawing.[8] This effect will dominate any other subtle effects that may arise due to bite-angle or steric considerations.

The bite-angle may play a role in the value for the $^{1}J_{PSe}$ coupling constant as monoselenide diphosphines have shown through space coupling to the other phosphorus.[126] This would result in a lower $^{1}J_{PSe}$ value than otherwise expected and the effect would be more pronounced with smaller bite-angles. In this case *t*-Bu-sixantphos has the lowest pK_b of the three ligands and also the smallest bite-angle, so a bite-angle effect may be present. However, the differences cannot be purely the result of the bite-angle as *t*-Bu-thixantphos has the largest $^{1}J_{PSe}$ value but *t*-Bu-xantphos has the largest bite-angle.

In addition to the influence of the bite-angle on the $^{1}J_{PSe}$ coupling constant there must exist another electronic effect contributing to the difference between the ligands. Both *t*-Bu-thixantphos and *t*-Bu-xantphos groups have an *ortho* ether and a *meta* alkyl group, in addition *t*-Bu-thixantphos has the thioether bridge. Thioethers are electron donating by resonance, but being in the *meta* position to the phosphorus the negative charge that could be generated is unable to interact with the phosphorus atom. With sulfur being slightly more electronegative

Table 2.7: Selected ^{31}P NMR data for *t*-Bu-xantphos selenides in 1:1 $CDCl_3$:CD_2Cl_2 ($\Delta\delta = \delta_{\text{phosphine selenide}} - \delta_{\text{diphosphine}}$).

	P		**P=Se**			
Diphosphine	δ/**ppm**	$\Delta\delta$/**ppm**	δ/**ppm**	$\Delta\delta$/**ppm**	$^{1}J_{PSe}$/**Hz**	pK_b
t-Bu-Sixantphos	15.9	7.5	102.7	94.3	689.1	5.67
t-Bu-Thixantphos	11.7	2.2	103.7	94.2	698.5	6.90
t-Bu-Xantphos	10.6	0.4	101.9	91.7	697.1	6.72

than carbon, a thioether is also slightly inductively electron withdrawing, which would result in the phosphorus being very slightly less basic in the case of *t*-Bu-thixantphos when compared to *t*-Bu-xantphos.

2.5 Summary

Two new *t*-Bu-xantphos ligands, *t*-Bu-sixantphos and *t*-Bu-thixantphos have been synthesised and an alternate synthesis of *t*-Bu-xantphos has been reported by lithiation of the appropriate backbone using *sec*-butyllithium with TMEDA and treatment with P^tBu_2Cl. Although this method requires long reactions times the only by-product is the mono-phosphine which can undergo the same process again to generate higher yields. NMR analysis of the three ligands showed a XAA'X' spin system for the *tert*-butyl protons, suggestive of through-space coupling of the two phosphorus atoms.

Natural bite-angles of 126.80, 126.98, and 127.56° were calculated using DFT for the *t*-Bu-sixantphos, *t*-Bu-thixantphos, and *t*-Bu-xantphos respectively. For comparative purposes the bite-angles for the Ph-xantphos ligands were also calculated: Ph-sixantphos (111.89°), Ph-thixantphos (112.65°), and Ph-xantphos (114.18°). The values for the Ph-xantphos ligands are slightly larger than those calculated using molecular mechanics, though the value for *t*-Bu-xantphos is lower than the previously reported value (140°) calculated with molecular mechanics. This is likely due to the molecular mechanics value overestimating the steric impact of the *tert*-butyl substituents. A comparison of the natural and median crystallographic bite-angles for a range of different diphosphine ligands showed a good correlation between the two, indicating that the natural bite-angles can be excellent predictors of coordination behaviour.

The three *t*-Bu-xantphos ligands react rapidly with one equivalent of acid to generate [(*t*-Bu-xantphos)H]$CH(SO_3CF_3)_2$. The proton moves between the two phosphorus atoms in room temperature solutions. This process was investigated using proton-coupled ^{31}P NMR spectroscopy and low temperature ^1H and ^{31}P NMR spectroscopy, revealing that the proton is isolated on a single phosphorus below -40 °C. The X-ray crystal structure of [(*t*-Bu-thixantphos)H]$CPh(SO_3CF_3)_2$ was obtained, and the phosphonium proton was able to be located: isolated on a single phosphorus.

The electronic properties of the *t*-Bu-xantphos ligands were investigated by the synthesis of phosphine selenides. In all cases the monoselenide formed with no evidence for a diselenide. The values of $^{1}J_{PSe}$ ranged from 689.1–698.5 Hz, which were converted into pK_b values of 5.67–6.90. These fall between the values of PPh_2Me and PMe_3 which is consistent with the strong electron donation from the *tert*-butyl substituents and the electron withdrawing nature of the aryl backbone. The pK_b value for Ph-xantphos is 13.55 showing the difference in the electronic properties of the *t*-Bu-xantphos ligands.

Overall this chapter provides an interesting introduction into the chemistry of the *t*-Bu-xantphos ligands and suggests that the coordination chemistry may be different to that of the Ph-xantphos ligands as a result of the much larger natural bite-angles and more electron-rich phosphorus atoms.

Chapter 3

Coordination Complexes with Silver

Silver is a precious metal that has been used in coins, jewellery and other ornamentation at least since 4000 B.C. Silver salts have a wide range of applications, such as photographic film, wound dressings, and water storage tanks.[146] Silver coordination complexes are also biologically active: bis-diphosphine silver complexes show anti-tumour and anti-fungal activity.[147,148] Metallic silver is used industrially as a catalyst for the conversion of ethene to ethylene glycol, and silver salts are occasionally used as co-catalysts in cross-coupling reactions.[149] Complexes of silver have been used as catalysts in a number of transformations, including Si-H activation,[150] asymmetric aldol conversions[151] and allylation of benzaldehyde.[56,152]

Silver coordination chemistry is interesting due to the wide range of different geometries available to the metal, resulting in a high degree of geometrical flexibility. The bite-angle, electronic influence of the diphosphine, and the coordination mode of any ancillary ligands can all impact the type of complex formed. Possible structures formed for an equimolar reaction of a silver salt with a diphosphine range from the straightforward monometallic complex, to multimetallic clusters with bridging diphosphines (Figure 3.1). For a detailed overview of silver coordination chemistry see Meijboom *et al.*[111]

Silver complexes with xantphos ligands have been reported previously.[56,153] In all cases the complexes are monometallic, and the majority of these structures

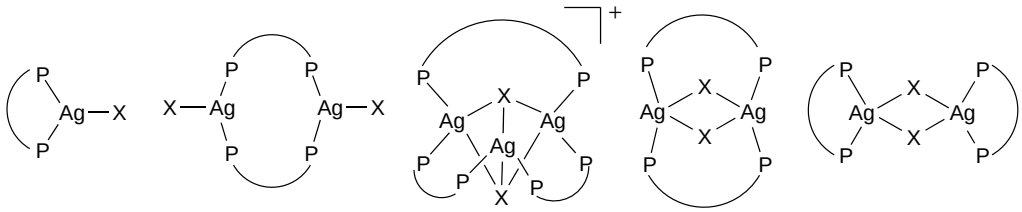

Figure 3.1: Possible structures for 1:1 silver diphosphine complexes, reproduced from Meijboom *et al.*[111]

are tetrahedral complexes of the type $[Ag(xantphos)(NN)]^+$ where NN represents a bidentate nitrogen ligand such as 2,2′-bipyridine. These $[Ag(xantphos)(NN)]^+$ complexes have been patented for their luminescent properties.[154–156] Other tetrahedral complexes with Ph-xantphos include a chelating ligand or two monodentate ligands (Figure 3.2). Only one trigonal silver Ph-xantphos complex has been reported (Figure 3.2c).[157] However, this is likely due to a lack of research rather than synthetic difficulties, as trigonal silver complexes with a chiral xantphos derivative have also been reported.[56]

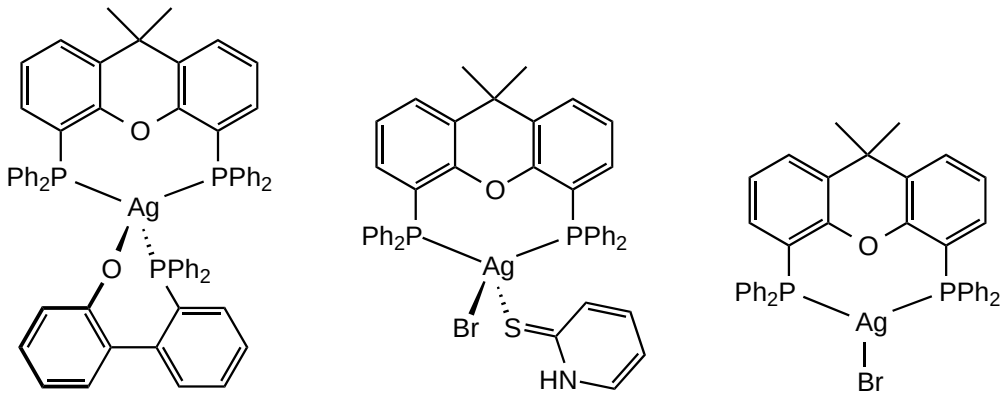

Figure 3.2: Tetrahedral and trigonal silver Ph-xantphos complexes.

Crystal structures of [AgBr(Ph-xantphos)] (Figure 3.3) and [AgBr(Ph-xantphos)(S-pyH)] (py = 2-pyridyl, Figure 3.4) have been reported.[157] In the trigonal structure the P-Ag-P angle is 109.38(7)° which increases to 111.507(17)° for [AgBr(Ph-xantphos)(S-pyH)]. The natural bite-angle for Ph-xantphos (111.7°)[67] is very close to the observed bite-angle. 2-Thiopyridine can act as a bidentate chelating ligand, however in this case the thione tautomer is formed and monodentate coordina-

tion through the sulfur is observed. In order for the 2-thiopyridine to chelate, the P-Ag-P angle would need to decrease significantly. In this instance the rigidity and steric bulk of Ph-xantphos prevents this from happening.[157]

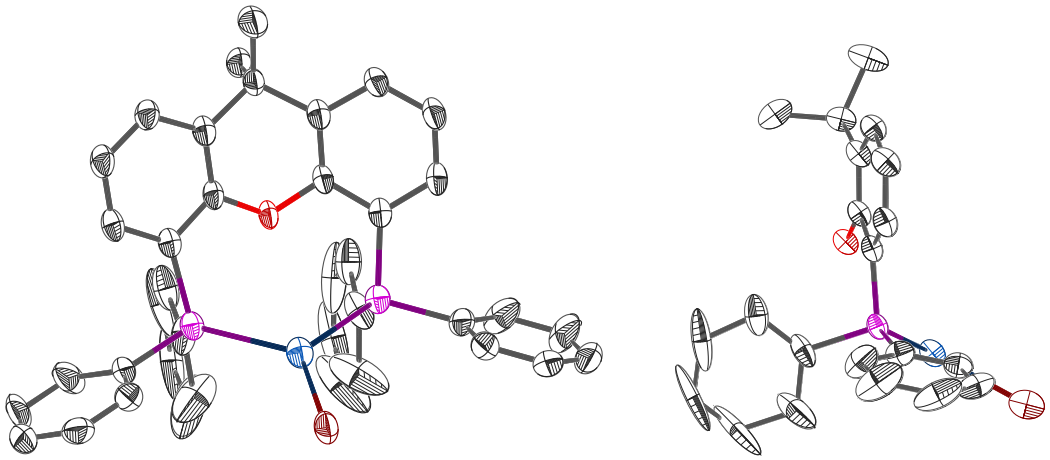

(a) (b)

Figure 3.3: X-ray crystal structure of [AgBr(Ph-xantphos)] showing the front (a) and side (b).[157] Hydrogen atoms omitted for clarity.

Silver is an excellent metal for investigating the coordination chemistry of xantphos ligands because it forms a wide range of different coordination geometries and has been shown to coordinate Ph-xantphos close to its natural bite-angle.[157] There are also a number of potential applications for silver complexes, such as catalysis, biological activity, and luminescent membranes. Silver is also especially suitable for study using ^{1}H, ^{13}C, and ^{31}P NMR spectroscopy as it consists of two stable spin $^{1}/_{2}$ isotopes, ^{107}Ag and ^{109}Ag, with natural abundances of 51.839 and 48.161% respectively. This allows further information to be obtained from the value of the silver-atom coupling constants. This chapter presents a study of the reactivity of the *t*-Bu-sixantphos, *t*-Bu-thixantphos, and *t*-Bu-xantphos ligands with two silver precursors: silver chloride and silver tetrafluoroborate.

3.1 Silver Chloride Complexes

Silver chloride complexes were synthesised by addition of each of the *t*-Bu-xantphos ligands to a suspension of silver chloride in $CDCl_3$ (Scheme 3.1), resulting in

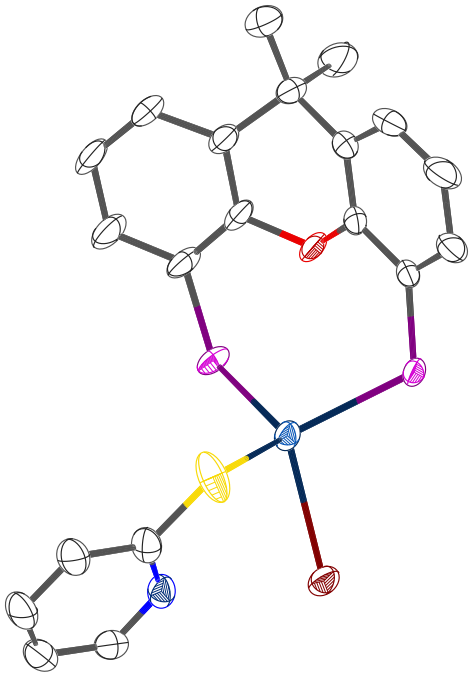

Figure 3.4: X-ray crystal structure of [Ag(Ph-xantphos)(HpyS)Br].[157] Phenyl rings and hydrogen atom omitted for clarity.

[AgCl(diphosphine)] complexes. In all cases, electrospray ionisation – mass spectrometry showed a clear peak for $[M-Cl]^+$ with no peaks observed for dimers or higher oligomers. The ^{31}P NMR spectra (see Figure 3.5 for an example) showed the expected pair of doublets in all cases, as summarised in Table 3.1. No relationship was observed between the natural bite-angle and the values of $^1J_{AgP}$. However, the change in the phosphorus chemical shift upon coordination ($\Delta\delta$) increases with decreasing bite-angle. This indicates that the decrease in shielding is larger for smaller bite-angles.

The ^1H NMR spectra for the [Ag(*t*-Bu-xantphos)Cl] complexes show half the expected number of aromatic signals, and one signal for the methyl groups and another for the *tert*-butyl substituents, indicating a complex with planes of symmetry in line with the backbone and perpendicular to it, running through the bridging atoms and the silver (representative spectrum for [Ag(*t*-Bu-sixantphos)Cl], Figure 3.5). The *tert*-butyl protons appear as a second order multiplet of the

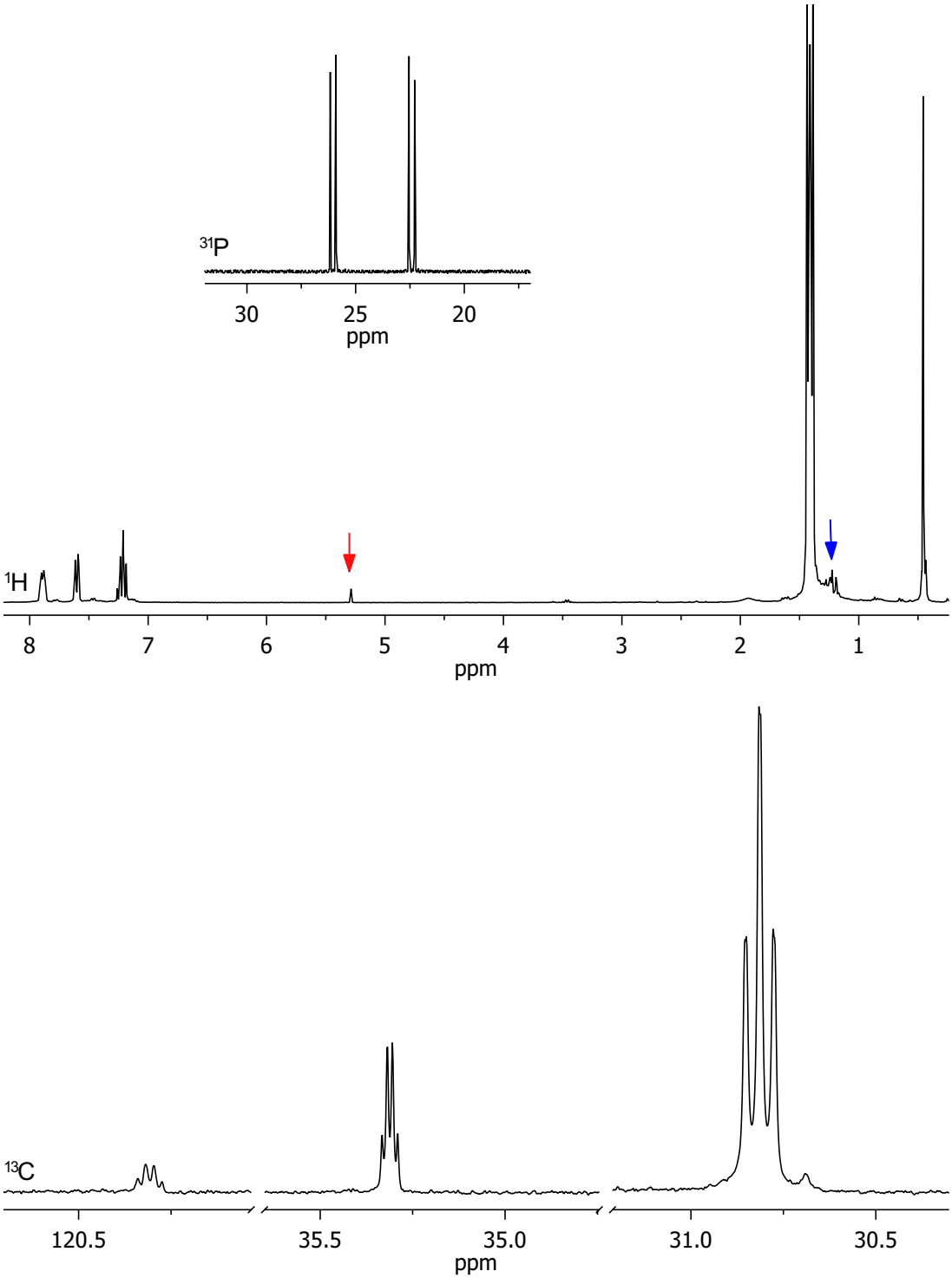

Figure 3.5: ^{31}P, ^{1}H and ^{13}C NMR spectra of [Ag(*t*-Bu-sixantphos)Cl] in $CDCl_3$. Arrows indicate impurities, CH_2Cl_2 indicated in red.

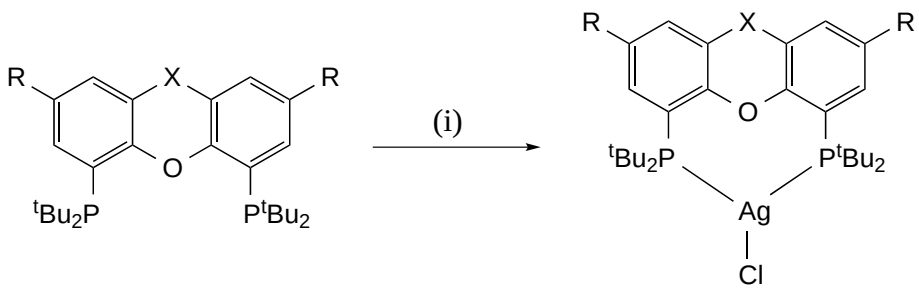

Scheme 3.1: Synthesis of [Ag(*t*-Bu-xantphos)Cl] complexes. *Reagents and conditions:* (i) AgCl, $CDCl_3$.

Table 3.1: Selected ^{31}P NMR data of [Ag(*t*-Bu-xantphos)Cl] complexes in $CDCl_3$ ($\Delta\delta = \delta_{\text{complex}} - \delta_{\text{free ligand}}$).

Compound	$\delta^{\mathbf{31}}\mathbf{P}/\mathbf{ppm}$	$\Delta\delta/\mathbf{ppm}$	$^{1}\boldsymbol{J}_{^{107}\mathbf{AgP}}/\mathbf{Hz}$	$^{1}\boldsymbol{J}_{^{109}\mathbf{AgP}}/\mathbf{Hz}$
t-Bu-Sixantphos	24.2	15.8	408.1	471.1
t-Bu-Thixantphos	21.8	12.3	406.7	469.6
t-Bu-Xantphos	20.7	10.5	409.3	472.2

$X_{18}AA'X_{18}'$ type, similar to the free ligand. The ^{13}C NMR spectra of the three complexes display some very distinctive signals (representative example, [Ag(*t*-Bu-sixantphos)Cl], Figure 3.5, bottom). The *ipso* phosphorus carbon on the aryl ring and the quaternary *tert*-butyl carbon appear as apparent quartets, while the signal for the terminal *tert*-butyl carbons is an apparent triplet of doublets. For each of these signals we would expect a doublet of virtual triplets or virtual triplet of doublets for each of the silver isotopologues. Owing to this complex spin system, values for the individual coupling constants were unable to be determined. The spectroscopic data for the three [Ag(*t*-Bu-xantphos)Cl] complexes show significant similarities, with no major discrepancies, indicating that all three complexes have the same overall geometries with only subtle differences.

Colourless crystals of [Ag(*t*-Bu-thixantphos)Cl] suitable for single-crystal X-ray diffraction were obtained by inwards diffusion of Et_2O into a CH_2Cl_2 solution of the complex. The crystal structure is shown in Figure 3.6, confirming the proposed monomeric trigonal structure. Selected bond lengths and angles, and crystallographic data are given in Tables 3.2 and 3.3 respectively. The [Ag(*t*-

Bu-thixantphos)Cl] complex crystallised in the $P2_1$ space group, while the similar complex [AgBr(Ph-xantphos)] crystallised in the higher symmetry $P2_1/m$ space group.[157] The P-Ag-P angle of 130.50(7)° is larger than the bite-angle for [AgBr(Ph-xantphos)] (109.37(1)°). However, both of these angles are very close to the natural bite-angle of their xantphos ligand. The natural bite-angle of *t*-Bu-thixantphos and Ph-xantphos were calculated to be 126.98° and 114.18° respectively (Section 2.2). This indicates that the natural bite-angle is a significant factor in determining the resulting P-Ag-P angle in these complexes. The silver oxygen distance of 3.007(6) Å indicates there no interaction between these atoms.

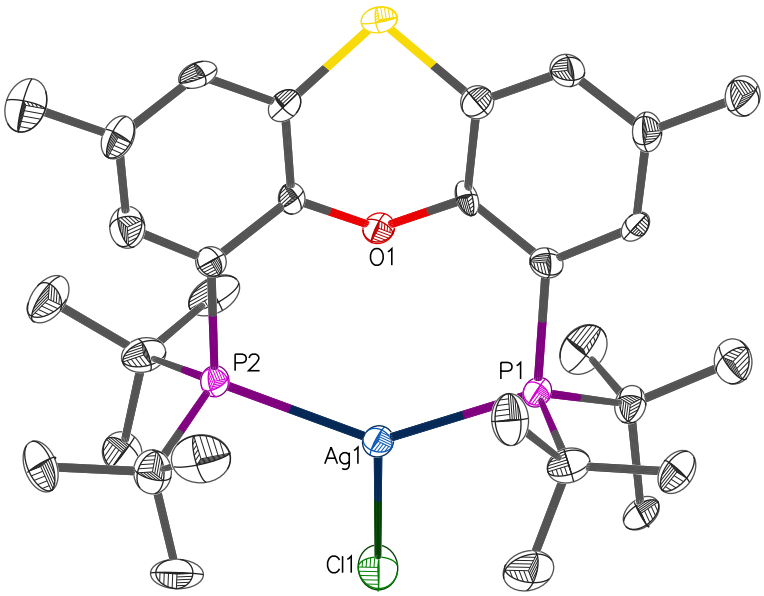

Figure 3.6: X-ray crystal structure of [Ag(*t*-Bu-thixantphos)Cl] (50% probability thermal ellipsoids). Hydrogen atoms omitted for clarity.

A side view of [Ag(*t*-Bu-thixantphos)Cl] given in Figure 3.7 shows the P-Ag-Cl angle relative to the ligand backbone. The chloride is not centred, with a difference in the P-Ag-Cl angles of 3.49°. This difference is likely the result of the backbone twisting with the chloride occupying the least sterically hindered site. The backbone is bent, resulting in two distinct faces of the molecule. In [Ag(*t*-Bu-thixantphos)Cl] the chloride sits on the convex face of the ligand while in [AgBr(Ph-xantphos)] (Figure 3.3) the bromide ligand occupies the concave

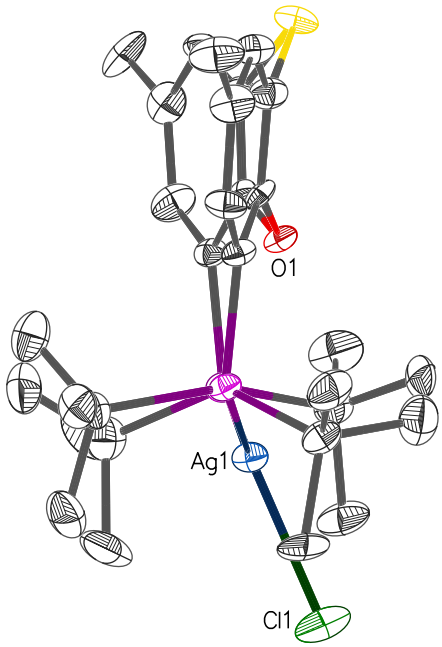

Figure 3.7: X-ray crystal structure of [Ag(*t*-Bu-thixantphos)Cl], side view (50% probability thermal ellipsoids). Hydrogen atoms omitted for clarity.

Table 3.2: Selected bond distances (Å) and angles (°) of [Ag(*t*-Bu-thixantphos)Cl].

Bond distances (Å)		**Bond angles (°)**	
P1...P2	4.416(3)	P1-Ag1-P2	130.50(7)
P1-Ag	2.430(2)	P1-Ag1-Cl1	116.46(8)
P2-Ag	2.433(2)	P2-Ag1-Cl1	112.95(8)
Ag...O1	3.007(6)	Aryl ring 1...Aryl ring 2	35.7(3)
Ag-Cl1	2.491(2)		

Table 3.3: Crystallographic data and structure refinement for [Ag(*t*-Bu-thixantphos)Cl]

Empirical formula	**$C_{30}H_{46}AgClOP_2S$**
Formula weight	659.99
Temperature/K	285.47(10)
Crystal system	monoclinic
Space group	$P2_1$
a/Å	8.6697(3)
b/Å	15.4417(6))
c/Å	11.9482(4)
$\alpha/^\circ$	90
$\beta/^\circ$	99.700(3)
$\gamma/^\circ$	90
Volume/$Å^3$	1576.70(10)
Z	2
ρ_{calc} mg/mm^3	1.390
µ/mm	7.636
F(000)	688.0
Crystal size/mm	0.3842 x 0.3421 x 0.1062
Radiation	CuKα (λ = 1.54184)
2θ range for data collection	7.506 to 147.890°
Index ranges	-10 $\leq$ h $\leq$ 10, -19 $\leq$ k $\leq$ 16, -14 $\leq$ l $\leq$ 14
Reflections collected	12454
Independent reflections	5818 [R_{int} = 0.0724, R_{sigma} = 0.0651]
Data/restraints/parameters	5818/1/339
Goodness-of-fit on F^2	1.138
Final R indexes [I>=2σ (I)]	R_1 = 0.0545, wR_2 = 0.1579
Final R indexes [all data]	R_1 = 0.0563, wR_2 = 0.1618
Largest diff. peak/hole / e $Å^{-3}$	0.88/-1.78
Flack parameter	-0.016(13)

face.[157] In addition, the C(aryl)-P-Ag-Cl dihedral angles of 159.8(3)° and 147.4(3)° in [Ag(*t*-Bu-thixantphos)Cl] are significantly larger then the corresponding dihedral angles in [Ag(Ph-xantphos)Br] of 109.6(4)°. The difference in the coordination plane between the two complexes, is likely the result of the steric influence of the *tert*-butyl groups compared to the phenyl rings; the chloride sits below the *tert*-butyl groups while intercalating with the phenyl rings. The backbone bending would result in two different sets of *tert*-butyl groups, which would have different NMR properties. However, this is not apparent in the NMR spectra of any of the [Ag(*t*-Bu-xantphos)Cl] complexes (Figure 3.5) indicating that the backbone is likely inverting rapidly in solution (Scheme 3.2). This inversion of the xantphos backbone has recently been observed for [Ru(CO)ClH(Ph-xantphos)(PPh_3)].[158]

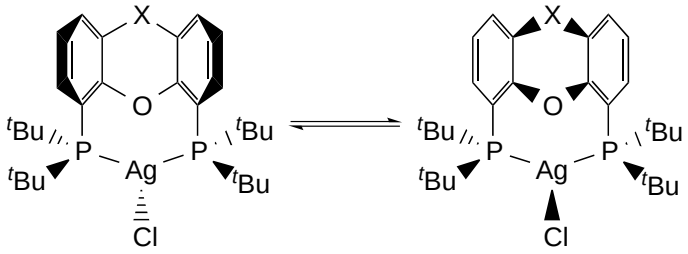

Scheme 3.2: Inversion of the xantphos backbone in [Ag(*t*-Bu-xantphos)Cl].

3.2 Reactions with Silver Tetrafluoroborate

Complexes of the type [Ag(*t*-Bu-xantphos)]BF_4 were synthesised in order to investigate the coordination of the diphosphine ligands in the absence of other ligands. Although tetrafluoroborate can coordinate to silver, it is unusual for it to do so, and numerous examples exist of silver complexes with free coordination sites that have a non-coordinated BF_4^- counterion (Figure 3.8).[159–161] Previous reports have shown that in the presence of an ether group and a tetrafluoroborate ion a linear diphosphine complex with mutually *trans* phosphorus atoms and no other ligands was synthesised.[162] In addition, coordination of the tetrafluoroborate to the silver will result in a shift of peak in the ^{19}F NMR spectrum.

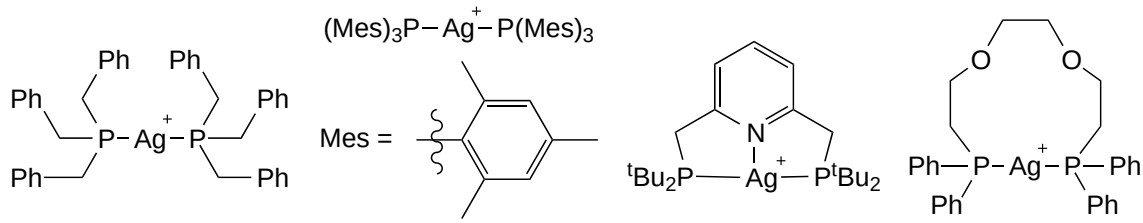

Figure 3.8: Examples of silver complexes with free coordination sites and non-coordinating BF_4^- counterions.[159–161]

The reaction between $AgBF_4$ and the *t*-Bu-xantphos ligands proceeded at room temperature in CH_2Cl_2, going to completion in under one hour (Scheme 3.3). The resulting [Ag(*t*-Bu-xantphos)]BF_4 complexes are light-sensitive in solution and in $CDCl_3$ solution completely degraded in 12 hours. For all three diphosphine ligands the ESI – mass spectra show a molecular ion peak corresponding to [Ag(diphosphine)]$^+$. In all cases the ^{31}P NMR spectra (for an example see Figure 3.9) show the expected pair of doublets, indicating chelation to a single silver atom. No relationship between the bite-angle and the $^1J_{^{107}AgP}$ or $^1J_{^{109}AgP}$ coupling constants was observed. The $^1J_{^{107}AgP}$ and $^1J_{^{109}AgP}$ coupling constants are larger than those for the silver chloride complexes (Table 3.4). This is consistent with their formulation as two-coordinate silver complexes, as the values of M-P coupling constants for d^{10} metals generally increase with decreasing coordination number.[16]

The ^{19}F NMR spectra of the three [Ag(*t*-Bu-xantphos)]BF_4 complexes show a single resonances between -151.3 and -151.9 ppm, indicating non-coordinating BF_4^- counterions. In the ^{1}H NMR spectra the *tert*-butyl resonances appear as a virtual triplet. Virtual triplets are commonly observed for $X_nAA'X'_n$ when A and A′ are strongly coupled such that $J_{AA'}$ is very much larger than the difference between J_{AX} and $J_{AX'}$.[124] In coordination compounds this condition is typically met if the two phosphorus atoms are in a *trans* configuration resulting in strong coupling of the spin systems.[16] In this case as the triplet is not a perfect 1:2:1 triplet it is likely that the phosphines are not strictly *trans* and the P-Ag-P angle is less than 180°.

The [Ag(*t*-Bu-xantphos)]BF_4 complexes show distinctive peaks in their ^{13}C NMR

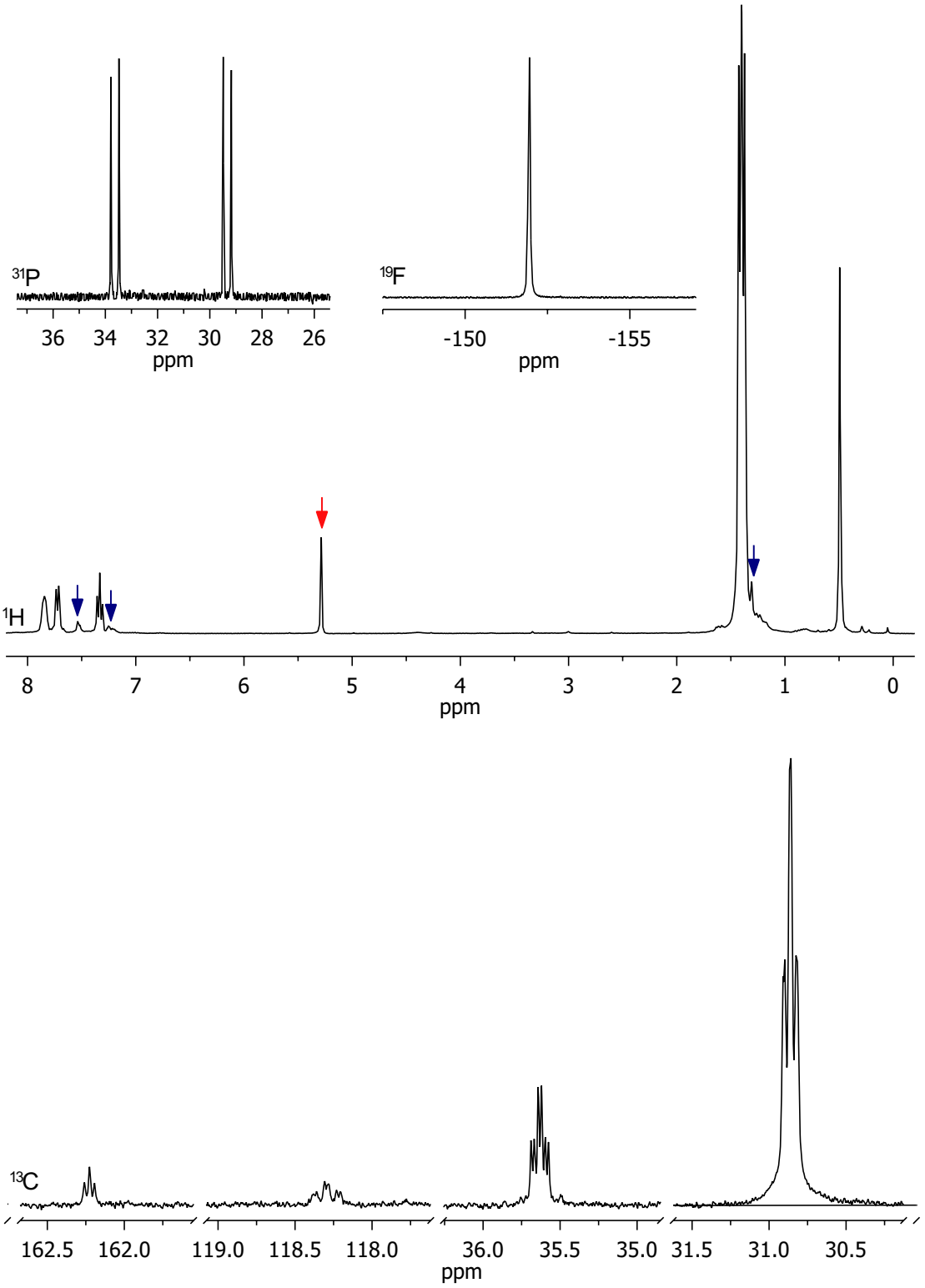

Figure 3.9: NMR spectra for [Ag(*t*-Bu-sixantphos)]BF_4 in $CDCl_3$. Arrows indicate impurities, CH_2Cl_2 indicated in red.

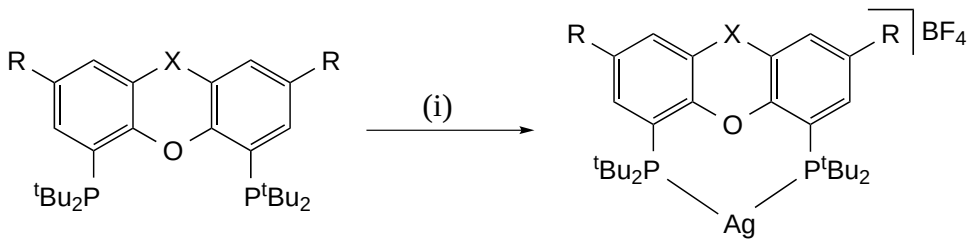

Scheme 3.3: Synthesis of [Ag(*t*-Bu-xantphos)]BF_4 complexes. *Reactions and conditions:* (i) $AgBF_4$, CH_2Cl_2.

Table 3.4: Selected NMR data of [Ag(*t*-Bu-xantphos)]BF_4 complexes ($\Delta\delta = \delta_{\text{complex}} - \delta_{\text{free ligand}}$).

	^{31}P				^{19}F
Diphosphine	δ/**ppm**	$\Delta\delta$/ **ppm**	$^1J_{^{107}\text{AgP}}$/**Hz**	$^1J_{^{109}\text{AgP}}$/**Hz**	δ/**ppm**
t-Bu-Sixantphos	31.5	23.1	482.9	557.4	-151.9
t-Bu-Thixantphos	28.4	18.9	486.7	562.2	-151.3
t-Bu-Xantphos	27.6	17.4	486.3	561.1	-151.9

spectra (see Figure 3.9 for a representative example), similar to those observed for the [Ag(*t*-Bu-xantphos)Cl] complexes (Section 3.1). The most downfield signal is for the aryl carbon attached to the oxygen atom (the *O-ipso* carbon). This signal appears as a virtual triplet, as expected for a XAA'X' system with strongly coupled phosphorus atoms. The signals for the *ipso* carbon attached to phosphorus, and the *tert*-butyl quaternary and terminal carbons, all appear as triplets of doublets due to coupling to phosphorus and both isotopes of silver. These signals would be expected to appear as a pair of virtual triplets of doublets; however, if the two leftmost peaks of one triplet of doublets overlapped with the two central peaks of the other triplet of doublets this could result in an apparent triplet of doublets (assuming that the virtual triplet is not a strict 1:2:1 triplet, which is likely applicable here as the ^{1}H NMR signal for the *tert*-butyl protons was not a 1:2:1 triplet).

The [Ag(*t*-Bu-xantphos)]BF_4 complexes have two free coordination sites; however, there is no evidence for either the ligand oxygen atom or the BF_4^- acting as

another ligand. This is likely due to the steric constraints of the larger bite-angle ligands and the bulky *tert*-butyl groups. Attempts were made to react the analogous [Ag(*t*-Bu-xantphos)]PF_6 complexes with ethene, ethyne and carbon monoxide, however no reactivity was observed.[163]

3.2.1 Reactions with LiCCPh

Silver acetylide complexes have gained attention recently due to their luminescent properties.[164–166] Silver acetylides supported by phosphine ligands tend to form cluster complexes with no monomeric structures currently reported in the CSD.[68] Attempts to synthesise a silver acetylide complex by reaction of the [Ag(*t*-Bu-xantphos)]BF_4 complexes with lithium phenylacetylide were marred by difficulties. The reaction was carried out in freshly distilled THF under argon, in the dark. After 12 hours the THF was removed *in vacuo* and the residue was extracted into a deuterated solvent and analysed by NMR spectroscopy. In $CDCl_3$ or acetone-d_6 a significant amount of DCCPh was observed in the ^{13}C NMR spectrum, indicating a reaction between the solvent and any acetylide complex that may have formed, or no reaction had occurred and the solvent was quenching the lithium acetylide. The ^{31}P NMR spectra showed a pair of doublets with different chemical shift and coupling constants to the starting material suggesting that a reaction between the [Ag(*t*-Bu-xantphos)]BF_4 complexes and LiCCPh had indeed occurred.

When the reaction was repeated and extracted into C_6D_6 the resulting NMR spectra were broad, with a pair of multiplets present in the ^{31}P NMR as would be expected if a silver cluster was formed. The ^{1}H and ^{13}C NMR spectra were also broad, however no peaks for free phenyl acetylene were observed, indicating that reaction had occurred with likely coordination. Unfortunately this complex was unstable and degraded completely in 24 hours to an insoluble black material. This material may be a higher order cluster, oligomer or polymeric species which commonly form with silver acetylide complexes. Further attempts at characterisation of the intermediate complex or the resulting degradation products were unsuccessful.

3.3 Summary

The coordination chemistry of *t*-Bu-sixantphos, *t*-Bu-thixantphos, and *t*-Bu-xantphos with silver(I) precursors has been investigated. [Ag(*t*-Bu-xantphos)Cl] complexes formed upon reaction of the ligands with AgCl. The X-ray crystal structure of [Ag(*t*-Bu-thixantphos)Cl] showed a trigonal geometry with a P-Ag-P angle of 130.50(7)°, which is slightly larger than the natural bite-angle (126.98°). The bite-angle in [Ag(*t*-Bu-thixantphos)Cl] is larger than the previously reported [Ag(Ph-xantphos)Br] (109.37(1)°) and chloride sits on the convex face whereas the bromide occupies the concave face. This shows the impact of the *tert*-butyl groups on the coordination chemistry. In solution the ligand backbones in the [Ag(*t*-Bu-xantphos)Cl] complexes are inverting rapidly, resulting in a single *tert*-butyl environment.

[Ag(*t*-Bu-xantphos)]BF_4 complexes were synthesised by reaction of the three *t*-Bu-xantphos ligands with $AgBF_4$. The NMR spectroscopy suggested that the P-Ag-P angle in these complexes was approaching 180°. Reaction of the [Ag(*t*-Bu-xantphos)]BF_4 complexes with lithium phenylacetylide in $CDCl_3$ or acetone-d_6 formed DCCPh but no change in the [Ag(*t*-Bu-xantphos)]BF_4 complexes. In C_6D_6 the resulting NMR spectra were broad with no peaks indicative of free phenyl acetylene. However, the product was unstable and degradation hindered characterisation. All of the characterised complexes in this chapter were monomeric species, indicating that the *t*-Bu-xantphos ligands preferentially chelate to a silver ion rather than bridging to form dimers/oligomers. The absence of any dimers and oligomers forming from the [Ag(*t*-Bu-xantphos)]BF_4 complexes suggests that the rigid backbone and bulky *tert*-butyl groups are able to stabilise electron deficient metal centres.

Chapter 4

Coordination Complexes with Rhodium

Rhodium is a very rare element forming only 0.001 ppm of the earth's crust.[167] The majority of the extracted rhodium (81%) is used in catalytic converters in cars to reduce harmful nitrogen oxides to nitrogen and oxygen.[168] Another important use of rhodium is in thermocouples where a rhodium-platinum alloyed wire is used, together with a pure platinum wire for use in high-temperature furnaces.[167] Rhodium coordination complexes form active catalysts, most commonly for hydroformylation and hydrogenation.[28,169,170] Wilkinson's catalyst, $[RhCl(PPh_3)_3]$, is one of the most widely known rhodium catalysts, used mainly for the hydrogenation of alkenes, but also for hydroboration of alkenes and selective hydrosilylation of α,β-unsaturated carbonyl compounds.[171–173]

The 2001 Nobel Prize in Chemistry was awarded to Knowles,[7] Noyori,[5] and Sharpless[174] for their work in asymmetric catalysis, including several rhodium catalysts. A derivative of Wilkinson's catalyst, where triphenylphosphine was replaced by the chiral phosphine (−)-PMePh^{i}Pr, was reported by Knowles and Sabacky in 1968.[175] This chiral version of Wilkinson's catalyst was the first asymmetric hydrogenation catalyst yielding an enantiomeric excess of 15% when hydrogenating α,β-unsaturated carbonyls (Scheme 4.1). This was improved by the development of the CAMP ligand (Figure 4.1), which gives an enantiomeric excess of 80% in the hydrogenation of dehydroamino acids, a key step in the commercial production of L-DOPA, a drug used in the treatment of Parkinson's disease.[176] Rhodium complexes containing chiral diphosphines also form active cat-

alysts, for example a [Rh(cod)(*S*)-BINAP] (Figure 4.1) catalyst is active for the asymmetric isomerisation of allylic amines, a key step in the industrial synthesis of (−)-menthol generating over 1000 tons per year.[5]

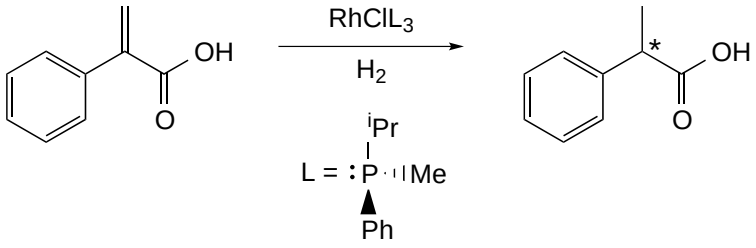

Scheme 4.1: Asymmetric catalytic hydrogenation developed by Knowles.[7]

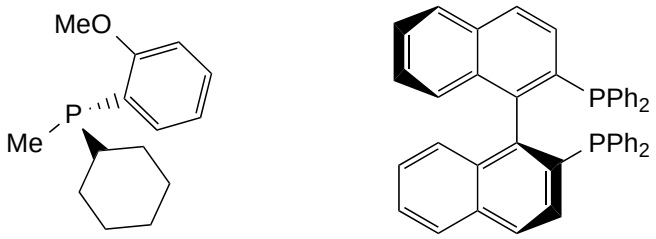

Figure 4.1: Chiral phosphine ligands CAMP (left) and (*S*)-BINAP (right), used in asymmetric catalysis.[5,176]

The xantphos class of ligands were first studied for potential use as ancillary ligands in rhodium-catalysed hydroformylation.[30] Small changes in the bite-angle can result in changes in reactivity and selectivity. For hydroformylation the larger bite-angle ligand, Ph-xantphos, showed a greater selectivity for the linear aldehyde than Ph-sixantphos or Ph-thixantphos. Xantphos ligands have the ability to coordinate to a metal centre in a number of different modes. The most common is the diphosphine κ*PP′* mode. Tridentate κ*P,O,P′* complexes of the xantphos ligands are also relatively common, especially in octahedral complexes. In this κ*P,O,P′* coordination mode, the xantphos ligand typically coordinates to the metal in a meridional manner, although facial complexes have also been reported.[177,178]

Subsequent to the research reported in this chapter being performed, one paper has been published, reporting the coordination chemistry of the *t*-Bu-xantphos

ligand with rhodium.[82] *t*-Bu-Xantphos was shown to react with [Rh(coe)(η-Cl)]$_2$ forming a [Rh(*t*-Bu-xantphos-κ*P,O,P′*)Cl] complex. This complex readily splits hydrogen to form a [Rh(*t*-Bu-xantphos-κ*P,O,P′*)Cl(H)$_2$] complex. Both of these complexes were also synthesised as part of the present study and comparison of the results will be discussed where relevant. Chloride abstraction from [Rh(*t*-Bu-xantphos-κ*P,O,P′*)Cl(H)$_2$] using $AgBF_4$ or $AgSbF_6$ generates the trigonal bipyramidal dihydride complex [Rh(*t*-Bu-xantphos-κ*P,O,P′*)(H)$_2$]$^+$. This dihydride reacts with ethene to give ethane and [Rh(*t*-Bu-xantphos-κ*P,O,P′*)(C_2H_4)], however no reaction with the commonly used hydrogen acceptors *t*-butylethylene or norbornene was observed, nor was any reaction with terminal alkenes. [Rh(*t*-Bu-xantphos-κ*P,O,P′*)Cl(H)$_2$] reacts with KO^{t}Bu resulting in a four coordinate monohydride species [Rh(*t*-Bu-xantphos-κ*P,O,P′*)H]. [Rh(*t*-Bu-xantphos-κ*P,O,P′*)H] is an active catalyst for the isomerisation of 1-hexene, with a TON of 2000 after 16 hours. Addition of ethene to this rhodium(I) hydride resulted in the reversible formation of an ethyl complex. This paper shows some of the interesting chemistry of *t*-Bu-xantphos with rhodium. However, to date the coordination chemistry of *t*-Bu-sixantphos and *t*-Bu-thixantphos has not been reported.

This chapter presents research into the coordination chemistry of *t*-Bu-sixantphos, *t*-Bu-thixantphos, and *t*-Bu-xantphos with rhodium. The goal was the synthesis and characterisation of complexes that may form as part of catalytic reactions. As such, this work focusses on the reactivity of a simple rhodium(I) complex towards small molecules, particularly the chemistry towards hydrogen and carbon monoxide, as these are common components of catalytic systems.

4.1 Synthesis of [Rh(κ*P,O,P′*)Cl] Complexes

Chlorido-bridged rhodium alkene dimers are commonly used starting materials for the formation of rhodium phosphine complexes. These dimers can react in a number of different ways depending on the phosphine ligand used (Figure 4.2). When two equivalents of a monophosphine react with [Rh(coe)$_2$Cl]$_2$, (coe = cyclooctene) the phosphine displaces one coe molecule from each rhodium atom forming a symmetric dimer.[179] These complexes are typically unstable. Further addition of phosphine displaces the remaining two coe molecules, while retaining the chlorido-bridged rhodium core.[180] Analogous complexes form when the

reaction is carried out with diphosphines.[181] In some cases, bidentate ligands can cleave the dimer resulting in a [Rh(LL)(coe)Cl] complex.[182] Tridentate ligands are also able to cleave the dimer and result in the mononuclear complexes [Rh(LLL)Cl].[183,184] With negatively charged tridentate ligands, a trigonal bipyramidal hydride chloride complex is formed (where the hydride forms *via* X-H activation of the central ligating atom).[185–187] Alternatively, a hydride can be abstracted from the ligand using a strong base prior to reaction with the rhodium dimer. Silver salts can also be added to remove the bridging chloride ligands and form a monomeric complex. In this case the remaining coordination site is occupied either by the anion from the silver salt, or by a cyclooctene molecule if a non-coordinating counterion is used.[188,189]

Reaction between $[Rh(coe)_2Cl]_2$ and the three *t*-Bu-xantphos ligands was carried out on an NMR scale in C_6D_6. No reaction occurred at room temperature overnight except in the case of *t*-Bu-xantphos, which displays a small amount of conversion, evident from the ^{1}H and ^{31}P NMR spectra. The lack of reactivity at room temperature may be the result of the poor solubility of $[Rh(coe)_2Cl]_2$ in C_6D_6. Upon heating to 60 °C coordination of the *t*-Bu-xantphos ligands proceeded, going to completion after 24 hours. For all three *t*-Bu-xantphos ligands the product is the expected [Rh(*t*-Bu-xantphos-κ*P,O,P*′)Cl] mononuclear complex (Scheme 4.2). This complex is directly analogous to an *i*-Pr-xantphos complex reported in 2013,[81] which was synthesised in the same manner. The *t*-Bu-xantphos ligands have a number of different possible coordination modes. In this case a meridional κ*P,O,P*′ pincer coordination is observed. It is likely that the reaction proceeds by substitution of one cyclooctene ligand with one of the phosphorus atoms, followed by a second to form a chlorido-bridged dimer. However, as the *t*-Bu-xantphos ligands have such large bite-angles and the potentially coordinating ether bridge, this can readily split the dimer resulting in the desired product. None of these intermediates were observed, indicating low activation barriers once the first substitution had occurred.

The ^{1}H, ^{13}C and ^{31}P NMR spectra for the three [Rh(*t*-Bu-xantphos-κ*P,O,P*′)Cl] complexes are consistent with the proposed structures. Representative ^{1}H and ^{31}P NMR spectra for [Rh(*t*-Bu-xantphos-κ*P,O,P*′)Cl] are shown in Figure 4.3 and selected NMR data for all three complexes is given in Table 4.1. In the ^{31}P NMR spectra the signals shift downfield by 35.8–37.5 ppm upon coordination, with the

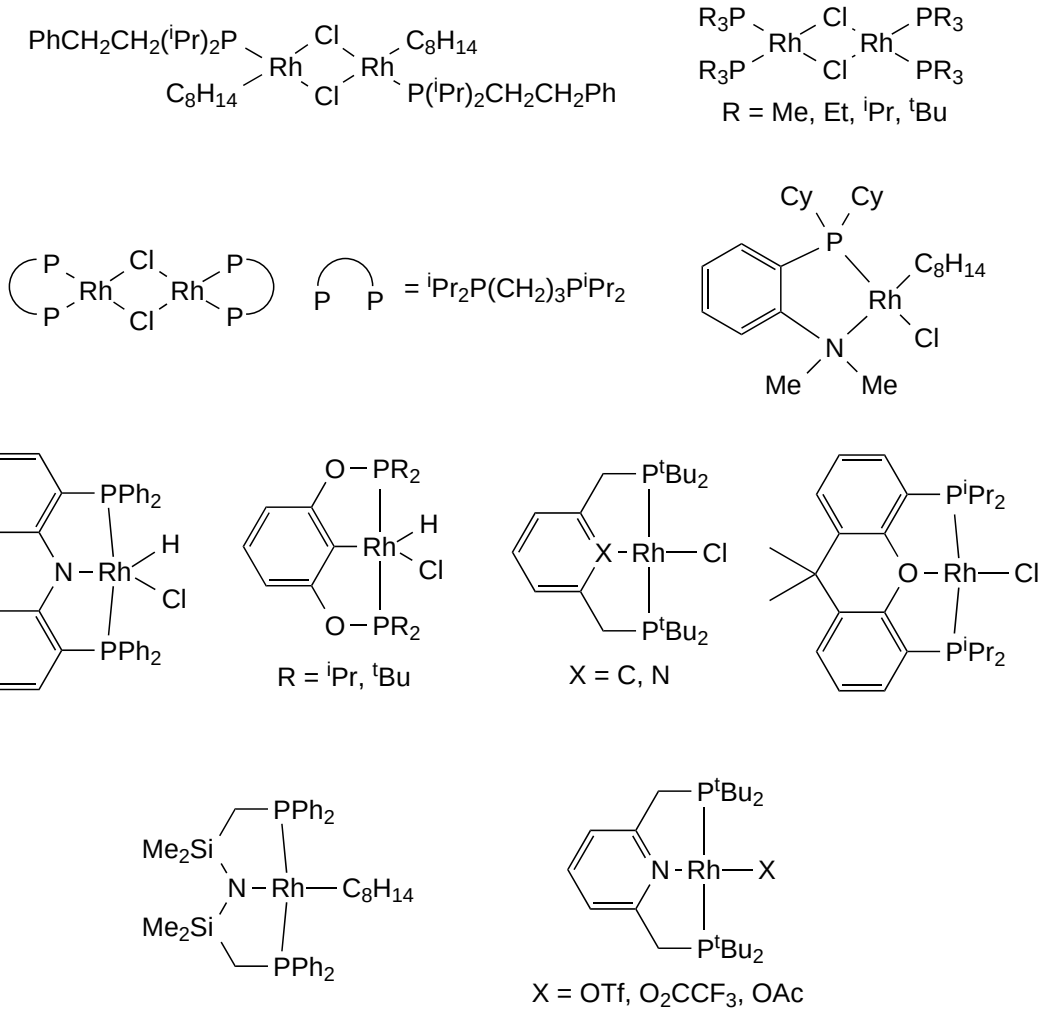

Figure 4.2: Complexes formed by reaction of $[Rh(coe)_2Cl]_2$ and phosphine ligands. First row: monophosphines in 2:1 and 4:1 ligand:$[Rh(coe)_2Cl]_2$, second row: bidentate ligands, third row: tridentate ligands in the absence of other reagents, fourth row: tridentate ligands using lithiated ligand (left) or a silver salt (right).

peaks for the complexes appearing at 44.2–47.7 ppm. The signals for the complexes are doublets with rhodium coupling of 140.0–142.3 Hz. This coupling is consistent with a rhodium(I) complex and is similar to the coupling constant for [Rh(*i*-Pr-xantphos-κ*P,O,P′*)Cl] (142.4 Hz).[81] The ^{1}H and ^{13}C NMR spectra support the proposed structure, as the *tert*-butyl proton and carbon signals all appear as virtual triplets, indicating strongly coupled phosphorus atoms, which typically occurs in a *trans* coordination geometry.[16,124] In the ^{13}C NMR spectrum the peak

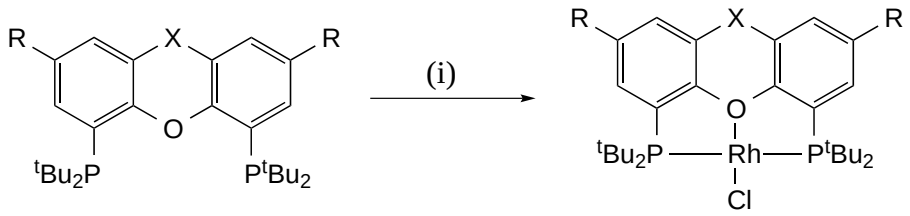

Scheme 4.2: Reaction of $[Rh(coe)_2Cl]_2$ and *t*-Bu-xantphos ligands. *Reagents and conditions:* (i) 0.5eq·$[Rh(coe)_2Cl]_2$, C_6D_6, 60 °C, 24 hours.

corresponding to the *O-ipso* carbon has shifted downfield relative to the free ligand, unlike the equivalent [Ag(*t*-Bu-xantphos)Cl] complexes where the oxygen is known to be non-coordinating (Table 4.2). This downfield shift is consistent with a coordinated oxygen. As the oxygen donates electron density to the metal this will inductively decrease electron density on the *O-ipso* carbon resulting in decreased shielding and thus a downfield shift of the NMR signal.

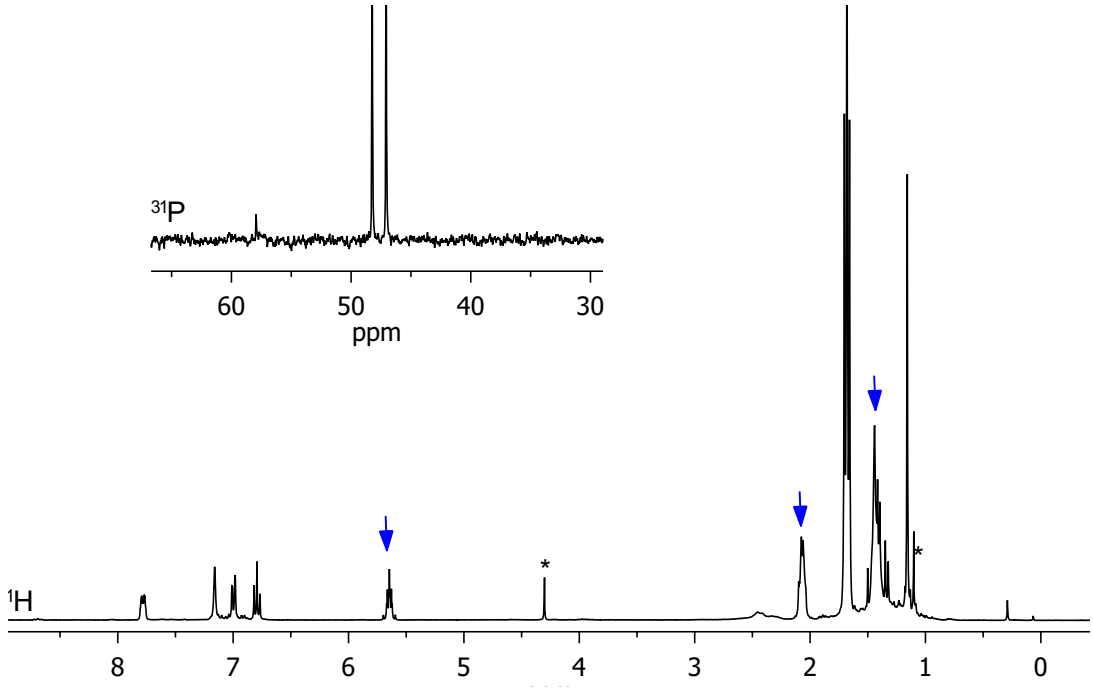

Figure 4.3: ^{31}P and ^{1}H NMR spectra for [Rh(*t*-Bu-xantphos)Cl] in C_6D_6. Blue arrows indicate displaced coe, asterisks denote impurities.

Subsequent to this work the [Rh(*t*-Bu-xantphos-κ*P,O,P'*)Cl] complex and X-ray

Table 4.1: Selected NMR data of [Rh(*t*-Bu-xantphos)Cl] complexes in C_6D_6 ($\Delta\delta$ = $\delta_{complex}$ - $\delta_{free\ ligand}$).

	^{31}P			^{1}H *t*-Bu	
Compound	δ/**ppm**	$\Delta\delta$/**ppm**	J_{RhP}/**Hz**	δ/**ppm**	J/**Hz**
t-Bu-Sixantphos	44.2	35.8	140.0	1.69	13.5
t-Bu-Thixantphos	46.5	37.0	141.5	1.67	13.7
t-Bu-Xantphos	47.7	37.5	142.3	1.68	13.4

crystal structure have been reported in the literature.[82] The literature method also used $[Rh(coe)_2Cl]_2$ as the starting material in benzene however, their reaction was complete in 24 hours at room temperature, which suggests that the heating to 60 °C is unnecessary. The NMR data reported herein is consistent with the literature values. The X-ray crystal structure of [Rh(*t*-Bu-xantphos-κ*P,O,P′*)Cl] (Figure 4.4) shows a square-planar geometry with a *t*-Bu-xantphos-κ*P,O,P′* coordination mode.

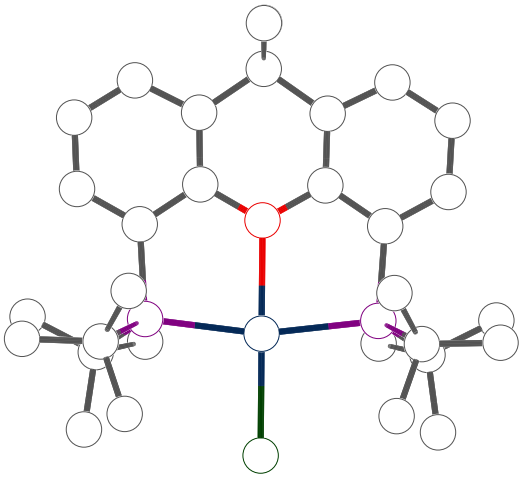

Figure 4.4: X-ray crystal structure of [Rh(*t*-Bu-xantphos-κ*P,O,P′*)Cl]. Hydrogen atoms omitted for clarity.[82]

Table 4.2: Chemical shift and coupling of the *O-ipso* carbon in the free ligand, [Ag(*t*-Bu-xantphos)Cl] ($CDCl_3$) and [Rh(*t*-Bu-xantphos)Cl] (C_6D_6) complexes ($\Delta\delta = \delta_{\text{complex}} - \delta_{\text{free ligand}}$).

	Ligand ($CDCl_3$)	**Ligand (C_6D_6)**	**[Ag(*t*-Bu-xantphos)Cl]**		**[Rh(*t*-Bu-xantphos)Cl]**	
Ligand	δ/**ppm**	δ/**ppm**	δ/**ppm**	$\Delta\delta$	δ/**ppm**	$\Delta\delta$
t-Bu-Sixantphos	164.3	164.5	163.9	-0.4	169.5	5.0
t-Bu-Thixantphos	155.3	155.9	155.5	0.2	157.4	1.5
t-Bu-Xantphos	155.8	156.0	156.5	0.7	158.9	2.9

4.2 Reaction with Hydrogen

Rhodium complexes are well-known as homogeneous hydrogenation and hydroformylation catalysts. Both of these processes involve the activation of molecular hydrogen at the rhodium centre. The catalytic cycle for hydrogenation using monophosphine ligands (Scheme 4.3) involves the addition of molecular hydrogen to [Rh(PR_3)$_2$Cl] generating a rhodium dihydride, which then coordinates an alkene and undergoes hydride-migration followed by reductive elimination to regenerate the starting rhodium complex and the alkane. In hydroformylation (Scheme 4.4) the alkene coordinates to an existing rhodium hydride complex. Hydride migration occurs followed by carbon monoxide coordination and migratory insertion into the rhodium alkyl bond. This is followed by the oxidative addition of dihydrogen, generating a rhodium(III) dihydride complex. The cycle concludes by reductive elimination, generating the aldehyde and the starting rhodium(I) complex. The influence of the bite-angle of Ph-xantphos complexes on the reactivity and selectivity of catalytic process was first studied for hydroformylation.[30] Since then hydroformylation has been studied extensively using a variety of xantphos derivatives.[25,32,34,60–62,64,114,116,190–204] Given the importance of the oxidative addition of molecular hydrogen for both hydrogenation and hydroformylation, and to investigate any possible differences of the wide bite-angle and steric bulk of the *t*-Bu-xantphos ligands we investigated the reactivity of the [Rh(*t*-Bu-xantphos-κ*P,O,P'*)Cl] complexes with dihydrogen.

The [Rh(*t*-Bu-xantphos-κ*P,O,P'*)Cl] complexes react readily with hydrogen, forming octahedral rhodium(III) dihydride complexes (Scheme 4.5). The dihydrogen undergoes oxidative addition forming two classical hydride ligands with a *cis* configuration. The *t*-Bu-xantphos ligands retain their meridional coordination, meaning that the hydride ligands are in different environments, one *trans* to the chloride and the other *trans* to the oxygen donor atom. As a result, the two faces of the *t*-Bu-xantphos ligands are now different causing two different environments for the bridgehead methyls in both *t*-Bu-sixantphos and *t*-Bu-xantphos, and the *tert*-butyl groups for all three *t*-Bu-xantphos ligands. However, the plane of symmetry perpendicular to the *t*-Bu-xantphos backbone is retained, such that the methyl substituents of *t*-Bu-thixantphos are in the same environment.

Two hydride resonances are evident in the ^{1}H NMR spectra of the three [Rh(*t*-Bu-

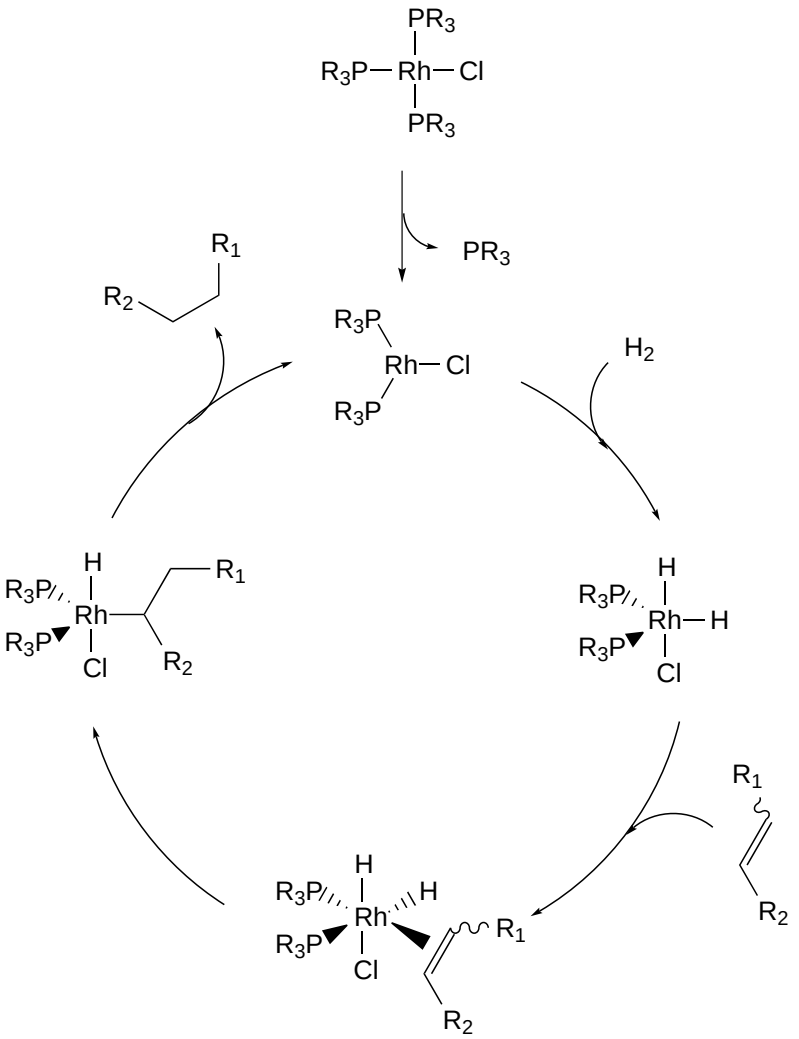

Scheme 4.3: Catalytic cycle for homogeneous hydrogenation using a rhodium chloride complex with monophosphine ligands.

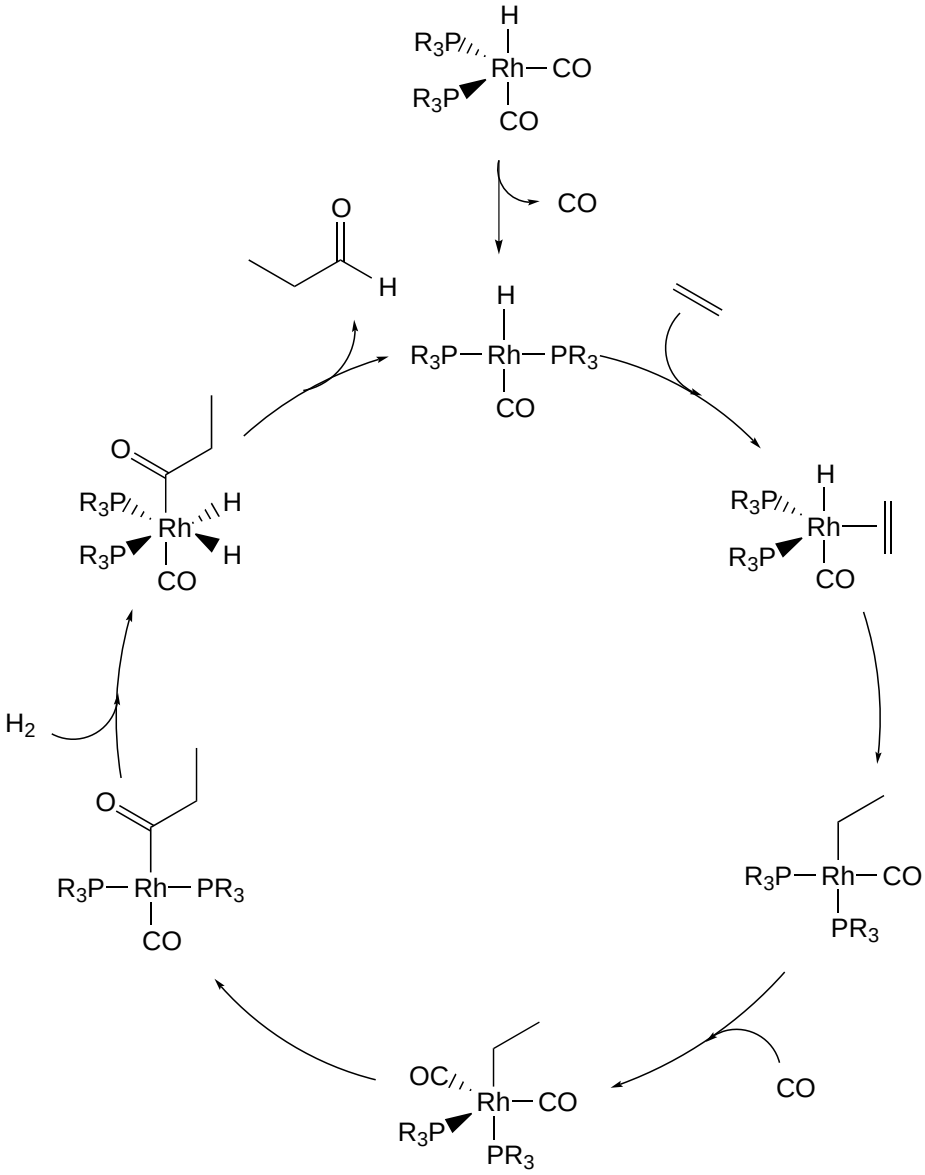

Scheme 4.4: Generic catalytic cycle for homogeneous hydroformylation.

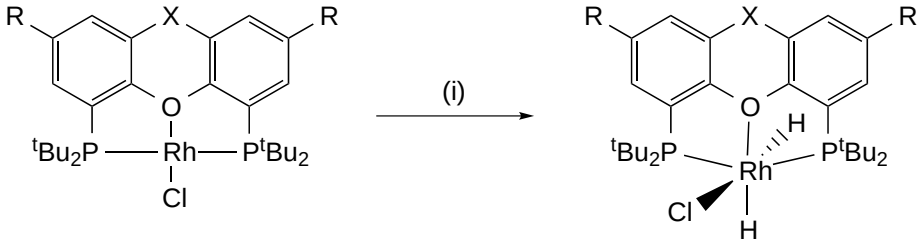

Scheme 4.5: Reaction of the Rh(*t*-Bu-xantphos)Cl] complexes with hydrogen. *Reagents and conditions:* (i) H_2, C_6D_6.

xantphos-κ*P,O,P'*)Cl$(H)_2$] complexes. The signals appear upfield as well defined doublets of triplets of doublets, coupling to the rhodium, two phosphorus atoms and each other (Figure 4.5, Table 4.3). The hydride *trans* to the chloride ligand (-16.92 to -17.04 ppm) shows very little difference in either the chemical shift or coupling constants between the three complexes. The hydride *trans* to the *t*-Bu-xantphos oxygen (-20.51 to -21.12 ppm) shows more variation in the chemical shift and coupling. The value of J_{RhH} decreases with increasing natural bite-angle, such that the *t*-Bu-xantphos complex has the lowest value and *t*-Bu-sixantphos the largest. This suggests that the *trans* influence of the ether bridge is highest for *t*-Bu-xantphos and lowest for *t*-Bu-sixantphos, which may be related to the amount of strain required for the ligand to achieve tridentate coordination.

The ^{31}P NMR spectra (example in Figure 4.5 for *t*-Bu-thixantphos) for the [Rh(*t*-Bu-xantphos-κ*P,O,P'*)Cl$(H)_2$] complexes each display a single resonance, downfield relative to the starting [Rh(*t*-Bu-xantphos-κ*P,O,P'*)Cl] complexes, as a doublet of doublets with some further coupling evident. Although ^{31}P NMR is ^{1}H decoupled, the decoupler is sometimes unable to fully decouple resonances that are so far outside the typical ^{1}H NMR range (-2 to 15 ppm) resulting in residual coupling. The values of J_{RhP} in the [Rh(*t*-Bu-xantphos-κ*P,O,P'*)Cl$(H)_2$] complexes are 116.1–117.8 Hz, a decrease of 23.7–25.3 Hz from the starting [Rh(*t*-Bu-xantphos-κ*P,O,P'*)Cl] complexes. This decrease is consistent with a change in the oxidation state from rhodium(I) to rhodium(III).[16] Two signals are observed in the ^{1}H NMR spectra for the *tert*-butyl protons in all three complexes consistent with the proposed geometry. Both signals are virtual triplets, confirming the mutually *trans* coordination of the phosphorus atoms, consistent with the proposed meridional coordination of the ligands. Two signals were also ob-

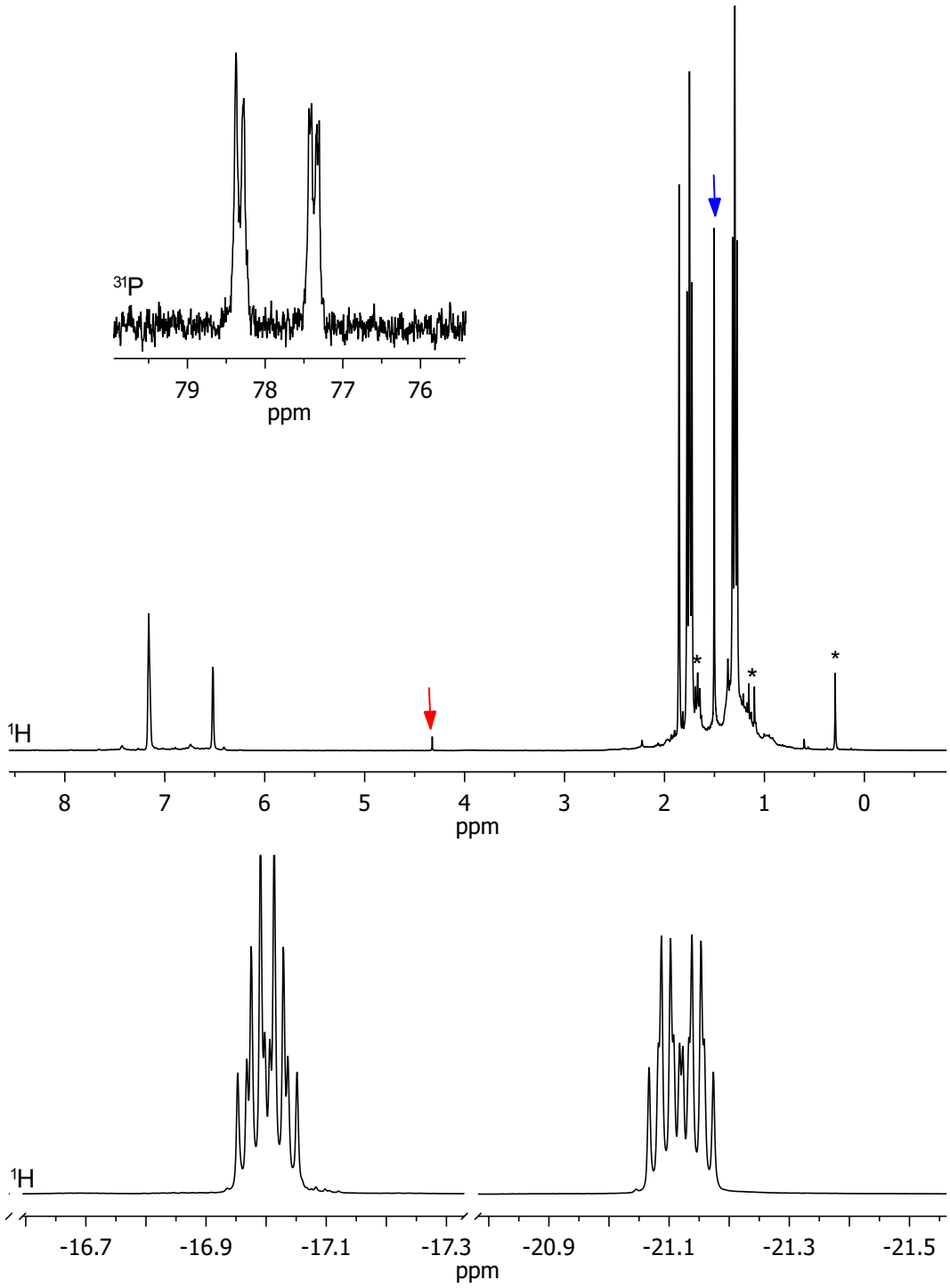

Figure 4.5: NMR spectra for [Rh(*t*-Bu-thixantphos)Cl$(H)_2$] in C_6D_6. Impurities are indicated by asterisks, CH_2Cl_2 is indicated by a red arrow and cyclooctane by a blue arrow.

Table 4.3: Hydride ^{1}H NMR data for Rh(*t*-Bu-xantphos-κ*P,O,P'*)Cl(H)$_2$] complexes in C_6D_6.

	H$^-$ *trans*-Cl$^-$				**H$^-$ *trans*-O**			
Diphosphine	δ/**ppm**	J_{RhH}/**Hz**	J_{PH}/**Hz**	J_{HH}/**Hz**	δ/**ppm**	J_{RhH}/**Hz**	J_{PH}/**Hz**	J_{HH}/**Hz**
t-Bu-Sixantphos	-16.92	22.7	13.5	9.4	-21.12	30.9	12.1	9.2
t-Bu-Thixantphos	-17.00	22.6	13.5	9.4	-21.13	30.5	12.4	9.4
t-Bu-Xantphos	-17.04	22.8	13.4	9.4	-20.51	28.8	12.2	9.4

served in the ^{1}H NMR spectra for the bridgehead methyls in [Rh(*t*-Bu-xantphos-κ*P,O,P'*)Cl(H)$_2$] and [Rh(*t*-Bu-sixantphos-κ*P,O,P'*)Cl(H)$_2$], again consistent with the proposed structure.

The [Rh(*t*-Bu-xantphos-κ*P,O,P'*)Cl(H)$_2$] complexes are similar to previously reported rhodium xantphos dihydride complexes, [Rh(H)$_2$(*i*-Pr-xantphos)X] (X = Cl, OTf)[81] and [Rh(H)$_2$(Ph-xantphos)X]$^+$ (X = P(Cyp)$_3$ Cyp = cyclopentyl, NCMe, OC(Me$_3$)$_2$, H$_3$BNMe$_3$-κ*H*).[72,177,205] In these cases the hydride *trans* to the oxygen atom was located in the ^{1}H NMR between -22.19 and -19.00 ppm with a rhodium coupling constant of 27.0–33.8 Hz. The ^{1}H NMR signals for the hydride ligands in the [Rh(*t*-Bu-xantphos-κ*P,O,P'*)Cl(H)$_2$] complexes are encompassed within these ranges (Table 4.3). For the reported *t*-Bu-xantphos complexes the ^{31}P NMR chemical shift is 77.8–79.0 ppm (J_{RhP} = 116.1–117.8 Hz). In comparison, the literature complexes appear at 36.9–45.4 ppm (J_{RhP} = 114–121 Hz) for Ph-xantphos and 64.8–67.2 ppm (J_{RhP} = 113–114 Hz) for *i*-Pr-xantphos. The coupling constants are consistent for the complexes, and although the absolute chemical shift varies significantly, the change in chemical shift on reaction with hydrogen from the [Rh(*t*-Bu-xantphos)Cl] complexes is consistent (28.7–31.1 ppm for *i*-Pr-xantphos compared to 31.3–34.0 ppm for *t*-Bu-xantphos, [Rh(Ph-xantphos)Cl] has not been reported in the literature).

The [Rh(H)$_2$(Ph-xantphos)X]$^+$ (X = P(Cyp)$_3$, H$_3$BNMe$_3$-κ*H*) complexes were reportedly only stable under a hydrogen atmosphere.[177,205] However, the [Rh(*t*-Bu-xantphos)Cl(H)$_2$] complexes were able to be placed under vacuum overnight with no evidence for loss of hydrogen. This difference is likely the result of the different electronics between *t*-Bu-xantphos and Ph-xantphos. The electron donating nature of the *tert*-butyl groups on *t*-Bu-xantphos enhances electron donation from the rhodium centre into the σ^* orbital of a dihydrogen ligand, thus favouring oxidative addition and the formation of two discrete hydrides. The Ph-xantphos ligand is more electron withdrawing than *t*-Bu-xantphos, due to the phenyl substituents on the phosphorus atoms. The lower electron donation will result in less back-bonding from the metal to the dihydrogen ligand and thus the barrier towards reforming the dihydrogen will be lower.

The synthesis of the [Rh(*t*-Bu-xantphos-κ*P,O,P'*)Cl] complexes from [Rh(coe)$_2$Cl]$_2$ generates cyclooctene as a by-product. This reaction mixture was used without further purification to determine the potential for the [Rh(*t*-Bu-xantphos-

κ*P,O,P'*)Cl] complexes to act as hydrogenation catalysts. Hydrogen gas was bubbled through a mixture of [Rh(*t*-Bu-xantphos-κ*P,O,P'*)Cl] and cyclooctene for 10 minutes before the reaction was sealed and allowed to proceed at room temperature. No evidence for cyclooctene was observed by ^{1}H NMR spectroscopy in the reaction mixture and a peak for cyclooctane was apparent (Figure 4.5). While further work to determine the activity of these complexes needs to be performed, this result indicates the potential for the [Rh(*t*-Bu-xantphos-κ*P,O,P'*)Cl] complexes to act as precatalysts for the hydrogenation of alkenes.

The [Rh(*t*-Bu-xantphos)Cl(H)$_2$] complex and its X-ray crystal structure have subsequently been published by another research group.[82] The X-ray crystal structure confirms the *t*-Bu-xantphos ligand coordinates in a κ*P,O,P'* meridional geometry with mutually *cis* hydrides. The spectroscopic data contained herein is consistent with the published values.

4.3 Rhodium Carbonyl Complexes

Metal carbonyl complexes are some of the most well-studied transition metal complexes for many reasons. Metal carbonyls are involved in a number of different catalytic processes including hydroformylation, hydroesterification and hydrocarboxylation to introduce oxygen functionality.[28,206,207] These reactions are of great synthetic importance and numerous industrial examples are known, such as the conversion of a benzylic alcohol to a carboxylic acid using a palladium catalyst in the synthesis of ibuprofen[208] and the hydroformylation of 1,3-butadiene to adipaldehyde, an intermediate for producing caprolactam and hexamethylene-1,6-diamine (HMDA), key monomers for nylon-6.6 and nylon-6 manufacture.[209] These catalytic processes involve the terminal coordination of the carbonyl to the metal centre. However, carbonyls can also act as bridging ligands, either solely through the carbon atom or in a side-on η^2 mode involving the π-system.

Transition metal carbonyl complexes have also been studied to investigate the electronic influence of other ligands. The stretching frequency of the C=O bond is a good measure of the electronic environment as carbonyl ligands are strong π-acceptor ligands, meaning that the metal centre will donate electron density into the π^*-orbital. This weakens the C=O bond and results in a shift of the infrared C=O stretch to lower frequency. The degree to which the back-bonding

occurs is related to the nature of the metal centre and the other ligands. As such, a number of series exist where this stretch has been used to quantify the electron donor capabilities of various ligands. These include the well-known Tolman Electronic Parameter using $[Ni(CO)_3L]$ complexes,[8,14] and $[Mo(CO)_5L]$ and $[Rh(CO)ClL_2]$ series,[9] although other methods are utilised such as the phosphine selenide coupling constants (see Section 2.4) and the J_{PtP} coupling in *cis*-$[PtCl_2P_2]$ complexes.[16]

The typical method for producing rhodium phosphine carbonyl complexes is to react the free phosphine or diphosphine ligand with either the chloro-bridged dicarbonyl dimer, $[Rh(CO)_2Cl]_2$, or by reaction with a chloro-bridged rhodium alkene dimer such as $[Rh(C_2H_4)_2Cl]_2$ or $[Rh(coe)_2Cl]_2$ under an atmosphere of carbon monoxide. The reaction is then purified either in the air or under inert atmosphere and in the majority of cases the product is *trans*-[Rh(CO)(PP)Cl] where PP is either two monophosphine ligands or a *trans*-spanning diphosphine. Using smaller bite-angle diphosphine ligands results in the *cis* isomer.

The reactivity of the [Rh(*t*-Bu-xantphos-κ*P,O,P'*)Cl] complexes towards carbon monoxide was investigated on an NMR scale by bubbling CO through a C_6D_6 solution of the complex for 10 minutes before sealing the NMR tube with a J. Young tap. An immediate colour change was observed, with the dark brown starting material changing to yellow (*t*-Bu-sixantphos) or orange (*t*-Bu-thixantphos and *t*-Bu-xantphos). NMR analysis of these samples showed the reaction was complete, forming a single product in under 15 minutes with no evidence of the starting material. All NMR spectra for these complexes were obtained under an atmosphere of CO.

The NMR spectra for the three resulting products show some differences. The ^{1}H and ^{13}C NMR spectra for the reaction of [Rh(*t*-Bu-thixantphos-κ*P,O,P'*)Cl] with CO are broad, while the ^{31}P NMR spectrum shows only slight broadening. This indicates possible dynamic behaviour. However, the spectra for the reaction of [Rh(*t*-Bu-sixantphos-κ*P,O,P'*)Cl] and [Rh(*t*-Bu-xantphos-κ*P,O,P'*)Cl] with CO are both well resolved (Figure 4.6 shows a selection of the NMR spectra for the *t*-Bu-xantphos complex). In all cases the ^{31}P NMR spectrum show a single peak at 69.3–71.6 ppm, split into a doublet by rhodium coupling of 120.0–122.2 Hz (Table 4.4). These are shifted downfield relative to the [Rh(*t*-Bu-xantphos-κ*P,O,P'*)Cl] starting material. The value of J_{RhP} has decreased from the starting [Rh(*t*-Bu-

xantphos-κ*P,O,P'*)Cl] complexes from 140.0–142.3 Hz to 120.0–122.2 Hz.

Table 4.4: Selected NMR data of [Rh(*t*-Bu-xantphos)$(CO)_2$Cl] complexes in C_6D_6 ($\Delta\delta = \delta_{complex} - \delta_{free\ ligand}$).

	^{31}P			^{13}C CO		
Ligand	δ/**ppm**	$\Delta\delta$ **ppm**	J_{RhP}/**Hz**	δ/**ppm**	J_{RhC}/**Hz**	J_{PC}/**Hz**
t-Bu-Sixantphos	70.8	26.6	120.0	195.5	84.4	13.0
t-Bu-Thixantphos	69.3	22.8	122.2		not observed	
t-Bu-Xantphos	71.6	23.9	120.0	194.9	84.4	12.4

The NMR spectra of the products from the reaction of the [Rh(*t*-Bu-xantphos)Cl] complexes with CO, indicate a high level of symmetry in the products. In the ^{1}H NMR spectra a single peak was observed for the *tert*-butyl groups and a singlet for the methyl groups for each of the three ligands. The number of aromatic signals in the ^{1}H NMR spectra indicate that two mirror planes exist, parallel to the backbone of the ligand and perpendicular to it (running through the oxygen and other bridging atom). For *t*-Bu-sixantphos and *t*-Bu-xantphos the *tert*-butyl groups appear as a virtual triplet indicating a *trans* or pseudo *trans* coordination geometry. For *t*-Bu-thixantphos the *tert*-butyl resonance displays some broadening, resulting in a singlet.

The number of signals in the ^{13}C NMR spectra is also suggestive of a highly symmetric product. Although the peaks were well resolved for the *t*-Bu-sixantphos and *t*-Bu-xantphos complexes, in the *t*-Bu-thixantphos complex all of the ^{13}C NMR peaks were broad except two, which can be attributed to the methyl groups and the aromatic carbon they are attached to, indicating that these carbons are unaffected by the dynamic process which leads to the broadening in this spectra. This process may be either exchange of the CO ligand with the uncoordinated CO, or a change in geometry such as a trigonal bipyramidal to square-planar equilibrium.

The reaction of the [Rh(*t*-Bu-xantphos)Cl] complexes with carbon monoxide was carried out with natural abundance CO. Despite this, a peak was observed for the coordinated carbonyl in the ^{13}C NMR spectra for the *t*-Bu-sixantphos and *t*-Bu-

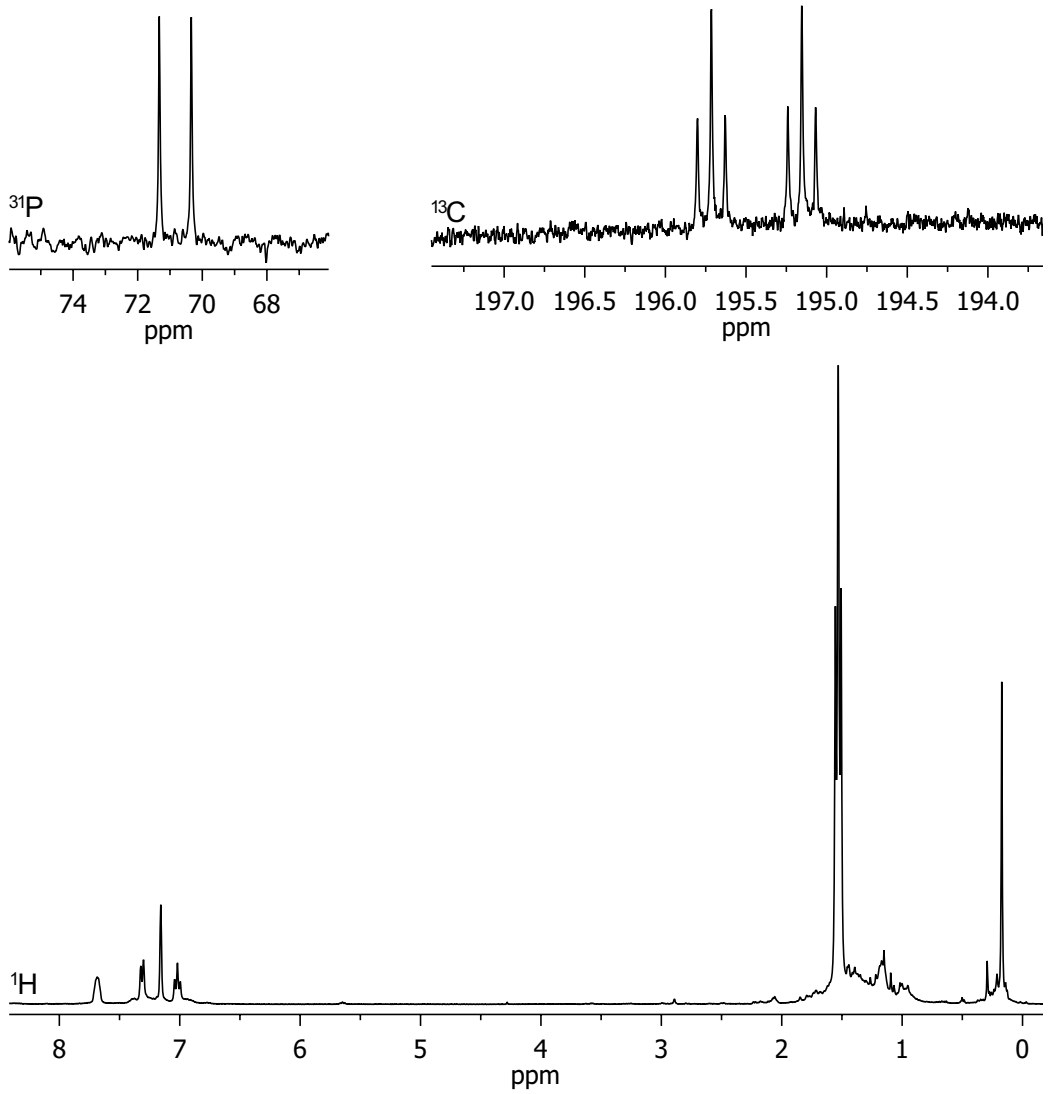

Figure 4.6: ^{31}P, ^{13}C and ^{1}H NMR spectra of the reaction of [Rh(*t*-Bu-sixantphos)Cl] with CO in C_6D_6.

xantphos products (Table 4.4 and Figure 4.6). This peak occurs at 195.5 ppm for *t*-Bu-sixantphos and 194.9 ppm for *t*-Bu-xantphos as a well resolved doublet of triplets indicating coupling to rhodium (J_{RhC} = 84.4 Hz for both) and two equivalent phosphorus atoms (J_{PC} = 13.0 and 12.4 Hz for *t*-Bu-sixantphos and *t*-Bu-xantphos respectively). These values are within the expected ranges for rhodium carbonyl complexes.

There are a number of different possible products for the reaction of the [Rh(*t*-Bu-xantphos-κ*P,O,P'*)Cl] complexes with carbon monoxide, due to the ability of rhodium(I) to form both square planar and trigonal bipyramidal structures, combined with the potential hemilability of the *t*-Bu-xantphos oxygen resulting in a κ*P,P'* bonding geometry. In addition, it is possible for either one or two carbonyl ligands to coordinate, displacing either the oxygen or the chloride ligand. The number of possibilities is decreased by the inability for the *t*-Bu-xantphos ligands to coordinate in a *cis* geometry on square planar centres (See Chapter 6 for further discussion) thus also eliminating trigonal bipyramidal products with the *t*-Bu-xantphos complex coordinated in a κ*P,P'* axial-equatorial position. Possible products from the reaction are outlined in Figure 4.7.

The majority of the possible structures outlined in Figure 4.7 can be discounted as they do no meet the symmetry requirements determined from the NMR spectra. The complexes consistent with the NMR spectra are the square planar complexes, [Rh(*t*-Bu-xantphos-κ*P,O,P'*)CO]Cl (B) and [Rh(*t*-Bu-xantphos-κ*P,P'*)$(CO)_2$]Cl (C); and the trigonal bipyramidal complexes, [Rh(*t*-Bu-xantphos-κ*P,O,P'*)$(CO)_2$]Cl (D) and *trans*-[Rh(*t*-Bu-xantphos-κ*P,P'*)$(CO)_2$Cl] (J). The mass spectra of the products from the reaction of the [Rh(*t*-Bu-xantphos)Cl] complexes with CO show a single major ion cluster. This cluster only differs for the three ligands due to the differences in the ligand structure. The cluster is consistent with a [Rh(*t*-Bu-xantphos)(CO)]$^+$ ion in both mass/charge ratio and isotopic distribution. While this supports the formulation of the product as a monocarbonyl entity, this ion cluster could result from any of the possible structures given in Figure 4.7 as mass spectrometry is performed under high vacuum, which may result in loss of CO from the dicarbonyl structures, and ionisation by loss of chloride ligands is very common for coordination complexes.[210]

As previously discussed (Section 4.1) the position of the *O-ipso* carbon peak in the ^{13}C NMR spectra for *t*-Bu-xantphos complexes can be used as a guide for the

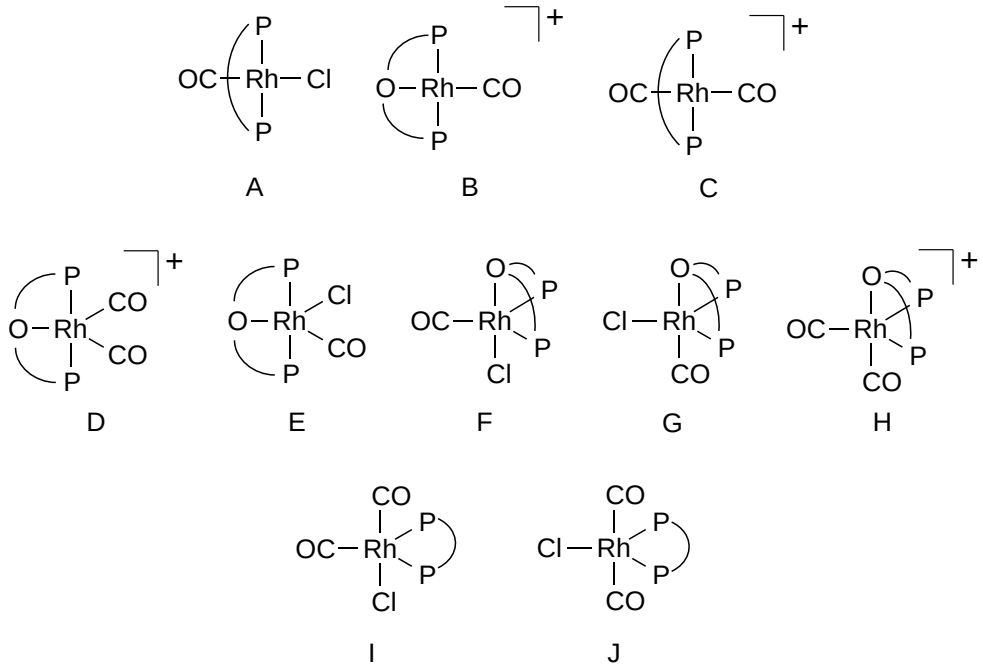

Figure 4.7: Possible products from reaction of [Rh(*t*-Bu-xantphos-κ*P,O,P'*)Cl] complexes with CO. First row: square planar complexes, second row: trigonal bipyramidal complexes with κ*P,O,P'* *t*-Bu-xantphos, and third row: trigonal bipyramidal complexes with κ*P,P'* *t*-Bu-xantphos ligands.

bonding mode of the ligand. A peak for the *O-ipso* carbon that has not shifted significantly from the *O-ipso* carbon peak for the free ligand is indicative of a κ*P,P'* coordination, while a peak shifted downfield by more than 2.0 ppm is indicative of a κ*P,O,P'* coordination. The products from this reaction show very little change in the position of the *O-ipso* peak compared to the free ligand (Table 4.5). Thus indicating that the coordination mode of the three *t*-Bu-xantphos ligands in these carbonyl complexes is most likely to be a bidentate κ*P,P'*mode.

The two possible square planar complexes [Rh(*t*-Bu-xantphos-κ*P,O,P'*)CO]Cl (B) and [Rh(*t*-Bu-xantphos-κ*P,P'*)$(CO)_2$]Cl (C) and one of the trigonal bipyramidal structures [Rh(*t*-Bu-xantphos-κ*P,O,P'*)$(CO)_2$]Cl (D) are positively charged. As such, poor solubility in C_6D_6 would be expected. However, the product of this reaction remains in a C_6D_6 solution with no signs of precipitation over a period of several weeks. This supports the formulation of the product as the trigonal bipyramidal *trans*-[Rh(*t*-Bu-xantphos)$(CO)_2$Cl] (J). Rhodium dicarbonyl com-

Table 4.5: ^{13}C Chemical shift and coupling for the *O-ipso* carbon in *t*-Bu-xantphos, [Rh(*t*-Bu-xantphos-κ*P,O,P'*)Cl] and carbonyl complexes ($\Delta\delta = \delta_{\text{complex}} - \delta_{\text{free ligand}}$).

	Free ligand		**[Rh(*t*-Bu-xantphos-κ*P,O,P'*)Cl]**			**[Rh(*t*-Bu-xantphos)(CO)$_2$Cl]**		
Ligand	δ^{13}**C/ppm**	J**/Hz**	δ^{13}**C/ppm**	$\Delta\delta$	J**/Hz**	δ^{13}**C/ppm**	$\Delta\delta$	J**/Hz**
t-Bu-Sixantphos	164.3	11.3	169.5	5.2	14.4	164.3	0.0	8.1
t-Bu-Thixantphos	155.3	13.0	157.4	2.1	16.8	154.9	-0.4	n.o.
t-Bu-Xantphos	155.8	12.0	158.9	3.1	16.3	155.6	-0.2	10.4

plexes are typically only stable below room temperature and under an atmosphere of carbon monoxide, readily losing CO under vacuum.[211,212] No change was observed in the ^{31}P or ^{1}H NMR spectra for the complexes in a C_6D_6 solution under an argon atmosphere after being under vacuum overnight. Likewise no change was observed for these samples after several weeks in a C_6D_6 solution under argon.

The infrared (IR) spectra of the [Rh(*t*-Bu-xantphos)$(CO)_2$Cl] complexes were obtained to determine any differences in the electronic properties of the three ligands. The C=O stretching frequency is sensitive to changes in the electron density on the metal centre. More electron rich metal centres will enhance the back-donation from the metal into the π^*-orbital on the carbonyl. As this is an anti-bonding orbital, increased electron density will result in decreased bond order observed as a lower C=O stretching frequency in the IR spectra. The IR spectra for the three [Rh(*t*-Bu-xantphos)$(CO)_2$Cl] complexes showed multiple stretches in the region where C=O stretches are observed. Indicative of multiple carbonyl ligands. The major C=O stretch occurs at 1979 cm^{-1} for all of the complexes irrespective of the *t*-Bu-xantphos ligand present. This indicates that the ligands are comparable in their electron donation capabilities in the $\kappa P,P'$ coordination mode.

Previous reports described the formation of *trans*-[Rh(CO)Cl(diphosphine)] complexes upon reaction of Ph-xantphos and DPEphos with $[Rh(CO)_2Cl]_2$.[213] These complexes appeared in the ^{31}P NMR spectra at 27.3 and 22.6 ppm with J_{RhP} = 119.2 and 123.5 Hz for Ph-xantphos and DPEphos respectively. In the ^{13}C NMR spectra singlets were observed for the carbonyl ligands at 180.9 and 183.3 ppm for Ph-xantphos and DPEphos respectively. The position of the carbonyl carbon in the *t*-Bu-xantphos complexes is at 195.5 or 194.9 ppm, indicating less shielding, which may be a result of the more electron rich rhodium centre in a five-coordinate complex. The rhodium chemistry of a more sterically demanding version of Ph-xantphos where the phenyl rings are replaced with *o*-tolyl groups has also been reported.[214] Again, this complex forms a *trans*-[Rh(CO)Cl(diphosphine)] complex. However, the analogous complexes with an iodide replacing the chloride ligand forms a square pyramidal structure with the oxygen coordinated to the rhodium. The C=O stretching frequencies for the *t*-Bu-xantphos carbonyl complexes (1979 cm^{-1}) occur between those for the *trans*-[Rh(CO)Cl(Ph-xantphos)] (1974 cm^{-1}) and *trans*-[Rh(CO)Cl(DPEphos)] (1985 cm^{-1}). The C=O stretch is

similar to [Rh(CO)Cl(PR_3)$_2$] with PR_3 = PPh_3 (1979 cm^{-1}) however, the strongly electron donating *tert*-butyl substituents on the *t*-Bu-xantphos ligands should result in a lower stretching frequency such as that where PR_3 = $PPhMe_2$ (1968 cm^{-1}).[9] This is further evidence that the *t*-Bu-xantphos complexes are not *trans*-[Rh(*t*-Bu-xantphos)(CO)Cl].

Based on this evidence we propose that the reaction of the [Rh(*t*-Bu-xantphos)Cl] complexes results in a trigonal bipyramidal structure with the *t*-Bu-xantphos ligand occupying two of the equatorial sites in a κ*P,P'* coordination mode. The remaining equatorial site is occupied by a chloride ligand and carbonyl ligands take up the two axial positions (Scheme 4.6). Trigonal bipyramidal structures (particularly those with carbonyl ligands) are known to undergo facile rearrangement to square pyramids.[212] This may be the cause of the broadening of the spectra for the *t*-Bu-thixantphos system, and the multiple peaks observed in the IR spectra. Ph-xantphos and DPEphos both form *trans*-[Rh(CO)Cl(diphosphine)], which would have a larger P-Rh-P angle than the [Rh(*t*-Bu-xantphos)(CO)$_2$Cl] complexes. This is counterintuitive as the natural bite-angle is larger for the *t*-Bu-xantphos ligands than for Ph-xantphos. However, it is possible that the *trans*-[Rh(CO)Cl(diphosphine)] are actually square pyramidal complexes with a weak interaction of the ether bridge in the diphosphine ligands, thus relieving the strain of such a wide bite-angle.

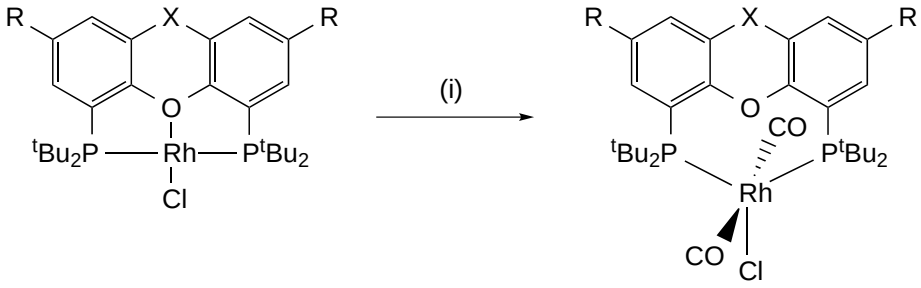

Scheme 4.6: Reaction of [Rh(*t*-Bu-xantphos)Cl] with carbon monoxide. *Reagents and conditions:* (i) 10 mins CO, C_6D_6, 3 days.

Dicarbonyl complexes have been reported for Ph-xantphos ligands, for example, Ph-sixantphos, Ph-thixantphos and Ph-xantphos form [Rh(CO)$_2$H(Ph-xantphos)] complexes.[30] The diphosphine ligands coordinate in a *bis*-equatorial-κ*P,P'* mode, while the hydride occupies an axial site and the two carbonyls are in one equa-

torial and one axial site. Little difference is observed between the three ligands with the ^{31}P NMR peaks between 21.1 and 23.4 ppm (J_{RhP}= 123.9–127.9 Hz). Interestingly, although the two carbonyl ligands are inequivalent, only one carbonyl peak was reported, occurring as a doublet of triplets at 201.1 ppm with J_{RhC} = 65.7 Hz, and J_{PC}= 10.6 Hz for the Ph-xantphos complex. No explanation was given for this but it may be due to the rapid exchange of one of the carbonyl ligands with free CO leading to broadening of the second ^{13}C peak.

4.4 Dioxygen and Oxo Complexes

The reaction of rhodium(I) complexes with oxygen is well established with numerous examples published.[215,216] Many aspects of the oxidation of Wilkinson's complex, [RhCl(PPh_3)$_3$], to form a distorted octahedral complex with a side-on η^2-O_2 ligand have been reported, including the synthesis,[217,218] degradation[219] and use as an oxidation catalyst.[220,221] Numerous other rhodium dioxygen complexes have been reported with monophosphine[222–231] and diphosphine[232–239] ligands. Reports of rhodium dioxygen complexes with heterobidentate[240–243] and tridentate[244–250] ligands are also numerous. However, despite the number of rhodium complexes of Ph-xantphos and other xantphos derivatives, no rhodium dioxygen complexes of these ligands have been reported. To address this, the reactivity of the [Rh(*t*-Bu-xantphos)Cl] and [Rh(*t*-Bu-xantphos)Cl(H)$_2$] complexes with all three ligands towards oxygen was investigated.

Bubbling air through a C_6D_6 solution of each of the [Rh(*t*-Bu-xantphos-κ*P,O,P'*)Cl] complexes resulted in the rapid formation of a new complex as expected (Scheme 4.7). The dihydride complexes, [Rh(*t*-Bu-xantphos-κ*P,O,P'*)Cl(H)$_2$], also reacted rapidly with air to form the same complexes. The ^{31}P NMR spectra of the resulting [Rh(*t*-Bu-xantphos)Cl(η^2-O_2)] complexes showed a single doublet (39.4–40.5) shifted upfield from the [Rh(*t*-Bu-xantphos)Cl] complex by between 4.8 and 7.5 ppm (Table 4.6). The value of J_{RhP} decreased by 37.8–41.6 Hz, to 100.7–102.2 Hz. This is consistent with a change in the oxidation state from rhodium(I) to rhodium(III) and the corresponding decrease in the s-character of the metal hybrid orbital, resulting from the change in coordination geometry from square planar to pseudo-octahedral.

Table 4.6: Selected NMR data for [Rh(*t*-Bu-xantphos-κ*P,O,P'*)Cl(η^2-O_2)] in C_6D_6 ($\Delta\delta = \delta_{\text{complex}} - \delta_{\text{free ligand}}$).

	^{31}P				^{13}C *O-ipso*		
Diphosphine	δ/**ppm**	$\Delta\delta$/**ppm**	J_{RhP}/**Hz**	ΔJ_{RhP}/**Hz**	δ/**ppm**	$\Delta\delta$/**ppm**	J/**Hz**
t-Bu-Sixantphos	39.4	4.8	102.2	37.8	166.7	2.4	9.8
t-Bu-Thixantphos	39.0	7.5	101.5	40.0	155.9	0.6	12.5
t-Bu-Xantphos	40.5	7.2	100.7	41.6	157.3	1.5	11.5

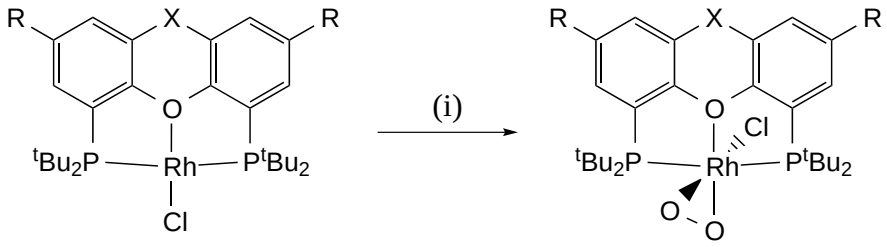

Scheme 4.7: Reaction of [Rh(*t*-Bu-xantphos)Cl] complexes with oxygen. *Reagents and conditions:* (i) 10 mins Air, C_6D_6, 24 hours.

The ^{1}H and ^{13}C NMR spectra for the three [Rh(*t*-Bu-xantphos)Cl(η^2-O_2)] complexes showed a loss of symmetry compared to the starting [Rh(*t*-Bu-xantphos)Cl] complexes. A single peak was observed for the methyl substituents on the aromatic rings of the *t*-Bu-thixantphos. However, two peaks were present for the methyl substituents on the carbon or silicon bridging atoms in both the *t*-Bu-xantphos and *t*-Bu-sixantphos complexes. In all three complexes, two different sets of peaks for the *tert*-butyl groups were observed. Together, this data indicates the presence of a plane of symmetry perpendicular to the backbone through the bridging atoms, and the absence of a plane of symmetry parallel to the backbone. Interestingly, the two methyl groups in the *t*-Bu-sixantphos and *t*-Bu-xantphos complexes occur in very different positions; one of the methyl groups is shifted upfield and the other downfield in both the ^{1}H and ^{13}C NMR spectra, compared to the [Rh(*t*-Bu-xantphos-κ*P,O,P'*)Cl] starting material and [Rh(*t*-Bu-xantphos-κ*P,O,P'*)Cl$(H)_2$]. The effect is more pronounced for *t*-Bu-xantphos than *t*-Bu-sixantphos. In addition, one of the *tert*-butyl groups in each of the three *t*-Bu-xantphos ligands is well resolved as a virtual triplet for all the ^{1}H and ^{13}C NMR environments, while the other *tert*-butyl group has a well resolved virtual triplet for the quaternary carbon while the terminal carbon and protons are broad.

In the ^{13}C NMR spectra for the [Rh(*t*-Bu-xantphos)Cl(η^2-O_2)] complexes, the shift in the position of the *O-ipso* carbon peak from the free ligand was lower than for the [Rh(*t*-Bu-xantphos)Cl] complexes (Table 4.6). In particular, the *t*-Bu-thixantphos dioxygen complex exhibited a shift in position of only 0.6 ppm. However, the effect is typically reduced for the *t*-Bu-thixantphos ligand system, in fact for [Rh(*t*-Bu-thixantphos)Cl$(H)_2$] a shift of only 0.1 ppm was observed despite a

κ*P,O,P'* coordination geometry. This difference may be due to the electron donation from the methyl groups on the aromatic system of *t*-Bu-thixantphos, which may mitigate the loss of electron density in the O-*ipso* carbon upon oxygen coordination. The shifts for *t*-Bu-sixantphos and *t*-Bu-xantphos are both consistent with κ*P,O,P'* coordination in the [Rh(*t*-Bu-xantphos)Cl(η^2-O_2)] complexes.

Slow evaporation of a C_6D_6 solution of [Rh(*t*-Bu-xantphos-κ*P,O,P'*)Cl(η^2-O_2)] produced dark red crystals suitable for X-ray diffraction. The crystal structure (Figure 4.8) displayed some substitutional disorder with the dioxygen ligand replaced in approximately 15% of the sites by an oxo ligand (Figure 4.9). The complexes co-crystallised in the orthorhombic space group *Pbca*. Crystallographic data is given in Table 4.7 and selected bond lengths and angles are given in Table 4.8.

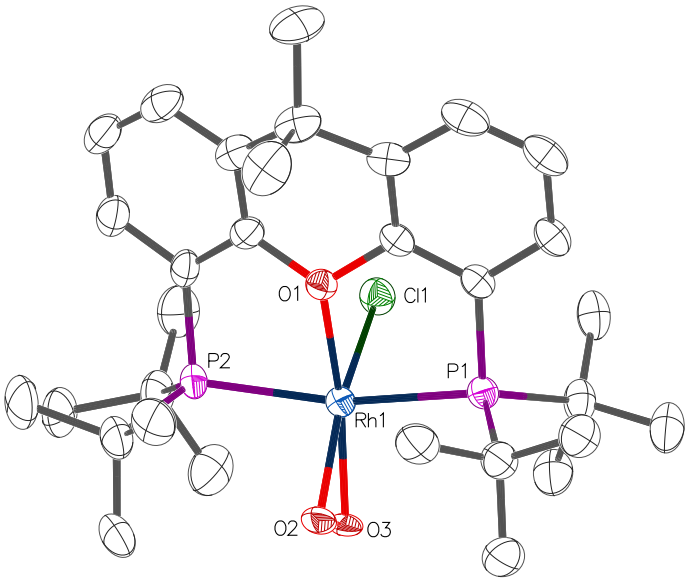

Figure 4.8: X-ray crystal structure of [Rh(*t*-Bu-xantphos)Cl(η^2-O_2)] (50% probability thermal ellipsoids). Hydrogen atoms omitted for clarity.

The O-O bond lengthens upon coordination due to back-bonding from the metal into the anti-bonding π^*-orbital of the ligand. In the crystal structure of [Rh(*t*-Bu-xantphos-κ*P,O,P'*)Cl(η^2-O_2)], the O2-O3 bond length is 1.424(5) Å, lengthened by 0.21 Å from the bond length in molecular oxygen of 1.21 Å.[251] This length is typical for rhodium dioxygen complexes with the average O-O bond length being 1.423 Å.[68] The Rh-O bond lengths for the dioxygen ligand are different, with the oxygen *trans* to chloride having a longer bond by 0.054 Å. The oxygen *trans* to

Table 4.7: Crystallographic Data and Structure Refinement of [Rh(*t*-Bu-xantphos)Cl(η^2-O_2)].

Empirical formula	**$C_{31}H_{48}ClO_{2.85}P_2Rh$**
Formula weight	666.53
Temperature/K	120.01(10)
Crystal system	orthorhombic
Space group	Pbca
a/Å	11.84223(17)
b/Å	20.2961(3)
c/Å	26.8069(4)
$\alpha/^\circ$	90
$\beta/^\circ$	90
$\gamma/^\circ$	90
Volume/Å^3	6443.06(17)
Z	8
ρ_{calc} mg/mm^3	1.374
µ/mm	6.206
F(000)	2790.0
Crystal size/mm	0.1092 x 0.0738 x 0.0159
Radiation	CuKα (λ = 1.54184)
2θ range for data collection	6.594 to 147.8°
Index ranges	-14 $\leq$ h $\leq$ 13, -25 $\leq$ k $\leq$ 21, -30 $\leq$ l $\leq$ 33
Reflections collected	45616
Independent reflections	6481 [R_{int} = 0.0631, R_{sigma} = 0.0332]
Data/restraints/parameters	6481/399/367
Goodness-of-fit on F^2	1.035
Final R indexes [I>=2σ (I)]	R_1 = 0.0439, wR_2 = 0.1145
Final R indexes [all data]	R_1 = 0.0550, wR_2 = 0.1226
Largest diff. peak/hole / e Å^{-3}	1.40/-0.78

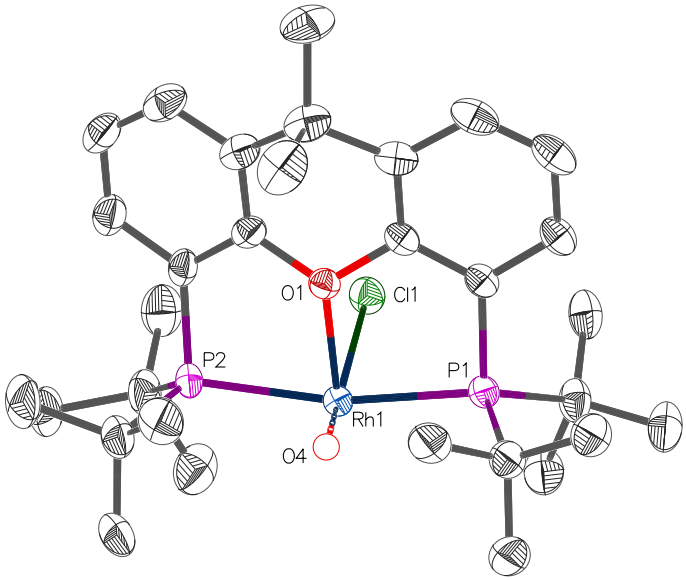

Figure 4.9: X-ray crystal structure of [Rh(*t*-Bu-xantphos-κ*P,O,P'*)Cl(O)] (50% probability thermal ellipsoids). Hydrogen atoms omitted for clarity.

Table 4.8: Selected bond distances (Å) and angles (°) of [Rh(*t*-Bu-xantphos)Cl(η^2-O_2)].

Bond distances (Å)		**Bond angles (°)**	
P1-Rh	2.3391(8)	P1-Rh-P2	166.01(3)
P2-Rh	2.3237(9)	Cl1-Rh-O2	158.18(10)
O1-Rh	2.193(2)	Cl1-Rh-O4	161.2(3)
O2-Rh	2.016(3)	O1-Rh-O3	161.33(12)
O3-Rh	1.962(3)	Ring1-Ring2	26.65(12)
Cl1-Rh	2.3871(9)	O1-C(bridge)-CH_3	165.9(3)
O2-O3	1.424(5)	O1-C(bridge)-CH_3	94.73
O4-Rh	1.669(10)		

chloride has a typical Rh-O bond length for rhodium dioxygen complexes (average = 2.017 Å), while the oxygen *trans* to the ether bridge is shorter than average with a length of 1.962(3) Å. This shorter bond results from the low *trans*-influence of the ether oxygen.[252,253] Only three complexes with shorter Rh-O bonds in a dioxygen complex have been reported (Figure 4.10).[254–256] These complexes have the dioxygen atoms *trans* to nitrogen or oxygen donor atoms, which are known to have low *trans*-influences.[252,253]

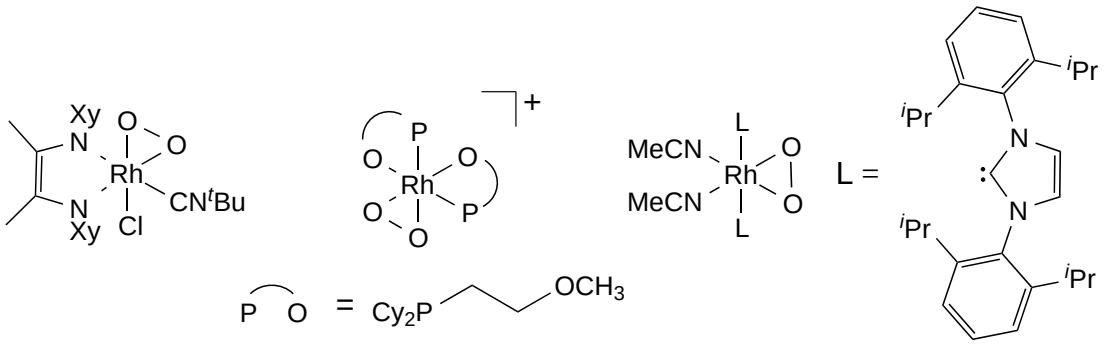

Figure 4.10: Rhodium dioxygen complexes with shorter Rh-O bonds than [Rh(*t*-Bu-xantphos-κ*P,O,P'*)Cl(η^2-O_2)].

The [Rh(*t*-Bu-xantphos-κ*P,O,P'*)Cl(η^2-O_2)] complexes, with *t*-Bu-sixantphos or *t*-Bu-xantphos, show two distinct methyl environments in the ^{1}H and ^{13}C NMR spectra for the bridgehead methyls. This indicates a loss of symmetry, giving two distinct faces of the *t*-Bu-xantphos ligands. From the crystal structure (Figure 4.8) the chloride ligand sits on the same side as the concave face of the ligand while the dioxygen ligand occupies the position pseudo-*trans* to the oxygen bridge of the ligand. This geometry leaves more space *trans* to the chloride, resulting in the curvature of the ligand to occupy this free space and the tipping of the methyl groups away from the chloride. The angle O1-C(bridge)-CH_3 is very different for the two methyl groups; 165.9(3) and 94.7(3)° for the concave and convex methyls, respectively and dihedral angles to the first C-H in the aromatic ring of 24.8 and 42.8°. This positioning results in quite different chemical environments for the two methyl groups, resulting in the different chemical shifts in the NMR spectra.

Although rhodium xantphos complexes are well studied due to their high catalytic activity and selectivity for hydroformylation, to the best of our knowledge,

no rhodium dioxygen complexes have been reported with any xantphos ligands. Only one transition metal complex with a xantphos related ligand and an η^2-O_2 ligand has been reported; [Ru(Ph-xantphos)(PPh_3)(η^2-O_2)H][BAr^F_4].[257] This complex formed by reaction of [Ru(Ph-xantphos)(PPh_3)HCl] with Na[BAr^F_4] followed by filtration then stirring in the air for 10 minutes. Similarly to the rhodium *t*-Bu-xantphos complexes, the *mer*-κ*P,O,P'* coordination is retained upon reaction with oxygen. The dioxygen ligand occupies the site *trans* to the hydride, where the chloride had previously been located.

The X-ray crystal structure of [Rh(*t*-Bu-xantphos)Cl(η^2-O_2)] contains substitutional disorder with approximately 15% of the dioxygen molecules replaced by an oxo ligand (Figure 4.9). The oxo complex shows a slightly distorted square-based pyramid structure with the ether bridge of the *t*-Bu-xantphos ligand occupying the apex, and *trans* coordination of the phosphorus atoms. The rhodium oxo bond (1.669(10) Å) is much shorter than the rhodium oxygen bond lengths in [Rh(*t*-Bu-xantphos)Cl(η^2-O_2)], consistent with a higher bond order. In addition, the rhodium oxo bond is the shortest crystallographically determined Rh-O bond.

To the best of our knowledge, this is the first example of crystallographic evidence for a rhodium(III) oxo complex. Only one previous crystal structure has been reported for a rhodium oxo complex (Figure 4.11).[258] The literature structure contains a rhodium(V) dimer with each rhodium atom coordinated to two oxo ligands, a DMSO ligand and an oxygen-nitrogen-sulfur heterotridentate ligand. The oxo *trans* to the DMSO ligand has a bond length of 1.701(5) Å, while the oxo *trans* to the nitrogen donor is slightly longer at 1.712(5) Å. Both of these are slightly longer than the Rh-O bond length in the [Rh(*t*-Bu-xantphos)Cl(O)] structure (1.669(10) Å). The average bond length for a transition metal oxo is 1.689 Å with a lower quartile at 1.671 Å.[68] This indicates that the bond length for the rhodium(III) oxo is in the lowest quarter of crystallographically determined bond lengths for transition metal oxo complexes; however, the bond is well within the range (1.106–2.956 Å).

Transition metal oxo complexes have long been studied as they have been implicated to have roles in biological systems,[259–262] C-H activation[263,264] and various oxidation reactions.[219,265,266] A terminal oxo ligand is a very strong π-donor ligand, thus the strongest coordination occurs with high oxidation state, early tran-

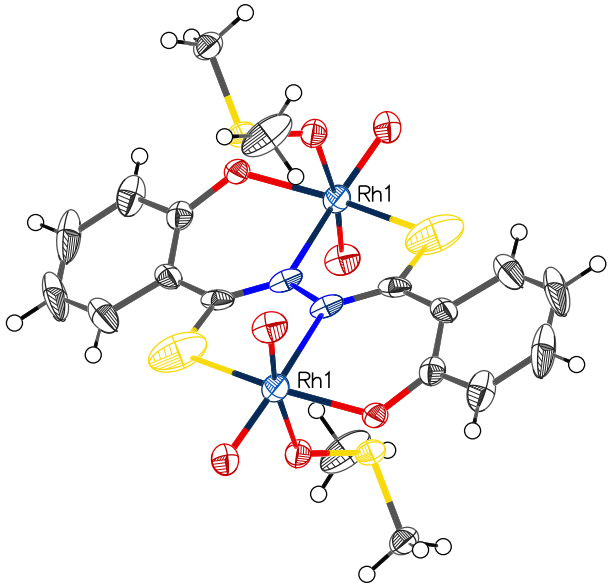

Figure 4.11: An X-ray crystal structure for the rhodium(V) oxo complex $[(RhO_2)_2(C_6H_4(O)-C(=S)-N=N-C(=S)(O)C_6H_4)(DMSO)_2]$.[258]

sition metals.[267] A review of transition metal oxo complexes published in 1987 stated that "M=O groups are stabilized at metal centres with an oxidation state of no less than +4 and no more than four d electrons".[265] This has led to the proposition of an "oxo-wall," a barrier between groups 8 and 9 of the periodic table, explaining the lack of tetragonal oxo complexes for group 9–11 transition metals.[268] This effect arises as the orbital splitting in an octahedral oxo complex lowers the symmetry of the t_{2g} orbitals to $b_2(d_{xy})$ and $e(d_{xz},d_{yz})$ and the metal-ligand antibonding e_g orbitals to $b_1(d_{x^2-y^2})$ and $a_1(d_{z^2})$ with the $e(d_{xx},d_{yz})$ and d_{z^2}, orbitals destabilised.[269] The more d-electrons that are present, the lower the bond order to the oxo, resulting in decreased stability. The [Rh(*t*-Bu-xantphos-κ*P*,*O*,*P*')Cl(O)] complex is of square pyramidal geometry so does not violate the oxo-wall proposition. The poor electron donation from the central ether bridge may lead to increased stability compared to other square pyramidal structures.

Despite the instability of terminal oxo complexes of the late transition metals, some examples do exist (Figure 4.12). A platinum(II) complex with a PCN pincer ligand was reacted with a freshly prepared acetone solution of dioxirane, resulting in formation of a platinum(IV) oxo complex.[266] This complex degrades over a period of 7–10 hours *via* an intramolecular oxygen transfer reaction from the

platinum to the phosphorus atom. The oxo also readily reacts with water (forming a bishydroxy, aquo complex), hydrogen (liberating water), carbon monoxide (forming CO_2 and a carbonyl complex), potassium hydride (to form a hydroxy complex) and oxidises triphenyl phosphine. This demonstrates a range of different potential uses for late transition metal oxo complexes. An iridium(V) oxo complex has also been reported, in this case the oxo complex was synthesised by reaction of [Ir(mes)$_3$] (mes = mesityl) with trimethylamine oxide (Figure 4.12).[270] A rhodium oxo complex was recently reported by Caulton *et al.* from reaction of a rhodium(III) hydride complex containing a metalled PNP ligand reacting with trimethylamine oxide, pyridine *N*-oxide or N_2O.[249,271] This complex undergoes oxo transfer reactions with trimethylphosphine and carbon monoxide.

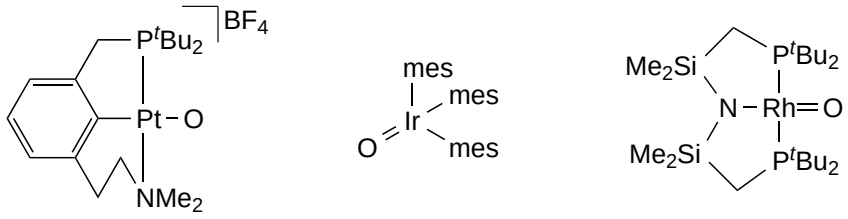

Figure 4.12: Previously reported late transition metal oxo complexes, mes = 2,4,6-trimethylphenyl.[249,266,271]

Given the novelty of the proposed rhodium(III) oxo complex, the synthesis of [Rh(*t*-Bu-xantphos-κ*P,O,P'*)Cl(O)] complexes with all three *t*-Bu-xantphos ligands was attempted using trimethylamine oxide, as this has been used previously in the synthesis of late transition metal oxo complexes,[270,271] and the by-product (trimethylamine) should be a poor ligand and result in little reactivity. Reaction between [Rh(*t*-Bu-sixantphos-κ*P,O,P'*)Cl] and trimethylamine oxide resulted in the immediate formation of the [Rh(*t*-Bu-sixantphos-κ*P,O,P'*)Cl(η^2-O_2)] complex, together with a small amount of the ligand oxide and uncoordinated *t*-Bu-sixantphos, over time peaks due to the [Rh(*t*-Bu-sixantphos-κ*P,O,P'*)Cl] complex began to reappear. This result may be due to the incomplete dissolution of [Rh(*t*-Bu-sixantphos-κ*P,O,P'*)Cl] in the CD_2Cl_2 reaction solvent, meaning that the amount in solution was over-oxidised before the remainder dissolved. Unfortunately, as [Rh(*t*-Bu-sixantphos-κ*P,O,P'*)Cl] is a dark brown colour it is challenging to gauge full dissolution. After four days at room temperature a small amount of product was evident in the ^{31}P NMR spectrum at 70.5 ppm (J_{RhP} = 114.1 Hz).

Reacting [Rh(*t*-Bu-thixantphos-κ*P,O,P'*)Cl] and trimethylamine oxide resulted in a mixture of compounds. Analysis by ^{31}P NMR showed 22.9% free *t*-Bu-thixantphos ligand indicating possible degradation of the rhodium complexes formed, [Rh(*t*-Bu-sixantphos-κ*P,O,P'*)Cl(η^2-O_2)] (8.6%), [Rh(*t*-Bu-thixantphos-κ*P,O,P'*)Cl] starting material (64.4%), and a new complex at 40.9 ppm (J_{RhP} = 90.4 Hz) (4.1%). After 10 days no [Rh(*t*-Bu-thixantphos-κ*P,O,P'*)Cl] or unidentified complex remained and the reaction mixture was primarily the dioxygen complex and a further new complex at 74.1 ppm (J_{RhP} = 116.3 Hz).

The reaction of [Rh(*t*-Bu-xantphos-κ*P,O,P'*)Cl] with trimethylamine oxide was initially carried out at -80 °C in order to prevent over-oxidation. However, initially the slow generation of the dioxygen species was observed with no evidence for any intermediate or otherwise. The reaction was allowed to warm to room temperature and after 24 hours a small signal was observed at 42.6 ppm (J_{RhP} = 90.4 Hz) comprising 4.2% of the reaction mixture. However, around 70.5% of the reaction mixture was the dioxygen complex and the remainder was the Rh(I) starting material. Similarly to the *t*-Bu-thixantphos reaction, this reaction slowly converted into a species at 75.1 ppm (J_{RhP} = 116.3 Hz).

The initial unknown complexes formed by the oxidation of [Rh(*t*-Bu-xantphos-κ*P,O,P'*)Cl] and [Rh(*t*-Bu-thixantphos-κ*P,O,P'*)Cl] had similar NMR spectra. In the ^{31}P NMR spectra a doublet was observed at 40.9 or 42.6 ppm, slightly downfield of the dioxygen complex. The values of J_{RhP} were identical with either ligand (90.4 Hz). The decrease from the values in the rhodium(I) starting materials (142.3 and 140.0 Hz for *t*-Bu-xantphos and *t*-Bu-thixantphos respectively) clearly indicates oxidation to a rhodium(III) species. ESI – Mass spectrometry was performed on the reaction mixtures for all three *t*-Bu-xantphos ligands. In all cases a molecular ion peak was observed consistent in both mass/charge ratio and isotopic pattern, indicative of an oxo complex ionising *via* loss of a chloride ligand.

Late transition metal oxo complexes are generally considered unstable and likely to undergo further reaction. The reactions of [Rh(*t*-Bu-xantphos-κ*P,O,P'*)Cl] with trimethylamine oxide were performed in CD_2Cl_2. As previously discussed (see Section 2.3) halocarbon molecules are not stable for extended periods of time in the light, undergoing a photo-catalysed degradation forming small amounts of hydrochloric acid (deuterium chloride in the case of NMR solvents).[138] Hereby we propose that the oxo complex likely reacted with the small amounts of deu-

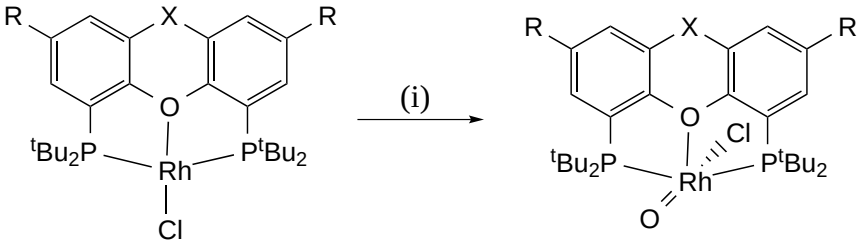

Scheme 4.8: Reaction of [Rh(*t*-Bu-xantphos)Cl] with trimethylamine oxide. *Reagents and conditions:* 1eq. $ONMe_3$, CD_2Cl_2.

terium chloride that formed over time, thus producing a hydroxy ligand (Scheme 4.9). The remaining coordination site on the metal would then likely be occupied by the chloride ion. The platinum oxo complex reported by Milstein *et al.* underwent reaction with water to form a bishydroxy complex while the rhodium oxo reported by Caulton *et al.* underwent metallation of one of the *tert*-butyl substituents on the phosphorus donor also forming a hydroxy ligand.[249]

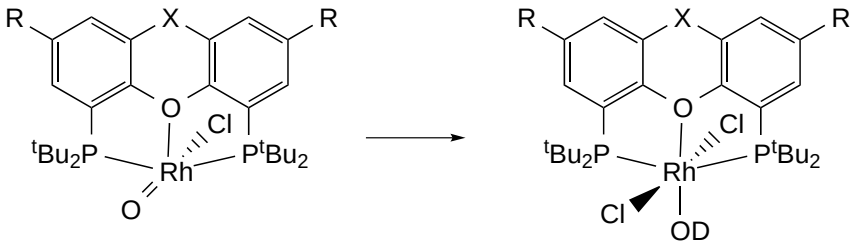

Scheme 4.9: Proposed reaction of [Rh(*t*-Bu-xantphos)Cl(O)] with DCl.

Unfortunately, due to time constraints, the formation of the rhodium oxo complexes was not studied in more depth.

4.5 Summary

The coordination chemistry of *t*-Bu-sixantphos, *t*-Bu-thixantphos, and *t*-Bu-xantphos with rhodium in both the +1 and +3 oxidation states was explored. The three ligands reacted readily with $[Rh(coe)_2Cl]_2$ forming [Rh(*t*-Bu-xantphos-κ*P,O,P'*)Cl]

complexes. These complexes readily split hydrogen to form [Rh(*t*-Bu-xantphos-κ*P,O,P'*)Cl(H)$_2$] complexes with a meridional *t*-Bu-xantphos ligand and *cis* hydrides. Little difference in the position and coupling constants of the hydride *trans* to the chloride was observed in the ^{1}H NMR spectra of the three complexes. The values of J_{RhH} for the hydride *trans* to the oxygen donor decreased with increasing bite-angle. Suggesting a *trans* influence series of *t*-Bu-xantphos > *t*-Bu-thixantphos > *t*-Bu-sixantphos. This difference may be related to the ease with which the ligands form wide bite-angle complexes.

The three [Rh(*t*-Bu-xantphos-κ*P,O,P'*)Cl] complexes were reactive towards carbon monoxide, forming [Rh(*t*-Bu-xantphosκ-*P,P'*)(CO)$_2$Cl]. In contrast, Ph-xantphos and DPEphos formed *trans*-[Rh(CO)Cl(diphosphine)] complexes. The *t*-Bu-xantphos ligands were coordinated in a κ-*P,P'* bisequatorial mode with an equatorial chloride and two axial carbonyl ligands. This shows a clear difference in the reactivity of the *t*-Bu-xantphos ligands when compared with Ph-xantphos.

The rhodium dioxygen complexes, [Rh(*t*-Bu-xantphos)Cl(η^2-O$_2$)] with the *t*-Bu-xantphos ligands were synthesised by reaction of [Rh(*t*-Bu-xantphos-κ*P,O,P'*)Cl] with the air. These are the first rhodium dioxygen complexes with xantphos ligands and only the second with any transition-metals. The X-ray crystal structure of [Rh(*t*-Bu-xantphos)Cl(η^2-O$_2$)] was reported showing a distorted octahedral configuration with a meridional coordination of the *t*-Bu-xantphos ligand. The O-O bond length was typical for rhodium dioxygen complexes. The Rh-O bond length for the oxygen *trans* to the oxygen donor of the *t*-Bu-xantphos ligand was the fourth shortest Rh-O length for a dioxygen complex that have been reported, indicating the low *trans*-influence of the *t*-Bu-xantphos oxygen.

The X-ray crystal structure of [Rh(*t*-Bu-xantphos)Cl(η^2-O$_2$)] was disordered with the dioxygen ligand replaced in around 15% of sites by an oxo ligand. To the best of our knowledge this is the first crystallographic evidence of a rhodium(III) oxo complex. The Rh-O bond length was 1.669(10) Å which is the shortest reported rhodium oxo bond length. The complex is a distorted square pyramid, so does not violate the "oxo-wall" theory. Attempts to synthesise [Rh(*t*-Bu-xantphos-κ*P,O,P'*)Cl(O)] by reaction of [Rh(*t*-Bu-xantphos-κ*P,O,P'*)Cl] with trimethylamine oxide were promising for *t*-Bu-thixantphos and *t*-Bu-xantphos, showing a new peak in the ^{31}P NMR spectra, which slowly converted into a different species, and mass spectra consistent with [Rh(*t*-Bu-xantphos-κ*P,O,P'*)(O)]$^+$.

Chapter 5

Coordination Complexes with Platinum(0) and Palladium(0)

Coordination complexes of palladium and platinum have a range of uses. Perhaps the most well-known platinum complex is $[PtCl_2(NH_3)_2]$ (cisplatin). Cisplatin, distributed under the trade name Platinol, is a widely used chemotherapeutic which is used in conjunction with other therapies for the treatment of various cancers, most commonly tumours including sarcomas, carcinomas and lymphomas.[2,3] A further two platinum complexes (carboplatin and oxaliplatin) have been approved for use in chemotherapy worldwide, with other complexes approved in select countries.[3,272]

Palladium complexes are some of the most common coordination complexes used for homogeneous catalysis, with applications in a wide-range of reactions including cross-coupling, allylic alkylation and various carbonylation reactions among many others.[6,32,149,273–276] These transformations are highly important for industrial processes and laboratory scale total syntheses.[277–279] The high reactivity of these species can make palladium complexes and their catalytic processes difficult to study. Platinum complexes are typically more inert than their corresponding palladium analogues to processes such as ligand exchange and redox changes.[280] The spin active isotope platinum-195 (34% abundant) can result in platinum coupling in the ^{1}H, ^{13}C, and ^{31}P NMR spectra, the coupling constants of which, can give additional information regarding the geometry and bonding in the complex. Platinum and palladium are otherwise very similar metals, which makes the additional insight gained from platinum models valuable when exam-

ining similar chemistry with palladium.

Prior to the start of this work four studies had been published investigating the catalytic activity of *t*-Bu-xantphos.[84–87] Two of these studies investigated the catalytic activity of *t*-Bu-xantphos palladium systems and one investigated platinum systems. In all cases little to no reactivity was observed with *t*-Bu-xantphos systems, whereas the corresponding Ph-xantphos reactions gave 40–99% conversions. This suggests differences in the coordination chemistry of the two ligands towards palladium and platinum. However, no studies have investigated the coordination chemistry of *t*-Bu-xantphos with either palladium or platinum, in order to explain the different activities. A crystal structure of [Pd(*t*-Bu-xantphos)Cl_2] was reported to the CSD in 2011 (CSD-XARXAR).[68] The crystal structure has three molecules in the asymmetric unit with bite-angles of 160.59(4), 161.97(3) and 161.31(4)°, compared to 100.61(5) and 100.92(7)° for [Pd(Ph-xantphos)Cl_2] with different solvates.[68,145,281] The difference in the bite-angles and geometries of the complexes that form may explain the difference in the catalytic reactivity of the complexes.

Since the start of this work, five further papers have been published investigating the catalytic activity of palladium complexes with *t*-Bu-xantphos.[93–95,97,98] In the palladium-catalysed Suzuki cross-coupling and the hydroesterification of methyl oleate little activity was observed with *t*-Bu-xantphos, whereas the Ph-xantphos complexes gave high yields.[97,98] However, in the *N*-alkylation of amines with primary and secondary alcohols, the *t*-Bu-xantphos system was more active than the Ph-xantphos system, with *t*-Bu-xantphos showing near quantitative conversion at 100 °C, while the Ph-xantphos system gave only 63% conversion at 110 °C. Similarly, the methylation of alkynyl C-H bonds with dimethyl sulfonium ylides using a palladium complex with *t*-Bu-xantphos went to 46% conversion, while Ph-xantphos gave only 15%.[95] A palladium complex with a monodentate Ph-xantphos or *t*-Bu-xantphos ligand was tested in the aminocarbonylation of heteroaryl bromides, and showed no reactivity with *t*-Bu-xantphos while Ph-xantphos gave a 92% isolated yield.[93] Together these studies support the premise that the coordination chemistry of *t*-Bu-xantphos and Ph-xantphos are distinct, likely as a result of the differences in the bite-angles and steric bulk between the ligands. However, no research into this area has yet been reported.

The coordination chemistry of Ph-xantphos with palladium has been the subject

of a number of different studies,[73–75,79,115,282,283] though no research into the coordination chemistry of the *t*-Bu-xantphos ligands with platinum has been reported. The main focus of this chapter is the investigation into the coordination chemistry of the three *t*-Bu-xantphos ligands with a range of platinum(0) and palladium(0) precursors. Some reactivity of the resulting complexes towards small molecules is also presented. A brief investigation into the coordination chemistry of Ph-thixantphos with platinum(0) will also be presented for comparative purposes. The subsequent chapter will address the coordination chemistry of the *t*-Bu-xantphos ligands with platinum(II) and palladium(II) starting materials.

5.1 Reactions of Ph-thixantphos with Platinum(0) Precursors

The 1:1 reaction between [Pt(nb)$_3$] (nb = norbornene, bicyclo[2.2.1]hept-2-ene) and Ph-thixantphos in C_6D_6 rapidly formed two products but did not progress further. The ^{31}P NMR spectrum shows one sharp peak at 20.0 ppm (J_{PtP} = 3470 Hz, 39.6%) and two overlapping broad singlets ranging from 0 to -10 ppm (60.4%). The platinum-phosphorus coupling constant on the sharp signal is consistent with a mono-alkene complex such as, [Pt(nb)(Ph-thixantphos)].[284] The ^{1}H NMR spectrum showed a number of aromatic signals together with peaks that can be ascribed to [Pt(nb)$_3$] and uncoordinated norbornene, as well as new alkyl and alkene proton signals. This suggests that the complex appearing at 20.0 ppm in the ^{31}P NMR spectrum is [Pt(nb)(Ph-thixantphos)], while the other complex has more than one molecule of Ph-thixantphos per platinum atom. Attempts to synthesise [Pt(nb)(Ph-thixantphos)] exclusively were unsuccessful, as were attempts to isolate the complex from the product mixture. As such, this species was not characterised fully.

The reaction between Ph-thixantphos and [Pt(nb)$_3$] was repeated using two equivalents of Ph-thixantphos per platinum. In this case only the broad species between 0 and -10 ppm was observed by ^{31}P NMR spectroscopy. Upon removal of the displaced norbornene from the system, the ^{1}H NMR spectrum displayed only aromatic signals. This indicates that the complex formed under these conditions does not contain an alkene ligand, nor is there any evidence for uncoordinated

Ph-thixantphos ligand. This is consistent with the formation of [Pt(Ph-thixantphos)$_2$] (Scheme 5.1).

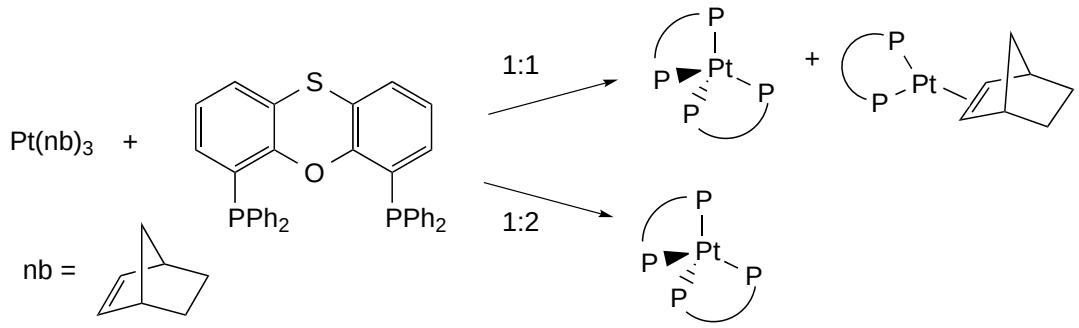

Scheme 5.1: Reaction of Ph-thixantphos with tris(norbornene)platinum.

Yellow crystals of [Pt(Ph-thixantphos$_2$]·2.5 CH_2Cl_2 were grown by inwards diffusion of diethyl ether into a dichloromethane solution of the complex. The complex crystallised in the monoclinic space group $C2/c$ with a well-defined main structure, though some disorder was present in the dichloromethane solvate. The crystal structure is shown in Figure 5.1, with Figure 5.2 showing the same structure without the phenyl substituents on the phosphorus atoms. Selected bond lengths and angles are given in Table 5.1, and crystallographic information is given in Table 5.2.

The X-ray crystal structure of [Pt(Ph-thixantphos$_2$] shows a distorted tetrahedral configuration with angles ranging from 103.741(18) to 119.313(17)°. This is likely due to the restrictions caused by having two rigid Ph-xantphos ligands around a single metal centre. There are two different phosphorus environments present in the crystal structure, such that each ligand has each of the two environments. One phosphine on each ligand is nearer to the adjacent ligand backbone whilst the other phosphine is nearer to the adjacent phenyl substituents. The backbone is bent away from planarity to allow the ligand to coordinate with bite angles of 106.377(16) and 108.059(17)°. These angles are close to the natural bite-angle calculated for this ligand of 109.4° from molecular mechanics and are slightly smaller than the DFT calculated value of 112.65°.[67]

Tetrahedral complexes of platinum with four phosphorus donors are well-known with numerous crystallographically determined structures.[68] One such structure with a xantphos ligand derivatised with ethyl groups on the phosphorus atoms was reported in 2004 (Figure 5.3a).[74] The [Pt(Et-xantphos$_2$] complex shows a

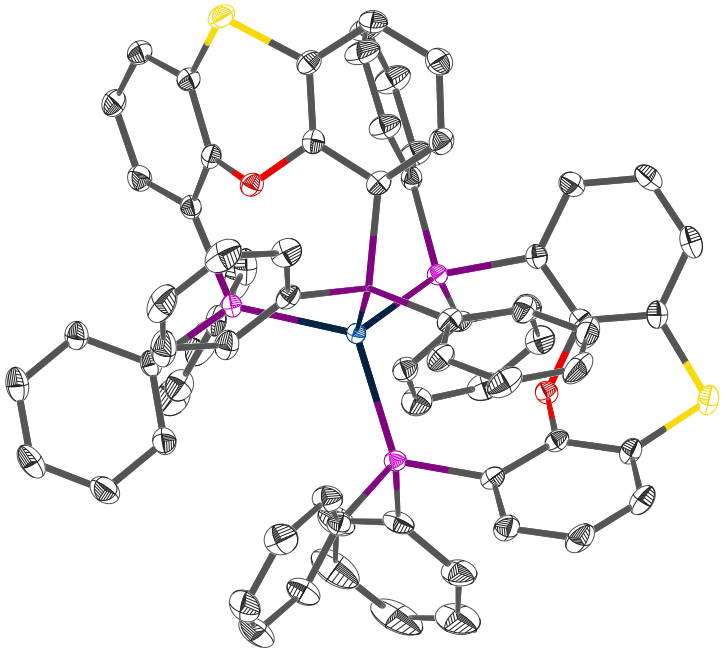

Figure 5.1: X-ray crystal structure of [Pt(Ph-thixantphos)$_2$] (50% probability thermal ellipsoids). Hydrogen atoms and dichloromethane solvate omitted for clarity.

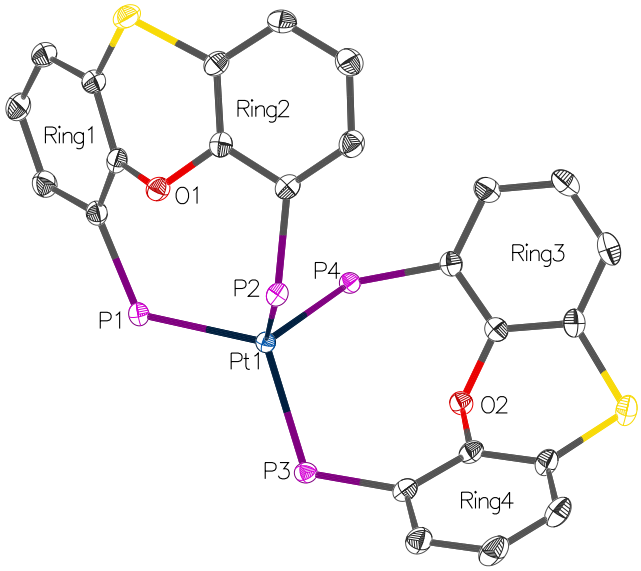

Figure 5.2: X-ray crystal structure of [Pt(Ph-thixantphos)$_2$] (50% probability thermal ellipsoids). Hydrogen atoms, dichloromethane solvate and phenyl rings omitted for clarity.

Table 5.1: Selected bond distances (Å) and angles (°) of [Pt(Ph-thixantphos)$_2$].

Bond distances (Å)		**Bond angles (°)**	
P1-Pt1	2.3325(6)	P1-Pt1-P2	108.059(17)
P2-Pt1	2.3209(5)	P1-Pt1-P3	105.501(17)
P3-Pt1	2.3242(4)	P1-Pt1-P4	119.313(17)
P4-Pt1	2.3249(5)	P2-Pt1-P3	114.224(19)
P1...P2	3.7661(7)	P2-Pt1-P4	103.741(18)
P1...P3	3.7068(7)	P3-Pt1-P4	106.377(16)
P1...P4	4.0194(7)	Ring 1-Ring 2	35.57(8)
P2...P3	3.9007(7)	Ring 3-Ring 4	45.39(8)
P2...P4	3.6544(7)		
P3...P4	3.7221(6)		
Pt1...O1	3.4977(14)		
Pt1...O2	3.5635(14)		

similar structure to [Pt(Ph-thixantphos)$_2$]. The bite-angles for the ethyl complex are 108.07(7) and 108.44(7)°, which are close to the Ph-thixantphos complex of 108.059(17) and 106.377(16)°. The P-Pt bond distances are slightly shorter for [Pt(Et-xantphos)$_2$] (2.312(2), 2.3119(16), 2.2916(17) and 2.289(2) Å) than for [Pt(Ph-thixantphos)$_2$] (2.3325(6), 2.3209(5), 2.3242(4) and 2.3249(5) Å) this is likely the result of the higher electron donation of ethyl substituents compared to phenyl rings. The bite-angles are also very similar to a [Pd(Ph-xantphos)$_2$] complex (Figure 5.3b), which has P-Pd-P angles of 106.34(2)°.[285] Given these similarities it is likely that the geometry of the complexes and the bite-angles of the ligands in these complexes are controlled primarily by valence angles.

The X-ray crystal structure of [Pt(Ph-thixantphos)$_2$] shows two different phosphorus environments for each Ph-thixantphos ligand (Figure 5.2). The backbone of the Ph-thixantphos ligand is bent resulting in one of the phosphorus atoms on one of the ligands sitting within the concave face of the other ligand's backbone while the other phosphorus atom sits away from the ligand backbone and has closer contacts with the phenyl substituents than the backbone. This indicates that while the two ligands are related overall, the two halves of a single ligand are in quite different spatial environments.

Table 5.2: Crystallographic data and structure refinement of [Pt(Ph-thixantphos)$_2$].

Empirical formula	$\mathbf{C_{149}H_{114}Cl_{10}O_4P_8Pt_2S_4}$
Formula weight	3089.07
Temperature/K	296.0
Crystal system	monoclinic
Space group	C2/c
a/Å	46.8743(16)
b/Å	13.1000(4)
c/Å	21.7852(7)
α/°	90
β/°	105.208(2)
γ/°	90
Volume/Å^3	12908.8(7)
Z	4
ρ_{calc} mg/mm^3	1.589
µ/mm	2.594
F(000)	6200.0
Crystal size/mm	0.61 x 0.18 x 0.15
Radiation	MoKα (λ = 0.71073)
2θ range for data collection	3.602 to 60.916°
Index ranges	-66 $\leq$ h $\leq$ 66, -18 $\leq$ k $\leq$ 17, -30 $\leq$ l $\leq$ 30
Reflections collected	172570
Independent reflections	19386 [R_{int} = 0.0370, R_{sigma} = 0.0207]
Data/restraints/parameters	19386/0/808
Goodness-of-fit on F^2	1.232
Final R indexes [I>=2σ (I)]	R_1 = 0.0219, wR_2 = 0.0565
Final R indexes [all data]	R_1 = 0.0338, wR_2 = 0.0716
Largest diff. peak/hole / e Å^{-3}	1.08/-1.07

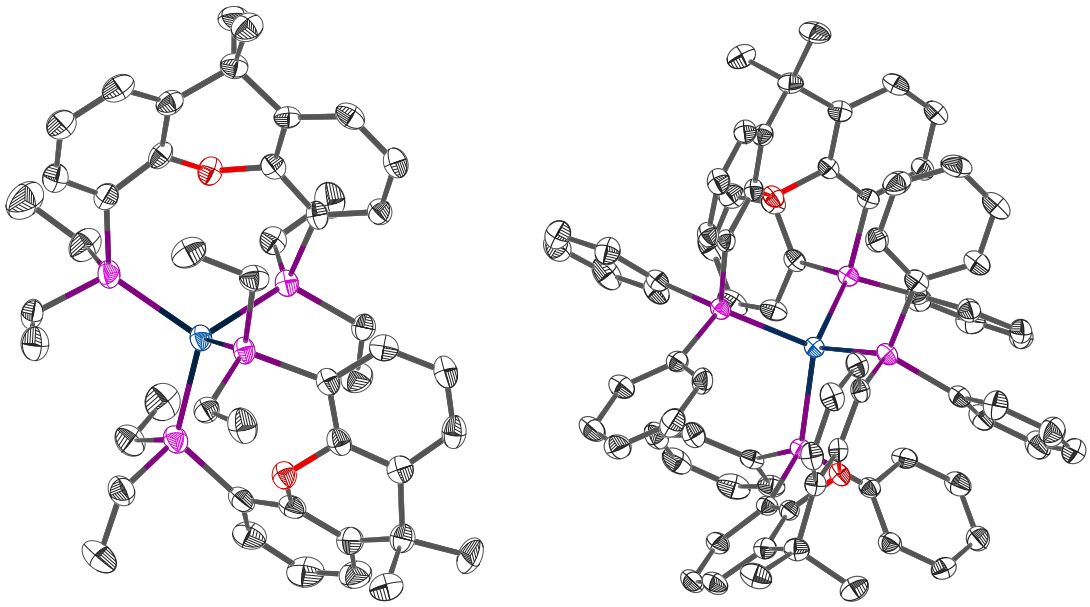

(a) (b)

Figure 5.3: X-ray crystal structures of [Pt(Et-xantphos)$_2$][285] (a) and [Pd(Ph-xantphos)$_2$][74] (b).

From the X-ray crystal structure of [Pt(Ph-thixantphos)$_2$], we would expect the ^{31}P NMR spectrum to show two different phosphorus environments. At room temperature both the ^{1}H and ^{31}P NMR spectra are very broad. While two environments are observed in the ^{31}P NMR spectrum, no coupling can be readily discerned, suggesting that a dynamic process is occurring. This behaviour was investigated using variable temperature ^{1}H and ^{31}P NMR analysis in CD_2Cl_2 (Figures 5.4 and 5.5). Lowering the temperature to 0 °C causes the ^{31}P NMR spectrum to sharpen with phosphorus coupling and platinum satellites resolved. The ^{31}P NMR spectrum continues to sharpen down to around -40 °C, below which no further changes are observed. The low temperature ^{1}H NMR spectra show a similar pattern: sharpening upon cooling to 0 °C, which continues down to -40 °C. However, unlike the ^{31}P NMR spectra, the ^{1}H NMR spectra at -60 and -80 °C begin to broaden once more.

The xantphos backbones frequently bend in order to achieve the coordination angles desired by the metal. However, while this is seen in the crystal structures of the complexes, the effects are not observed in the NMR spectra due to rapid

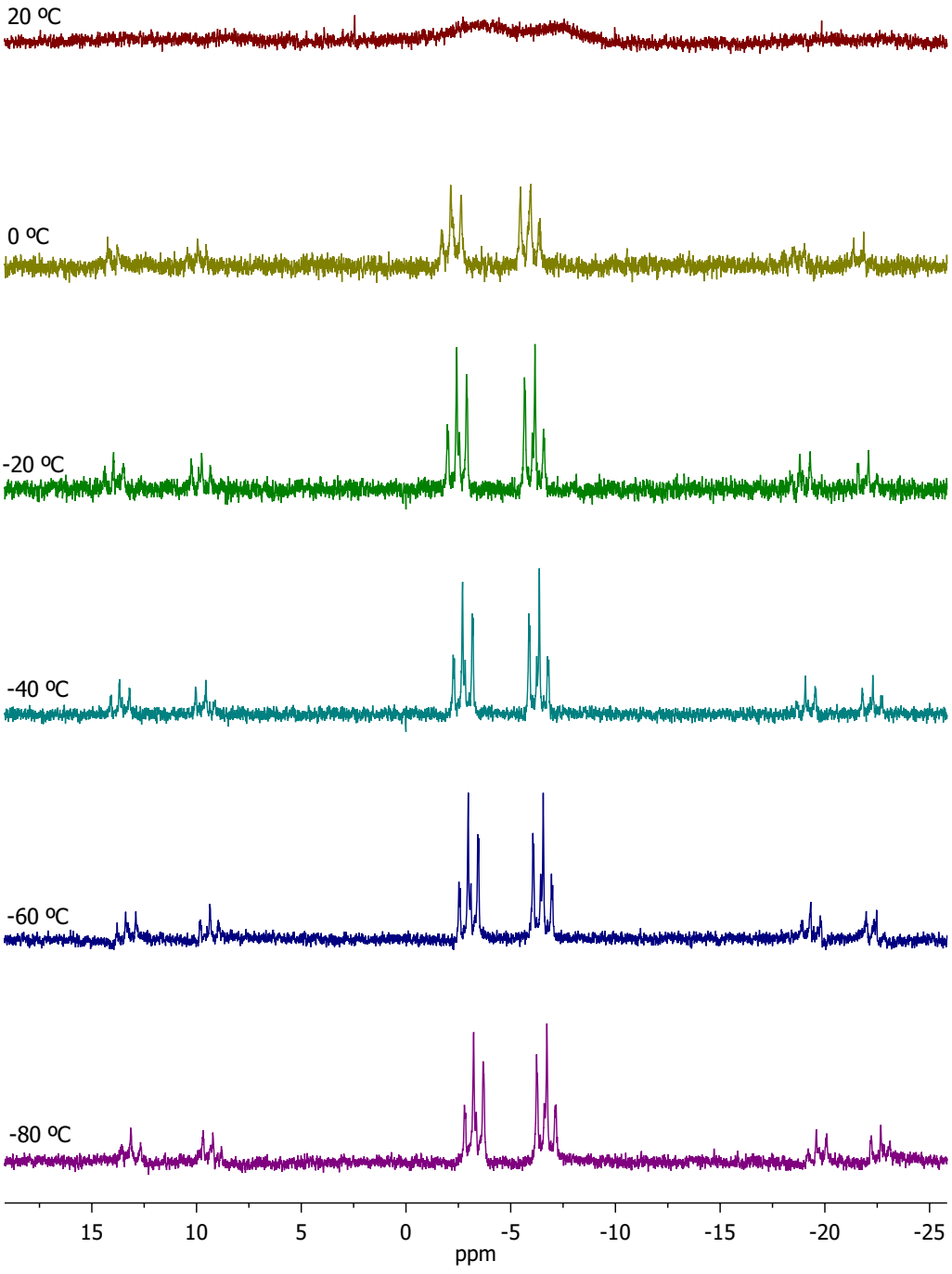

Figure 5.4: Low temperature ^{31}P NMR spectra of [Pt(Ph-thixantphos)$_2$] in CD_2Cl_2.

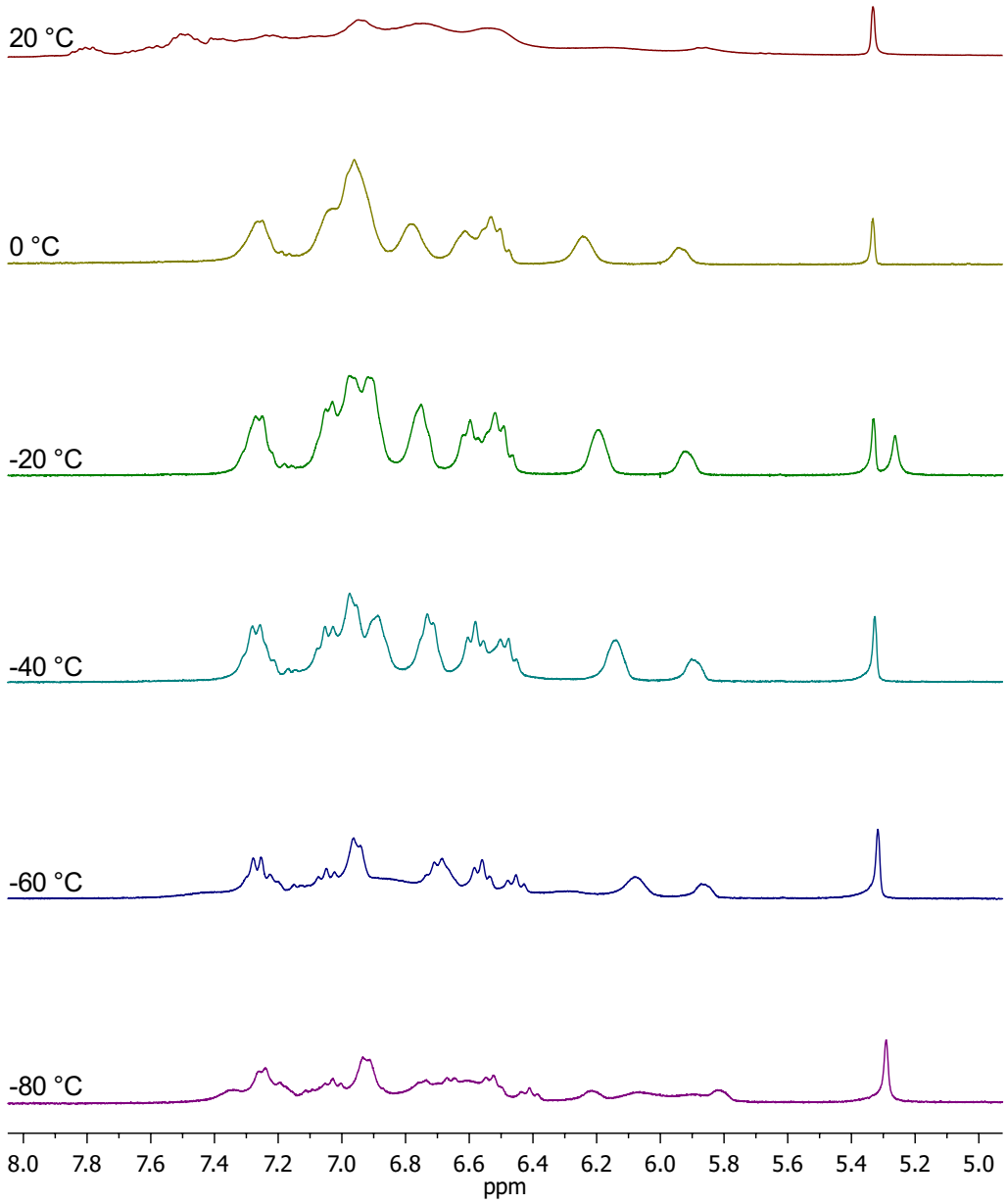

Figure 5.5: Low temperature ^{1}H NMR spectra of [Pt(Ph-thixantphos)$_2$] in CD_2Cl_2, showing the aromatic region.

inversion of the ligand such that both faces of the backbone are averaged on the NMR timescale. In the case of [Pt(Ph-thixantphos)$_2$], the X-ray crystal structure shows two different spatial phosphorus environments, which should result in different chemical shifts in the ^{31}P NMR spectrum. This system is sufficiently crowded around the metal centre to reduce the ability of the xantphos system to invert. As such, cooling to 0 °C is sufficient to lock the backbones of [Pt(Ph-thixantphos)$_2$] in a single configuration, thus allowing the two different ^{31}P environments to become visible. Even at room temperature two different signals are apparent, indicating that although the inversion is occurring, the rate is slow enough compared to the NMR timescale to allow some distinction between the two phosphorus atoms. The inversion of the xantphos backbones stops, on the NMR timescale, upon cooling to around -20 °C. However, while the ^{31}P NMR spectrum remains sharp below this temperature, the ^{1}H NMR spectrum begins to broaden again. This may be the result of restricted rotation of some or all of the phenyl rings, which may occur due to the steric demands of the system.

The ^{31}P NMR spectrum of [Pt(Ph-thixantphos)$_2$] at -80 °C shows some interesting features. Two peaks are observed as triplets at -2.43 and -6.16 ppm with phosphorus-phosphorus coupling of 55.0 Hz and platinum-phosphorus coupling of 3976 and 3864 Hz respectively. The value for the phosphorus-phosphorus coupling was slightly larger than that reported for the analogous [Pt(Et-xantphos)$_2$] complex, which showed two triplets at -6.82 and -19.65 ppm with two-bond phosphorus-phosphorus coupling of 48 Hz.[74] The phosphorus-platinum coupling constants were also similar between the two complexes. The Ph-thixantphos complex had coupling constants of 3976 and 3864 Hz, whereas the Et-xantphos complex J_{PtP} = 4086 and 3602 Hz. However, the ^{31}P NMR spectrum of [Pt(Et-xantphos)$_2$] was sharp at room temperature in toluene-d_8, while the spectrum for [Pt(Ph-thixantphos)$_2$] did not fully resolve until -40 °C, indicating that the propensity for the ligands in these complexes to undergo inversion differs.[74]

A useful platinum(0) starting material is [Pt(C_2H_4)$_3$], as the ethene ligands are readily displaced by other ligands, although [Pt(C_2H_4)$_3$] is only stable under an ethene atmosphere.[286,287] Transition metal ethene complexes are important from an industrial perspective as ethene is a common feedstock used in industrial-scale syntheses.[288,289] The 1:1 reaction between [Pt(C_2H_4)$_3$] and Ph-thixantphos was carried out on an NMR scale to allow the identification of any intermediates that may form. The reaction was rapid and the solution turned orange after

only 10 minutes at room temperature. The ^{31}P NMR spectrum showed [Pt(Ph-thixantphos)$_2$] was the major product accounting for 93% of the phosphorus containing species, while the remaining 7% was [Pt(C_2H_4)(Ph-thixantphos)], analogous to the [Pt(nb)(Ph-thixantphos)] formed in reaction with [Pt(nb)$_3$]. Interestingly, the ratio of the alkene to bis complex formed appears to be dependent on the alkene used. The small amount of [Pt(C_2H_4)(Ph-thixantphos)] formed suggests that the free ligand prefers to react with the alkene complex to form [Pt(Ph-thixantphos)$_2$] rather than react with [Pt(C_2H_4)$_3$]. This indicates that the initial coordination of the diphosphine to form [Pt(C_2H_4)(Ph-thixantphos)] activates the system to react further with free Ph-thixantphos. However, in the norbornene case we observe 60.4% [Pt(Ph-thixantphos)$_2$], indicating that while the uncoordinated diphosphine does prefer to react with [Pt(nb)(Ph-thixantphos)] over the [Pt(nb)$_3$], the effect is not as significant as for the ethene system.

5.2 Reaction of *t*-Bu-xantphos Ligands with [Pt(nb)$_3$]

The equimolar reaction of [Pt(nb)$_3$] with Ph-thixantphos instantaneously formed [Pt(Ph-thixantphos)$_2$] and [Pt(nb)(Ph-thixantphos)] as the major and minor products respectively. The same reaction with *t*-Bu-thixantphos in C_6D_6 was slower, requiring heating at 60 °C for four days in order to go to completion. In a similar manner to the reaction with Ph-thixantphos, the reaction of *t*-Bu-thixantphos with [Pt(nb)$_3$] also produces two products. One of these products is the same in both cases, [Pt(nb)(xantphos)] (xantphos = Ph-thixantphos, *t*-Bu-thixantphos). However, rather than a bis(diphosphine) complex forming, as observed with Ph-thixantphos, using *t*-Bu-thixantphos generated a reactive, 14-electron [Pt(*t*-Bu-thixantphos)] complex (60.8%, Scheme 5.2). Although 14-electron complexes are electron-deficient, several examples have been reported, with [Pt(PPh_3)$_2$] first reported in 1966[290] followed by [Pt(PCy_3)$_2$],[291] [Pt(P^tBu_3)$_2$], [Pt(P^tBu_2Ph)$_2$], and [Pt(P^iPr_3)$_2$].[292]

The [Pt(*t*-Bu-thixantphos)(nb)] complex exhibits a broad resonance at 55.6 ppm with platinum satellites in the ^{31}P NMR spectrum. The value of J_{PtP} (3612 Hz) is typical for trigonal platinum alkene complexes.[284] The alkene protons appear at 2.37 ppm in the ^{1}H NMR spectrum as a broad singlet with no discernable phosphorus coupling but platinum coupling of 67.8 Hz. A similarly broad singlet in

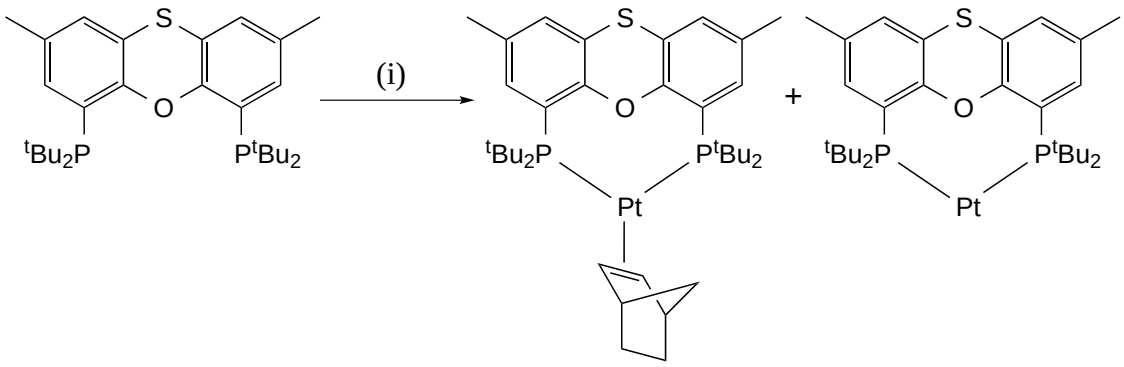

Scheme 5.2: Reaction between tBu-thixantphos and [Pt(nb)$_3$]. *Reagents and conditions:* (i) [Pt(nb)$_3$], C_6D_6, 60 °C.

the ^{13}C NMR spectrum at 51.9 ppm with J_{PtC} = 343.9 Hz was observed for the alkene carbons. Half of the expected number of norbornene and *t*-Bu-thixantphos NMR signals are observed indicating a symmetrical complex.

The reaction between *t*-Bu-sixantphos and [Pt(nb)$_3$] under the same conditions formed an analogous 14-electron [Pt(*t*-Bu-sixantphos)] complex as the major product after 24 hours at 60 °C, appearing in the ^{31}P NMR spectrum at 79.5 ppm (J_{PtP} = 4827 Hz). Two other products are also observed, appearing at 59.3 ppm (J_{PtP} = 3572 Hz) and 34.7 ppm (J_{PtP} = 2677 Hz). As the complex at 59.3 ppm is similar in both chemical shift and coupling constant to [Pt(*t*-Bu-thixantphos)(nb)], it is proposed to be [Pt(*t*-Bu-sixantphos)(nb)]. The features of the complex at 34.7 ppm are surprising. The value of J_{PtP} is similar to a number of Pt(II) complexes with *trans* phosphorus atoms (for examples see Chapter 6). Unfortunately the complexes could not be separated to gain further insight into their structures.

The major product in the reaction between *t*-Bu-xantphos and [Pt(nb)$_3$] was different to the other xantphos ligands. A small amount of a complex with a signal at 78.9 ppm in the ^{31}P NMR spectrum was formed, consistent with a [Pt(*t*-Bu-xantphos)] complex (the signal was too weak to observe any platinum coupling). However, the major product, and the only species present after 24 hours at 60 °C was a complex in the ^{31}P NMR spectrum at 46.7 ppm (J_{PtP} = 3246 Hz). The ^{1}H NMR spectrum of this complex showed a triplet at -18.49 ppm, with J_{PH} of 13.1 Hz and J_{PtH} of 1107 Hz. The chemical shift of this signal and the value of J_{PtH} are consistent with a hydride positioned *trans* to a ligand with a low *trans*-influence.

The value of J_{PH} is consistent with a *cis* arrangement of the hydride with the two phosphorus atoms. The ^{1}H and ^{13}C NMR signals for the *tert*-butyl substituents are broad which may suggest a dynamic process is occurring. The *O-ipso* carbon shows a downfield shift of 2.8 ppm which is consistent with coordination of the oxygen atom. This suggests a platinum(II) complex of the type [Pt(*t*-Bu-xantphos-κ*P,O,P'*)H]X (Scheme 5.3). However, complexes of this type typically have platinum-phosphorus coupling constants of between 2300 and 2800 Hz (see Chapter 6), while the value of J_{PtP} for this complex is higher at 3246 Hz. The nature of the counterion and the hydride source were not determined.

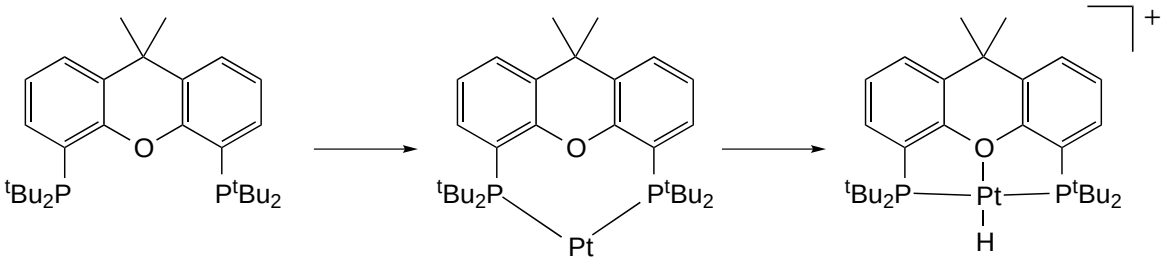

Scheme 5.3: Reaction between *t*-Bu-xantphos and [Pt(nb)$_3$]· *Reagents and conditions:* [Pt(nb)$_3$], C_6D_6, 60 °C, 24 hours.

The formation of the proposed [Pt(*t*-Bu-xantphos-κ*P,O,P'*)H]X complex likely results from the [Pt(*t*-Bu-xantphos)] complex undergoing reaction with another molecule in the system. Despite the number of [Pt(monophosphine)$_2$] complexes, isolable [Pt(diphosphine)] complexes are relatively rare as diphosphine ligands typically provide less protection of the metal centre due to the restrictions of their bite-angle. Although [Pt(diphosphine)] complexes are frequently proposed as intermediates, few have been isolated.[293–295] [Pt(diphosphine)] complexes will typically coordinate to any possible ligands that are present. The proposed 14-electron complex [Pt(dcype)] (dcype = 1,2-bis(dicyclohexylphosphino)ethane) reacts with alkenes and alkynes to form [Pt(alkene)(dcype)] or [Pt(alkyne) (dcype)], and reacts with alkanes to form [Pt(alkyl)(dcype)H] complexes.[294] [Pt(dcype)] also reacts with benzene to form [Pt(C_6H_5)(dcype)H]. Although in the [Pt(*t*-Bu-xantphos-κ*P,O,P'*)H]X system no evidence of a coordinated alkyl, phenyl or other fragment was observed, this may explain the formation of the hydride species, which then loses the other ligand to form a counterion. The hydride is unlikely to result from water as all solvents that were used were dried over molecular

sieves prior to use and the water content of solvents dried in this manner is too small to account for the complete transformation to a hydride complex.[296]

The [Pt(*t*-Bu-thixantphos)] complex can be isolated by removal of the norbornene from the sample, under reduced pressure, while the analogous *t*-Bu-sixantphos complex only formed as a mixture and the *t*-Bu-xantphos complex went on to form [Pt(*t*-Bu-xantphos-κ*P,O,P'*)H] with full conversion after 24 hours preventing their isolation and full characterisation. The ^{31}P NMR data for the complexes is given in Table 5.3. The complexes all exhibit a single peak in the ^{31}P NMR spectra shifted downfield from the free ligand by 68–71 ppm ($\Delta\delta$). A study of the ^{31}P NMR properties of [Pt(PR$_3$)$_2$] complexes showed that all of the 14-electron complexes of this type that were studied display a downfield shift of the phosphorus signal by between 48 and 58 ppm upon coordination, with platinum-phosphorus coupling constants between 4100 and 4600 Hz.[12] The change in chemical shift for the *t*-Bu-xantphos complexes is larger than that reported for monophosphines. This may be the result of strain placed on the system to achieve such a large bite-angle, or the result of a slightly bent complex which may form to allow bidentate coordination. The platinum-phosphorus coupling is also larger than those previously reported, by over 200 Hz. The largest previously reported Pt-P coupling for these complexes is 4592 Hz for [Pt(P^{t}Bu$_2$Ph)$_2$], and coupling constants of between 4370 and 4424 Hz have been reported by our group for substituted [Pt(P^{t}Bu$_2$Bn)$_2$] complexes.[297,298] The larger coupling constants for the *t*-Bu-xantphos species likely indicates a distortion of the system from the linearity observed with monophosphine systems.

Table 5.3: ^{31}P NMR data for [Pt(*t*-Bu-xantphos)] complexes. J_{PtP} was not observed for *t*-Bu-xantphos ($\Delta\delta = \delta_{complex} - \delta_{free\ ligand}$).

	^{31}P		
Diphosphine	**δ/ppm**	**$\Delta\delta$/ppm**	**J_{PtP}/Hz**
t-Bu-Sixantphos	79.5	71.1	4827
t-Bu-Thixantphos	78.6	69.1	4810
t-Bu-Xantphos	78.9	68.7	n.o.

5.3 Reaction of *t*-Bu-thixantphos with [Pt(cod)$_2$]

[Pt(cod)$_2$] (cod = 1,5-cyclooctadiene) is a commonly used starting material for the formation of platinum(0) phosphine complexes as the cod ligands can be readily displaced by phosphines.[291,299] The reaction between *t*-Bu-thixantphos and [Pt(cod)$_2$] was carried out on an NMR scale in C_6D_6. The only phosphorus containing product from the reaction was [Pt(*t*-Bu-thixantphos)]. However, conversion of only 28% was achieved. After 48 hours at room temperature the reaction had become black and despite heating no further reaction was observed. Together with the absence of unreacted [Pt(cod)$_2$] in the ^{1}H NMR spectrum this suggests that the [Pt(cod)$_2$] was unstable under the reaction conditions. Analysis of the reaction mixture by ^{1}H and ^{13}C NMR spectroscopy showed the presence of 1,3- and 1,4-cyclooctadiene in addition to 1,5-cyclooctadiene. A weak signal in the ^{1}H NMR spectrum was observed at -18.2 ppm as a triplet (J_{PH} = 13.7 Hz) with platinum satellites (J_{PtH} = 1100 Hz). This signal is in a similar position and has similar coupling constants to the peak in the ^{1}H NMR of [Pt(*t*-Bu-xantphos)H]X. This may indicate that the 14-electron [Pt(*t*-Bu-thixantphos)] complex is able to catalyse the isomerisation of 1,5-cyclooctadiene. This process may involve the oxidative addition of an allylic C-H of the cod ligand to the platinum forming an η^3-allyl and a hydride ligand, which could then reductively eliminate to form 1,3-cyclooctadiene. Given the poor reactivity of [Pt(cod)$_2$] with *t*-Bu-thixantphos the analogous reactions with *t*-Bu-sixantphos and *t*-Bu-xantphos were not attempted.

5.4 Reaction of *t*-Bu-xantphos Ligands and [Pt(C_2H_4)$_3$]

Both ethene and norbornene are monodentate alkene ligands whilst cod is a bidentate ligand which typically chelates to metal centres. Hence, the reactivity of the *t*-Bu-xantphos ligands with [Pt(C_2H_4)$_3$] is expect to be more similar to that observed with [Pt(nb)$_3$] than that with [Pt(cod)$_2$]. Furthermore ethene is more readily displaced than norbornene as the coordination of norbornene relieves the strain associated with the bicyclic system. However, ethene is a smaller ligand than norbornene. Hence investigating the reactivity of the *t*-Bu-xantphos ligands with [Pt(C_2H_4)$_3$] gives an opportunity to probe the relative importance of elec-

tronic and steric effects in controlling the coordination of alkene ligands to [Pt(*t*-Bu-xantphos)] complexes. The three *t*-Bu-xantphos ligands were reacted on an NMR scale in C_6D_6 with freshly prepared [Pt(C_2H_4)$_3$], made from [Pt(cod)$_2$] under an ethene atmosphere. All three ligands initially formed a complex of the type [Pt(*t*-Bu-xantphos)(C_2H_4)] (Scheme 5.4). However, while the ethene complex was the only product for the reaction with *t*-Bu-thixantphos, the reaction with *t*-Bu-xantphos progressed to form [Pt(*t*-Bu-xantphos)H]X. Again the nature of the counterion in this species was unable to be determined. The reaction between *t*-Bu-sixantphos and [Pt(C_2H_4)$_3$] showed 11.1% of [Pt(*t*-Bu-sixantphos)(C_2H_4)] after four hours. However, the reaction did not progress further.

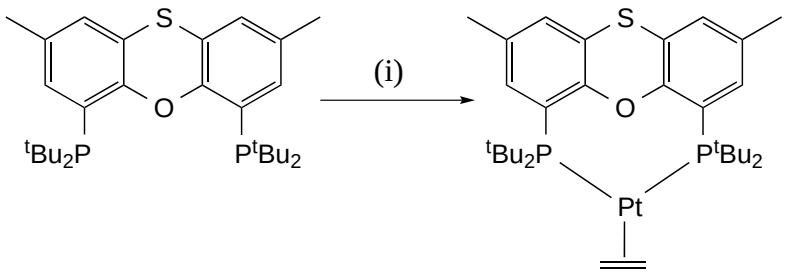

Scheme 5.4: Reaction between *t*-Bu-thixantphos and [Pt(C_2H_4)$_3$]. *Reagents and conditions:* (i) [Pt(C_2H_4)$_3$], C_6D_6, 48 hours, under C_2H_4.

Selected NMR data for the [Pt(*t*-Bu-xantphos)(C_2H_4)] complexes is given in Table 5.4. In all cases the ^{31}P NMR spectrum showed a singlet between 53.4 and 55.7 ppm, shifted downfield by between 43.2 and 46.2 ppm from the corresponding free ligand. All of the J_{PtP} values are within the expected range for complexes of this type.[16] [Pt(*t*-Bu-sixantphos)(C_2H_4)] has a J_{PtP} value almost 400 Hz lower than that observed for the corresponding *t*-Bu-thixantphos and *t*-Bu-xantphos complexes. The lower coupling constant may indicate that the ethene ligand is more strongly coordinated to the platinum centre in [Pt(*t*-Bu-sixantphos)(C_2H_4)]. This may be the result of the smaller bite-angle of the *t*-Bu-sixantphos ligand allowing more room for the ethene ligand to interact with the platinum. The ^{1}H NMR spectra showed peaks at 2.50 and 2.52 ppm corresponding to the ethene protons for [Pt(*t*-Bu-thixantphos)(C_2H_4)] and [Pt(*t*-Bu-xantphos)(C_2H_4)] respectively. The peak corresponding to coordinated ethene was obscured in the ^{1}H NMR spectrum for the *t*-Bu-sixantphos complex. The dramatic upfield shift of

the ^{1}H signal for the ethene ligand is consistent with coordination to a metal centre such at platinum (uncoordinated ethene appears at 5.25 ppm[300]). As both the *t*-Bu-sixantphos and *t*-Bu-xantphos ethene complexes reacted further to produce mixtures, the ^{13}C NMR peak for the ethene ligand was only observed in [Pt(*t*-Bu-thixantphos)(C_2H_4)]. The ethene carbon signal appeared at 34.2 ppm as a broad singlet with a J_{PtC} value of 223.2 Hz.

Table 5.4: ^{31}P NMR data for [Pt(*t*-Bu-xantphos)(C_2H_4)] complexes in C_6D_6 ($\Delta\delta$ = $\delta_{complex}$ - $\delta_{free\ ligand}$).

	^{31}P			^{1}H	
Diphosphine	δ/**ppm**	$\Delta\delta$/**ppm**	J_{PtP}/**Hz**	δ/**ppm**	J_{PtH}/**Hz**
t-Bu-Sixantphos	53.7	45.3	3499		
t-Bu-Thixantphos	55.7	46.2	3899	2.50	59.5
t-Bu-Xantphos	53.4	43.2	3878	2.52	58.0

The reaction of *t*-Bu-thixantphos with the three different platinum alkene complexes showed markedly different properties: [Pt(nb)$_3$] forms an equilibrium between [Pt(*t*-Bu-thixantphos)(nb)] and [Pt(*t*-Bu-thixantphos)]; [Pt(cod)$_2$] forms [Pt(*t*-Bu-thixantphos)]; and [Pt(C_2H_4)$_3$] forms [Pt(*t*-Bu-thixantphos)(C_2H_4)]. [Pt(*t*-Bu-thixantphos)(nb)] was converted entirely to the [Pt(*t*-Bu-thixantphos)] complex by placing a sample under vacuum for one hour, while the [Pt(*t*-Bu-thixantphos)(C_2H_4)] complex showed no change under the same conditions. Bubbling argon through a solution of [Pt(*t*-Bu-thixantphos)(C_2H_4)] for 10 mins, resulted in the formation of only small amounts of [Pt(*t*-Bu-thixantphos)]. This indicates that ethene is more strongly coordinated to the platinum centre than norbornene and is less prone to dissociation. In general dialkyl substituted alkenes coordinate more weakly than ethene, as shown in the straightforward synthesis of [Pt(C_2H_4)$_3$] from [Pt(cod)$_2$].[291,301] However, coordination of norbornene relieves some of the ring-strain which means it coordinates more strongly than cod. [Pt(nb)$_3$] is an air-stable solid, while [Pt(C_2H_4)$_3$] degrades if not stored under ethene, indicating that norbornene coordinates more strongly than ethene.

5.5 Formation of Platinum Dioxygen Complexes

[Pt(P_2)] complexes (P = monophosphine, P_2 = diphosphine) are reactive towards small molecules, particularly those with diphosphine ligands as was observed in the formation of [Pt(*t*-Bu-xantphos)H]X.[294] The reactivity of [Pt(*t*-Bu-thixantphos)] is lower than the reactivity of the corresponding *t*-Bu-sixantphos and *t*-Bu-xantphos complexes. Both the *t*-Bu-sixantphos and *t*-Bu-xantphos complexes were unstable in solution, while the *t*-Bu-thixantphos complex was stable in C_6D_6, under argon, at room temperature for at least several days. However, [Pt(*t*-Bu-thixantphos)] reacts rapidly with oxygen forming [Pt(*t*-Bu-thixantphos)(η^2-O_2)] upon exposure to air (Scheme 5.5). Bubbling air through a sample containing [Pt(*t*-Bu-thixantphos)] and [Pt(*t*-Bu-thixantphos)(nb)] or a sample of [Pt(*t*-Bu-thixantphos)(C_2H_4)] resulted in complete conversion (by ^{31}P NMR spectroscopy) to [Pt(*t*-Bu-thixantphos)(η^2-O_2)]. This reaction is quite common for complexes of the type [Pt(PR_3)$_2$].[302,303]

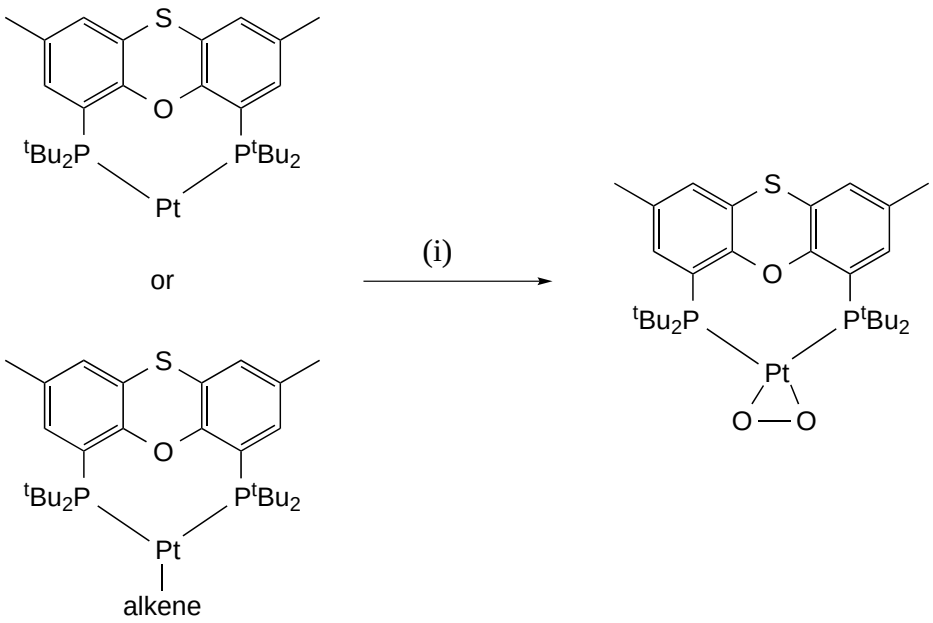

Scheme 5.5: Reaction of [Pt(alkene)(*t*-Bu-thixantphos)] and [Pt(*t*-Bu-thixantphos)] with air. Alkene = C_2H_4 or norbornene. *Reagents and conditions:* (i) Air, 10 mins, C_6D_6.

Upon reaction of [Pt(*t*-Bu-thixantphos)] with oxygen, the ^{31}P NMR signal shifts

upfield from 78.6 to 38.4 ppm with an associated reduction in the magnitude of the phosphorus-platinum coupling from 4810 to 4488 Hz. The reduction in coupling constant is due to the decrease in the s-character of the platinum bond orbitals upon changing the geometry of the complex.[16] The value of the J_{PtP} coupling constant is larger than those previously reported (3930–4112 Hz).[297,302] Similarly to the NMR data obtained for [Pt(*t*-Bu-thixantphos)], these values may be different from the literature data due to the constraints of the diphosphine ligand over the monophosphines reported in the literature. The ^{1}H and ^{13}C NMR spectra of [Pt(*t*-Bu-thixantphos)(η^2-O_2)] show doublets for the *tert*-butyl proton and carbon environments, rather than the virtual triplets observed for [Pt(*t*-Bu-thixantphos)]. This is consistent with the change in geometry as virtual triplets indicate strongly coupled phosphorus atoms which generally occurs with *trans* coordination.[124]

Colourless single crystals of [Pt(*t*-Bu-thixantphos)(η^2-O_2)] were obtained by allowing oxygen to diffuse slowly into a C_6D_6 solution containing a mixture of [Pt(*t*-Bu-thixantphos)(nb)] and [Pt(*t*-Bu-thixantphos)]. The complex crystallised in the Pbca space group with two molecules of C_6D_6 as solvate. The crystal structure is shown in Figure 5.6 with a side view in Figure 5.7. Selected bond lengths and angles for the complex are summarised in Table 5.5 and crystallographic data is given in Table 5.6.

Table 5.5: Selected bond distances (Å) and angles (°) of [Pt(*t*-Bu-thixantphos)(η^2-O_2)] · 2 C_6D_6.

Bond distances (Å)		**Bond angles (°)**	
P1-Pt	2.3159(13)	P1-Pt-P2	117.26(5)
P2-Pt	2.3056(13)	P1-Pt-O2	101.26(14)
O1-Pt	3.383(3)	P2-Pt-O3	100.11(13)
O2-Pt	2.024(4)	O2-Pt-O3	41.38(18)
O3-Pt	2.022(4)	Ring 1 - Ring 2	133.90(18)
O1-O2	1.429(6)		

The crystal structure of [Pt(*t*-Bu-thixantphos)(η^2-O_2)] shows a planar geometry around the platinum with the sum of the angles = 360.01°. The backbone of

Table 5.6: Crystallographic data and structure refinement of [Pt(*t*-Bu-thixantphos)(η^2-O_2)] · 2 C_6D_6.

Empirical formula	**$C_{42}H_{46}D_{12}O_3P_2PtS$**
Formula weight	912.04
Temperature/K	120.01(10)
Crystal system	orthorhombic
Space group	Pbca
a/Å	17.7892(3)
b/Å	15.8129(3)
c/Å	28.4025(5)
$\alpha/^\circ$	90
$\beta/^\circ$	90
$\gamma/^\circ$	90
Volume/Å^3	7989.6(2)
Z	8
ρ_{calc} mg/mm^3	1.516
µ/mm	3.682
F(000)	3664.0
Crystal size/mm	0.21 x 0.16 x 0.15
Radiation	MoKα (λ = 0.71073)
2θ range for data collection	5.348 to 65.882°
Index ranges	-27 $\leq$ h $\leq$ 26, -22 $\leq$ k $\leq$ 24, -43 $\leq$ l $\leq$ 40
Reflections collected	118275
Independent reflections	14395 [R_{int} = 0.0668, R_{sigma} = 0.0383]
Data/restraints/parameters	14395/0/456
Goodness-of-fit on F^2	1.101
Final R indexes [I>=2σ (I)]	R_1 = 0.0638, wR_2 = 0.1563
Final R indexes [all data]	R_1 = 0.0824, wR_2 = 0.1718
Largest diff. peak/hole / e Å^{-3}	7.62/-3.06

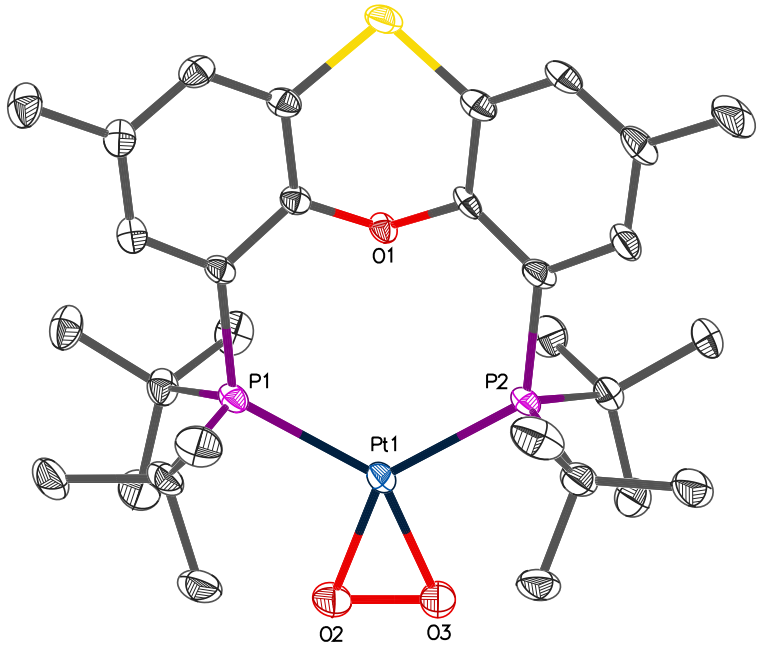

Figure 5.6: [Pt(*t*-Bu-thixantphos)(η^2-O_2)] · 2 C_6D_6 (50% probability thermal ellipsoids). Hydrogen atoms and solvent molecules omitted for clarity.

the ligand is bent to achieve a bite-angle of 117.26(5)°, smaller than the calculated bite-angle of 126.98° (Section 2.2). The bite-angle of the *t*-Bu-thixantphos ligand in [Pt(*t*-Bu-thixantphos)(η^2-O_2)] is similar to the bite-angle in [Ag(*t*-Bu-thixantphos)Cl] (116.46(8)°, Table 3.2). No interaction between the ether-bridge oxygen and the platinum is observed, with a distance of 3.383(3) Å between the two atoms. All of the bond lengths and angles have typical values. Surprisingly only four crystal structures of platinum dioxygen complexes have been reported in the CSD, three of which are for [Pt(η^2-O_2)(PPh_3)$_2$] with different solvates, (C_6H_6, $CHCl_3$ and C_7H_8).[304–306] However, the data quality for the structure with a toluene solvate was poor.[306] The other reported crystal structure is for [Pt(η^2-O_2)(P^tBu_2Ph)$_2$].[307] The P^tBu_2Ph ligand has similar steric and electronic properties to the *t*-Bu-xantphos ligands, though the *t*-Bu-xantphos ligands are restricted by the backbone. The P-Pt-P angle in [Pt(η^2-O_2)(P^tBu_2Ph)$_2$] (113.1(2)°) is smaller than that observed for [Pt(*t*-Bu-thixantphos)(η^2-O_2)], indicating the role of the rigid backbone in determining the bite-angle of transition metal complexes. The Pt-O, and O-O bond lengths, and the O-Pt-O angle show little difference

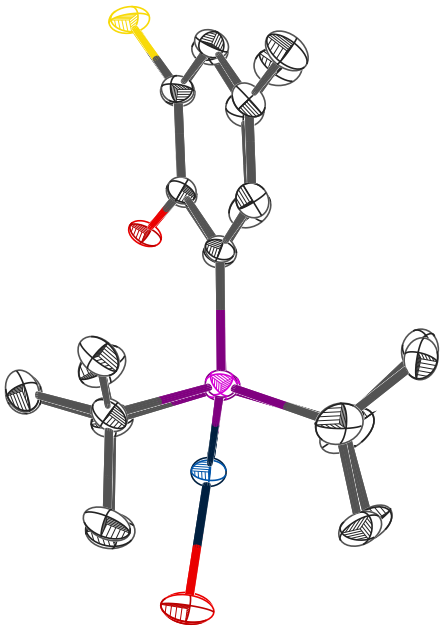

Figure 5.7: [Pt(*t*-Bu-thixantphos)(η^2-O_2)] · $2C_6D_6$, side view (50% probability thermal ellipsoids). Hydrogen atoms and solvent molecules omitted for clarity.

between the three reported structures and [Pt(*t*-Bu-thixantphos)(η^2-O_2)] (Table 5.7).

The O-O bond length (1.429(6) Å) in [Pt(*t*-Bu-thixantphos)(η^2-O_2)] is longer than the bond length of molecular oxygen (1.21 Å) indicating a reduction in the bond order upon coordination to the metal centre. Transition metal complexes with O-O bond lengths of 1.4–1.5 Å are regarded formally as peroxide complexes with an O_2^{2-} ligand and a platinum(II) centre.[308] The O-O bond length is slightly shorter in [Pt(*t*-Bu-thixantphos)(η^2-O_2)] than the analogous PPh_3 or P^tBu_2Ph complexes (although within error for the P^tBu_2Ph value).[304–307] *t*-Bu-Thixantphos would be expected to be more electron-donating than PPh_3, and to have similar electronic properties to P^tBu_2Ph. A longer O-O bond length is expected if more electron-donating ligands are used as this would add to the O_2 anti-bonding π^*-orbital through back-donation, which should reduce the bond order and thus increase the O-O bond length. However, the P-Pt-P angle is larger for *t*-Bu-thixantphos than the other ligands. This may indicate that the O-O bond length is restrained by the sterics of the *t*-Bu-thixantphos ligand. Hence the O-O bond length in these

Table 5.7: Selected bond distances (Å) and angles (°) of [Pt(PP)(η^2-O_2)].

	Bond distances (Å)			Bond angles (°)	
Compound	**O-O**	**Pt-O**	**Pt-O′**	**O-Pt-O′**	**P-Pt-P**
[Pt(η^2-O_2)(P^tBu_2Ph)$_2$)]	1.42(2)	2.02(1)	2.02(1)	41.5(5)	113.1(2)
[Pt(η^2-O_2)(PPh_3)$_2$] · C_6H_6	1.45(4)	2.01(3)	2.01(2)	43(1)	101.2(4)
[Pt(η^2-O_2)(PPh_3)$_2$] · $CHCl_3$	1.505(16)	2.006(7)	2.006(7)	44.06(40)	101.23(12)
[Pt(*t*-Bu-thixantphos)(η^2-O_2)] · $2C_6D_6$	1.429(6)	2.024(4)	2.022(4)	41.38(18)	117.26(5)

complexes is likely the result of a combination of both steric and electronic effects.

5.6 Reactions of [Pt(*t*-Bu-thixantphos)(η^2-O_2)]

The bond length of the dioxygen molecule increases upon coordination, indicating a decrease in the bond order and strength. As such, the oxygen molecule should be activated, and more likely to undergo reactions with small molecules, with several examples reported in the literature.[215,216,231,237,302,309–312] Some examples of reversible coordination of dioxygen to a palladium centre have also been reported, with removal of the dioxygen ligand either by vacuum, substitution or reaction with other ligands.[215,307,313] As such the reversibility of the formation of [Pt(*t*-Bu-thixantphos)(η^2-O_2)] was investigated by vacuum and by reaction with C_2H_4, and the activation of the oxygen ligand was explored by reaction with various small molecules; C_2H_2, H_2, CO, CO_2, NH_4PF_6 and 1,3,5-triaza-7-phosphaadamantane (pta).

The [Pd(η^2-O_2)(P^tBu_2Ph)$_2$] complex readily loses dioxygen under vacuum, although the dioxygen ligand in [Pt(η^2-O_2)(P^tBu_2Ph)$_2$] does not dissociate under the same conditions.[307] Recent work in our group showed that [Pt(η^2-O_2)(P^tBu_2Bn)] can also lose oxygen under vacuum.[297,298] The dioxygen ligand in the [Pt(*t*-Bu-thixantphos)(η^2-O_2)] complex was not observed to dissociate despite heating the reaction under vacuum. This result is not unexpected as the *t*-Bu-thixantphos system is more sterically and electronically similar to P^tBu_2Ph than P^tBu_2Bn. However, the larger P-Pt-P angle in the *t*-Bu-thixantphos complex (117.26(5)°) compared to the P^tBu_2Ph complex (113.1(2)°) may been expected to promote the loss of the dioxygen ligand.[307]

[Pt(*t*-Bu-thixantphos)(η^2-O_2)] can also be formed through reaction of [Pt(*t*-Bu-thixantphos)(C_2H_4)] with air. However, bubbling ethene through an NMR sample of [Pt(*t*-Bu-thixantphos)(η^2-O_2)] in C_6D_6 for 10 minutes showed no conversion to the ethene complex. Leaving the sample under an atmosphere of ethene for a further 48 hours showed no evidence by NMR spectroscopy for conversion to [Pt(*t*-Bu-thixantphos)(C_2H_4)], indicating that the reaction is not readily reversible.

Complexes [Pd(η^2-O_2)($P^tBu_2{}^nBu$)$_2$] and [Pd(η^2-O_2)($PAd_2{}^nBu$)$_2$] (Ad = 1-adamantyl) have been used as stable precatalysts for palladium catalysed formylations and alkoxycarbonylations due to their reduction to the 14-electron palladium complexes by reaction with hydrogen (5 bar) at 40 °C for 16 hours.[313] Reaction of [Pt(*t*-Bu-thixantphos)(η^2-O_2)] with hydrogen gas was attempted by bubbling the gas through the reaction mixture then sealing under an atmosphere of hydrogen. No reaction was observed after three days at room temperature, indicating the stability of the dioxygen complex. However, this cannot be taken as a direct comparison of stability between [Pt(*t*-Bu-thixantphos)(η^2-O_2)] and the [Pd(η^2-O_2)($P^tBu_2{}^nBu$)$_2$] and [Pd(η^2-O_2)($PAd_2{}^nBu$)$_2$] (Ad = 1-adamantyl) complexes, as the reaction was not attempted at the higher temperatures and pressures used in the literature method.[313]

Having established that the reaction of [Pt(*t*-Bu-thixantphos)] with dioxygen is not readily reversible, the reactivity of the coordinated dioxygen ligand was investigated. The platinum dioxygen complexes [Pt(η^2-O_2)(PR_3)$_2$] (PR_3 = PCy_3, P^iPr_3, $P^tBu_2{}^nBu$, P^tBu_2Me, PPh_3) readily react with alkynes showing 1,2-addition of the dioxygen across the triple bond forming metallacyclic compounds.[309] Reaction of [Pt(*t*-Bu-thixantphos)(η^2-O_2)] with ethyne showed no reaction after two days at room temperature. The absence of any reactivity may be due to the inactivity of ethyne towards dioxygen complexes (the literature examples used electron poor alkynes for this reaction), rather than any inherent stability of the dioxygen complex.

Platinum dioxygen complexes can react with carbon monoxide to form carbonate complexes and with carbon dioxide to form peroxycarbonates.[302] No reaction was observed between [Pt(*t*-Bu-thixantphos)(η^2-O_2)] and carbon dioxide, possibly due to the steric demands of the *t*-Bu-thixantphos ligand. However, the reaction with carbon monoxide proved to be more complex than those previously reported, proceeding through several intermediates before forming a single stable species after seven days at room temperature. In order to assist in identification of these intermediates, the reaction was repeated using ^{13}C-enriched CO and the reaction was followed by ^{1}H, ^{13}C and ^{31}P NMR spectroscopy. However, due to the complexity of the system, little information could be gained from the ^{1}H NMR spectra.

The first step in the reaction of [Pt(*t*-Bu-thixantphos)(η^2-O_2)] with carbon monox-

ide results in the expected product, with the carbon monoxide inserting into the O-O bond to form a κ^2O^1,O^2-carbonate ligand. The ^{13}C NMR spectrum contains a triplet peak at 167.9 ppm (J_{PC} = 3.9 Hz) with platinum satellites (J_{PtC} = 64.4 Hz). The ^{31}P NMR spectrum shows an associated peak at 15.6 ppm with J_{PtP} of 4055 Hz. Previously, this reaction has been observed with [Pt(η^2-O_2)(P^tBuPh_2)$_2$] and [Pt(η^2-O_2)($P^tBu_2{}^nBu$)$_2$] which experienced upfield shifts of 9.7 and 16.3 ppm, and a decrease in the value of J_{PtP} by 364 and 330 Hz respectively upon reaction with CO.[302] In the *t*-Bu-thixantphos reaction an upfield shift of 22.8 ppm and a decrease in the value of J_{PtP} of 433 Hz was observed. While the shift is greater than expected for the *t*-Bu-thixantphos complex, the chemical shift of [Pt(η^2-CO_3)(PP)] complexes with mono, or diphosphines varies substantially (-12.0–58.7 ppm), and although reported coupling constants (3377–3697 Hz)[16,302] are smaller than for [Pt(*t*-Bu-thixantphos)(CO_3-κ^2O^1,O^2)] (4055 Hz) it has been shown throughout this chapter that the *t*-Bu-xantphos platinum complexes typically have larger J_{PtP} values than other complexes of the same type.

The [Pt(*t*-Bu-thixantphos)(CO_3-κ^2O^1,O^2)] complex converts over the course of several days into another intermediate. This intermediate has two different signals in the ^{31}P NMR spectrum in a 1:1 ratio at 50.5 and -38.7 ppm with platinum satellites of 1893 and 2854 Hz respectively. This shows a loss of the symmetry of the *t*-Bu-thixantphos ligand with the two phosphorus atoms now appearing in different environments. The large upfield shift (48.2 ppm from the free ligand) is typical for formation of a four-membered ring including the phosphorus atom.[314] The phosphorus atom at 50.5 ppm has a coupling constant indicative of a *trans* ligand with a high *trans*-influence such as an alkyl group. From this a *cis* arrangement of the phosphorus atoms with metallation of one of the *tert*-butyl substituents creating an alkyl group *trans* to the non-metallated phosphorus can be proposed. If metallation had occurred *via* a C-H activation an upfield signal in the ^{1}H NMR spectrum would be expected indicative of a platinum hydride. No such peak was observed, instead a strongly downfield ^{1}H signal was observed at 17.6 ppm indicating the presence of an acidic proton. From this information the conversion of the κ^2O^1,O^2-carbonate ligand into a κ^2O^1,O^2-bicarbonate incorporating the hydrogen from the metallated *tert*-butyl group is proposed. Unfortunately this complex is too short-lived to investigate by ^{13}C NMR spectroscopy

The final product in the reaction of [Pt(*t*-Bu-thixantphos)(η^2-O_2)] with carbon

monoxide forms by loss of carbon dioxide gas (observed in the ^{13}C NMR spectrum) from the [Pt(*t*-Bu-thixantphos-H-κ*P,P′,C*)(O_2COH-κ^2*O*^{1},*O*^{2})] complex. The final product shows two peaks in the ^{31}P NMR spectrum: one at -49.2 ppm (J_{PtP} = 3943 Hz) and the other at 38.2 ppm (J_{PtP} = 1794 Hz). This indicates the retention of the *t*-Bu-thixantphos ligand with one metallated *tert*-butyl group from the bicarbonate complex. The platinum-phosphorus coupling constants show that the non-metallated phosphorus is *trans* to the metallated *tert*-butyl group, while the metallated phosphorus is *trans* to a ligand with a weak *trans* influence. This ligand is proposed to be a hydroxyl, as this would result from loss of CO_2 from a bicarbonate, and hydroxyl ligands have a low *trans* influence. The final product shows a signal in the ^{13}C NMR spectrum for the metallated carbon at 15.7 ppm as a doublet of doublets with coupling of 81.6 Hz to the *trans* phosphorus and 35.6 Hz to the *cis* phosphorus, though no platinum satellites could be observed. The position of this peak is consistent with other platinum alkyls that occur *trans* to phosphorus.[315–317] No signal for the hydroxyl proton was observed in the ^{1}H NMR spectrum, which may indicate exchange with a deuterium from the solvent (CD_2Cl_2). The mass spectrum was also unable to confirm the presence of a hydroxyl ligand as a peak was observed for [M-OH]$^+$, as transition metal complexes frequently ionise by loss of weakly coordinated ligands.[210] The overall reaction showing the intermediates is given in Scheme 5.6.

The final two structures in the reaction of [Pt(*t*-Bu-thixantphos)(η^2-O_2)] with carbon monoxide (Scheme 5.6) are particularly noteworthy due to the *cis* coordination of the phosphines. Metallation of *i*-Pr-xantphos has been reported on iridium[81] with *i*-Pr-xantphos coordinating in a κ*P,P′,O,C* mode. However, the present example of [Pt(*t*-Bu-thixantphos-H-κ*P,P′,C*)OH] is the only example of κ*P,P′,C* coordination of a xantphos ligand. Sterically bulky ligands show a distinct preference for *trans* coordination (discussed further in Chapter 6). The metallacyclobutane must coordinate in two *cis* sites. However, the *t*-Bu-xantphos could still maintain a *trans* coordination. It is plausible that metallation of the *tert*-butyl group relieves the steric constraints of the system allowing for *cis* chelation of the phosphorus atoms. The P-Pt-C angle in the metallacyclobutane is also likely to be less than 90° resulting in additional room around the platinum centre.

Despite such unexpected chemistry with CO, [Pt(*t*-Bu-thixantphos)(η^2-O_2)] shows

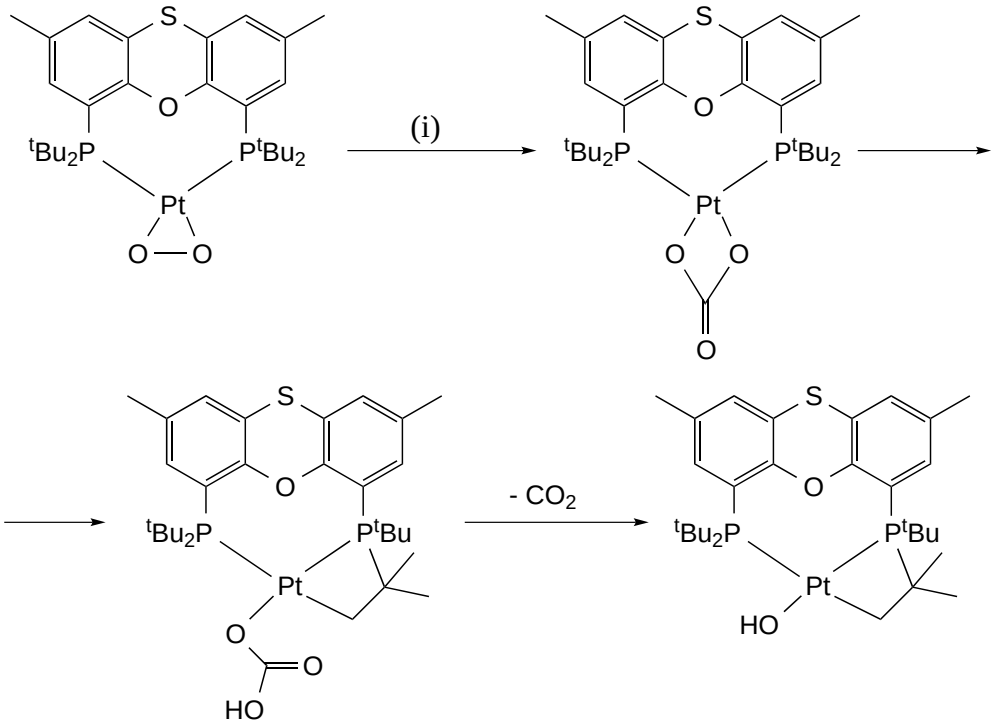

Scheme 5.6: Reaction between [Pt(*t*-Bu-thixantphos)(η^2-O_2)] and CO.

a distinct stability towards other small molecules. No reaction with ammonium hexafluorophosphate or with methane was observed. However, a straightforward reaction does occur with pta. Pta is a phosphine ligand with a very small cone angle making it an ideal choice to react with the sterically encumbered system.[318] Addition of pta to a solution of [Pt(*t*-Bu-thixantphos)(η^2-O_2)] showed immediate changes in the ^{31}P NMR spectrum, with new peaks appearing at 9.5 and -74.1 ppm (J_{PtP} = 3562 Hz). The peak at 9.5 ppm did not show any coupling to platinum and is consistent with an uncoordinated *t*-Bu-thixantphos ligand. The peak at -74.1 ppm is consistent with the literature reported [Pt(pta)$_4$] complex.[319] The ^{1}H and ^{13}C NMR data confirm these assignments. No intermediates were observed due to the speed of the reaction. This suggests that pta is able to displace both the dioxygen and the *t*-Bu-thixantphos ligand from the platinum, and thus is too reactive to gain any insight into the activation of the dioxygen moiety.

5.7 Reactions with Palladium(0) Precursors

Platinum complexes are frequently synthesised as models for the analogous palladium species as they are frequently more stable, and the presence of ^{195}Pt allows for additional information in the NMR spectra, which can be useful in characterisation. However, palladium complexes are of particular interest due to their use in a wide range of catalytic processes. These systems often involve both palladium(0) and palladium(II) complexes. A number of papers regarding the catalytic activity of palladium *t*-Bu-xantphos systems have also been reported though no investigation into the coordination chemistry has been published. As such, the reactivity of the *t*-Bu-xantphos ligands towards palladium(0) starting materials was investigated. All reactions discussed in this section were carried out on an NMR scale.

Initial investigations focussed on the reactivity of *t*-Bu-thixantphos towards palladium(0) precursors commonly used in catalysis. Allyl-(cyclopentadienyl)palladium(II) [Pd(C_3H_5)Cp] can react with phosphine ligands to give palladium(0) complexes. The reaction between *t*-Bu-thixantphos and [Pd(C_3H_5)Cp] in C_6D_6 was slow. After 24 hours at room temperature no changes in the NMR spectra were observed. After 48 hours at 50 °C no unreacted *t*-Bu-thixantphos was observed in the ^{31}P NMR spectrum. However, the ^{31}P and ^{1}H NMR spectra showed a number of different products, which were unable to be separated or analysed further.

[$Pd_2(dba)_3$] (dba = dibenzylideneacetone) is another common palladium(0) complex used as a precatalyst. The reaction between *t*-Bu-thixantphos and [$Pd_2(dba)_3$] generated a mixture of products. However, a single major product was observed at 40.0 ppm in the ^{31}P NMR spectrum (C_6D_6), after heating at 40 °C for four days. The major product integrated for 67% of the ^{31}P containing species while uncoordinated *t*-Bu-thixantphos accounted for 17% of the reaction mixture. The species was not [Pd(*t*-Bu-thixantphos)] (this will be discussed shortly). However, the product was unable to be isolated from the reaction mixture and the presence of large amounts of uncoordinated dba hampered the further characterisation of this species. It is possible that the species was [Pd(*t*-Bu-thixantphos)(dba)] although little evidence to support this could be obtained.

Platinum alkene complexes, such as the air-stable solids [$Pt(cod)_2$] and [$Pt(nb)_3$],

make excellent starting materials for the formation of platinum(0) complexes.[291,299] Although [Pt(C_2H_4)$_3$] is only stable under an ethene atmosphere it is readily synthesised *in situ*, *via* reaction of ethene with [Pt(cod)$_2$].[320] Unfortunately the corresponding palladium complexes are typically unstable at room temperature in solution and are not practical to be used as starting materials.[321] However, given the slow reactivity of *t*-Bu-thixantphos with [Pd(C_3H_5)Cp] and [Pd$_2$(dba)$_3$], coupled with the desire to investigate the analogues of the platinum alkene complexes discussed earlier, the reactivity of *t*-Bu-thixantphos towards [Pd(nb)$_3$] was studied. [Pd(nb)$_3$], like other palladium alkene complexes, is unstable in solution, with significant degradation observed at room temperature.[321] However, the amount of degradation can be reduced by addition of excess norbornene to the reactions.

Reaction of *t*-Bu-thixantphos with [Pd(nb)$_3$] was rapid compared to the other palladium(0) starting materials, going to completion in 72 hours at room temperature. The reaction formed a mixture of [Pd(*t*-Bu-thixantphos)(nb)] (38.0%) and [Pd(*t*-Bu-thixantphos)] (62.0%). As such, the reaction was also carried out with *t*-Bu-sixantphos and *t*-Bu-xantphos. The reaction of *t*-Bu-xantphos with [Pd(nb)$_3$] was complete in under one hour forming a mixture including, [Pd(*t*-Bu-xantphos)(nb)] (12.6%) and [Pd(*t*-Bu-xantphos)] (73.1%). Using *t*-Bu-sixantphos resulted in only 43.4% product in the ^{31}P NMR spectrum after 24 hours (the remainder being free ligand). No further progress in the reaction between *t*-Bu-sixantphos and [Pd(nb)$_3$] was observed by NMR spectroscopy after 48 hours. However, after five months at room temperature the reaction had progressed to 68% complex indicating that the lack of reactivity was not necessarily due to degradation of the [Pd(nb)$_3$].

The major products from the reaction of the *t*-Bu-xantphos ligands with [Pd(nb)$_3$] appear at 41.9–42.9 ppm in the ^{31}P NMR spectra. Given the similarity in the ^{31}P chemical shift and the inability to isolate the *t*-Bu-sixantphos and *t*-Bu-xantphos complexes, the *t*-Bu-thixantphos complex was the only product explored in depth. Once the product was formed, the norbornene was removed under vacuum with no degradation of the resulting complex. The complex displays no resonances in the ^{1}H and ^{13}C NMR spectra apart from those corresponding to a coordinated *t*-Bu-thixantphos ligand. The quarternary and terminal *tert*-butyl carbon and proton signals appear as virtual triplets, consistent with a *trans* coordination of phosphorus atoms. Hence, the complexes formed in these three

reactions are [Pd(*t*-Bu-xantphos)] species (Scheme 5.7).

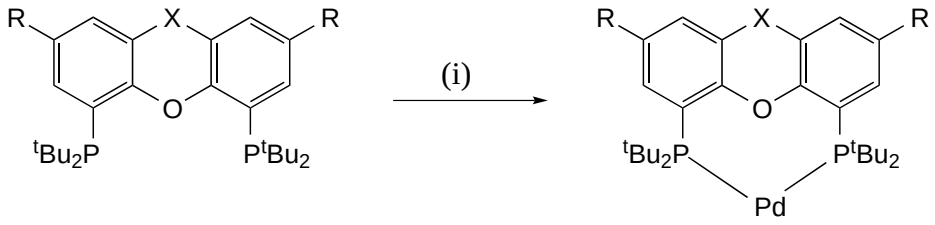

Scheme 5.7: Formation of the major product in the reaction between the *t*-Bu-xantphos ligands and [Pd(nb)$_3$]. *Reagents and conditions:* (i) [Pd(nb)$_3$], C_6D_6.

5.7.1 Reaction of [Pd(*t*-Bu-thixantphos)] with Oxygen

The [Pt(*t*-Bu-thixantphos)] complex reacts rapidly and irreversibly with dioxygen to form [Pt(*t*-Bu-thixantphos)(η^2-O_2)] (Section 5.5). Previous examples have indicated that the coordination of dioxygen to palladium is frequently reversible even if the platinum analogue is not.[307] Reaction of [Pd(*t*-Bu-thixantphos)] with oxygen occurs rapidly forming a green [Pd(*t*-Bu-thixantphos)(η^2-O_2)] complex. The ^{31}P NMR spectrum shows a smaller change in chemical shift than is observed with the platinum analogue (9.1 compared to 40.2 ppm) and the shift is downfield rather than upfield as in the platinum case. This is likely due to marked differences in the 14-electron complexes rather than the dioxygen complexes as the ^{31}P NMR signal for [Pt(*t*-Bu-thixantphos)] appears at 78.6 ppm, whereas the signal for [Pd(*t*-Bu-thixantphos)] is at 42.9 ppm. The *tert*-butyl signals in the ^{1}H and ^{13}C NMR spectra of [Pd(*t*-Bu-thixantphos)(η^2-O_2)] appear as doublets indicating the loss of the *trans* arrangement of the phosphorus atoms.

The reaction of [Pd(*t*-Bu-thixantphos)] with dioxygen was observed to be readily reversible. Removal of the solvent from the NMR sample under vacuum for a few minutes was sufficient for the dioxygen to dissociate and undergo complete reversion to [Pd(*t*-Bu-thixantphos)]. This is consistent with the literature, which indicates that coordination of dioxygen to palladium complexes is typically reversible.[307] This may be due to the reduced back-bonding of palladium compared to platinum, which results in less activation of the O-O bond upon coordination, such that on palladium the dioxygen is more like a neutral O_2 ligand,

whereas on platinum the dioxygen becomes more like a peroxy O_2^{2-}.

5.8 Computational Results

It has been observed throughout this chapter that the differences in the coordination chemistry of the three *t*-Bu-xantphos ligands with platinum and palladium is subtle, often forming mixtures of products and some readily reversible systems. However, a number of the complexes were unable to be isolated and fully characterised. As such, we have investigated the conversion of the [M(*t*-Bu-xantphos)] complexes to [M(*t*-Bu-xantphos)(nb)] or [M(*t*-Bu-xantphos)(η^2-O_2)] (M = Pd, Pt) using DFT. Structural models of the complexes were optimised and their vibrational frequencies calculated using a B3LYP functional,[131–134] with the def2-TZVP basis set.[135,136]

Selected bond lengths and angles are given in Tables 5.8, 5.9 and 5.10 for [M(*t*-Bu-xantphos)], [M(*t*-Bu-xantphos)(nb)] and [M(*t*-Bu-xantphos)(η^2-O_2)] respectively. The P-M-P angles are larger in the [M(*t*-Bu-xantphos)] complexes than in the [M(*t*-Bu-xantphos)(nb)] and [M(*t*-Bu-xantphos)(η^2-O_2)] as expected. However, the P-M-P angles in the [M(*t*-Bu-xantphos)] complexes are smaller than the idealised 180° expected for a two-coordination platinum(0) complex. The rigid backbone of the *t*-Bu-xantphos ligands likely prevents larger bite-angles from forming without introducing coordination to the oxygen bridge in the backbone. In this case the M-O distances are larger than expected for Pt-O or Pd-O bonds, indicating that no bonding interaction is present. The C=C and O-O distances for the norbornene in [M(*t*-Bu-xantphos)(nb)] and the dioxygen in [M(*t*-Bu-xantphos)(η^2-O_2)] are longer on platinum than palladium, consistent with the higher π-aciditiy of platinum compared to palladium.[280]

The Gibbs free energies of the complexes were calculated and the values of ΔG for the reaction of the [M(*t*-Bu-xantphos)] (M = Pd, Pt) complexes with norbornene were calculated (Table 5.11). The value of ΔG for the reaction between the [M(*t*-Bu-xantphos)] complexes and norbornene is positive, indicating that the reaction would not occur spontaneously and the 14-electron complex is the lower energy system. This is consistent with the experimental results for the palladium complexes. However, in the platinum system mixtures of the norbornene and the 14-electron complexes were observed for both *t*-Bu-sixantphos and *t*-

Table 5.8: Calculated bond lengths and angles for [M(*t*-Bu-xantphos)].

Ligand	**P-Pt-P**/°	**P-Pd-P**/°	**Pt-O**/ Å	**Pd-O** /Å
t-Bu-Sixantphos	152.5	150.2	2.7982	2.7954
t-Bu-Thixantphos	151.8	149.4	2.8290	2.8283
t-Bu-Xantphos	151.5	149.3	2.7791	2.7723

Table 5.9: Calculated bond lengths and angles for [M(*t*-Bu-xantphos)(nb)].

Ligand	**P-Pt-P**/°	**P-Pd-P**/°	**C=C (Pt)** /Å	**C=C (Pd)** /Å
t-Bu-Sixantphos	114.8	115.4	1.4359	1.4055
t-Bu-Thixantphos	115.6	116.2	1.4353	1.4046
t-Bu-Xantphos	116.0	116.6	1.4355	1.4055

Table 5.10: Calculated bond lengths and angles for [M(*t*-Bu-xantphos)(η^2-O_2)].

Ligand	**P-Pt-P**/°	**P-Pd-P**/°	**O-O (Pt)** /Å	**O-O (Pd)** /Å
t-Bu-Sixantphos	115.3	118.7	1.4083	1.3714
t-Bu-Thixantphos	116.8	118.6	1.4078	1.3710
t-Bu-Xantphos	117.2	119.6	1.4070	1.3705

Bu-thixantphos. In the case of *t*-Bu-xantphos, the [Pt(*t*-Bu-xantphos)] complex was formed initially but this converted to [Pt(*t*-Bu-xantphos-κ*P,O,P'*)H]$^+$. This hydride complex is likely the result of the 14-electron complex undergoing reaction with another component of the system. Although the [Pt(*t*-Bu-xantphos)] complexes are formed as the major products experimentally, an equilibrium with the norbornene complex is likely present. These calculations do not take into account the effect of having a large excess of norbornene present in solution, which may result in an equilibrium between the [Pt(*t*-Bu-xantphos)] and [Pt(*t*-Bu-xantphos)(nb)] complexes.

The values for the Gibbs free energies of the [M(*t*-Bu-xantphos)(η^2-O_2)] (M = Pd, Pt) complexes were also calculated together with the ΔG values for their formation from the [M(*t*-Bu-xantphos)] complexes (Table 5.12). All of the ΔG values are negative, indicating that the formation of the dioxygen complex is spontaneous. The ΔG values for the palladium complexes are more negative than the platinum ones. This suggests that the palladium complexes should be more stable than the platinum system to reversibility. However, this was not observed experimentally for the *t*-Bu-thixantphos system where the platinum dioxygen complex was very stable and the palladium dioxygen complex readily converted to the [Pd(*t*-Bu-thixantphos)] species. From Table 5.10 we can see that the P-M-P angle is consistently larger in the palladium complexes than the platinum, while the O-O bond length is smaller for the palladium complexes. This suggests that there is less back-donation from the metal centre into the oxygen π^*-orbital. Hence, the dioxygen ligand on palladium is less strongly coordinated than on platinum and may have a lower activation barrier towards dissociation.

5.9 Summary

Ph-Thixantphos was shown to react with [Pt(nb)$_3$] and [Pt(C_2H_4)$_3$] forming [Pt(Ph-thixantphos)$_2$] as the major product in both 1:1 and 2:1 reactions. [Pt(Ph-thixantphos)(alkene)] (alkene = nb, C_2H_4) were present as minor components in the 1:1 reactions. [Pt(Ph-thixantphos)] was characterised by X-ray crystallography showing a tetrahedral environment around the platinum. The ^{1}H and ^{31}P NMR spectra of [Pt(Ph-thixantphos)] at room temperature are broad, possibly due to inversion of the backbone. However, cooling to -40 °C resolved a pair of triplets

Table 5.11: Gibbs free energies calculated for reaction of [M(*t*-Bu-xantphos)] with norbornene (M = Pd, Pt). All values are in kJ mol^{-1}, Norbornene G = -715998.2 kJ mol^{-1}.

PP	**[Pd(PP)]**	**[Pd(PP)(nb)]**	**Pd ΔG**	**[Pt(PP)]**	**[Pt(PP)(nb)]**	**Pt ΔG**
t-Bu-Sixantphos	-6163451.1	-6879350.9	98.4	-6140995.8	-6856897.4	96.6
t-Bu-Thixantphos	-6445645.2	-7161551.4	92.1	-6423187.2	-7139098.3	87.1
t-Bu-Xantphos	-5503258.5	-6219169.0	87.8	-5480799.2	-6196709.7	87.7

Table 5.12: Gibbs free energies calculated for reaction of [M(*t*-Bu-xantphos)] with oxygen (M = Pd, Pt). All values are in kJ mol^{-1} oxygen G = -394857.8 kJ mol^{-1}.

PP	**[Pd(PP)]**	**[Pd(η-O_2)(PP)]**	**Pd ΔG**	**[Pt(PP)]**	**[Pt(η-O_2)(*t*-Bu-xantphos)]**	**Pt ΔG**
t-Bu-Sixantphos	-6163451.1	-6558323.8	-14.8	-6140995.8	-6535862.4	-8.8
t-Bu-Thixantphos	-6445645.2	-6840520.9	-17.8	-6423187.2	-6818062.4	-17.4
t-Bu-Xantphos	-5503258.5	-5898134.9	-18.6	-5480799.2	-5875674.2	-17.2

with platinum satellites.

No evidence for a bis(diphosphine) complex was observed in the reactions of the *t*-Bu-xantphos ligands with [Pt(nb)$_3$], [Pt(cod)$_2$],[Pt(C_2H_4)$_3$], and [Pd(nb)$_3$] starting materials. Reaction with [Pd(nb)$_3$] formed mixtures with [Pd(*t*-Bu-xantphos)] as the major product. Similarly, reaction of *t*-Bu-thixantphos with [Pt(nb)$_3$] formed a mixture of [Pt(*t*-Bu-thixantphos)] and [Pt(*t*-Bu-thixantphos)(nb)]. Analogues of these two complexes were also observed in the analogous reaction with *t*-Bu-sixantphos, in addition to an unknown complex with a coupling constant indicative of platinum(II). The reaction between [Pt(nb)$_3$] and *t*-Bu-xantphos formed [Pt(*t*-Bu-xantphos)] as a minor component which converted into [Pt(*t*-Bu-xantphos)H]X.

The reactions of the *t*-Bu-xantphos ligands with [Pt(C_2H_4)$_3$] resulted in [Pt(*t*-Bu-xantphos)(C_2H_4)] complexes. [Pt(*t*-Bu-xantphos)(C_2H_4)] went on to produce [Pt(*t*-Bu-xantphos)H]X. Reacting *t*-Bu-thixantphos with [Pt(cod)$_2$] formed only [Pt(*t*-Bu-thixantphos)], though the yield was low due to degradation.

[Pd(*t*-Bu-thixantphos)], [Pt(*t*-Bu-thixantphos)], and [Pt(*t*-Bu-thixantphos)(C_2H_4)] all react rapidly with air forming [M(*t*-Bu-thixantphos)(η^2-O_2)] (M = Pd, Pt). With palladium this reaction was readily reversibly in a few minutes under vacuum. On platinum the coordination of oxygen was not reversible either by vacuum, or reaction with C_2H_4 or H_2. [Pt(*t*-Bu-thixantphos)(η^2-O_2)] was characterised by X-ray crystallography, displaying a planar molecule with a bent *t*-Bu-thixantphos backbone. The bite-angle was 117.26(5), smaller than the natural bite-angle of (126.98°), but the largest P-Pt-P angle of the five [Pt(η^2-O_2)(P_2)] complexes that have been characterised crystallographically.

[Pt(*t*-Bu-thixantphos)(η^2-O_2)] was tested for reactivity towards a range of different small molecules. No reaction was observed with ethyne, ammonium hexafluorophosphate or carbon dioxide. Reaction with the small phosphine pta produce uncoordinated *t*-Bu-thixantphos and [Pt(pta)$_4$], going to completion when four equivalents of pta were used. Reaction of [Pt(*t*-Bu-thixantphos)(η^2-O_2)] with carbon monoxide initially formed the expected carbonate complex. However, this continued to react, undergoing metallation of a *tert*-butyl methyl to form a bicarbonate, which loses carbon dioxide leaving a hydroxyl ligand coordinated to the platinum centre.

The [M(*t*-Bu-xantphos)], [M(*t*-Bu-xantphos)(nb)], and [M(*t*-Bu-xantphos)(η^2-O_2)] (M = Pd, Pt) complexes were explored computationally. The O-O bond were longer in the platinum complexes than in the palladium, which may explain the ready dissociation of the dioxygen from the palladium complex while the platinum complex was not reversible. The ΔG values for the formation of the norbornene and the dioxygen complexes from the 14-electron complexes were also calculated. The results indicated that the formation of the dioxygen complex is spontaneous, although the formation of the norbornene complex from the [Pt(*t*-Bu-xantphos)] complexes is not. While this does not take into account the effect of having excess norbornene in solution which may effect the position of the equilibrium.

Overall this chapter provides an account into the coordination chemistry of *t*-Bu-sixantphos, *t*-Bu-thixantphos, and *t*-Bu-xantphos with platinum(0) and palladium(0) and the reactivity of Ph-thixantphos towards [Pt$(nb)_3$] and [Pt$(C_2H_4)_3$]. Several new complexes have been synthesised including two characterised by X-ray crystallography. In a number of cases the reactivity of the three *t*-Bu-xantphos ligands was different, indicating the role of the bite-angle on the coordination chemistry of these compounds.

Chapter 6

Coordination Complexes with Platinum(II) and Palladium(II)

Coordination complexes of palladium are used as catalysts for a wide range of reactions including cross-coupling, allylic alkylation and various carbonylation reactions, which are important on both laboratory and industrial scales.[6,32,149,273–279] The high reactivity of palladium complexes can render them difficult to characterise and study. Platinum and palladium have similar overall reactivity patterns. However, platinum complexes are typically more inert than their corresponding palladium analogues to processes such as ligand exchange and redox changes.[280] The presence of a spin active isotope ^{195}Pt (34% abundant) can result in coupling in the NMR spectra, which can give additional information about the nature of the complexes. This makes platinum a useful model for the chemistry of palladium.

Seven reports have been published investigating the catalytic activity of palladium complexes using *t*-Bu-xantphos. These include the N-arylation and alkylation of amines, cross-coupling of thiols and aryl bromides or triflates, Suzuki cross-coupling, hydroesterificaton of methyl oleate, aminocarbonylation of hetero(aryl) bromides, and the methylation of alkynyl C-H bonds with dimethyl sulfonium ylides.[84,87,93–95,97,98] In the N-arylation of heterocyclic diamines the *t*-Bu-xantphos system showed little activity ($< 1\%$), whereas the Ph-xantphos system was more successful (40%).[87] In the N-alkylation of aniline with benzyl alcohol the *t*-Bu-xantphos system gave 100% conversion at 100 °C while the Ph-xantphos reaction at 110 °C only gave 63%.[94] The cross-coupling of butane thiol with

phenyl triflates in xylene at 140 °C produced only trace amounts of the product using *t*-Bu-xantphos while an 80% yield was obtained with Ph-xantphos.[84] The Ph-xantphos complex was also more reactive in the Suzuki cross-coupling of 2-(4-bromophenyl)-5-chloropyrazine with a benzimidazole boronic ester giving a 83% yield compared to only 5% with *t*-Bu-xantphos.[97] The same lack of activity was observed for the hydroesterification of methyl oleate, with no conversion obtained for *t*-Bu-xantphos compared to 70% for Ph-xantphos. In the methylation of alkynyl C-H bonds with dimethyl sulfonium ylides, the *t*-Bu-xantphos ligand produced a greater yield than the Ph-xantphos ligand (46% compared to 15%).[95] Together, these studies suggest differences in the coordination chemistry and reactivity of the *t*-Bu-xantphos and Ph-xantphos ligands. However, little research into the coordination chemistry of *t*-Bu-xantphos has been performed.

Only two palladium complexes of *t*-Bu-xantphos have been reported. The X-ray crystal structure of [Pd(*t*-Bu-xantphos)Cl_2] was reported to the CSD in 2011 (CSD-XARXAR),[68] however a research paper including synthetic details has not been published. The crystal structure (Figure 6.1) has three molecules in the asymmetric unit each showing a distorted *trans* geometry with P-Pd-P angles of 160.59(4), 161.97(3) and 161.31(4)°. These are larger than the 100.61(5) and 100.92(7)° for [Pd(Ph-xantphos)Cl_2] with different solvates.[68,145,281] The difference in the bite-angles and geometries of the complexes that form may explain the difference in the catalytic reactivity of the complexes. The other complex reported for *t*-Bu-xantphos showed an unusual monodentate coordination mode (Figure 6.2).[93] This is not a common coordination mode for the xantphos ligands and the same complex was also formed with Ph-xantphos. In an aminocarbonylation reaction the Ph-xantphos complex gave a 92% isolated yield, while no product was observed using the *t*-Bu-xantphos system. The reason for this difference was not addressed in the publication.

Metal halide complexes are ubiquitous in coordination chemistry. They form a number of complexes that are active catalysts, and are widely used as starting points for the synthesis of more complex systems. Platinum halide complexes are also of interest due to their potential as chemotherapeutics. Complexes such as, *cis*-platin [$PtCl_2(NH_3)_2$] and its derivatives are now an important part of several treatment protocols and have improved the prognosis for many cancer patients, for example, the cure rate of testicular cancer has increased from less than 10% to over 90%.[3]

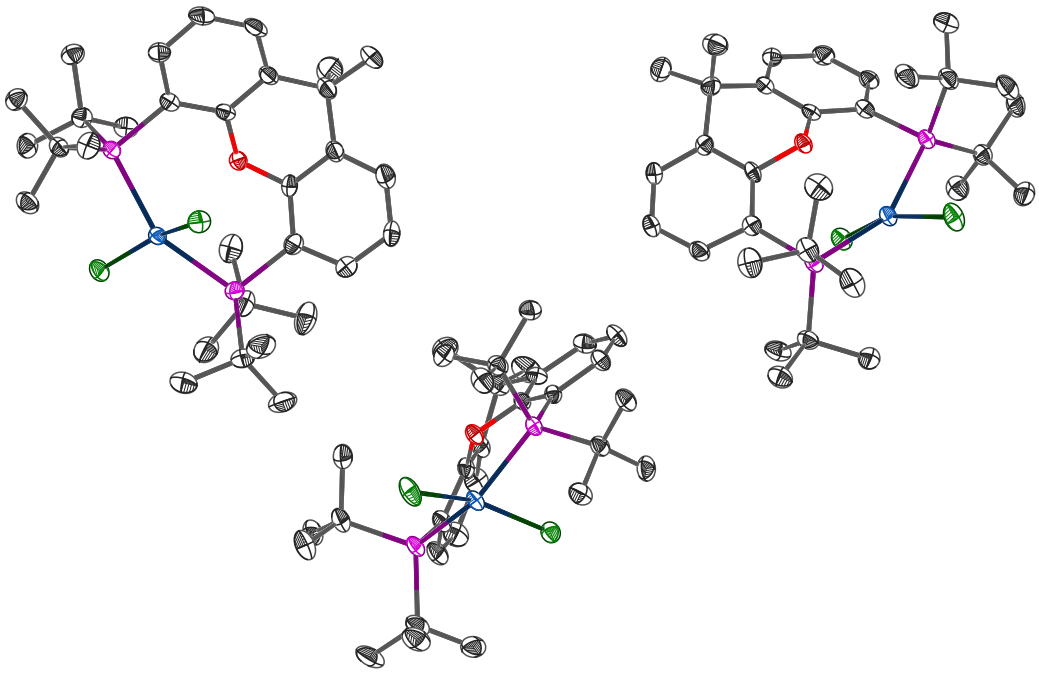

Figure 6.1: X-ray crystal structure of [Pd(*t*-Bu-xantphos)Cl_2] (CSD-XARXAR).[68] Hydrogen atoms and solvent of crystallisation omitted for clarity.

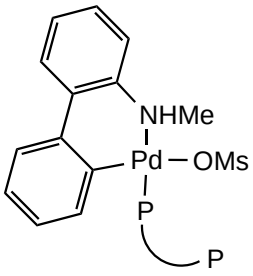

Figure 6.2: Previously reported palladium complex with PP = *t*-Bu-xantphos or Ph-xantphos.[93]

The coordination chemistry of Ph-xantphos on palladium has been the subject of a number of studies,[73–75,79,115,282,283] though few have investigated the coordination chemistry with platinum. Catalytic systems frequently involve palladium in both the 0 and +2 oxidation states, hence it is important that both are studied.[31] Investigation into the coordination chemistry of the *t*-Bu-xantphos ligands with platinum and palladium(0) was reported in Chapter 5. This chapter will present work on the coordination chemistry of the three *t*-Bu-xantphos ligands with platinum and palladium(II) in order to investigate the differences and similarities in the chemistry of the *t*-Bu-xantphos ligands with the Ph-xantphos ligands.

6.1 Reactions with Platinum Dichloride Starting Materials

The reactivity of the *t*-Bu-xantphos ligands towards platinum dichloride starting materials was initially investigated by studying the reaction of *t*-Bu-thixantphos with a range of different starting materials in both *cis* and *trans* geometries: [$PtCl_2$(hex)], (hex = hexa-1,5-diene) *cis*-[$PtCl_2(SEt_2)_2$], *cis*-[$PtCl_2(MeCN)_2$], *trans*-[$PtCl_2$(MeCN)], and *trans*-[$PtCl_2(^tBuCN)_2$]. In a number of cases, the reaction was very slow and protonation of the *t*-Bu-thixantphos ligand occurred faster than the formation of a platinum complex. If a platinum complex was produced, it was the same species irrespective of the starting material or conditions of the reaction. The most successful result went to completion after 72 hours in toluene at 50 °C using [$PtCl_2$(hex)], which contains a readily displaced diene ligand. In C_6D_6 the product appears in the ^{31}P NMR spectrum as a singlet at 32.9 ppm with a J_{PtP} value of 2700 Hz. The value of the one-bond phosphorus-platinum coupling constant can give important information regarding the geometry of the complex. In particular, the value of J_{PtP} is highly dependent on the *trans*-influence of the ligand *trans* to the phosphorus atom.[16] A value of 2700Hz for J_{PtP} is characteristic of mutually *trans* phosphorus atoms, rather than phosphorus *trans* to a chloride (J_{PtP} = 3200–3800 Hz).[252,253,322] Hence, the product of the reaction between *t*-Bu-thixantphos and [$PtCl_2$(hex)] is *trans*-[Pt(*t*-Bu-thixantphos)Cl_2] (Scheme 6.1).

[Pt(*t*-Bu-thixantphos)Cl_2] is dark red in both C_6D_6 solution and the solid state.

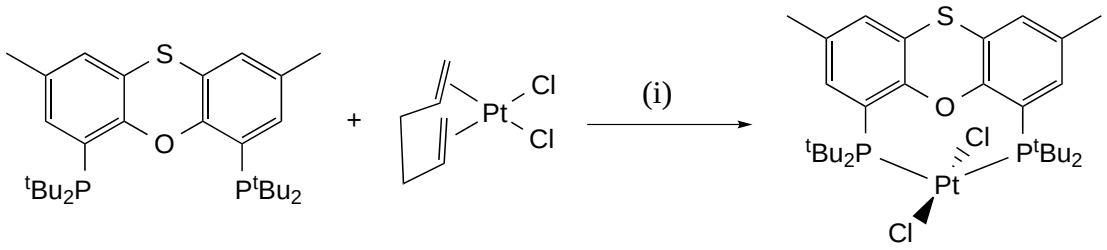

Scheme 6.1: Synthesis of [Pt(*t*-Bu-thixantphos)Cl_2]. *Reagents and conditions:* (i) toluene, 50 °C, 3 days.

This is unusual as platinum dichloride complexes are typically pale, or yellow in colour. Indeed the previously reported [Pt(Ph-xantphos)Cl_2] complex is a white solid.[86] This suggests that [Pt(*t*-Bu-thixantphos)Cl_2] is unusual from an electronic perspective, which may be the result of a strained coordination geometry.

Dark red crystals of [Pt(*t*-Bu-thixantphos)Cl_2] suitable for X-ray diffraction were grown by inwards diffusion of diethyl ether into a dichloromethane solution of the complex. The structure is shown in Figure 6.3, with a side-on view in Figure 6.4. The complex crystallises in the monoclinic crystal system in the space group $P2_1/c$. Selected bond lengths and angles are given in Table 6.1, and the crystallographic data is given in Table 6.2.

Table 6.1: Selected bond distances (Å) and angles (°) of [Pt(*t*-Bu-thixantphos)Cl_2].

Bond distances (Å)		**Bond angles (°)**	
P1...P2	4.5037(6)	P1-Pt-P2	151.722(15)
P1-Pt	2.3205(4)	Cl1-Pt-Cl2	164.235(15)
P2-Pt	2.3239(4)	P1-Pt-Cl1	87.11(15)
Pt-Cl1	2.3209(4)	P1-Pt-Cl2	95.939(16)
Pt-Cl2	2.3098(4)	P2-Pt-Cl1	86.699(14)
Pt...O	2.8016(11)	P2-Pt-Cl2	96.917(15)
		Ring 1-Ring 2	139.11(6)

The crystal structure of [Pt(*t*-Bu-thixantphos)Cl_2] (Figure 6.3) is distorted from the square-planar geometry typically observed for Pt(II) complexes. The τ_5 pa-

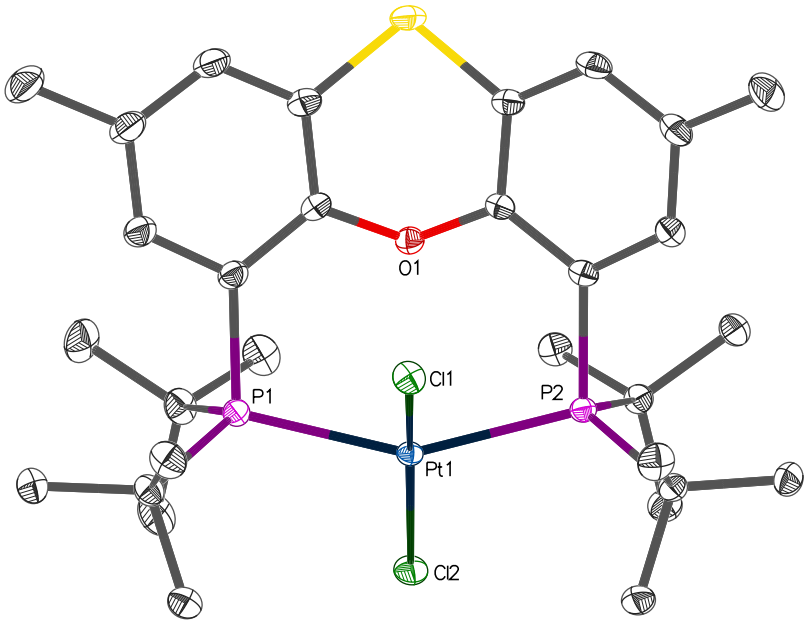

Figure 6.3: X-ray crystal structure of [Pt(*t*-Bu-thixantphos)Cl_2] (50% probability thermal ellipsoids). Hydrogen atoms omitted for clarity.

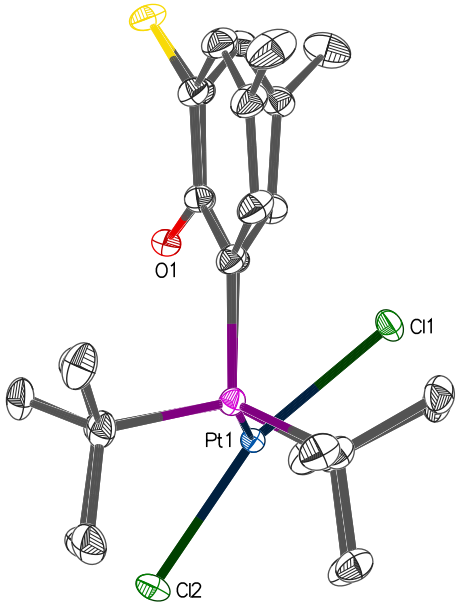

Figure 6.4: X-ray crystal structure of [Pt(*t*-Bu-thixantphos)Cl_2], side view (50% probability thermal ellipsoids). Hydrogen atoms omitted for clarity.

Table 6.2: Crystallographic data and structure refinement of [Pt(*t*-Bu-thixantphos)Cl_2].

Empirical formula	**$C_{30}H_{46}Cl_2OP_2PtS$**
Formula weight	782.66
Temperature/K	284.87(10)
Crystal system	monoclinic
Space group	$P2_1/c$
a/Å	15.26769(8)
b/Å	10.98650(7)
c/Å	19.05134(13)
$\alpha/^\circ$	90
$\beta/^\circ$	95.2318(5)
$\gamma/^\circ$	90
Volume/$Å^3$	3182.33(3)
Z	4
ρ_{calc} mg/mm^3	1.634
µ/mm	4.766
F(000)	1568.0
Crystal size/mm	0.27 x 0.14 x 0.08
Radiation	MoKα (λ = 0.71073)
2θ range for data collection	5.264 to 75.522°
Index ranges	-25 $\leq$ h $\leq$ 25, -15 $\leq$ k $\leq$ 18, -32 $\leq$ l $\leq$ 31
Reflections collected	49341
Independent reflections	16242 [R_{int} = 0.0277, R_{sigma} = 0.0333]
Data/restraints/parameters	16242/0/348
Goodness-of-fit on F^2	1.076
Final R indexes [I>=2σ (I)]	R_1 = 0.0240, wR_2 = 0.0445
Final R indexes [all data]	R_1 = 0.0351, wR_2 = 0.0486
Largest diff. peak/hole / e $Å^{-3}$	1.46/-1.27

rameter has been used for many years to describe the shapes of five-coordinate complexes.[323] In 2007 a related τ_4 parameter was introduced to describe the distortion of four-coordinate copper complexes between the ideal tetrahedral and square planar geometries.[324] The parameter is defined in Equation 6.1 where α and β are the two largest L-M-L angles in the four-coordinate complex. The value of τ_4 vary between 0 for an ideal square-planar complex to 1 for a tetrahedral complex. Using the two largest angles for [Pt(*t*-Bu-thixantphos)Cl_2] (P1-Pt-P2 = 151.722 and Cl1-Pt-Cl2 = 164.235) gives a value for τ_4 of 0.31. This indicates severe distortion from the expected square-planar geometry with the structure closest to a seesaw geometry.

$$\tau_4 = \frac{360 - (\alpha + \beta)}{141} \tag{6.1}$$

The bite-angle of the *t*-Bu-thixantphos ligand is 151.722(15)° in [Pt(*t*-Bu-thixantphos)Cl_2], which is significantly larger than the natural bite-angle determined by DFT (126.98°, Section 2.2). This deviation is likely due to the influence of the platinum centre, which prefers a coordination geometry close to square-planar. The bite-angle is unusual for complexes of the type [Pt(PP)Cl_2], where PP is either two monophosphine ligands or one diphosphine ligand. A search of the CSD showed that the P-Pt-P angles of these complexes are very bi-modal, showing clear preference for the *cis* 90° or the *trans* 180° (Figure 6.5).[68] The *t*-Bu-thixantphos angle (151.722(15)°) is situated between these two regions, with the closest *bis*-monophosphine complex at 167.261, and the closest chelating diphosphine at 171.9(4)°. Seven other *trans*-dichloridoplatinum complexes which have chelating diphosphines have been reported (Figure 6.6).[33,325–330] All of these have larger P-Pt-P angles than the *t*-Bu-thixantphos complex (171.9(4)–180.00(0)°). The chelate ring size for these molecules (Figure 6.6) ranges from 10–14 atoms, with the cyclodextrin-derived system having a ring size of 21 atoms (Figure 6.6g). In contrast, the *t*-Bu-thixantphos chelate ring contains only 8 atoms. This relatively small chelation ring size, combined with the rigidity of the backbone is likely the reason for the distortion around the platinum centre as the *trans* chelation puts strain on the *t*-Bu-thixantphos ligand.

The P-Pt-P angle of [Pt(*t*-Bu-thixantphos)Cl_2] (151.722(15)°) is much larger than in the closest *cis*-[$PtCl_2(P_2)$] (P_2 = chelating diphosphine) complexes (113.39(3))°

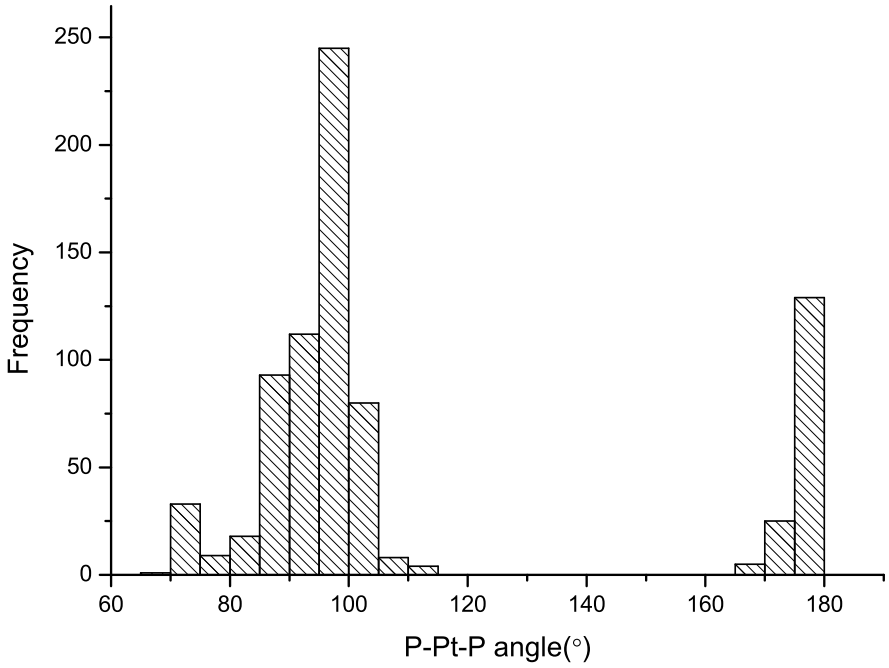

Figure 6.5: Distribution of the P-Pt-P angles in crystal structures of $[PtCl_2(P_2)]$ where P = tertiary phosphine ligand, P_2 = chelating diphosphine ligand.

and 113.43(6)°). Both of these complexes contain xantphos ligands, indicating that the rigid xantphos backbone plays a role in forming species with larger bite-angles.[331,332] In addition to the two already mentioned, three other crystal structures for $[PtCl_2(xantphos)]$ complexes have been reported (Figure 6.7).[333–335] These complexes have crystallographically determined bite-angles of 99.17(3), 99.64(4) and 100.87(8)°. Although these are all *cis* dichloride complexes it can be seen that the xantphos ligands have access to larger bite-angles than the ideal 90° of the square-planar platinum(II) complexes. In [Pt(*t*-Bu-thixantphos)Cl_2] it is likely that the *trans* coordination of the chloride ligands is the result of the increased steric demand of the *tert*-butyl substituents, which results in the larger observed bite-angle.

The angle of the coordination plane relative to the backbone of the $[PtCl_2(xantphos)]$ complexes appears to be related to the bite-angle. The three xantphos complexes with bite-angles of 99–100° (Figure 6.8) have a coordination plane

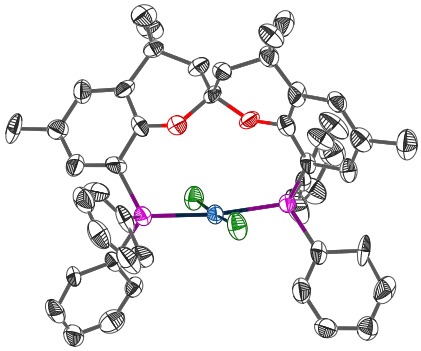

(a) 10 atoms, 171.9(4)° [33]

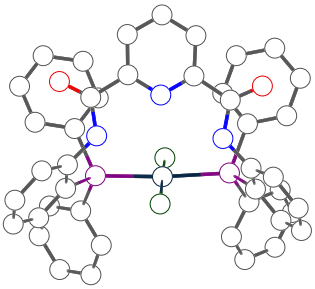

(b) 14 atoms, 172.25(4)° [329]

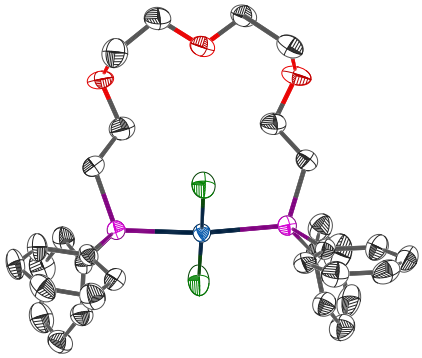

(c) 14 atoms, 173.01(6)° [328]

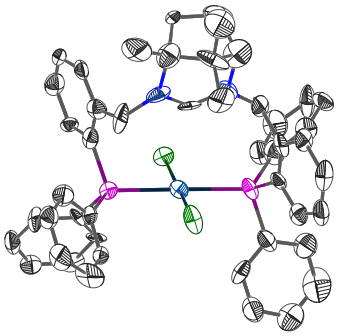

(d) 12 atoms, 174.9(3)° [327]

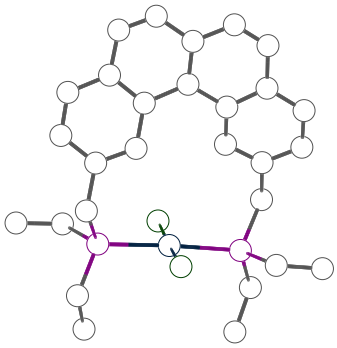

(e) 12 atoms, 177.1(3)° [325]

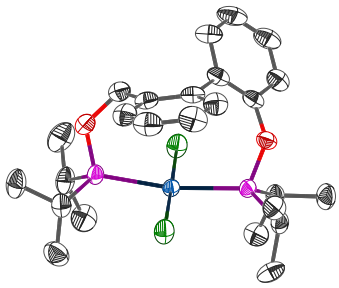

(f) 10 atoms, 177.77(6)° [330]

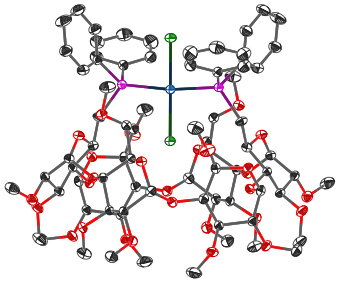

(g) 21 atoms, 180.00(0)° [326]

Figure 6.6: X-ray crystal structures of dichloridoplatinum complexes with *trans*-spanning diphosphine ligands. The values given are the P-Pt-P angles.

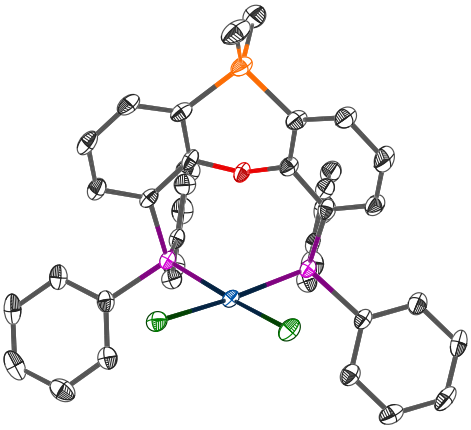

(a) 99.17(3)° [334]

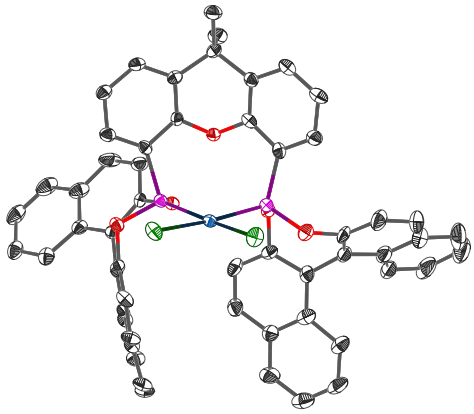

(b) 99.64(4)° [333]

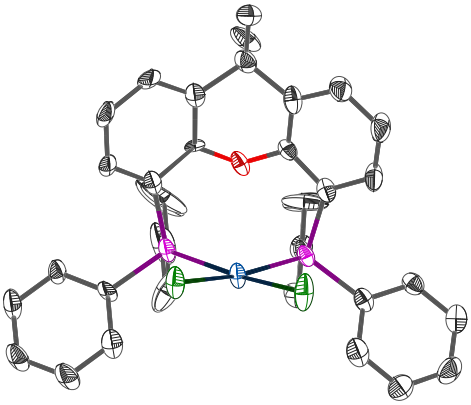

(c) 100.87(8)° [335]

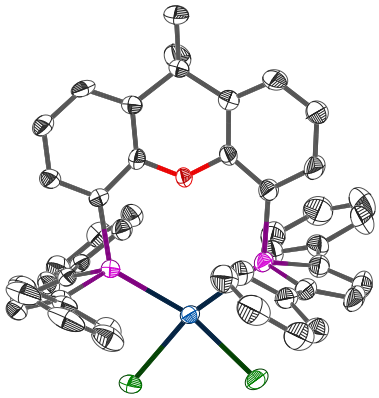

(d) 113.39(3)° [332]

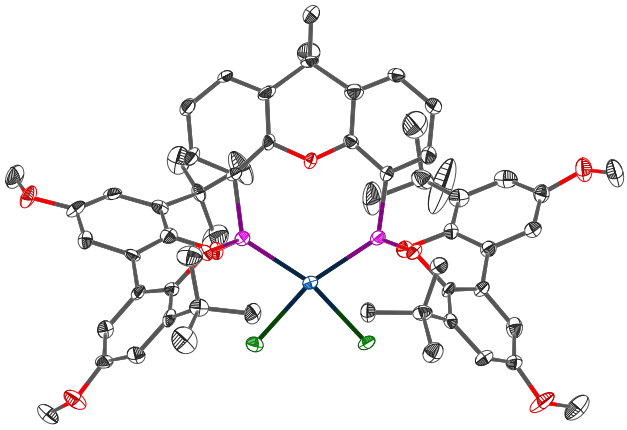

(e) 113.43(6)° [331]

Figure 6.7: X-ray crystal structures of complexes of the type [$PtCl_2$(xantphos)]. The P-Pt-P angle is indicated.

that is almost perpendicular to the plane of the xantphos backbone (105.90(12)°, 74.42(13)° and 77.0(4)°). In contrast, the two xantphos complexes with bite-angles of 113.39(3) and 113.43(6)° show coordination planes that are in-line with the xantphos backbone (176.9(2)° and 178.63(10)°). This is likely the result of the cyclic bulky substituents on the phosphorus atoms of these complexes. In contrast, the [Pt(*t*-Bu-thixantphos)Cl_2] complex, with a much larger bite-angle of 151.722(15)°, shows an angle of 140.48(5)° between the P-Ar bonds and the Pt coordination plane. This shows the marked difference between the [Pt(*t*-Bu-thixantphos)Cl_2] complex and the other [$PtCl_2$(xantphos)] complexes. The change in the position of the coordination plane relative to the backbone is due to the bulky *tert*-butyl-substituents causing a distorted *trans* coordination geometry. In all of the xantphos crystal structures the ligand backbone is bent, which is clear in the side-on view (Figures 6.4 and 6.8). This bending results in a concave face that is less sterically hindered than the convex face. Hence the coordination plane tilts such that the chloride on the concave face is closer to the backbone than the chloride on the convex face.

While the geometry of [Pt(*t*-Bu-thixantphos)Cl_2] is unusual when compared to other platinum complexes, there are 805 bis-phosphine dichloridopalladium complexes in the CSD, with 18 of these having P-Pd-P angles between 150 and 167° (no platinum complexes of this type with a bite-angle in this region have been reported).[68] All of these complexes include diphosphine ligands, indicating the importance of the ligand in controlling the coordination geometry of the complex. Of particular interest is the structure of [Pd(*t*-Bu-xantphos)Cl_2].[68] This structure has three distinct molecules of [Pd(*t*-Bu-xantphos)Cl_2] within the unit cell, with bite-angles of 152.30(4), 152.91(4) and 152.83(4)°. These are all slightly larger than the P-Pt-P angle in [Pt(*t*-Bu-thixantphos)Cl_2], which is expected due to the larger natural bite-angle of *t*-Bu-xantphos. In other respects the crystal structures are very similar.

The bond lengths for the coordinating atoms in [Pt(*t*-Bu-thixantphos)Cl_2] are all close to the average values determined from the Cambridge Crystallographic Data Centre (Table 6.1). The Pt-O distance is 2.8016(11) Å, significantly longer than the average reported Pt-O bond length (2.053 Å) indicating that there is no interaction between the two atoms. However, this is shorter than the five other complexes with xantphos derived backbones (3.174-3.466 Å) indicating that there is a relationship between the bite-angle of the diphosphine and the proximity of

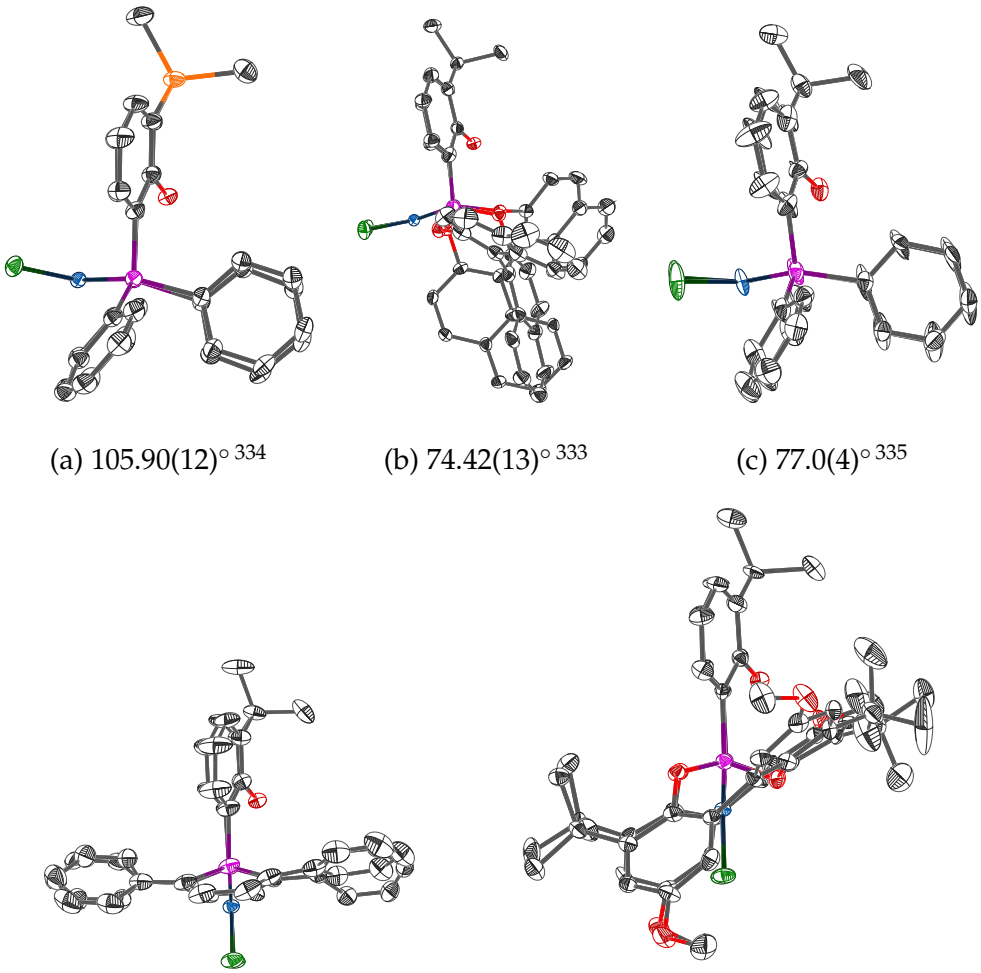

(a) 105.90(12)° [334] (b) 74.42(13)° [333] (c) 77.0(4)° [335]

(d) 178.63(10)° [332] (e) 176.9(2)° [331]

Figure 6.8: Side-on view of X-ray crystal structures of complexes of the type [$PtCl_2$(xantphos)] showing the coordination plane relative to the xantphos backbone. The value of the angle between the mean coordination plane and the P-backbone bond is given beneath each structure.

the oxygen atom.

The ^{1}H and ^{13}C NMR spectra of *trans*-[Pt(*t*-Bu-thixantphos)Cl_2] in C_6D_6 show two different sets of *tert*-butyl carbon and proton resonances. One of the sets appears as clearly resolved virtual triplets for both carbon environments and the proton environment. The other set has a well resolved virtual triplet for the quaternary carbon, whereas the other carbon and the proton signal are broad singlets. The reason for the appearance of two different *tert*-butyl environments is apparent from the solid-state structure (Figures 6.3 and 6.4). The backbone of the *t*-Bu-thixantphos ligand is bent, resulting in a concave and a convex side. If the ligand is not inverting in solution then this will result in two different *tert*-butyl environments: the two on the concave side, and the two on the convex side. The broadness that is observed for the methyl groups in one of the sets may be due to the steric constraints of this structure.

The *trans*-[Pt(*t*-Bu-thixantphos)Cl_2] complex showed a solvent dependent NMR spectrum. In C_6D_6 a single sharp peak was observed at 32.9 ppm (J_{PtP}= 2700 Hz) in the ^{31}P NMR spectrum. However, in acetone-d_6 this peak became very broad, at 35 ppm, while in CD_2Cl_2 or $CDCl_3$ the peak shifted to 46.4 ppm. The colour of the complex changes dramatically depending on the solvent. In the solid state the crystals have been determined to be *trans*-[Pt(*t*-Bu-thixantphos)Cl_2] without any solvent of crystallisation and are deep red in colour. Benzene and toluene solutions retain this colour. However, acetone solutions are orange, while in chloroform or dichloromethane the solution is yellow. Although colour changes for systems with solvent interactions or strong intermolecular interactions are well-known this is unlikely to be the case here. Instead it is likely that solvent-dependent coordination is occurring. In non-polar solvents such as benzene and toluene [Pt(*t*-Bu-thixantphos)Cl_2] is present. However, polar solvents like acetone or chloroform are more likely than benzene or toluene to stabilise charged species. Hence, in polar solvents it is proposed that one of the chloride ligands dissociates and the ether oxygen associates to form [Pt(*t*-Bu-thixantphos-κ*P,O,P'*)Cl]Cl (Scheme 6.2). In acetone the broadness of the spectrum combined with the intermediate colour likely indicates the rapid interconversion of the complexes.

To test the chloride dissociation theory, the [Pt(*t*-Bu-thixantphos)Cl_2] complex was dissolved in acetone and reacted with ammonium hexafluorophosphate. The

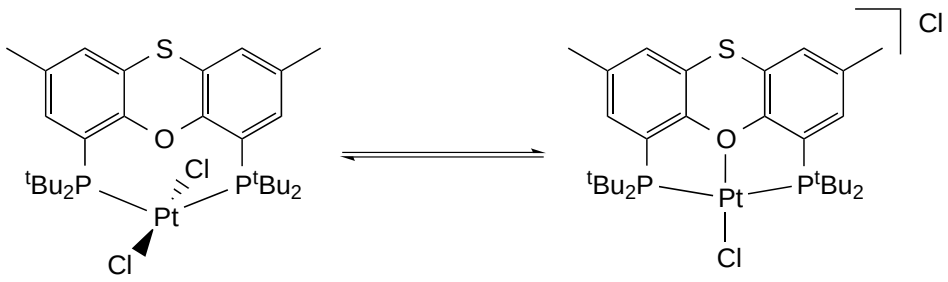

Scheme 6.2: Equilibrium between [Pt(*t*-Bu-thixantphos)Cl_2] and Pt(*t*-Bu-thixantphos)Cl]Cl.

solution changed colour over 30 minutes from deep orange to yellow, and a precipitate of ammonium chloride formed. The product appeared at 46.4 ppm (J_{PtP}= 2347 Hz) in the ^{31}P NMR spectrum with an associated septet at -144.5 (J_{PF} = 710.6) ppm indicative of PF_6. The value of J_{PtP} had decreased from the dichloride complex by 353 Hz, which may be the result of changes in the coordination geometry of the platinum centre. A shift of the signal in the ^{13}C NMR spectrum for the O-*ipso* carbon occurred from 155.8 ppm to 157.4 ppm, indicative of the oxygen coordinating to the metal centre.

6.1.1 Reactions of [$PtCl_2$(hex)] with *t*-Bu-sixantphos and *t*-Bu-xantphos

Several starting materials were investigated for the synthesis of *trans*-[Pt(*t*-Bu-thixantphos)Cl_2]. The best results occurred using [$PtCl_2$(hex)], which proceeded in C_6D_6 at 40 °C showing 75% conversion after 72 hours, or in toluene at 50 °C with 100% conversion in the same time. Due to the success of these conditions over other choices of starting material, temperature, and solvent, the synthesis of analogous *trans*-[$PtCl_2P_2$] complexes with *t*-Bu-sixantphos and *t*-Bu-xantphos was attempted using [$PtCl_2$(hex)], in toluene at 50 °C.

The reaction between *t*-Bu-xantphos and [$PtCl_2$(hex)] proceeded as expected. After 72 hours at 50 °C in toluene an orange solid was isolated which was further purified by recrystallisation, *via* inwards diffusion of diethyl ether into a dichloromethane solution of the product. The ^{31}P NMR spectrum showed one major product at 32.4 ppm (J_{PtP} = 2721 Hz, C_6D_6). The downfield shift of the peak

in the ^{31}P NMR spectrum is indicative of complexation. The value of 2721 Hz is consistent with a phosphorus *trans* to another phosphorus donor, rather than *trans* to a chloride ligand.[252,253,322] The position of the peak and the value of the one-bond platinum-phosphorus coupling constant are very similar to those for *trans*-[Pt(*t*-Bu-thixantphos)Cl_2] (32.9 ppm, J_{PtP} = 2700 Hz), suggesting the formation of an analogous product, *trans*-[Pt(*t*-Bu-xantphos)Cl_2].

The reaction between *t*-Bu-sixantphos and [$PtCl_2$(hex)] was not straightforward. After 72 hours at 50 °C the reaction contained unreacted *t*-Bu-sixantphos (53.4%), [(*t*-Bu-sixantphos)H]$^+$ (22.8%), and a platinum complex. Although the protonation of *t*-Bu-thixantphos did occur in a number of the reactions with various different [$PtCl_2L_2$] starting materials, this side-reaction was only observed when chlorinated solvents were used. Hence the formation of [(*t*-Bu-thixantphos)H]$^+$ can be attributed to the formation of small amounts of hydrochloric acid due to the UV-catalysed degradation of chlorinated solvents. However, the formation of [(*t*-Bu-sixantphos)H]$^+$ also occurred in toluene and C_6D_6. There are two possible proton sources, either small amounts of water which may have entered the reaction, or reaction with the surface of the glassware. The solvents were all degassed and dried over molecular sieves in accordance with Armarego and Chai.[336] This should result in a water concentration of 0.9 ppm for toluene, which is insufficient to account for the conversion.[296] Furthermore, the *t*-Bu-sixantphos ligand synthesis involves a dichloromethane/water liquid/liquid separation and no protonation was evident in the ^{1}H or ^{31}P NMR spectra of the *t*-Bu-sixantphos ligand after this step. This makes it unlikely that water is the proton source in this reaction.

Analysis of the *t*-Bu-xantphos selenides (Section 2.4) showed that *t*-Bu-sixantphos is the most basic of all of the ligands with a pK_b of 5.67 compared to 6.90 and 6.72 for *t*-Bu-thixantphos and *t*-Bu-xantphos respectively. Hence the *t*-Bu-sixantphos ligand is significantly more susceptible to protonation, leading to the observed difficulties. The *t*-Bu-sixantphos ligand has the smallest calculated bite-angle of the three ligands (Section 2.2) which would result in additional strain when forming the *trans*-[Pt(*t*-Bu-sixantphos)Cl_2] complex compared to the other two ligands. The reaction with *t*-Bu-thixantphos requires 72 hours at 50 °C to reach completion. It is likely that the reaction with *t*-Bu-sixantphos would require additional time or harsher conditions to go to completion. Hence the formation of *trans*-[Pt(*t*-Bu-sixantphos)Cl_2] has a larger activation barrier compared with the

t-Bu-thixantphos or *t*-Bu-xantphos ligands, making the alternative protonation reaction more likely to occur.

Despite the significant amounts of [(*t*-Bu-sixantphos)H]$^+$ that formed, one species that displays platinum coupling in the ^{31}P NMR spectrum is formed. This species was not isolated and due to the complexity of the ^{1}H and ^{13}C NMR spectra for the reaction mixture these were unable to be fully assigned. The peak for the platinum containing species appears in the ^{31}P NMR spectrum at 34.7 ppm (J_{PtP} = 2686 Hz, C_6D_6). The value of J_{PtP} is indicative of a *trans* arrangement of phosphorus atoms.[252,253,322] The position of the ^{31}P NMR signal and the value of J_{PtP} are similar to the *trans*-[Pt(*t*-Bu-thixantphos)Cl_2] complex which appears at 32.9 ppm (J_{PtP} = 2700 Hz, C_6D_6). Based on this evidence the product of the reaction between *t*-Bu-sixantphos and [$PtCl_2$(hex)] is *trans*-[Pt(*t*-Bu-sixantphos)Cl_2]. The mass spectrum shows a peak with a consistent mass and isotopic distribution for [$C_{30}H_{48}ClOP_2PtSi$]$^+$, which could result from loss of a chloride from *trans*-[Pt(*t*-Bu-sixantphos)Cl_2].[210]

[$PtCl_2$(xantphos)] complexes have been reported for Ph-sixantphos, Ph-thixantphos and Ph-xantphos.[337] Unlike the *trans*-[Pt(*t*-Bu-xantphos)Cl_2] complexes the Ph-xantphos complexes form *cis*-[Pt(Ph-xantphos)Cl_2] with J_{PtP} values over 3600 Hz (Table 6.3), indicative of phosphorus *trans* to a chloride ligand. The J_{PtP} values for the *trans*-[Pt(*t*-Bu-xantphos)Cl_2] complexes are almost 1000 Hz lower, indicative of *trans* coordination of the phosphorus atoms. The *cis* geometries of the Ph-xantphos complexes have been confirmed by X-ray crystallography of *cis*-[Pt(Ph-sixantphos)Cl_2][334] and *cis*-[Pt(Ph-xantphos)Cl_2].[335] The pseudo-*trans* geometry of *trans*-[Pt(*t*-Bu-thixantphos)Cl_2] has been determined crystallographically (Figure 6.3).

The ^{1}H and ^{13}C NMR spectra for all three *trans*-[Pt(*t*-Bu-xantphos)Cl_2] complexes display broad signals for the *tert*-butyl proton and carbon environments. The NMR spectra of *trans*-[Pt(*t*-Bu-thixantphos)Cl_2] showed two different sets of *tert*-butyl peaks. Based on the crystal structure these were determined to be on the concave or convex side of the bent backbone. For the *t*-Bu-xantphos complex the backbone may be inverting on a similar timescale to the NMR spectroscopy. This results in a single signal for the *tert*-butyl groups but broadened due to the similar timescale to the NMR analysis. The ^{13}C NMR signals for the *O-ipso* carbon shifted very slightly upon coordination (less than 1.1 ppm), which indicates that

the oxygen atom is not coordinated to the metal centre, consistent with the crystal structure of *trans*-[Pt(*t*-Bu-thixantphos)Cl_2].

Table 6.3: Selected NMR data for [Pt(xantphos)Cl_2] complexes. Values for Ph-xantphos complexes are in $CDCl_3$ [110] and values for *t*-Bu-xantphos complexes are in C_6D_6. ^{13}C data for the Ph-xantphos complexes was not reported ($\Delta\delta = \delta_{complex} - \delta_{free\ ligand}$).

	^{31}P			^{13}C *O-ipso*	
Diphosphine	δ/**ppm**	$\Delta\delta$/**ppm**	J_{PtP}	δ/**ppm**	$\Delta\delta$/**ppm**
Ph-Sixantphos	7.6	25.2	3663		
Ph-Thixantphos	8.4	25.7	3641		
Ph-Xantphos	6.6	24.1	3695		
t-Bu-Sixantphos	34.7	26.3	2686		
t-Bu-Thixantphos	32.9	23.4	2700	155.8	-0.1
t-Bu-Xantphos	32.4	22.2	2721	157.1	1.1

The solvent-dependent coordination that was observed in the synthesis of [Pt(*t*-Bu-thixantphos)Cl_2] was also observed for [Pt(*t*-Bu-xantphos)Cl_2], and was studied in more depth for this complex. Selected NMR data for [Pt(*t*-Bu-xantphos)Cl_2] dissolved in $CDCl_3$, CD_2Cl_2 and C_6D_6 are given in Table 6.4. The complex was also analysed in acetone-d_6 however the ^1H, ^{13}C and ^{31}P NMR spectra were very broad likely indicating the rapid interconversion between [Pt(*t*-Bu-xantphos)Cl_2] and [Pt(*t*-Bu-xantphos-κ*P,O,P'*)Cl]Cl. The peak in the ^{31}P NMR spectrum shifts by around 15 ppm upon changing the solvent from C_6D_6 to $CDCl_3$ or CD_2Cl_2. The value of J_{PtP} is lower by more than 370 Hz, consistent with coordination of the oxygen to the metal centre. The pseudo-*trans* geometry of the *trans*-[Pt(*t*-Bu-xantphos)Cl_2] complexes results in significant strain in the *t*-Bu-xantphos ligands. Coordination of the oxygen to the metal centre can relieve the strain and allow much larger P-M-P angles to form. With a larger P-Pt-P angle the phosphorus atoms are closer to a mutually *trans* configuration. The closer to *trans* the atoms become, the greater the influence of the other phosphorus atom and thus the value of J_{PtP}.

The ^1H and ^{13}C NMR data for [Pt(*t*-Bu-xantphos)Cl_2] and [Pt(*t*-Bu-xantphos)Cl]Cl all show virtual triplet peaks for the *tert*-butyl protons and carbons. This indi-

Table 6.4: Selected NMR data for [Pt(*t*-Bu-xantphos)Cl_2] and [Pt(*t*-Bu-xantphos)Cl]Cl ($\Delta\delta = \delta_{complex} - \delta_{free\ ligand}$).

		^{31}P			^{13}C *O*-ipso	
Solvent	**Complex**	δ/**ppm**	$\Delta\delta$/**ppm**	J_{PtP}	δ/**ppm**	$\Delta\delta$/**ppm**
C_6D_6	[Pt(*t*-Bu-xantphos)Cl_2]	32.4	22.2	2721.0	157.1	1.1
$CDCl_3$	[Pt(*t*-Bu-xantphos)Cl]Cl	47.7	37.5	2349.6	158.5	2.7
CD_2Cl_2	[Pt(*t*-Bu-xantphos)Cl]Cl	47.8	37.6	2345.3	158.8	3.0

cates strongly coupled phosphorus atoms, which typically occurs with mutually *trans* phosphorus atoms. However, the ^{13}C peak for the *O-ipso* carbon in the *t*-Bu-xantphos ligand shows a shift of only 1.1 ppm (from the free ligand) when in C_6D_6, but a shift ($\Delta\delta$) of 2.7 or 3.0 ppm in $CDCl_3$ and CD_2Cl_2 respectively. This shift has been observed for a number of rhodium complexes with the *t*-Bu-xantphos ligands coordinated as tridentate κ*P,O,P'* pincer ligands (Chapter 4). The downfield shift upon coordination of the oxygen is due to the oxygen donating electron density to the metal, which inductively decreases the electron density on the adjacent carbon atoms, resulting in decreased shielding.

The solvent dependent formation of [Pt(*t*-Bu-xantphos)Cl]Cl complexes was confirmed by reaction of [Pt(*t*-Bu-xantphos)Cl]Cl and [Pt(*t*-Bu-thixantphos)Cl]Cl with NH_4PF_6. [Pt(*t*-Bu-sixantphos)Cl_2] could not be isolated and therefore was not investigated for this reaction. The two complexes react visibly with NH_4PF_6, changing a dichloromethane solution from orange/red to yellow over a one hour period. The excess NH_4PF_6 and NH_4Cl by-product are readily removed by concentration of the solution and filteration through a plug of alumina. Selected NMR data is given in Table 6.5. The ^{31}P NMR spectra clearly show the presence of the PF_6 counterion appearing as a septet at -144.5 ppm (J_{PF} = 710.5 Hz) for both *t*-Bu-thixantphos and *t*-Bu-xantphos. The ^{19}F NMR spectra further confirms this with a clear doublet at -73.4 ppm (J_{PF} = 710.6 Hz).

The ^{1}H and ^{13}C NMR spectra for the [Pt(*t*-Bu-xantphos-κ*P,O,P'*)Cl]PF_6 complexes show virtual triplet peaks for all of the *tert*-butyl environments, indicative of *trans* coordination of the phosphorus atoms. The position of the *O-ipso* carbon has also shifted relative to both the free ligand and the [Pt(*t*-Bu-xantphos)Cl_2]

Table 6.5: Selected NMR data for [Pt(*t*-Bu-xantphos)Cl]X complexes (X = Cl, PF_6) in CD_2Cl_2 ($\Delta\delta = \delta_{complex} - \delta_{free\ ligand}$).

	^{31}P					^{13}C *O*-ipso	
Complex	δ/**ppm**	$\Delta\delta$/**ppm**	J_{PtP}/**Hz**	δ/**ppm**	J_{PF}/**Hz**	δ/**ppm**	$\Delta\delta$/**ppm**
[Pt(*t*-Bu-thixantphos)Cl]PF_6	46.4	36.9	2347	-144.5	710.5	157.4	2.1
[Pt(*t*-Bu-xantphos)Cl]PF_6	47.8	37.6	2350	-144.5	710.4	158.8	3.0
[Pt(*t*-Bu-xantphos)Cl]Cl	47.8	37.6	2345	N/A	N/A	158.8	3.0

complexes (Table 6.5). The shift from the free ligand is in excess of 2.0 ppm, indicative of the decreased shielding of the *O-ipso* carbon that occurs upon coordination of the oxygen to a transition metal.

6.2 Reactions with [Pd(cod)Cl_2]

Palladium dichloride complexes are ubiquitous in coordination chemistry, the CSD contains over 3000 X-ray crystal structures of palladium dichlorides.[68] The interest in these complexes is due to their relative ease of synthesis and high reactivity, which enables their wide use as pre-catalysts in a range of different catalytic processes such as the many palladium catalysed cross-coupling reactions.[31]

The reactivity of the *t*-Bu-xantphos ligands with palladium(II) was explored with a common palladium(II) starting material, [Pd(cod)Cl_2] (cod = 1,5-cyclooctadiene). This complex is very similar to the [$PtCl_2$(hex)] that was used to explore the analogous chemistry with platinum; hexa-1,5-diene and cod are both readily displaced by phosphine ligands. The reactions between the *t*-Bu-xantphos ligands and [Pd(cod)Cl_2] were straightforward, producing only one product in all cases, determined to be the *trans*-[Pd(*t*-Bu-xantphos)Cl_2] complex (Figure 6.3).

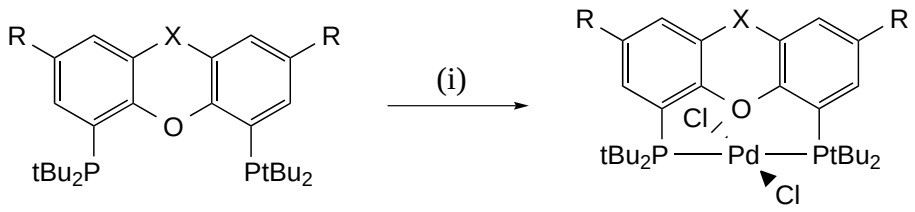

Scheme 6.3: Synthesis of [Pd(*t*-Bu-xantphos)Cl_2] complexes. *Reagents and conditions:* (i) [Pd(cod)Cl_2], toluene, 40 °C, 3 days.

Selected NMR data for the *trans*-[Pd(*t*-Bu-xantphos)Cl_2] complexes is given in Table 6.6. The ^{31}P NMR spectra each show one singlet, while the ^{1}H and ^{13}C NMR spectra display half the total expected number of peaks indicating the presence of a plane of symmetry. The chemical shift of the ^{31}P signal varies between 30.5 and 43.9 ppm for the three complexes. A downfield shift of this magnitude is consistent with coordination to a transition metal.[16] In [Pd(*t*-Bu-xantphos)Cl_2] both

of the *tert*-butyl carbon signals and the proton signal appear as virtual triplets, consistent with a *trans* coordination. However, the complexes with *t*-Bu-sixantphos and *t*-Bu-thixantphos both have resolved virtual triplets for the *tert*-butyl protons and quaternary carbon environments, while the terminal carbon signals display some broadening. The position of the *O-ipso* carbon can be indicative of tridentate coordination of the xantphos ligands. In this case the shift upon coordination ranges from -0.2 to 1.1 ppm. These are all smaller than would be expected if a chloride had dissociated and a pincer complex had formed.

Table 6.6: Selected NMR data for [Pd(*t*-Bu-xantphos)Cl_2] complexes in CD_2Cl_2 ($\Delta\delta = \delta_{complex} - \delta_{free\ ligand}$).

	^{31}P		^{13}C *O*-ipso	
Diphosphine	δ/**ppm**	$\Delta\delta$/**ppm**	δ/**ppm**	$\Delta\delta$/**ppm**
t-Bu-Sixantphos	46.7	38.3	165.4	1.1
t-Bu-Thixantphos	40.0	30.5	155.1	-0.2
t-Bu-Xantphos	54.1	43.9	156.6	0.8

Unlike the [Pt(*t*-Bu-xantphos)Cl_2] complexes, the [Pd(*t*-Bu-xantphos)Cl_2] complexes do not display solvent dependent coordination. NMR spectroscopy of the complexes in $CDCl_3$, CD_2Cl_2, and C_6D_6 showed no substantial changes in either the chemical shift of the ^{31}P NMR signal or the *O-ipso* carbon. Selected NMR data for *t*-Bu-sixantphos in different solvents is given in Table 6.7.

Table 6.7: Selected NMR data for [Pt(*t*-Bu-sixantphos)Cl_2] in different solvents ($\Delta\delta = \delta_{complex} - \delta_{free\ ligand}$).

	^{31}P		^{13}C *O*-ipso	
Solvent	δ/**ppm**	$\Delta\delta$/**ppm**	δ/**ppm**	$\Delta\delta$/**ppm**
C_6D_6	42.0	33.6	164.9	0.4
$CDCl_3$	45.7	37.3	165.1	0.8
CD_2Cl_2	46.7	38.3	165.4	1.1

6.2.1 Formation of [Pd(*t*-Bu-xantphos-κ*P,O,P'*)Cl]PF_6 Complexes

The [Pt(*t*-Bu-xantphos)Cl_2] complexes displayed solvent dependent dissociation of one of the chloride ligands. The pincer complex [Pt(*t*-Bu-xantphos-κ*P,O,P'*)Cl]$^+$ was trapped by counterion exchange with NH_4PF_6. Although the [Pd(*t*-Bu-xantphos)Cl_2] complexes do not display the same solvent dependent coordination, reaction with NH_4PF_6 resulted in the analogous [Pd(*t*-Bu-xantphos)Cl]PF_6 complexes (Scheme 6.4). An associated colour change from the deep red dichloride complexes to bright yellow pincer species was observed for all three of the ligands.

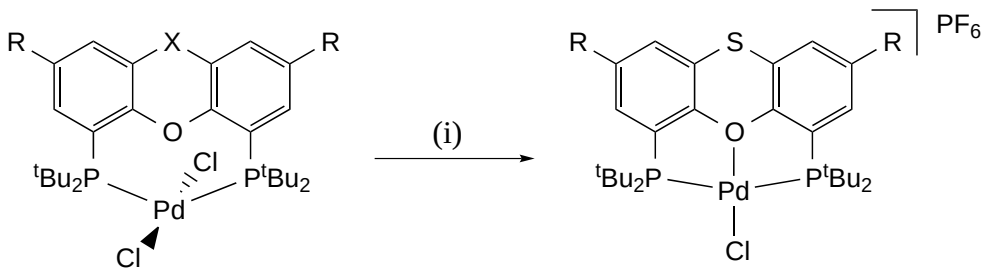

Scheme 6.4: Synthesis of [Pd(*t*-Bu-xantphos-κ*P,O,P'*)Cl]PF_6. *Reagents and conditions:* (i) NH_4PF_6, CH_2Cl_2, 24 hours.

Selected NMR data of the [Pd(*t*-Bu-xantphos-κ*P,O,P'*)Cl]PF_6 complexes is given in Table 6.8. The PF_6^- counterion is clearly apparent as a septet in the ^{31}P NMR spectrum at -144.5 ppm and a doublet in the ^{19}F NMR spectrum at -73.4 ppm, indicating a non-coordinating counterion. The ^{31}P NMR signals for the *t*-Bu-xantphos ligands have all shifted downfield. The *tert*-butyl ^{1}H and ^{13}C environments for all three complexes now appear as well-resolved virtual triplets indicating *trans* chelation of the phosphorus atoms. A reaction has occurred in all cases indicated by a shift in the ^{31}P NMR spectrum and the changes of other peaks in the ^{1}H and ^{13}C NMR spectra. Although the change in the chemical shift of the *O-ipso* carbon of *t*-Bu-sixantphos from the uncoordinated ligand ($\Delta\delta$) is indicative of oxygen coordination, the values for *t*-Bu-thixantphos and *t*-Bu-xantphos are not. This may mean that the oxygen is only very weakly coordinating to the palladium centre and in solution a T-shaped palladium complex is present, or that the complex may be stabilised by other interactions such as weak agostic interactions with the *tert*-butyl methyl groups or between the palladium atom

and the PF_6 counterion.

Table 6.8: Selected NMR data for [Pd(*t*-Bu-xantphos)Cl]PF_6 in CD_2Cl_2 ($\Delta\delta$ = $\delta_{complex}$ - $\delta_{free\ ligand}$).

	^{31}P				^{13}C	
Ligand	δ/**ppm**	$\Delta\delta$/**ppm**	δ/**ppm**	J_{PF}/**Hz**	δ/**ppm**	$\Delta\delta$/**ppm**
t-Bu-Sixantphos	52.4	5.7	-144.5	710.3	168.4	4.1
t-Bu-Thixantphos	56.4	16.4	-144.5	710.5	154.9	-0.4
t-Bu-Xantphos	58.3	4.2	-144.5	710.4	156.7	0.9

6.3 Computational Results

The [Pt(*t*-Bu-xantphos)Cl_2] complexes displayed solvent dependent coordination forming [Pt(*t*-Bu-xantphos-κ*P,O,P'*)Cl]Cl. This pincer complex was trapped by the exchange of the counterion using ammonium hexafluorophosphate. The palladium analogue did not display the same solvent-induced dissociation, although the [Pd(*t*-Bu-xantphos-κ*P,O,P'*)Cl]Cl complexes could be readily synthesised by reaction with ammonium hexafluorophosphate. This reactivity, particularly the solvent dependent exchange was investigated further using density functional theory. The geometries of all structures were optimised and frequencies were calculated using a B3LYP functional,[131–134] with the def2-TZVP basis set.[135,136] The energies of the systems were then calculated with incorporation of a solvent model (SMD).

Structures were optimised for the complexes [M(*t*-Bu-xantphos)Cl_2] and [M(*t*-Bu-xantphos-κ*P,O,P'*)Cl]$^+$ (M = Pd, Pt) with the three different *t*-Bu-xantphos ligands. The change in energy for the dissociation of a chloride ligand was calculated and the results for each of these reactions are summarised in Figure 6.9. Typical DFT calculations are performed for molecules in the gas phase. However, this is not always an appropriate description of the system, particularly when conversions between uncharged and charged species are involved as solvent stabilisation can become important. This is apparent for the dichloride to pincer conversion. In the gas phase, the systems show that the pincer complexes are

around 400 kJ mol^{-1} higher in energy than the corresponding dichloride complex. This indicates that the reaction would be highly endothermic, although it may still be favoured entropically.

Figure 6.9: Energy change on conversion from the [M(*t*-Bu-xantphos)Cl_2] to [M(*t*-Bu-xantphos)Cl]Cl.

[Pt(diphosphine)Cl_2]→ [Pt(POP)Cl] + Cl^-

	ΔE, kJ mol^{-1}				
Ligand	**Solvent Free**	**$(CH_3)_2CO$**	**C_6H_6**	**$CHCl_3$**	**CH_2Cl_2**
t-Bu-sixantphos	393.5	-2.2	150.7	59.0	20.4
t-Bu-thixantphos	400.2	4.3	157.9	66.0	27.3
t-Bu-xantphos	384.5	-14.6	140.1	47.7	8.6

[Pd(diphosphine)Cl_2]→ [Pd(POP)Cl] + Cl^-

	ΔE, kJ mol^{-1}				
Ligand	**Solvent Free**	**$(CH_3)_2CO$**	**C_6H_6**	**$CHCl_3$**	**CH_2Cl_2**
t-Bu-sixantphos	397.4	0.8	155.0	62.7	23.7
t-Bu-thixantphos	405.3	7.9	163.1	70.3	31.4
t-Bu-xantphos	391.7	-7.9	83.2	55.0	15.6

Single point energy calculations for the [M(*t*-Bu-xantphos)Cl_2] and [M(*t*-Bu-xantphos-κ*P,O,P'*)Cl]$^+$ in a range of solvents were performed on the structures that had been optimised in the gas phase (Figure 6.9). The results show that the introduction of any solvent reduces the energy required by more than half. For both the platinum and palladium complexes, the reaction in benzene requires the most energy of any of the solvents studied. This is consistent with the experimental results, as the platinum complexes are present as [Pt(*t*-Bu-xantphos)Cl_2] in benzene. For the platinum complexes conversion to [Pt(*t*-Bu-xantphos-κ*P,O,P'*)Cl]Cl was observed experimentally in chloroform and dichloromethane and the spectrum in acetone was broad, likely indicating some conversion. Interestingly, the computational results indicate that the lowest energy change occurs for the reaction in acetone, as these values are either close to zero or even negative, while the dichloromethane values are 8.6–27.3 kJ mol^{-1} and the chloroform values are

higher still 47.7–66.0 kJ mol^{-1}. These values do not include entropic effects which are likely to be significant as the disorder is increased. Although the calculations suggest that the chloride dissociation is an endothermic process, the reactions may be spontaneous due to entropy.

The results for the palladium complexes show similar overall trends to the platinum complexes (Figure 6.9). However, most of the palladium reactions require slightly more energy than the platinum complexes. This is consistent with the observation that the reaction is spontaneous for platinum (under certain conditions) while it is not for palladium. The energy for the palladium complexes in dichloromethane are lower than the energy for the platinum reaction in chloroform, which was observed to be spontaneous experimentally, again indicating that entropy is likely playing a significant role for this reaction.

6.4 Reactions with Platinum Dimethyl Starting Materials

Transition metal alkyl complexes are among the most important organometallic complexes as they can be intermediates in a wide range of catalytic transformations, including polymerisation and carbonylation reactions.[113,338] The synthesis of isolatable transition metal alkyl complexes is important, as studying their chemistry can give insight into the reactions occurring in catalytic systems.[339] Methyl complexes have gained attention in recent years, as protonation of a rhodium methyl complex led to a σ-methane complex which was characterised by NMR spectroscopy.[340] Platinum methyl complexes were investigated as part of this study as the stronger σ-donor character of the methyl ligand may lead to different reactivity than that of the platinum dichloride complexes.[252]

The reactivity of the *t*-Bu-xantphos ligands with [Pt(hex)Me_2)] was first studied using the *t*-Bu-thixantphos ligand. *t*-Bu-Thixantphos was combined with [Pt(hex)Me_2] in an NMR tube in C_6D_6 under argon to enable the progress to be followed by NMR spectroscopy. After 24 hours at room temperature no reaction was observed, so the sample was heated to 60 °C. The progress of the sample was monitored at regular intervals. However, after 28 days at 60 °C no changes were observed. The ^{31}P NMR spectrum showed a single peak indicative

of uncoordinated *t*-Bu-thixantphos, and the ^{1}H NMR spectrum showed a mixture with [Pt(hex)Me_2]. This indicates that the lack of reactivity was not the result of degradation of either the platinum starting material or the *t*-Bu-thixantphos ligand.

One equivalent of the strong acid CHPh$(SO_2CF_3)_2$ was added to the mixture of *t*-Bu-thixantphos and [Pt(hex)Me_2] in an attempt to protonate the platinum complex and remove one of the methyl ligands as methane, thus forming a free coordination site to promote reaction with the *t*-Bu-thixantphos. As discussed in Section 2.3, the *t*-Bu-xantphos ligands can act as Brønsted bases and have pK_b values of 5.67–6.90. As such, the *t*-Bu-thixantphos ligand reacted with the acid quickly and completely forming [(*t*-Bu-thixantphos)H]CPh$(SO_2CF_3)_2$ (Scheme 6.5). Although the mixture was subsequently followed for several days by NMR spectroscopy, no reaction was observed between the protonated *t*-Bu-thixantphos ligand and the [Pt(hex)Me_2] complex.

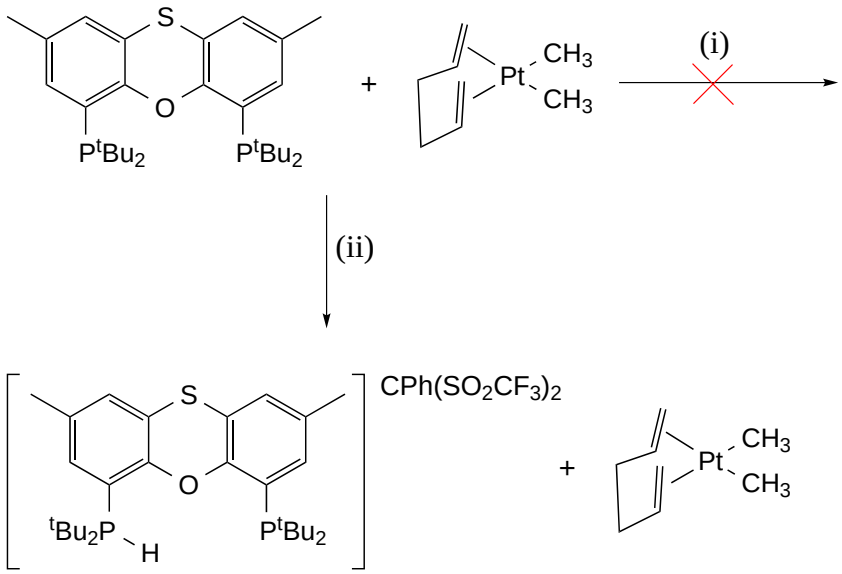

Scheme 6.5: Attempted reaction of [Pt(hex)Me_2] and *t*-Bu-thixantphos. *Reagents and conditions:* (i) C_6D_6, 60 °C, (ii) HCPh$(SO_2CF_3)_2$.

When the *t*-Bu-xantphos ligands were reacted with [$PtCl_2L_2$] complexes (L = SEt_2, MeCN, *t*-BuCN, L_2 = 1,5-hexadiene) no *cis* products were observed regardless of the starting material, and the reaction was fastest when the *cis* complex [$PtCl_2$(hex)] was used due to the lability of the diene. Due to the steric bulk of the

tert-butyl substituents on the phosphorus atoms and the rigidity of the *t*-Bu-xantphos backbone these ligands would be expected to act as *trans*-spanning diphosphines or tridentate κ*P,O,P'* pincer ligands rather than forming *cis* chelates. Thus, in order for a reaction to occur between *t*-Bu-xantphos and [Pt(hex)Me_2] the system must undergo a *cis-trans* isomerism process. For the dichlorides this is easily facilitated by loss of one of the chloride ligands followed by re-coordination in a *trans* configuration. However, methyl ligands are strong σ-donors and coordinate very strongly to Pt(II).[252] The first step of the reaction likely proceeds with one of the phosphorus donors displacing one half of the diene (Scheme 6.6). From this position the other phosphorus needs to displace the alkene forming a *cis*-*t*-Bu-xantphos complex. This could then undergo *cis-trans* isomerism; or the complex could isomerise first and then the phosphine could displace the alkene. In the first case, the *cis*-*t*-Bu-xantphos complex would be highly disfavoured due to the very large natural bite-angle of these ligands. In either case, for the *cis-trans* isomerism to occur, the complex must lose a methyl ligand and these are too strongly coordinated for this to occur, especially combined with the low *trans*-influence of the hexa-1,5-diene ligand and the moderate *trans*-influence of the phosphorus donors.[252,253,322]

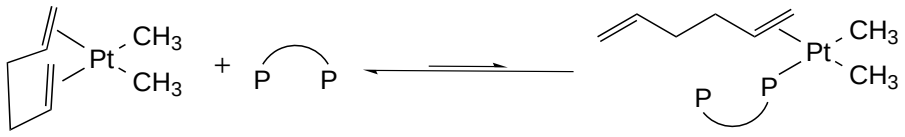

Scheme 6.6: Proposed reaction between [Pt(hex)Me_2] and a *t*-Bu-xantphos diphosphine ligand (PP).

6.5 Reactions with [PtCl(hex)Me]

Chloridomethylplatinum complexes are interesting due to the different properties of the chloride and methyl ligands. The methyl ligand is a much stronger σ-donor than a chloride ligand, meaning that the methyl imparts a much stronger *trans*-influence.[252,253,322] The difference in the donor properties of the chloride and methyl ligands can result in asymmetric reactivity as the chloride will undergo substitution more readily than the methyl ligand. If a *cis*-[PtClMe(PP)]

complex was formed, the two phosphorus atoms would be in different environments, which could lead to asymmetric reactions of the diphosphine. In the more likely scenario for the *t*-Bu-xantphos ligand system, that *trans*-[Pt(*t*-Bu-xantphos)ClMe] complex forms, then the strong *trans*-influence of the methyl group may promote the dissociation of the chloride ligand

[PtCl(hex)Me] was chosen as the starting material due to the success of the reactions of the *t*-Bu-xantphos ligands with [$PtCl_2$(hex)]. Reaction between the *t*-Bu-xantphos ligands and [PtCl(hex)Me] was performed on an NMR-scale in C_6D_6 to allow the reactions to be studied as they progressed and identify any intermediates that may form. As the reaction progressed the product precipitated out as an off-white solid. This solid was insoluble in most common solvents except acetone-d_6. The *t*-Bu-xantphos ligands and [PtCl(hex)Me] are insoluble in acetone, meaning that this was not suitable as the reaction solvent. In all cases, the solution was decanted from the precipitate and the solid was dissolved in acetone-d_6, where only one species, ([Pt(*t*-Bu-xantphos)Me]Cl) was observed, indicating complete reaction (Scheme 6.7).

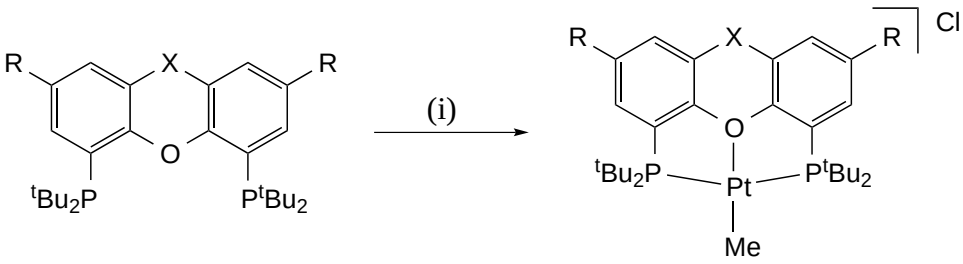

Scheme 6.7: Reaction between [PtCl(hex)Me] and *t*-Bu-xantphos ligands. *Reagents and conditions:* (i) [PtCl(hex)Me], 24 hours, room temperature (50 °C *t*-Bu-sixantphos).

The speed of the reaction varied between the three ligands. With *t*-Bu-xantphos the reaction was fastest, reaching completion in 48 hours at room temperature. *t*-Bu-Thixantphos reacted slightly more slowly, with completion observed after 72 hours. *t*-Bu-Sixantphos was the slowest of the three systems; little reaction was observed after 72 hours at room temperature, however after 24 hrs of heating at 50 °C the reaction was complete by NMR spectroscopy. This difference in reactivity is likely the result of the bite-angle of the ligand and the amount of energy

required to achieve a *trans*-geometry. With the larger calculated bite-angle of the *t*-Bu-xantphos ligand the amount of energy required to achieve a pincer geometry would be lower than that for the other ligands. Similarly *t*-Bu-sixantphos, with the smallest of the three natural bite-angles, would require more energy in order to achieve the coordination geometry of the product.

Selected NMR data for the three [Pt(*t*-Bu-xantphos)Me]Cl complexes is summarised in Table 6.9. In the ^{31}P NMR spectra only one signal is observed for each of the complexes, indicating identical environments for both phosphorus atoms which implies symmetrical complexes. Given that [PtCl(hex)Me] is asymmetrical and a symmetrical complex is formed, this is evidence for *trans*-coordination of the *t*-Bu-xantphos ligands. The ^{31}P NMR signal has shifted downfield by around 40 ppm to 48.7, 50.5, or 51.0 ppm for *t*-Bu-sixantphos, *t*-Bu-thixantphos and *t*-Bu-xantphos, respectively. The peak for each complex is a singlet with J_{PtP} coupling ranging from 2763 to 2793 Hz. If the phosphorus atom was *trans* to a chloride we would typically expect coupling constants larger than 3000 Hz, while if it was *trans* to a methyl ligand we would expect values below 2000 Hz. A coupling constant of around 2800 Hz is generally indicative of phosphorus *trans* to an atom with a similar *trans*-influence, in this case another phosphorus. Furthermore this coupling is of similar magnitude to the coupling constant observed for the [Pt(*t*-Bu-xantphos)Cl_2] complexes (2686–2721 Hz). Both of these points strongly indicate a *trans*-coordination geometry for the complex.

The position of the *O-ipso* carbon in the ^{13}C NMR spectrum can be indicative of coordination of the oxygen to a metal centre. In this particular case the peak for *t*-Bu-sixantphos moves 3.0 ppm downfield from the uncoordinated ligand, while the peak for *t*-Bu-xantphos shifts by only 0.3 ppm downfield and the peak for *t*-Bu-thixantphos shifts 1.5 ppm upfield comparing the free ligand with the [Pt(*t*-Bu-xantphos)Me]Cl complexes. This is no clear indication of whether the oxygen is coordinated to the metal centre or not. One of the reasons for this inconsistency is the insolubility of the free ligand in acetone, meaning that we are comparing the data for the free ligand in $CDCl_3$ with the complex in acetone-d_6. Peaks frequently shift depending on the solvent, meaning that no conclusions can be drawn from the position of the *O-ipso* ^{13}C NMR signal in this case. The solubility of the complex is indicative of the chloride dissociating from the metal centre. The [Pt(*t*-Bu-xantphos)Me]Cl complexes are insoluble in the non-polar C_6D_6, whereas they are very soluble in polar acetone-d_6. This is consistent with a

Table 6.9: Selected NMR Data for [Pt(*t*-Bu-xantphos)Me]Cl complexes in acetone-d_6 Values for the J_{PtX} coupling constants are given in brackets ($\Delta\delta = \delta_{complex} - \delta_{free\ ligand}$).

	^{31}P		^{1}H	^{13}C	
Diphosphine	δ/**ppm**	$\Delta\delta$/**ppm**	**Pt−CH$_3$** δ/**ppm**	**Pt−CH$_3$** δ/**ppm**	$\Delta\delta$ **C-O** /**ppm**
t-Bu-Sixantphos	48.7 (2763)	40.3	2.01 (98.6)	-22.7 (780.5)	3.0
t-Bu-Thixantphos	50.5 (2793)	41.0	1.94 (97.4)	-23.8 (777.2)	-1.5
t-Bu-Xantphos	51.0 (2788)	40.8	1.92 (97.4)	-23.9 (774.6)	0.3

charged species forming in solution which could result from the loss of the chloride ligand. Furthermore, in the [Pt(*t*-Bu-xantphos)Cl_2] complexes the chloride was observed to dissociate readily. In this case the high *trans*-influence character of the methyl ligand would promote the loss of the chloride ligand. In addition, the strong σ-donor ability of the methyl ligand would mean that the oxygen atom would be coordinated in an extremely weak fashion and would donate less electron density when in [Pt(*t*-Bu-xantphos)Me]Cl compared with [Pt(*t*-Bu-xantphos)Cl]Cl.

The peaks for the methyl ligand in the ^{1}H and the ^{13}C NMR spectra can give additional information about the nature of the complex. In the ^{1}H NMR spectrum the peak appears between 1.92 and 2.01 ppm as a triplet with platinum satellites. Coupling to two phosphorus atoms in the same environment generates the triplet with a three-bond J_{PH} coupling constant of 5.4–5.5 Hz, indicative of a *cis* relationship between the phosphorus atoms and the methyl ligand, consistent with a *trans*-spanning diphosphine ligand. The value of the two-bond platinum-proton coupling constant on the methyl ligand ranges from 97.4 Hz for both *t*-Bu-xantphos and *t*-Bu-thixantphos, to 98.6 Hz for *t*-Bu-sixantphos. This is a very large coupling constant for a platinum methyl ligand and is indicative of a ligand *trans* to the methyl which has a very low *trans*-influence. This is also reflected in the ^{13}C NMR spectrum where the methyl ligands appear at between -22.7 and -23.9 ppm with coupling constants of 774.6–780.5 Hz. The large upfield shift of the methyl ligand from the typical position of an organic methyl substituent (5-30 ppm[341]) arises from the additional electron density as a result of coordination. The chemical shift of the methyl carbon, together with the value of J_{PC} is largely the result of the ligand in the *trans* position. Previous work both in our group[315,316] and by others[342] has shown that methyl ligands *trans* to a moderate σ donor such as a phosphorus appear at 5–15 ppm in the ^{13}C NMR spectrum, with a platinum-carbon coupling constant of around 700 Hz. In contrast, when the methyl is *trans* to a weak σ-donor ligand such as a nitrogen donor the methyl shifts upfield to around -10– -25 ppm with larger coupling constants of around 800 Hz. In this case values of -22.7 to -23.9 for the ^{13}C chemical shift and values of J_{PtC} between 774.6–780.5 Hz clearly indicate that the methyl ligand is *trans* to a weak σ-donor such as a chloride or an oxygen. The value of J_{PtC} is lowest for *t*-Bu-xantphos and highest for *t*-Bu-sixantphos suggesting a series of O-*trans* influence for the three ligands of *t*-Bu-sixantphos $<$ *t*-Bu-thixantphos $<$ *t*-Bu-xantphos.

Based on the relative reactivity of the *t*-Bu-xantphos ligands with [PtCl(hex)Me] and the NMR data, [Pt(*t*-Bu-xantphos)Me]Cl is proposed as the product. However, the coordination of the oxygen has not been established conclusively. Two related complexes have been reported: $[PdMe(P^tBu_3)_2]^+$ and $[PtMe(P^iPr_3)_2]^+$, the solid state structures of which have been determined by X-ray crystallography (Figure 6.10).[343,344] Both complexes are stabilised in the solid-state by an agostic interaction from one of the isopropyl or *tert*-butyl methyl substituents, although they were synthesised in the presence of coordinating solvents. The NMR spectra of each showed symmetrical molecules with no evidence for an agostic interaction, even down to -80 °C, indicating rapid exchange of the agostic interaction between the numerous C-H bonds available. Low temperature ^1H and ^{31}P NMR analysis of [Pt(*t*-Bu-sixantphos)Me] was carried out from 20 to -80 °C. No changes in the spectra were observed, except for a slight broadening of the signals due to precipitation. This indicates that if an agostic-bond is present, the presence of 12 different *tert*-butyl CH_3 groups (i.e. 36 different agostic possibilities) means there is ample opportunity for exchange, resulting in the apparent symmetry at room temperature.

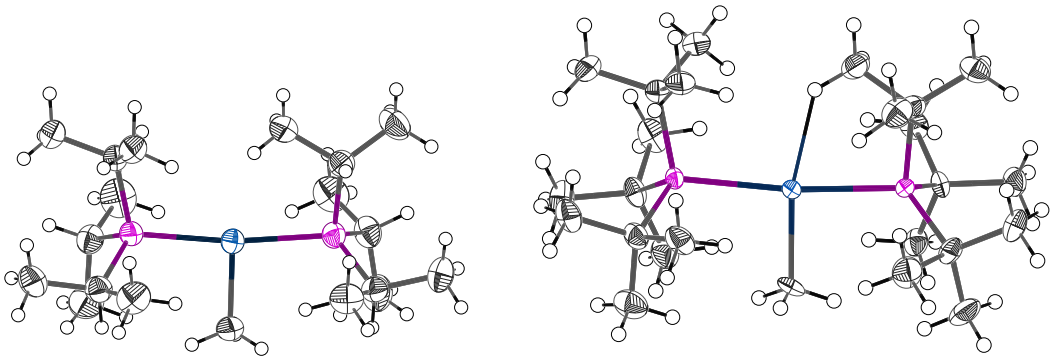

(a) $[PtMe(P^iPr_3)_2]^+$ (b) $[PdMe(P^tBu_3)_2]^+$

Figure 6.10: X-ray crystal structures of $[PtMe(P^iPr_3)_2]^+$[343] and $[PdMe(P^tBu_3)_2]^+$.[344] Counterions omitted for clarity.

On the basis of the spectroscopic analysis and the structures of similar compounds there are three plausible structures for the product from reaction between [PtCl(hex)Me] and the *t*-Bu-xantphos ligands; all contain the *t*-Bu-xantphos ligand in a *trans*-configuration and a methyl group. The fourth coordination site on the platinum could either be occupied by a chloride ligand, an agostic interaction from one of the many *tert*-butyl C-H bonds, or by a very weak interaction

with the oxygen in the backbone of the *t*-Bu-xantphos ligands. The absence of the chloride ligand was confirmed by reaction between [Pt(*t*-Bu-xantphos)Me]Cl and NH_4PF_6 on an NMR-scale. Over the course of several days no change was observed in the ^{1}H, ^{13}C or ^{31}P NMR spectra except for the appearance of a septet in the ^{31}P NMR spectrum and a doublet in the ^{19}F NMR spectrum indicative of a non-coordinating PF_6^- counterion (NH_4PF_6 is insoluble in acetone-d_6). As no change was observed in the NMR spectra upon cooling to -80 °C, the fourth coordination site could be occupied either a rapidly exchanging agostic interaction or the oxygen in the backbone (Scheme 6.8).

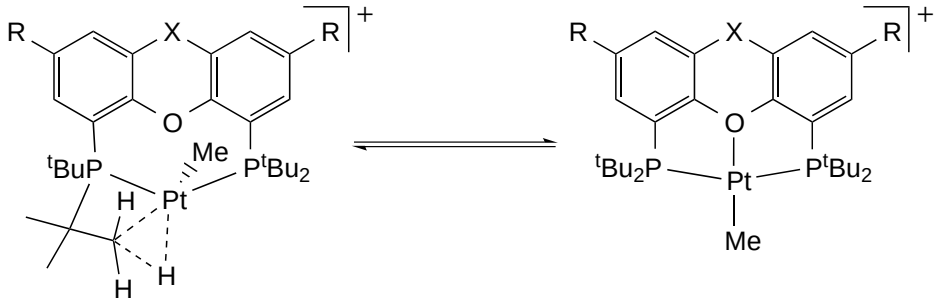

Scheme 6.8: Equilibrium between [Pt(*t*-Bu-xantphos)Me] and [Pt(*t*-Bu-xantphos-κ*P,O,P'*)Me].

6.5.1 Computational Results

Computational modelling was used to determine whether the three [Pt(*t*-Bu-xantphos)Me]X complexes take the form of a pincer complex [Pt(*t*-Bu-xantphos-κ*P,O,P'*)Me]$^+$, or whether an agostic interaction from the *tert*-butyl groups is formed instead. Structural models of both of these isomers were optimised and their vibrational frequencies were calculated using density functional theory using a B3LYP functional[131–134] with the def2-TZVP basis set.[135,136] Selected bond lengths and angles are given in Table 6.10 and 6.11 for the agostic and pincer complexes respectively.

Little variation is present in the bond lengths and bite-angles for the three ligands in either the pincer or the agostic complex. The platinum-methyl bond length varies by only 0.001 Å between the three agostic and the three pincer complexes,

Table 6.10: Selected bond lengths and angles calculated for the agostic complexes [Pt(*t*-Bu-xantphos)Me]$^+$.

Ligand	**Pt-Me** /Å	**Pt-H** /Å	**P-Pt-P** /°
t-Bu-Sixantphos	2.051	2.763	153.9
t-Bu-Thixantphos	2.052	2.828	153.7
t-Bu-Xantphos	2.051	2.868	153.2

Table 6.11: Selected bond lengths and angles calculated for the pincer complexes [Pt(*t*-Bu-xantphos-κ*P,O,P'*)Me]$^+$.

Ligand	**Pt-Me** /Å	**Pt-O** /Å	**P-Pt-P** /°
t-Bu-Sixantphos	2.052	2.323	165.7
t-Bu-Thixantphos	2.053	2.277	164.4
t-Bu-Xantphos	2.053	2.256	164.4

and by only 0.002 Å across all six of the structures. Similarly, the bite-angles show little difference among the complexes despite the difference in the natural bite-angles for the ligands. The platinum-oxygen bond length for the pincer complex shows a decrease with the increasing natural bite-angle of the ligand such that the *t*-Bu-sixantphos complex has the longest Pt-O bond. A similar trend is present for the Pt-H bond length in the agostic complexes, where the longest Pt-H distance is for the *t*-Bu-sixantphos system and the shortest Pt-H distance is for the *t*-Bu-xantphos complex. These are consistent with the observed changes in the ^{13}C NMR spectrum for the methyl ligand, whereby the *t*-Bu-sixantphos complex has the largest value of J_{PtC} and *t*-Bu-xantphos has the smallest. Decreasing the Pt-O or Pt-H bond lengths will increase the *trans* influence of the ligand as a result of increased σ donation from the ligand to the platinum, leading to a lower platinum-carbon coupling constant.

The Gibbs free energy for the each of the complexes was also calculated (Table 6.12). The agostic complexes were consistently higher in energy than the pincer complexes, indicating that conversion from the agostic to the pincer is an exothermic process generating 106, 111, or 122 kJ mol^{-1} of energy. This suggests that the pincer complex is likely the thermodynamically favoured product in the reaction between [PtCl(hex)Me] and the three *t*-Bu-xantphos ligands (Scheme 6.8). The value for ΔG appears to be correlated with the natural bite-angle of the ligands. This indicates that although the three diphosphine ligands produce complexes with similar bite-angles, the natural bite-angle of the ligand can impact the stability of the starting and final complexes.

Table 6.12: Gibbs free energies calculated for the agostic and pincer complexes [Pt(*t*-Bu-xantphos-κ*P,O,P'*)Me]$^+$. All values are in kJ mol^{-1}

Ligand	**Agostic *G***	**Pincer *G***	**ΔG**
t-Bu-Sixantphos	-6245006	-6245113	-106
t-Bu-Thixantphos	-6527190	-6527301	-111
t-Bu-Xantphos	-5584828	-5584950	-122

While the relative thermodynamic preference between the pincer and the agostic has been established, the reaction occurring is actually dissociation of a chlo-

ride from the [Pt(*t*-Bu-xantphos)ClMe] complexes forming either the pincer or the agostic complex. The energy changes for these reactions are given in Tables 6.13 and 6.14. In this case we see that under standard gas-phase DFT conditions, neither the pincer nor the agostic complex is lower in energy than the [Pt(*t*-Bu-xantphos)ClMe] starting material. However, significantly less energy is required for the conversion to the pincer than to the agostic.

Table 6.13: Energy change for the conversion of the [Pt(*t*-Bu-xantphos)ClMe] to the pincer complex.

[Pt(*t*-Bu-xantphos)ClMe] $\rightarrow$ [Pt(*t*-Bu-xantphos-κ*P,O,P'*)Me] + Cl^-

	Δ**E,** kJ mol^{-1}				
Ligand	**Solvent Free**	**$(CH_3)_2CO$**	**C_6H_6**	**$CHCl_3$**	**CH_2Cl_2**
t-Bu-sixantphos	341.2	-45.6	100.4	11.7	-24.7
t-Bu-thixantphos	349.7	-38.3	109.2	20.0	-17.0
t-Bu-xantphos	337.5	-52.7	97.2	7.4	-30.4

Table 6.14: Energy change for the conversion of the [Pt(*t*-Bu-xantphos)ClMe] to the agostic complex [Pt(*t*-Bu-xantphos)Me]$^+$.

[Pt(*t*-Bu-xantphos)ClMe] $\rightarrow$ [Pt(*t*-Bu-xantphos)Me]$^+$ + Cl^-

	Δ**E,** kJ mol^{-1}				
Ligand	**Solvent Free**	**$(CH_3)_2CO$**	**C_6H_6**	**$CHCl_3$**	**CH_2Cl_2**
t-Bu-sixantphos	454.2	54.9	210.0	117.0	78.2
t-Bu-thixantphos	462.4	59.8	217.6	123.8	84.1
t-Bu-xantphos	462.7	60.4	218.9	124.9	84.8

Typical DFT computations are carried out for single molecules in the gas phase. While this is applicable to a range of applications, when dealing with conversions between uncharged and charged molecules the solvent can have a significant impact on the thermodynamics of the reaction. It has been observed experimentally with the platinum and palladium dichloride complexes that the solvent can also play a role in the formation of the pincer complexes. As such, single-point energy calculations with a solvent correction were performed for the conversion of [Pt(*t*-Bu-xantphos)ClMe] into the pincer or the agostic complexes. The energy changes

are summarised in Tables 6.13 and 6.14 for the pincer and the agostic respectively. The inclusion of any of the solvents drastically decreases the amount of energy required to form the product, thus indicating that the solvent is important for these reactions. Under experimental conditions the reaction is performed in benzene from which the product precipitates as a white solid that is only soluble in acetone (of the solvents examined).

The energy change for conversion of the [Pt(*t*-Bu-xantphos)ClMe] complexes into the pincer is much lower than that required to form the agostic complex, regardless of solvent. This indicates that the pincer is thermodynamically preferred over the agostic complex. Interestingly, for the pincer complex the reaction in benzene requires the most energy, whereas the reaction in chloroform, although still an overall positive ΔE value, only requires at most 20.0 kJ mol^{-1}. Based on the computational results the proposed product in the reaction between the *t*-Bu-xantphos ligands and [PtCl(hex)Me] is the pincer [Pt(*t*-Bu-xantphos-κ*P,O,P'*)Me]Cl complex.

The reaction of a number of xantphos ligands with [Pd(cod)ClMe] has previously been studied experimentally.[73] Me-xantphos is a xantphos derivative with methyl substituents on the phosphorus atoms. Reaction of [Pd(cod)ClMe] with Me-xantphos produces exclusively *cis*-[PdClMe(Me-xantphos)]. All of the Ph-xantphos ligands formed [PdClMe(Ph-xantphos)] complexes that displayed *cis*-*trans*-isomerism at room temperature. At low temperature both the *cis* and *trans* isomers were observed for Ph-thixantphos and Ph-xantphos, while only the *cis* complex was observed for Ph-xantphos. Reaction of the [PdClMe(xantphos)] complexes with $AgSO_3CF_3$ produces the pincer complexes [PdClMe(xantphos-κ*P,O,P'*)][SO_3CF_3] with all four ligands that were studied. The difference in the coordination behaviour of these ligands and the *t*-Bu-xantphos complexes indicates that the direct formation of the [Pt(*t*-Bu-xantphos)Me]Cl complexes is most likely the result of the higher steric demands of the *t*-Bu-xantphos ligands compared to the Ph-xantphos or Me-xantphos ligands.

6.6 Summary

t-Bu-Xantphos and *t*-Bu-thixantphos were shown to react with [$PtCl_2$(hex)] forming exclusively *trans*-[Pt(*t*-Bu-xantphos)Cl_2] complexes, unlike the Ph-xantphos

ligands which form exclusively *cis* dichlorides. The same reaction with *t*-Bu-sixantphos produced the *trans*-[Pt(*t*-Bu-sixantphos)Cl_2] complex together with *t*-Bu-sixantphosH^+, even in toluene and benzene, possibly due to reaction with the glass. All of the dichloride complexes were dark red in colour, although most platinum dichloride complexes are pale or yellow. This colour is possibly due to the unusual coordination geometry of the platinum, shown by X-ray crystallography of [Pt(*t*-Bu-thixantphos)Cl_2]. The complex has a bite-angle of 151.722(15)° and the sum of the angles around the platinum is 499.006° showing significant distortion from the ideal square-planar geometry typically observed for platinum(II). Analogous [Pd(*t*-Bu-xantphos)Cl_2] complexes were synthesised for *t*-Bu-sixantphos, *t*-Bu-thixantphos, and *t*-Bu-xantphos by reaction with [Pd(cod)Cl_2].

The [Pt(*t*-Bu-xantphos)Cl_2] and [Pt(*t*-Bu-thixantphos)Cl_2] complexes showed dissociation of a chloride ligand, forming [Pt(*t*-Bu-xantphos-κ*P,O,P'*)Cl]Cl in $CDCl_3$ and CD_2Cl_2. The same behaviour was not observed for the palladium analogues. The pincer complexes [M(*t*-Bu-xantphos-κ*P,O,P'*)Cl]$^+$ could be formed for both platinum and palladium by counterion exchange with NH_4PF_6. Computational investigation into the chloride dissociation showed that although the formation of the pincer complexes is endothermic in almost all cases, the presence of any solvent more than halved the required energy and the reactions in chloroform and dichloromethane were less endothermic than in benzene. The reactions in acetone were close to neutral energy requirements with some exothermic results. The palladium reactions required slightly more energy in all cases, consistent with the experimental results. The calculations do not include entropy which is likely to be significantly in favour of the pincer complexes.

The pincer complexes [Pt(*t*-Bu-xantphos-κ*P,O,P'*)Me]Cl were observed to form as the sole product from reaction of the *t*-Bu-xantphos ligands with [PtCl(hex)Me]. The NMR data was unclear regarding the coordination of the oxygen atom to the platinum and previous literature suggested that the platinum centre may be stabilised by an agostic interaction with one of the *tert*-butyl C-H bonds. Computational investigation showed that for all three *t*-Bu-xantphos ligands the pincer complex is lower in energy suggesting that this the fourth coordination site on the platinum is occupied by the backbone oxygen. From the values of J_{PC} for the methyl ligand the *t*-Bu-sixantphos ligand has the weakest *trans* influence and the *t*-Bu-xantphos ligand has the strongest. This suggests that although compu-

tationally the bite-angles of the three ligands are the same, the natural bite-angle can predict the donor properties of the backbone oxygen.

This chapter has presented a number of new platinum and palladium complexes with the *t*-Bu-sixantphos, *t*-Bu-thixantphos, and *t*-Bu-xantphos. No *cis* complexes were observed at any point, indicating the influence of *tert*-butyl groups on the coordination modes of the ligands. The *trans* complexes have the smallest observed bite-angles for square-planar complexes with *trans*-spanning diphosphine ligands. A number of *t*-Bu-xantphos pincer complexes were also reported, with [Pt(*t*-Bu-xantphos)Cl]$^+$ and [Pt(*t*-Bu-xantphos)Me]Cl forming spontaneously with appropriate solvent choice.

Chapter 7

Conclusion

The *t*-Bu-xantphos ligand has been tested in a number of catalytic reactions with varying results.[84–87,90,93,96–98] The conversions are typically very different to those obtained with Ph-xantphos suggesting differences in their coordination behaviour. However, few studies had investigated the coordination chemistry of the *t*-Bu-xantphos ligand. This thesis aimed to address that deficit by synthesising two new *t*-Bu-xantphos ligands, and investigating the properties and coordination chemistry of the three ligands, with a particular focus on transition metals used in catalysis.

Two new *t*-Bu-xantphos ligands with a $SiMe_2$ (*t*-Bu-sixantphos) or a sulfur atom (*t*-Bu-thixantphos) in place of the CMe_2 bridging group in *t*-Bu-xantphos were synthesised. The synthetic method for *t*-Bu-sixantphos and *t*-Bu-thixantphos was also used successfully to synthesise *t*-Bu-xantphos. This synthesis is advantageous as the only by-products are the monophosphines, which can be reused in a further cycle to produce additional diphosphine. The bite-angles of the *t*-Bu-xantphos and Ph-xantphos were calculated using DFT methods with the *t*-Bu-xantphos ligands found to have larger bite-angles (126.80–127.56°) than the Ph-xantphos ligands (111.89–114.18°). The values calculated for the Ph-xantphos ligands using DFT are consistent with the literature values calculated using molecular mechanics.

The *t*-Bu-xantphos ligands are both Brønsted and Lewis bases. The three ligands reacted rapidly with strong acids forming (*t*-Bu-xantphos)H^+ with a single proton that exchanged rapidly between the two phosphorus atoms at room temper-

ature. This process has a coalescense temperature of around -40 °C in solution. Synthesis of the *t*-Bu-xantphos selenides and analysis of their $^{1}J_{PSe}$ values gave pK_b values of 5.67 for *t*-Bu-sixantphos, 6.90 for *t*-Bu-thixantphos, and 6.72 for *t*-Bu-xantphos. These are much lower than the value for Ph-xantphos of 13.55, as expected due to greater electron density on the phosphorus atoms in *t*-Bu-xantphos resulting from the *tert*-butyl substituents.

The coordination chemistry of the *t*-Bu-xantphos ligands was investigated with silver, rhodium, platinum, and palladium. Two types of silver complexes were reported, [Ag(*t*-Bu-xantphos)Cl] and [Ag(*t*-Bu-xantphos)]BF_4. Both are monomeric despite the free-coordination site in [Ag(*t*-Bu-xantphos)]BF_4. The *t*-Bu-thixantphos ligand in the x-ray crystal structure of [Ag(*t*-Bu-thixantphos)Cl] had a bite-angle of 130.50(7)°, which is larger than the bite-angle in the previously reported [Ag(Ph-xantphos)Br] complex (109.37(1)°). Both of these are close to the natural bite-angle of the xantphos ligand, indicating that the coordination geometry around the silver is controlled by the diphosphine ligand. Although the crystal structure of [Ag(*t*-Bu-thixantphos)Cl] suggested that the *tert*-butyl substituents should have different NMR signals, this was not observed spectroscopically, likely due to the rapid inversion of the xantphos backbone.

Rhodium complexes are used as catalysts for hydrogenation and hydroformylation which are performed under hydrogen or a mixed hydrogen/carbon monoxide atmosphere. [Rh(*t*-Bu-xantphos-κ*P,O,P'*)Cl] complexes were formed for all three *t*-Bu-xantphos ligands. The reactivity of these complexes towards H_2, CO, and O_2 was investigated, forming [Rh(*t*-Bu-xantphos-κ*P,O,P'*)Cl$(H)_2$], [Rh(*t*-Bu-xantphos)$(CO)_2$Cl], and [Rh(*t*-Bu-xantphos-κ*P,O,P'*)Cl(η^2-O_2)] complexes. The value of the J_{RhH} coupling constant for the hydride *trans* to the oxygen atom in the [Rh(*t*-Bu-xantphos-κ*P,O,P'*)Cl$(H)_2$] complexes was largest for the *t*-Bu-sixantphos complex, followed by *t*-Bu-thixantphos then *t*-Bu-xantphos. This shows that the ligands have differing *trans* influences; *t*-Bu-sixantphos < *t*-Bu-thixantphos < *t*-Bu-xantphos. The X-ray crystal structure of [Rh(*t*-Bu-xantphos-κ*P,O,P'*) Cl(η^2-O_2)] was disordered with the dioxygen ligand replaced in 15% of the sites by an oxo. This is the first crystallographic evidence for a rhodium(III) oxo complex, and only the third rhodium oxo complex that has been reported. Attempts to synthesis the oxo complex directly were promising, with a new peak present in the ^{31}P NMR spectrum for a short-lived species. However, further research and characterisation is necessary.

Upon reaction of Ph-thixantphos with [Pt(nb)$_3$] or [Pt(C_2H_4)$_3$] the major product was [Pt(Ph-thixantphos)$_2$]; this was the only product observed in a 2:1 reaction, and was characterised crystallographically. The coordination chemistry with platinum(0) and palladium(0) showed some differences between the three *t*-Bu-xantphos ligands. *t*-Bu-Thixantphos reacts with [Pt(nb)$_3$] to form a mixture of [Pt(*t*-Bu-thixantphos)] and [Pt(*t*-Bu-thixantphos)(nb)]. Analogues of these complexes were formed in the reaction between [Pt(nb)$_3$] and *t*-Bu-sixantphos. However, over time a complex with NMR data consistent with platinum(II) is observed. Using *t*-Bu-xantphos small amounts of [Pt(*t*-Bu-xantphos)] forms, but the final product is [Pt(*t*-Bu-xantphos)H]X, possibly through reaction of the 14-electron complex with a component of the reaction mixture. The ability to isolate [Pt(*t*-Bu-thixantphos)], indicates the protection that the wide bite-angle and size of the *tert*-butyl substituents can impart to a metal centre. Isolable complexes of the type [Pt(diphosphine)] are rare, although examples with monophosphines are known. Reaction of the *t*-Bu-xantphos ligands with [Pd(nb)$_3$] formed [Pd(*t*-Bu-xantphos)] and [Pd(*t*-Bu-xantphos)(nb)] complexes for all three ligands. [Pt(*t*-Bu-xantphos)(C_2H_4)] complexes *via* reaction with [Pt(C_2H_4)$_3$]. [Pd(*t*-Bu-thixantphos)], [Pt(*t*-Bu-thixantphos)], and [Pt(*t*-Bu-thixantphos)(C_2H_4)] all react with oxygen. On palladium the oxygen is readily removed *in vacuo*, whereas the platinum complex does not lose oxygen under vacuum. [Pt(*t*-Bu-thixantphos)(η^2-O_2)] is unreactive towards C_2H_2, H_2, CO_2, NH_4PF_6 and pta. However, CO can insert into the O-O bond forming a carbonate, complex which progresses through two intermediates resulting in [Pt(*t*-Bu-thixantphos-H-κ-*C,P,P'*)OH]. This reactivity is unprecedented in the literature.

The coordination chemistry of the *t*-Bu-xantphos ligands with platinum(II) and palladium(II) starting materials was also explored. Regardless of the geometry of the starting material exclusively *trans*-[M(*t*-Bu-xantphos)Cl_2] (M = Pd, Pt) complexes were formed. The reaction of *t*-Bu-sixantphos with [PtCl_2(hex)] was hindered due to the competing protonation of the ligand due to the higher basicity of *t*-Bu-sixantphos compared to *t*-Bu-thixantphos and *t*-Bu-xantphos. The X-ray crystal structure of [Pt(*t*-Bu-xantphos)Cl_2] is unique among [PtCl_2(PP)] complexes, with a P-Pt-P angle of 151.722(15)°, with no similar angles reported in the CSD. The platinum dichloride complexes underwent solvent-dependent dissociation of a chloride ligand, forming [Pt(*t*-Bu-xantphos-κ*P,O,P'*)Cl]$^+$ in $CDCl_3$ and CD_2Cl_2. The solvent-dependent behaviour was not observed for the palladium

complexes. Computational investigations showed that, although the pincer complexes are consistently higher in energy than the dichloride complexes, the energy difference is much lower in polar solvents. Entropy would also promote the dissociation of the chloride ligand leading to the experimentally observed spontaneity. No reaction occurred between *t*-Bu-thixantphos and [Pt(hex)Me_2], likely due to the stronger coordination of the methyl ligands. The reactions of the *t*-Bu-xantphos ligands with [PtCl(hex)Me] formed only [Pt(*t*-Bu-xantphos)Me]$^+$ pincer complexes with no chlorido-methyl species observed. This is likely the result of the high *trans*-influence of the methyl ligand promoting loss of the chloride. Computational investigation showed that the fourth coordination site is occupied by the oxygen in the backbone of the *t*-Bu-xantphos ligands. The value of the J_{PtC} coupling constant is largest for *t*-Bu-sixantphos, then *t*-Bu-thixantphos, then *t*-Bu-xantphos consistent with the O-*trans* influence series observed in the rhodium complexes; *t*-Bu-sixantphos $<$ *t*-Bu-thixantphos $<$ *t*-Bu-xantphos.

Overall this thesis provides an account into the synthesis, properties and coordination chemistry of *t*-Bu-sixantphos, *t*-Bu-thixantphos, and *t*-Bu-xantphos with four late-transition metals; silver, rhodium, platinum, and palladium. The ligands showed: formation of monomeric silver complexes with κ-*P,P′* coordination; rhodium complexes with meridional κ*P,O,P′* coordination in square-planar, octahedral and trigonal bipyramidal complexes, and κ-*P,P′* coordination in trigonal bipyramidal species; platinum(0) and palladium(0) complexes with κ-*P,P′* coordination in the presence and absence of other ligands and; exclusive *trans*-κ-*P,P′*coordination to platinum(II) and palladium(II) and κ*P,O,P′* bonding modes. The final mode observed was the metallation of the *tert*-butyl group on platinum to form a κ-*C,P,P′* ligand. X-ray crystallography showed that the *t*-Bu-thixantphos ligand can achieve κ-*P,P′* coordination with bite-angles ranging from 117–151°.

Chapter 8

Experimental

8.1 General Procedures

All reactions and manipulation of products and reagents were carried out under an inert nitrogen or argon atmosphere using standard Schlenk line techniques unless stated otherwise. All reactions using silver compounds were performed in the dark. Unless otherwise stated the starting materials used in this work were obtained from Sigma-Aldrich, Merck Chemical Companies, Thermo Fisher Scientific, and BOC Industrial Gases, and used without further purification. Analytical grade reagents and high purity solvents were degassed and purged with argon before use, and dried over molecular sieves. Diethyl ether and tetrahydrofuran were distilled under an argon atmosphere from sodium benzophenone ketyl immediately prior to use. 1,3,5-triaza-7-phosphaadamantane,[345] *sec*-Butyllithium,[346] 2,8-dimethylphenoxathiin,[347] 10,10-dimethylphenoxasilin,[30] $CH_2(SO_2CF_3)_2$,[348] $[Pt(nb)_3]$,[349] $[Rh(coe)_2Cl]_2$,[350] $[Pt(C_2H_4)_3]$,[320] $[PtCl_2(NCMe)_2]$,[351] $[Pt(cod)_2]$,[352] $[Pt(C_6H_{10})Cl_2]$,[353] $[PtCl_2(SEt_2)_2]$,[46] $[PtCl_2(^tBuCN)_2]$,[354] $[Pd(nb)_3]$,[321] $[Pt(C_6H_{10})ClMe]$,[355] $[Pd(cod)Cl_2]$, and $[Pt(C_6H_{10})Me_2]$,[349] were prepared according to literature procedures.

NMR spectra were recorded using a Varian Unity Inova 300 (300 MHz for ^1H, 75 MHz for ^{13}C, 121 MHz for ^{31}P and 282 MHz for ^{19}F), a Varian Unity Inova 500 (500 MHz for ^1H and 125 MHz for ^{13}C), or a Varian DirectDrive 600 (600 MHz for ^1H and 150 MHz for ^{13}C) spectrometer. The 600 MHz instrument was equipped with a Varian inverse-detected triple-resonance HCN cold probe operating at

25 K. All direct-detected ^{1}H and ^{13}C chemical shifts were referenced to the residual solvent peak.[300] NMR samples were prepared under an inert nitrogen or argon atmosphere unless otherwise stated, using C_6D_6, $CDCl_3$, CD_2Cl_2, acetone-d_6 and toluene-d_8. Variable temperature NMR spectroscopy was carried out using a Varian Unity Inova 300 MHz NMR spectrometer. Infrared spectra were recorded with a PerkinElmer Spectrum One FT-IR spectrophotometer in absorbance mode. Electrospray ionisation mass spectrometry was recorded using an Agilent 6530 Q-TOF mass spectrometer, or performed by the Carbohydrate Chemistry Group at Industrial Research Limited, Lower Hutt, using a Waters Q-TOF Premier Tandem mass spectrometer.

Single crystal X-ray diffraction data was solved using the Superflip program[356] (except for [Ag(*t*-Bu-thixantphos)Cl] which was solved using the SHELX program) and refined using the SHELX program[357] with OLEX2 (version 1.2.5)[358] as a front-end. Unless stated otherwise the hydrogen atoms were placed in calculated positions. Crystallographic data was collected by the X-ray Crystallography Laboratory at the University of Canterbury, using either a Bruker SMART APEX-II CCD diffractometer or an Agilent SuperNova (Dual Source) CCD diffractometer. Data were reduced using Bruker SAINT or Agilent CrysAlisPro software. Absorption correction was performed using SADABS or SCALE3 ABSPACK. Theoretical calculations were performed using the Gaussian 09 Revision B.01 program[359,360] running on the Victoria University of Wellington School of Chemical and Physical Sciences Heisenberg cluster, consisting of sixteen processing nodes with two 2.53 GHz Xeon X3440 quad-core processors per node and 1 GB of memory per core. All searches of the Cambridge Structural Databank used version 5.35 (November 2013).[68]

8.2 Ligands and Non-Transition Metal Derivatives

2,8-Dimethyl-4,6-bis(di-*tert*-butylphosphino)phenoxathiin (*t*-Bu-thixantphos)

sec-Butyllithium (5.32 mL, 1.2 M in cyclohexane) was added dropwise to a stirred solution of 2,8-dimethylphenoxathiin (0.71 g, 3.1 mmol) and TMEDA (0.92 mL, 6.2 mmol) in diethyl ether (30 mL) at -78 °C. The resulting yellow solution was al-

lowed to warm to room temperature and stirred for a further 16 hours over which time a dark red colour developed. The reaction was cooled to -78 °C and chlorodi-*t*-butylphosphine (1.18 mL, 6.2 mmol) was added dropwise. The reaction mixture was stirred for a further seven days resulting in a yellow solution with a white precipitate of lithium chloride. The solvent was removed *in vacuo* giving an orange oil. This oil was dissolved in dichloromethane (25 mL) and washed with water (3 x 15 mL). The organic layer was passed through a column of magnesium sulfate and solvent was removed *in vacuo*. The product was recrystallised from *n*-propanol giving small white crystals (1.36 g, 85%). This compound can be handled in the air for short periods however, should be stored under an inert atmosphere. ^{31}P NMR (121 MHz, $CDCl_3$): δ 9.5 (s). ^{1}H NMR (500 MHz, $CDCl_3$): δ 7.29 (s, PC(Ar)C*H*), 6.88 (s, SCC*H*), 2.25 (s, C(Ar)C*H*$_3$), 1.22-1.24 (m, PC(C*H*$_3$)$_3$). ^{13}C NMR (125 MHz, $CDCl_3$): δ 155.3 (vt, J_{PC} = 13.0 Hz, PC*C*O), 134.6 (s, PC(Ar)*C*H), 131.9 (s, *C*(Ar)CH$_3$), 128.0 (dd, J = 22.5, 17.7 Hz, P*C*(Ar)), 127.4 (s, SC*C*H), 120.1 (vt, J_{PC} = 2.4 Hz, SC*C*H), 32.9 (dd, J = 15.8, 13.4 Hz, P*C*(CH$_3$)$_3$), 30.8 (vt, J_{PC} = 18.2 Hz, PC(*C*H$_3$)$_3$), 20.9 (s, C(Ar)*C*H$_3$). HRMS calcd for $C_{30}H_{47}OP_2S$ [M+H]$^+$ m/z = 517.2817; found = 517.2819.

4,6-Bis(di-*tert*-butylphosphino)-10,10-dimethylphenoxasilin (*t*-Bu-sixantphos)

This compound was prepared similarly to *t*-Bu-thixantphos using 10,10-dimethylphenoxasilin (0.40 g, 1.8 mmol) giving the title compound as white crystals (0.127 g, 14%).

^{31}P NMR (121 MHz, CD_2Cl_2): δ 8.4 (s, $^4J_{PSi}$ = 4.8 Hz). ^{1}H NMR (500 MHz, CD_2Cl_2): δ 7.87 (d, J = 7.4 Hz, PC(Ar)C*H*), 7.53 (d, J = 7.1 Hz, SiCC*H*), 7.12 (t, J = 7.5 Hz, PCCC*H*), 1.29 (vt, J_{PH} = 5.6 Hz, PC(C*H*$_3$)$_3$), 0.46 (s, Si(C*H*$_3$)$_2$), ^{13}C NMR (125 MHz, CD_2Cl_2): δ 164.3 (vt, J_{PC} = 11.3 Hz, PC*C*O), 138.5 (s, PC(Ar)*C*H), 134.8 (s, SiC*C*H), 128.0 (s, P*C*(Ar)), 121.4 (s, PCC*C*H), 119.4 (s, Si*C*CH), 33.2 (dd, J_{PC} = 16.3, 13.9 Hz, P*C*(CH$_3$)$_3$), 31.0 (vt, J_{PC} = 9.6 Hz, PC(*C*H$_3$)$_3$), -0.09 (s, Si(*C*H$_3$)$_2$). HRMS calcd for $C_{30}H_{49}OP_2Si$ [M + H]$^+$ m/z = 515.3022; found = 515.3021.

9,9-Dimethyl-4,6-bis(diphenylphosphino)xanthene (*t*-Bu-xantphos)

9,9-dimethylxanthene (0.50 g, 2.38 mmol) and TMEDA (1.07 mL, 7.13 mmol) were dissolved in diethyl ether (20 mL). Added s-BuLi dropwise causing the reaction to change to yellow then a deep red. After stirring for 24 hours chlorodi(*tert*-butyl)phosphine (1.36 mL, 7.13 mmol) was added dropwise. After six days of stirring a white precipitate had formed and a pale yellow solution remained. The solvent was removed *in vacuo* and the resulting yellow oil was taken up in dichloromethane (20 mL) and washed with degassed water (10 mL). The aqueous layer was further extracted with dichloromethane (20 mL) and the combined organic layers were washed with water (3 x 10 mL). The organic layers were dried over magnesium sulfate and the solvent was removed *in vacuo*. The resulting pale yellow solid was recrystallised from n-propanol yielding the title compound as fine white needles (0.44 g, 37%).

The ^{1}H and ^{13}C NMR data are consistent with the literature values.[84] However, the literature reported ^{31}P chemical shift is 12.4 ppm. Due to this discrepancy full characterisation data for this compound is given below.

^{31}P NMR (121 MHz, $CDCl_3$): δ 10.2 (s), ^{1}H NMR (500 MHz, $CDCl_3$): δ 7.60 (d, J = 7.6 Hz, PC(Ar)C*H*), 7.38 (dd, 7.8, 1.5 Hz, C(bridge)CC*H*), 7.03 (t, J = 7.6 Hz, PCCC*H*), 1.57 (s, C(bridge)(CH_3)$_2$), 1.21-1.25 (m, PC(CH_3)$_3$). ^{13}C NMR (125 MHz, $CDCl_3$): δ 155.8 (vt, J_{PC} = 12.0 Hz, PC*C*O), 133.7 (bs, PC(Ar)*C*H), 130.7 (vt, J_{PC} = 2.0 Hz, C(bridge)*C*CH), 126.6 (dd, J_{PC} = 21.6, 15.4 Hz, P*C*(Ar)), 125.5 (s, C(bridge)CCH), 121.5 (s, PCCCH), 35.0 (bs, *C*(bridge)), 32.7 (dd, J_{PC} = 16.1, 12.7 Hz, P*C*(CH$_3$)$_3$), 31.1 (s, C(bridge)(*C*H$_3$)$_2$), 30.8 (vt, J_{PC} = 18.8 Hz, PC(*C*H$_3$)$_3$). HRMS calcd for $C_{31}H_{49}OP_2$ $[M+H]^+$ m/z = 499.3253; found = 499.3241.

2,6-bis(di-*tert*-butylphosphino)phenoxathiin

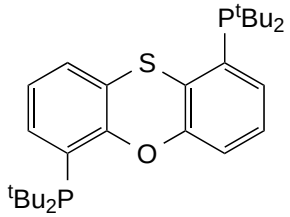

Phenoxathiin (0.20 g, 1.00 mmol) and TMEDA (0.43 mL, 2.27 mmol) were dissolved in heptane (6 mL). A solution of *sec*-butyllithium (1.0 M in cyclohexane, 2.27 mL) was added dropwise. The mixture was stirred for 24 hours resulting in a yellow solution with a white precipitate. P^tBu_2Cl (0.55 mL, 2.90 mmol) was added dropwise to the reaction and the resulting mixture was heated at 60 °C for 24 hours. The solvent was removed under reduced pressure and the resulting yellow oil was taken up in dichloromethane (10 mL) and washed with degassed water (2 x 10 mL). The organic layer was dried by passing through a plug of $MgSO_4$ before removed the solvent *in vacuo*. The resulting oil was recrystallised from hot n-propanol yielding the title compound as a yellow microcrystalline solid (0.316 g, 65%).

^{31}P NMR (121 MHz, $CDCl_3$): δ 17.7 (d, J = 2.2 Hz, *P*CCO) 11.7 (d, J = 2.3 Hz, *P*CCS) ^{1}H NMR (500 MHz, $CDCl_3$): δ 7.49 (d, J= 7.6 Hz, 1H, Ar), 7.40 (d, J= 7.3 Hz, 1H, Ar), 7.17 (dd, J= 7.7 Hz, 1.3 Hz, 1H, Ar), 7.13 (d, J= 7.6 Hz, 1H, Ar), 7.07 (t, J= 7.7 Hz, 1H, Ar), 6.94 (t, J= 7.6 Hz, 1H, Ar), 1.21 (d, J= 12.3 Hz, 18H, PC(C*H*$_3$)$_3$), 1.20 (d, J= 12.0 Hz, 18H, PC(C*H*$_3$)$_3$). ^{13}C NMR (150 MHz, $CDCl_3$): δ 156.4 (d, J_{PC}= 17.9 Hz, 1C, Ar), 151.6 (d, J_{PC}= 10.4 Hz, 1C, Ar), 134.1 (s, 1C, Ar), 134.0 (s, 1C, Ar), 133.8 (s, 1C, Ar), 130.5 (d, J_{PC}= 3.4 Hz, 1C, Ar), 127.9 (s, 1C, Ar), 126.2 (d, J_{PC}= 31.8 Hz, 1C, Ar), 125.6 (d, J_{PC}= 7.0 Hz, 1C, Ar), 122.8 (s, 1C, Ar), 122.3 (d, J_{PC}= 17.9 Hz, 1C, Ar), 119.4 (s, 1C, Ar) 33.1 (d, J_{PC}= 21.4 Hz, P*C*(CH$_3$)$_3$), 32.4 (d, J_{PC}= 23.7 Hz, P*C*(CH$_3$)$_3$), 30.7 (d, J_{PC}= 15.1 Hz, PC(*C*H$_3$)$_3$), 30.4 (d, J_{PC}= 14.4 Hz, PC(*C*H$_3$)$_3$).

Synthesis of [(*t*-Bu-xantphos)H]CH(SO_2CF_3)

A solution of $CH_2(SO_2CF_3)_2$ (0.009 g, 0.032 mmol) in $CDCl_3$ (0.5 mL) was added to *t*-Bu-xantphos (0.016 g, 0.032 mmol) in an NMR tube. The reaction was instantaneous and quantitative conversion was observed by NMR spectroscopy. Removal of the solvent *in vacuo* gave the product as a white solid in quantitative yield.

^{31}P NMR (121 MHz, $CDCl_3$): δ 17.4 (bs). ^{1}H NMR (600 MHz, $CDCl_3$): δ 9.05 - 8.09 (m, P*H*), 7.67-7.74 (m, 4H, Ar), 7.39 (bs, 2H, Ar), 4.06 (bs, C*H*(SO_2CF_3)$_2$), 1.65 (s, C(bridge)(C*H*$_3$)$_2$), 1.37-1.43 (m, PC(C*H*$_3$)$_3$). ^{19}F NMR (282 MHz, $CDCl_3$): δ -80.9 (s, C*F*$_3$) ^{13}C NMR (150 MHz, $CDCl_3$): δ 153.6-153.8 (m, PC*C*O), 132.5

(bs), 130.3 (bs), 125.0 (bs), 121.0 (quartet, J_{CF} = 317.9 Hz, CH(SO_2CF_3)$_2$), 54.1 (s, *C*H(SO_2CF_3)$_2$), 35.5 (s, *C*(bridge)), 34.0 (bs, P*C*(CH_3)$_3$), 30.8 (s, C(bridge)(*C*H$_3$)$_2$), 29.4 (bs, PC(*C*H$_3$)$_3$). HRMS calcd for $C_{31}H_{49}OP_2$ $[M]^+$ m/z = 499.3253; found = 499.3254.

Synthesis of [(*t*-Bu-thixantphos)H]CH(SO_2CF_3)

This product was synthesised similarly to [*t*-Bu-xantphos(H)]CH(SO_2CF_3)$_2$ using *t*-Bu-thixantphos (0.041 g, 0.079 mmol) giving the title compound in quantitative yield as a pale yield solid. X-ray quality crystals were grown by performing the reaction in C_6D_6 and allowing the solvent to slowly evaporate.

^{31}P NMR (121 MHz, CD_2Cl_2): δ 15.8 (s) ^{1}H NMR (500 MHz, CD_2Cl_2): δ 8.99 (m, P*H*), 7.29 (s, SCC*H*), 7.22 (s, PC(Ar)C*H*), 3.83 (s, C*H*(SO_2CF_3)), 2.36 (s, C(Ar)C*H*$_3$), 1.41-1.44 (m, PC(C*H*$_3$)$_3$). ^{13}C NMR (125 MHz, CD_2Cl_2): δ 152.9 (s, PC*C*O), 136.2 (s, *C*(Ar)CH$_3$), 132.5 (s, SC*C*H), 131.8 (s, PC(Ar)*C*H), 122.2 (s, S*C*CH), 121.5 (quartet, J_{CF} = 325.6 Hz, CF_3), 115.3 (s, P*C*(Ar)), 34.4 (s, P*C*(CH_3)$_3$), 29.5 (s, PC(*C*H$_3$)$_3$). One peak (*C*H(SO_2CF_3)) obscured by solvent. HRMS calcd for $C_{30}H_{47}OP_2S$ $[M]^+$ m/z = 517.2817; found = 517.2817.

Synthesis of [(*t*-Bu-sixantphos)H]CH(SO_2CF_3)

[*t*-Bu-Sixantphos(H)]CH(SO_2CF_3)$_2$ was synthesised in a similar manner to [*t*-Bu-xantphos(H)]CH(SO_2CF_3) using *t*-Bu-sixantphos (0.020 g, 0.039 mmol). The product was produced as a white solid in quantitative yield.

^{31}P NMR (121 MHz, $CDCl_3$): δ 14.3 (s) ^{1}H NMR (500 MHz, $CDCl_3$): δ 9.57 (m, P*H*), 7.85-7.87 (m, PC(Ar)C*H*), 7.79 (d, 6.6 Hz, SiCC*H*), 7.41 (t, 7.5 Hz, PCCC*H*), 4.06 (bs, C*H*(SO_2CF_3)$_2$), 1.43 (vt, J_{PH} = 7.5 Hz, PC(C*H*$_3$)$_3$), 0.53 (s, Si(C*H*$_3$)$_2$). ^{19}F NMR (282 MHz, $CDCl_3$): δ -80.8 (s, C*F*$_3$) ^{13}C NMR (125 MHz, $CDCl_3$): δ 161.5 (vt, J_{PC} = 5.3 Hz, PC*C*O), 139.1 (s, SiC*C*H), 136.9 (s, PC(Ar)*C*H), 124.0 (vt, J_{PC} = 2.4 Hz, PCC*C*H), 121.1 (s, Si*C*CH), 121.1 (quartet, J_{CF} = 327.2 Hz, CH(SO_2CF$_3$)$_2$), 115.0 (bs, P*C*(Ar)), 53.6 (s, *C*H(SO_2CF_3)$_2$), 34.2 (vt, J_{PC} = 3.9 Hz, P*C*(CH_3)$_3$), 29.5 (vt, J_{PC} = 4.3 Hz, PC(*C*H$_3$)$_3$), -0.4 (s, Si(*C*H$_3$)$_2$). HRMS calcd for $C_{30}H_{49}OP_2Si$ $[M]^+$ m/z = 515.3022; found = 515.3023.

t-Bu-SixantphosSe

A solution of *t*-Bu-xantphos (0.031 g, 0.060 mmol) in toluene (5 mL) was added to grey selenium (0.095 g, 1.20 mmol) in toluene (5 mL). The reaction was heated to reflux with stirring for 3 days. The resulting yellow solution was allowed to cool, filtered and reduced *in vacuo* to give a pale yellow solid (0.036 g, 100%).

^{31}P NMR (121 MHz, 1:1, $CDCl_3$:CD_2Cl_2): δ 15.9 (s, P), 102.7 (s, $^1J_{PSe}$ = 689.1 Hz, P=Se). ^{1}H NMR (300 MHz, 1:1, $CDCl_3$:CD_2Cl_2): δ 9.13 (bs, 1H, Ar), 7.81 (d, J = 7.5 Hz, 1H, Ar), 7.66-7.16 (m, 4H, Ar), 1.61 (d, J = 22.5 Hz, P(=Se)C(C*H3*)$_3$), 1.10 (d, J = 11.5 Hz, PC(C*H*$_3$)$_3$), 0.36 (s, Si(C*H*$_3$)$_2$), 0.07 (s, Si(C*H*$_3$)$_2$). HRMS calcd for $C_{30}H_{49}OP_2SeSi$ $[M+H]^+$ m/z = 595.2190; found = 595.2172.

t-Bu-ThixantphosSe

A solution of *t*-Bu-thixantphos (0.042 g, 0.081 mmol) in toluene (5 mL) was added to grey selenium (0.128 g, 1.62 mmol) in toluene (5 mL). The reaction was heated to reflux with stirring for 3 days. The resulting yellow solution was allowed to cool, filtered and reduced *in vacuo* to give the title compound as a yellow solid (0.047 g, 98%).

^{31}P NMR (121 MHz, $CDCl_3$): δ 11.7 (s, P), 101.9 (s, $^1J_{PSe}$ = 698.5 Hz, P=Se). ^{1}H NMR (300 MHz, $CDCl_3$): δ 8.85 (d, J = 16.2 Hz, P(=Se)CC*H*), 7.26 (s, 1H, Ar), 6.96 (s, 1H, Ar), 6.89 (s, 1H, Ar), 2.27 (s, 3H, C(Ar)C*H*$_3$), 2.25 (s, 3H, C(Ar)C*H*$_3$), 1.62 (d, J = 16.6 Hz, 18H, P(=Se)C(C*H3*)$_3$), 1.15 (d, J = 11.9 Hz, 18H, PC(C*H*$_3$)$_3$). HRMS calcd for $C_{31}H_{49}OP_2SSe$ $[M+H]^+$ m/z = 597.1984; found = 597.1919.

t-Bu-XantphosSe

A solution of *t*-Bu-xantphos (0.041 g, 0.082 mmol) in toluene (5 mL) was added to grey selenium (0.130 g, 1.65 mmol) in toluene (5 mL). The reaction was heated to reflux with stirring for 3 days. The resulting yellow solution was allowed to cool, filtered and reduced *in vacuo* to give a pale yellow solid (0.038 g, 80%).

^{31}P NMR (121 MHz, 1:1, $CDCl_3$:CD_2Cl_2): δ 10.6 (s, P), 101.9 (s, $^1J_{PSe}$ = 697.1 Hz, P=Se). ^{1}H NMR (500 MHz, 1:1, $CDCl_3$:CD_2Cl_2): δ 9.26 (dd, 17.4,

7.8 Hz, P(=Se)CC*H*), 7.67 (d, *J* = 7.6 Hz, PC(Ar)C*H*), 7.60 (d, *J* = 7.5 Hz, P(=Se)CCCC*H*), 7.50 (d, *J* = 7.5 Hz, PCCCC*H*), 7.24 (t, *J* = 7.8 Hz, P(=Se)CCC*H*), 7.19 (t, *J* = 7.6 Hz, PCCC*H*), 1.66 (d, *J* = 16.6 Hz, P(=Se)C(C*H3*)$_3$), 1.57 (s, C(bridge)(C*H*$_3$)$_2$), 1.19 (d, *J* = 11.8 Hz, PC(C*H*$_3$)$_3$). ^{13}C NMR (125 MHz, 1:1 $CDCl_3$:CD_2Cl_2): δ 157.0 (d, J_{PC} = 21.1 Hz, PC*C*O), 154.2 (s, P(=Se)C*C*O), 143.5 (d, J_{PC} = 11.6 Hz, P(=Se)C*C*H), 136.0 (s, PC(Ar)*C*H), 132.8 (s, PCC*C*C(bridge)), 132.0 (d, J_{PC} = 4.8 Hz, P(=Se)CC*C*C(bridge)), 129.2 (d, J_{PC} = 2.4 Hz, P(=Se)CCC*C*H), 126.3 (s, PCCC*C*H), 125.3 (d, J_{PC} = 35 Hz, P*C*(Ar)), 123.2 (s, 2C, P(=Se)CC*C*H, PCC*C*H), 115.4 (d, J_{PC} = 39.8 Hz, P(=Se)*C*(Ar)), 39.2 (d, J_{PC} = 34.6 Hz, P(=Se)*C*(CH3)3), 35.3 (s, *C*(bridge)), 33.5 (d, J_{PC} = 26.9 Hz, P*C*(CH_3)$_3$), 31.2 (d, J_{PC} = 15.4 Hz, PC(*C*H$_3$)$_3$), 30.9 (dd, 7.7, 2.0 Hz, P(=Se)C(*C*H$_3$)$_3$). 30.8 (s, C(bridge)*C*H$_3$). HRMS calcd for $C_{31}H_{49}OP_2Se$ $[M+H]^+$ m/z = 579.2421; found = 579.2381.

8.3 Silver Complexes

[Ag(*t*-Bu-thixantphos)Cl]

This reaction was carried out in the dark. *t*-Bu-Thixantphos (88 mg, 0.17 mmol) and silver chloride (24 mg, 0.17 mmol) were combined CH_2Cl_2 (4 mL) in a Schlenk tube. After 5 days stirring the solution was passed through a plug of alumina, washing with dichloromethane (4 x 1 mL). The solvent was removed *in vacuo* giving a cloudy oil. The oil was triturated with hexane (2 mL) yielding the title compound as a white powder (94 mg, 84%). The resulting silver complex is light sensitive and care should be taken to exclude light.

^{31}P NMR (121 MHz, $CDCl_3$): δ 21.81 (d, $^1J_{^{107}AgP}$ = 406.7 Hz, d, $^1J_{^{109}AgP}$ = 469.6 Hz). ^{1}H NMR (600 MHz, $CDCl_3$): δ 7.39 (d, J_{PH} = 1.0 Hz, PC(Ar)C*H*), 7.11 (d, J_{PH} = 1.6 Hz, SCC*H*), 2.31 (s, C(Ar)C*H*$_3$) 1.41 (m, PC(C*H*$_3$)$_3$). ^{13}C NMR (150 MHz, $CDCl_3$): δ 155.5 (vt, J_{PC} = 6.6 Hz, PC*C*O), 134.8 (d, J_{PC} = 4.9 Hz, PC(Ar)*C*H), 133.1 (d, J_{PC} = 1.5 Hz, *C*(Ar)CH$_3$), 130.3 (s, SC*C*H), 122.8 (vt, J_{PC} = 3.0 Hz, S*C*CH), 120.9 (m, P*C*(Ar)) 35.3 (m, P*C*(CH_3)$_3$) 30.9 (vt, J_{PC} = 5.6 Hz, PC(*C*H$_3$)$_3$), 20.8 (s, C(Ar)*C*H$_3$). HRMS calcd for $C_{30}H_{46}OP_2SAg$ $[M-Cl]^+$ m/z = 623.1796; found = 623.1805.

[Ag(*t*-Bu-sixantphos)Cl]

This reaction was carried out in the dark. *t*-Bu-Sixantphos and silver chloride were combined in an NMR tube, dissolved in $CDCl_3$, and sonicated for 5 mins. After four days the reaction was sonicated for 6 x 5 mins. The solution was decanted and the resulting solid was washed with dichloromethane (3 x 1 mL). The solvent was removed *in vacuo* yielding the title compound as a white solid (31 mg, 97%). The resulting silver complex is light sensitive and care should be taken to exclude light.

^{31}P NMR (121 MHz, $CDCl_3$): δ 24.2 (d, $^{1}J_{^{107}AgP}$ = 408.1 Hz, d, $^{1}J_{^{109}AgP}$ = 471.1 Hz) ^{1}H NMR (600 MHz, $CDCl_3$): δ 7.88 (m, PC(Ar)C*H*), 7.61 (dd, 7.0, 1.8 Hz, SiCC*H*), 7.21 (t, 7.3 Hz, PCCC*H*), 1.42 (m, PC(C*H*$_3$)$_3$), 0.46 (s, Si(C*H*$_3$)$_2$). ^{13}C NMR (150 MHz, $CDCl_3$): δ 163.9 (vt, J_{PC} = 5.2 Hz, PC*C*O), 138.2 (d, J_{PC} = 4.4 Hz, PC(Ar)*C*H), 136.3 (s, SiC*C*H), 122.2 (s, Si*C*CH), 122.1 (s, PCC*C*H), 120.5 (m, P*C*(Ar)) 35.5 (m, P*C*(CH$_3$)$_3$) 31.0 (vt, J_{PC} = 5.6 Hz, PC(*C*H$_3$)$_3$), -1.3 (s, C(Ar)*C*H$_3$). HRMS calcd for $C_{30}H_{48}OP_2Ag$ [M-Cl]$^+$ *m/z* = 621.2001; found = 621.2021.

[Ag(*t*-Bu-xantphos)Cl]

This reaction was carried out in the dark. *t*-Bu-Xantphos (0.017 g, 0.034 mmol) and silver chloride (0.005 g, 0.035 mmol) were combined in an NMR tube and dissolved in $CDCl_3$. After 48 hours the reaction mixture was sonicated 10 x 5 mins. The solution was decanted and the resulting solid was dried under reduced pressure leaving the title compound as a white powder (0.017 g, 78%). The resulting silver complex is light sensitive and care should be taken to exclude light.

^{31}P NMR (121 MHz, $CDCl_3$): δ 20.7 (d, $^{1}J_{^{107}AgP}$ = 409.3 Hz, d, $^{1}J_{^{109}AgP}$ = 472.2 Hz) ^{1}H NMR (500 MHz, $CDCl_3$): δ 7.68 (d, J_{PH} = 6.9 Hz, PC(Ar)C*H*), 7.53 (dd, 7.6, 1.2 Hz, C(bridge)CC*H*), 7.19 (t, 7.7 Hz, PCCC*H*), 1.56 (s, C(bridge)(C*H*$_3$)$_2$), 1.40-1.43 (m, PC(C*H*$_3$)$_3$). ^{13}C NMR (125 MHz, $CDCl_3$): δ 156.5 (vt, J_{PC} = 6.5 Hz, PC*C*O), 133.7 (m, PC(Ar)*C*H), 130.7 (s, C(bridge)*C*CH), 126.8 (s, C(bridge)C*C*H), 122.7 (s, PCC*C*H), 119.3 (m, P*C*(Ar)), 35.6 (m, *C*(bridge)), 35.1 (m, P*C*(CH$_3$)$_3$), 30.8 (vt, J_{PC} = 5.6 Hz, PC(*C*H$_3$)$_3$), 28.5 (s, C(bridge)(*C*H$_3$)$_2$). HRMS calcd for $C_{31}H_{48}OP_2Ag$ [M-Cl]$^+$ *m/z* = 605.2226; found = 605.2163.

[Ag(*t*-Bu-sixantphos)]BF_4

This reaction was carried out in the dark. *t*-Bu-Sixantphos (0.027 g, 0.052 mmol) and silver tetrafluoroborate (0.010, 0.052 mmol) were combined in an NMR tube and dissolved in $CDCl_3$. After 3 days the reaction was complete by NMR spectroscopy. The solution was removed under reduced pressure yielding the title compound as a white solid (0.024 g, 0.034 mmol, 64%).

^{31}P NMR (121 MHz, $CDCl_3$): δ 31.5 (d, $^1J_{^{107}AgP}$ = 482.9 Hz, d, $^1J_{^{109}AgP}$ = 557.4 Hz). ^{1}H NMR (500 MHz, $CDCl_3$): δ 7.84 (bs, PC(Ar)C*H*), 7.73 (d, 6.8 Hz, SiCC*H*), 7.34 (t, 7.3 Hz, PCCC*H*), 1.40 (vt, J_{PH} = 15.9 Hz, PC(C*H*$_3$)$_3$), 0.49 (s, Si(C*H*$_3$)$_2$). ^{13}C NMR (125 MHz, $CDCl_3$): δ 162.3 (vt, J_{PC} = 8.7 Hz, PC*C*O), 138.2 (s, SiC*C*H), 138.1 (d, J_{PC} = 6.7 Hz, PC(Ar)*C*H), 123.1 (d, J_{PC} = 1.9 Hz, PCC*C*H), 122.1 (s, Si*C*CH), 118.4 (m, P*C*(Ar)), 35.7 (m, P*C*(CH$_3$)$_3$), 30.9 (m, PC(*C*H$_3$)$_3$), -0.6 (s, Si(*C*H$_3$)$_2$). ^{19}F NMR (282 MHz, $CDCl_3$): δ -151.9 (s, BF_4^-). HRMS calcd for $C_{30}H_{48}OP_2AgSi$ [M-BF_4^-]$^+$ m/z = 621.2001; found = 621.2032.

[Ag(*t*-Bu-thixantphos)]BF_4

This reaction was carried out in the dark. A solution of *t*-Bu-thixantphos (0.026 g, 0.050 mmol) in 0.5 mL of $CDCl_3$ was added to silver tetrafluoroborate (0.010 g, 0.051 mmol) in an NMR tube. After 3 days the reaction NMR showed complete conversion into the title complex. The solvent was removed under reduced pressure yielding the product as a white solid (0.030 g, 0.042 mmol, 84%).

^{31}P NMR (121 MHz, $CDCl_3$): δ 28.4 (d, $^1J_{^{107}AgP}$ = 486.7 Hz, d, $^1J_{^{109}AgP}$ = 562.2 Hz). ^{1}H NMR (500 MHz, $CDCl_3$): δ 7.32 (s, PC(Ar)C*H*), 7.16 (s, SCC*H*), 2.33 (s, C(Ar)C*H*$_3$), 1.40 (vt, J_{PH} = 15.8 Hz, PC(C*H*$_3$)$_3$). ^{13}C NMR (125 MHz, $CDCl_3$): δ 153.9 (vt, J_{PC} = 11.0 Hz, PC*C*O), 134.4 (d, J_{PC} = 1.7 Hz, *C*(Ar)CH$_3$), 134.2 (d, J_{PC} = 6.30 Hz, PC(Ar)*C*H), 131.1 (s, SC*C*H), 122.3 (s, S*C*CH), 119.4 (m, P*C*(Ar)), 35.5 (m, P*C*(CH$_3$)$_3$), 30.8 (m, PC(*C*H$_3$)$_3$), 20.7 (s, C(Ar)*C*H$_3$). ^{19}F NMR (282 MHz, $CDCl_3$): δ 151.3 (s, BF_4^-). HRMS calcd for $C_{30}H_{46}OP_2SAg$ [M-BF_4^-]$^+$ m/z = 623.1796; found = 623.1826.

[Ag(*t*-Bu-xantphos)]BF_4

This reaction was carried out in the dark as silver compounds are typically light sensitive. *t*-Bu-Xantphos (0.017 g, 0.034 mmol) and silver tetrafluoroborate (0.008 g, 0.041 mmol) were combined in an NMR tube and dissolved in $CDCl_3$. After 48 hours the reaction was complete by NMR spectroscopy. The solvent was removed under reduced pressed yielding a white solid in quantitative yield.

^{31}P NMR (121 MHz, $CDCl_3$): δ 27.6 (d, $^1J_{^{107}AgP}$ = 486.3 Hz, d, $^1J_{^{109}AgP}$ = 561.1 Hz) ^1H NMR (500 MHz, $CDCl_3$): δ 7.63-7.67 (m, C(bridge)CC*H*, PC(Ar)C*H*), 7.29 (t, 7.7 Hz, PCCC*H*), 1.59 (s, C(bridge)(CH_3)$_2$), 1.39-1.42 (m, PC(CH_3)$_3$). ^{13}C NMR (125 MHz, $CDCl_3$): δ 154.9 (vt, J_{PC} = 5.6 Hz, PC*C*O), 133.5 (vt, J_{PC} = 1.9 Hz, PC(Ar)*C*H), 133.5 (d, J_{PC} = 5.8 Hz, C(bridge)*C*CH), 128.4 (s, C(bridge)C*C*H), 123.8 (s, PCC*C*H), 117.8 (s, P*C*(Ar)), 35.6 (vtd, J_{PC} = 5.3, 2.4 Hz, *C*(bridge)), 35.3 (m, P*C*(CH_3)$_3$), 30.6 (m, PC(*C*H_3)$_3$), 29.4 (s, C(bridge)(*C*H_3)$_2$). ^{19}F NMR (282 MHz, $CDCl_3$): δ -151.9 (s, BF_4^-) HRMS calcd for $C_{31}H_{48}OP_2Ag$ [M-BF_4^-]$^+$ *m/z* = 605.2226; found = 605.2217.

Reaction of [Ag(*t*-Bu-sixantphos)]BF_4 with LiCCPh

A solution of n-butyllithium in cyclohexanes (1.6 M 0.12 mL) was added to a solution of phenylacetylene (0.021 mL) in THF (40 mL). The mixture was stirred for 10 minutes, then a solution of [Ag(*t*-Bu-sixantphos)]BF_4 (0.34 g) in THF (2.0 mL) was added. The reaction mixture was stirred in the dark for 2 hours. The solvent was removed *in vacuo* and the residue taken up in acetone-d_6 for NMR analysis.

^{31}P NMR (121 MHz, acetone$-d_6$): δ 26.4 (d, $^1J_{^{107}AgP}$ = 418.5 Hz, d, $^1J_{^{109}AgP}$ = 482.9 Hz) ^1H NMR (500 MHz, acetone$-d_6$): δ 8.06 (m, 2H, Ar), 7.86 (dd, *J* = 7.1, 1.5 Hz, 2H, Ar), 7.41 (t, *J* = 7.4 Hz, PCCC*H*), 1.47-1.45 (m, PC(CH_3)$_3$), 0.51 (s, Si(CH_3)$_2$). ^{19}F NMR (282 MHz, acetone$-d_6$): δ -152.3 (s, BF_4^-).

Reaction of [Ag(*t*-Bu-thixantphos)]BF_4 with LiCCPh

A solution of n-butyllithium in cyclohexanes (1.6 M 0.11 mL) was added to a solution of phenylacetylene (0.020 mL) in THF (40 mL). The mixture was stirred

for 10 minutes, then 17 mL of the solution was added to a solution of [Ag(*t*-Bu-thixantphos)]BF_4 in (0.055 g) in THF (3.0 mL). The reaction mixture was stirred in the dark for 12 hours. The solvent was removed *in vacuo* and the residue taken up in acetone-d_6 or C_6D_6 for NMR analysis.

^{31}P NMR (121 MHz, C_6D_6): δ 23.4, (bs) 19.9, (bs) ^{1}H NMR (300 MHz, C_6D_6): δ 7.7-6.8 (m, 6H, Ar), 1.96 (bs, C(Ar)CH_3), 1.42 (bs, PC(CH_3)$_3$). ^{19}F NMR (282 MHz, C_6D_6): δ -156.9 (s, BF_4^-)

^{31}P NMR (121 MHz, acetone−d_6): δ 23.1 (d, $^1J_{^{107}AgP}$ = 410.3 Hz, d, $^1J_{^{109}AgP}$ = 474.1 Hz). ^{1}H NMR (300 MHz, acetone−d_6): δ 7.61 (s, 2H, Ar) 7.36 (s, 2H, Ar) 2.39 (s, C(Ar)CH_3), 1.51-1.46 (m, PC(CH_3)$_3$). ^{19}F NMR (282 MHz, acetone−d_6): δ -152.1 (s, BF_4^-).

Reaction of [Ag(*t*-Bu-xantphos)]BF_4 with LiCCPh

A solution of n-butyllithium in cyclohexanes (1.6 M 0.11 mL) was added to a solution of phenylacetylene (0.020 mL) in THF (40 mL). The mixture was stirred for 10 minutes, then 16.2 mL of the solution was added to a solution of [Ag(*t*-Bu-xantphos)]BF_4 in (0.051 g) in THF (3.0 mL). The reaction mixture was stirred in the dark for 12 hours. The solvent was removed *in vacuo* and the residue taken up in acetone-d_6 for NMR analysis.

^{31}P NMR (121 MHz, acetone−d_6): δ 20.7 (d, $^1J_{^{107}AgP}$ = 407.4 Hz, d, $^1J_{^{109}AgP}$ = 471.1 Hz). ^{1}H NMR (500 MHz, acetone−d_6): δ 7.86 (d, J = 7.5 Hz, 2H, Ar), 7.76 (dd, J = 7.6, 0.9 Hz, 2H, Ar), 7.37 (t, J = 7.6 Hz, PCCCH), 1.61 (s, C(bridge)(CH_3)$_2$), 1.46-1.44 (m, PC(CH_3)$_3$). ^{19}F NMR (282 MHz, acetone−d_6): δ -152.6 (s, BF_4^-).

8.4 Rhodium Complexes

[Rh(*t*-Bu-sixantphos-κ*P,O,P'*)Cl]

A solution of *t*-Bu-sixantphos (0.032 g, 0.062 mmol) in C_6D_6 was added to solid $[Rh(coe)_2Cl]_n$ (0.027 g, 0.075 mmol, 1.2 eq. of Rh) in a Young's tap NMR tube. The tube was sealed under argon and heated to 60 °C for 24 hours. The solution was

decanted and the solvent removed *in vacuo* to yield the title compound as a dark red solid in quantitative yield (0.041 g, 0.062 mmol, 100%).

^{31}P NMR (121 MHz, C_6D_6): δ 44.2 (d, J_{RhP} = 140.0 Hz). ^{1}H NMR (600 MHz, C_6D_6): δ 8.05 (m, PC(Ar)C*H*), 7.13 (dd, J = 6.8, 1.8 Hz, SiCC*H*), 6.84 (t, J = 7.2 Hz, PCCC*H*), 1.69 (vt, J_{PH} = 13.5 Hz, PC(C*H*$_3$)$_3$), 0.07 (s, Si(C*H*$_3$)$_2$). ^{13}C NMR (125 MHz, C_6D_6): δ 169.5 (PC*C*O, J_{PC} = , Hz,) (s, 138.4)PC(Ar)*C*H, 136.0 (s, SiC*C*H), 127.0 (m, P*C*(Ar)), 122.8 (s, PCC*C*H), 121.5 (SiC*C*H, J_{PC} = , Hz,) (37.7, J_{PC} = vt Hz, 9.9)P*C*(CH$_3$)$_3$, 31.0 (vt, J_{PC} = 8.1 Hz, PC(*C*H$_3$)$_3$), -0.7 (s, Si(*C*H$_3$)$_2$). HRMS calcd for $C_{30}H_{48}OP_2RhSi$ [M-Cl]$^+$ m/z = 617.1999; found = 617.1998.

[Rh(*t*-Bu-thixantphos-κ*P,O,P'*)Cl]

This compound was synthesised similarly to [Rh(*t*-Bu-sixantphos)Cl] using, *t*-Bu-thixantphos (0.025 g, 0.048 mmol) and [Rh(coe)$_2$Cl]$_n$ (0.021 g, 0.059 mmol). The title compound was obtained as an air-sensitive brown solid in quantitative yield (0.032 g, 0.048 mmol, 100%).

^{31}P NMR (121 MHz, C_6D_6): δ 46.5 (d, J_{RhP} = 141.5 Hz) ^{1}H NMR (600 MHz, C_6D_6): δ 7.43 (d, J = 1.5 Hz, PC(Ar)C*H*), 6.39 (s, SCC*H*), 1.81 (s, C(Ar)C*H*$_3$), 1.67 (vt, J = 13.6 Hz, PC(C*H*$_3$)$_3$). ^{13}C NMR (150 MHz, C_6D_6): δ 157.4 (vt, J_{PC} = 16.8 Hz, PC*C*O), 134.0 (vt, J_{PC} = 3.6 Hz, *C*(Ar)CH$_3$), 133.7 (s, PC(Ar)*C*H), 128.5 (s, SC*C*H), 127.4 (vt, J_{PC} = 8.1 Hz, SC*C*H), 117.9 (vt, J_{PC} = 7.6 Hz, P*C*(Ar)), 37.7 (vt, J_{PC} = 9.2 Hz, P*C*(CH$_3$)$_3$), 30.9 (vt, J_{PC} = 7.5 Hz, PC(*C*H$_3$)$_3$), 19.8 (s, C(Ar)*C*H$_3$). HRMS calcd for $C_{30}H_{46}OP_2RhS$ [M-Cl]$^+$ m/z = 619.1794; found = 619.1795.

[Rh(*t*-Bu-xantphos-κ*P,O,P'*)Cl]

The compound was synthesised similarly to [Rh(*t*-Bu-sixantphos)Cl] using *t*-Bu-xantphos (0.019 g, 0.038 mmol) and [Rh(coe)$_2$Cl]$_n$ (0.016 g, 0.038 mmol). A dark red solid was obtained in quantitative yield (0.024 g, 0.038 mmol, 98.9%).

^{31}P NMR (121 MHz, C_6D_6): δ 47.7 (d, J_{RhP} = 142.3 Hz) ^{1}H NMR (500 MHz, C_6D_6): δ 7.78 (d, J = 7.3 Hz, PC(Ar)C*H*), 7.01 (d, J = 7.6 Hz, C(bridge)CC*H*), 6.80 (t, J = 7.7 Hz, PCCC*H*), 1.68 (vt, J_{PH} = 13.4 Hz, PC(C*H*$_3$)$_3$), 1.16 (s, C(bridge)(C*H*$_3$)$_2$). ^{13}C NMR (125 MHz, C_6D_6): δ 158.9 (vt, J_{PC} = 16.3 Hz, PC*C*O), 133.6 (s, PC(Ar)*C*H),

131.3 (vt, J_{PC} = 6.23 Hz, C(bridge)*C*CH), 127.7 (s, C(bridge)C*C*H), 125.7 (vt, J_{PC} = 12.0 Hz, P*C*(Ar)), 123.8 (s, PCC*C*H), 37.6 (vt, J_{PC} = 10.1 Hz, P*C*$(CH_3)_3$), 32.5 (s, *C*(bridge)), 33.8 (s, C(bridge)(*C*$H_3)_2$), 30.8 (vt, J_{PC} = 7.7 Hz, PC(*C*$H_3)_3$). HRMS calcd for $C_{31}H_{48}OP_2Rh$ $[M\text{-}Cl]^+$ m/z = 601.2230; found = 601.2222.

(*OC*-6-43)-[Rh(*t*-Bu-sixantphos-κ*P,O,P'*)Cl$(H)_2$]

C_6D_6 (0.5 mL) was stirred vigorously under hydrogen for 10 mins, before using to dissolve [Rh(*t*-Bu-sixantphos)Cl] (0.037 g, 0.057 mmol) in a Young's tap NMR tube. Hydrogen was bubbled through the solution for 10 mins before sealing the tube under hydrogen. After 48 hours removal of the solvent *in vacuo* yielded the title compound as a brown solid in quantitative yield (0.037 g, 0.056 mmol).

^{31}P NMR (121 MHz, C_6D_6): δ 78.2 (ddd, J_{RhP} = 116.1, J_{PH} = 12.1, 2.7 Hz). ^{1}H NMR (600 MHz, C_6D_6): δ 7.71 (m, PC(Ar)C*H*), 7.23 (dd, J = 7.1, 1.7 Hz, SiCC*H*), 6.93 (t, J = 7.4 Hz, PCCC*H*), 1.75 (vt, J = 14.7 Hz, PC(C*H*$_3)_3$), 1.29 (vt, J = 13.7 Hz, PC(C*H*$_3)_3$), 0.17 (s, Si(C*H*$_3)_2$), 0.10 (s, Si(C*H*$_3)_2$), -16.92 (dtd, J_{RhH} = 22.7, J_{PH} = 13.5, J_{HH} 9.4, H$^-$ *trans* Cl$^-$), -21.12 (dtd, J_{RhH} = 30.9, J_{PH} = 12.1, J_{HH} 9.2, H$^-$ *trans* O). ^{13}C NMR (150 MHz, C_6D_6): δ 165.6 (vt, J = 11.0 Hz, PC*C*O), 137.5 (s, PC(Ar)*C*H), 136.4 (s, SiC*C*H), 126.5 (vt, J = 15.0 Hz, P*C*(Ar)), 122.6 (vt, J = 4.6 Hz, PCC*C*H), 122.0 (s, Si*C*CH), 38.4 (vt, J = 10.9 Hz, P*C*$(CH_3)_3$), 36.7 (vtt, J = 20.8, 2.8 Hz, P*C*$(CH_3)_3$), 33.5 (vt, J = 8.5 Hz, PC(*C*$H_3)_3$), 30.0 (bs, PC(*C*$H_3)_3$), -0.7 (s, Si(*C*$H_3)_2$), -0.9 (s, Si(*C*$H_3)_2$). HRMS calcd for $C_{30}H_{50}OP_2RhSi$ $[M\text{-}Cl]^+$ m/z = 619.2156; found = 619.2137.

(*OC*-6-43)-[Rh(*t*-Bu-thixantphos-κ*P,O,P'*)Cl$(H)_2$]

The reaction was performed using the same method as the synthesis of [Rh(*t*-Bu-sixantphos)Cl$(H)_2$], using *t*-Bu-thixantphos (0.034 g, 0.052 mmol). NMR analysis after 48 hours showed the title compound as the only product. The solvent was removed under reduced pressure, yielding the title compound as a brown solid in quantitative yield (0.034 g).

^{31}P NMR (121 MHz, C_6D_6): δ 77.8 (ddd, J_{RhP} = 117.8, J_{PH} = 11.9, 3.7). ^{1}H NMR (600 MHz, C_6D_6): δ 7.15 (d, J = 2.1 Hz, PC(Ar)C*H*), 6.51 (s, SCC*H*), 1.85 (s, C(Ar)C*H*$_3$), 1.75 (vt, J = 14.6 Hz, PC(C*H*$_3)_3$), 1.29 (vt, J = 13.9 Hz, PC(C*H*$_3)_3$), -17.00 (dtd, J_{RhH}

= 22.6, J_{PH} = 13.5, J_{HH} 9.4, H^- *trans* Cl^-), -21.13 (dtd, J_{RhH} = 30.5, J_{PH} = 12.4, J_{HH} 9.4, H^- *trans* O). ^{13}C NMR (150 MHz, C_6D_6): δ 155.4 (vt, J = 13.8 Hz, PC*C*O), 133.8 (vt, J = 4.6 Hz, *C*(Ar)CH_3), 133.1 (s, PC(Ar)*C*H), 129.1 (s, SC*C*H), 126.7 (vt, J = 16.2 Hz, S*C*CH), 120.2 (vt, J = 6.9 Hz, P*C*(Ar)), 38.3 (vt, J = 10.9 Hz, P*C*$(CH_3)_3$), 36.5 (vtt, J = 19.1, 2.5 Hz, P*C*$(CH_3)_3$), 33.2 (vt, J = 8.1 Hz, PC(*C*$H_3)_3$), 30.1 (bs, PC(*C*$H_3)_3$), 20.1 (s, C(Ar)*C*H_3).

(*OC*-6-43)-[Rh(*t*-Bu-xantphos-κ*P,O,P'*)Cl(H)$_2$]

This reaction was performed using the same method as the synthesis of [Rh(*t*-Bu-sixantphos)Cl(H)$_2$], using [Rh(*t*-Bu-xantphos)Cl] (0.023 g, 0.036 mmol). After 48 hours the solvent was removed in vacuo yielding the title compound as a brown solid in quantitative yield (0.023 g).

^{31}P NMR (121 MHz, C_6D_6): δ 79.0 (ddd, J_{RhP} = 117.0, J_{PH} = 11.9, 5.2). ^{1}H NMR (600 MHz, C_6D_6): δ 7.48 (m, PC(Ar)C*H*), 7.08 (d, J = 7.5 Hz, C(bridge)CC*H*), 6.88 (t, J = 7.6 Hz, PCCC*H*), 1.77 (vt, J = 14.8 Hz, PC(C*H*$_3)_3$), 1.30 (vt, J = 13.7 Hz, PC(C*H*$_3)_3$), 1.25 (s, C(bridge)(C*H*$_3)_2$), 1.22 (s, C(bridge)(C*H*$_3)_2$), -17.04 (dtd, J_{RhH} = 22.8, J_{PH} = 13.4, J_{HH} 9.4, H^- *trans* Cl^-), -20.51 (dtd, J_{RhH} = 28.8, J_{PH} = 12.2, J_{HH} 9.4, H^- *trans* O). ^{13}C NMR (150 MHz, C_6D_6): δ 156.2 (vt, J = 13.3 Hz, PC*C*O), 132.9 (s, C(bridge)C*C*H), 132.4 (vt, J = 5.2 Hz, C(bridge)*C*CH) 127.8 (vt, J = 8.1 Hz, PC(Ar)*C*H), 125.1 (vt, J = 17.9 Hz, P*C*(Ar)), 123.5 (vt, J = 4.6 Hz, PCC*C*H), 38.1 (vt, J = 11.6 Hz, P*C*$(CH_3)_3$), 36.5 (vtt, J = 19.1 Hz, P*C*$(CH_3)_3$), 34.8 (s, *C*(bridge)), 33.5 (vt, J = 7.5 Hz, PC(*C*$H_3)_3$), 32.4 (s, C(bridge)(*C*$H_3)_2$), 30.4 (s, C(bridge)(*C*$H_3)_2$), 30.0 (bs, PC(*C*$H_3)_3$).

(*TBPY*-5-33)-[Rh(*t*-Bu-sixantphos-κ^2-*P,P'*)(CO)$_2$Cl]

[Rh(*t*-Bu-sixantphos)Cl] (0.041 g, 0.063 mmol) was dissolved in C_6D_6 (0.5 mL) in a Young's tap NMR tube, under an argon atmosphere. Carbon monoxide was bubble through the solution for 10 mins, before the tube was sealed under a carbon monoxide atmosphere. After three days the reaction was complete by ^{31}P NMR spectroscopy. The orange solution was decanted and the solvent was removed under reduced pressure, yielding the title complex as an orange solid (0.027 g, 0.038 mmol, 60%).

^{31}P NMR (121 MHz, C_6D_6): δ 70.8 (d, J_{RhP} = 120.0 Hz). ^{1}H NMR (600 MHz, C_6D_6): δ 7.69 (m, PC(Ar)C*H*), 7.32 (d, J = 6.8 Hz, SiCC*H*), 7.02 (t, J = 7.2 Hz, PCCC*H*), 1.53 (vt, J = 14.0 Hz, PC(CH_3)$_3$), 0.18 (s, Si(CH_3)$_2$). ^{13}C NMR (150 MHz, C_6D_6): δ 195.5 (dt, J = 84.4, 13.0 Hz, Rh*C*O) 164.3 (vt, J = 8.1 Hz, PC*C*O), 138.1 (s, PC(Ar)*C*H), 136.5 (s, SiC*C*H), 124.9 (vt, J = 24.2 Hz, P*C*(Ar)), 123.2 (s, Si*C*CH), 122.4 (s, PCC*C*H), 38.4 (vt, J = 13.9 Hz, P*C*(CH_3)$_3$), 31.5 (bs, PC(*C*H$_3$)$_3$), -1.5 (bs, Si(*C*H$_3$)$_2$). HRMS calcd for $C_{31}H_{48}O_2P_2RhSi$ [M-COCl]$^+$ m/z = 645.1948; found = 645.1959.

(*TBPY*-5-33)-[Rh(*t*-Bu-thixantphos-κ^2-*P,P'*)(CO)$_2$Cl]

This compound was synthesised similarly to [Rh(*t*-Bu-sixantphos)(CO)$_2$Cl], using [Rh(*t*-Bu-thixantphos)Cl] (0.032 g, 0.049 mmol) generating [Rh(*t*-Bu-thixantphos)(CO)$_2$Cl] as a yellow solid, (0.025 g, 0.035 mmol, 72%).

^{31}P NMR (121 MHz, C_6D_6): δ 69.3 (d, J_{RhP} = 122.2 Hz) ^{1}H NMR (600 MHz, C_6D_6): δ 7.15 (s, Ar), 6.88 (bs, Ar), 1.88 (s, C(Ar)C*H*$_3$), 1.52 (bs, PC(C*H*$_3$)$_3$). ^{13}C NMR (150 MHz, C_6D_6): δ 154.9 (bs, PC*C*O), 134.1 (s, Ar), 132.5 (bs, Ar), 129.5 (bs, Ar), 125.6 (bs, Ar), 121.7 (bs, Ar), 38.2 (bs, C(bridge)(*C*H$_3$)$_2$), 31.5 (bs, P*C*(CH$_3$)$_3$), 20.3 (s, *C*(bridge)). HRMS calcd for $C_{31}H_{46}O_2P_2RhS$ [M-COCl]$^+$ m/z = 647.1743; found = 647.1754.

(*TBPY*-5-33)-[Rh(*t*-Bu-thixantphos-κ^2-*P,P'*)(CO)$_2$Cl]

This compound was synthesised similarly to [Rh(*t*-Bu-sixantphos)(CO)$_2$Cl], using [Rh(*t*-Bu-xantphos)Cl] (0.024 g, 0.038 mmol) generating the title compound as a yellow solid, (0.018 g, 0.026 mmol, 67%).

^{31}P NMR (121 MHz, C_6D_6): δ 71.6 (d, J_{RhP} = 120.0 Hz). ^{1}H NMR (600 MHz, C_6D_6): δ 7.46 (m, PC(Ar)C*H*), 7.15 (partially obscured by residual solvent peak, C(bridge)CC*H*), 6.94 (t, J = 7.6 Hz, PCCC*H*), 1.54 (vt, J = 13.8 Hz, PC(C*H*$_3$)$_3$), 1.24 (s, C(bridge)(C*H*$_3$)$_2$). ^{13}C NMR (150 MHz, C_6D_6): δ 194.9 (dt, J = 84.4, 12.4 Hz, Rh*C*O), 155.6 (vt, J = 10.4 Hz, PC*C*O), 133.4 (vt, J = 4.6 Hz, C(bridge)*C*CH), 133.3 (s, PC(Ar)*C*H), 127.0 (s, C(bridge)C*C*H), 123.9 (vt, J = 25.4 Hz, P*C*(Ar)), 122.7 (vt, J = 5.3 Hz, PCC*C*H), 38.1 (vt, J = 13.9 Hz, P*C*(CH$_3$)$_3$), 35.3 (s, *C*(bridge)),

31.4 (bs, PC(CH$_3$)$_3$), 29.5 (bs, C(bridge)(CH$_3$)$_2$). HRMS calcd for $C_{32}H_{48}O_2P_2Rh$ [M-COCl]$^+$ m/z = 629.2179; found = 629.2186.

[Rh(*t*-Bu-sixantphos)Cl(η^2-O$_2$)]

Air was bubbled through an NMR sample of [Rh(*t*-Bu-sixantphos)Cl] (0.050 g) in C_6D_6 for 10 mins. After 24 hours at room temperature, NMR spectroscopy showed quantitative conversion to [Rh(*t*-Bu-sixantphos)Cl(η^2-O$_2$)].

^{31}P NMR (121 MHz, C_6D_6): δ 39.4 (d, J_{RhP} = 102.2 Hz). ^{1}H NMR (600 MHz, C_6D_6): δ 7.62 (m, PC(Ar)CH), 7.18 (dd, J = 7.0, 1.6 Hz, SiCCH), 6.89 (t, J = 7.2 Hz, PCCCH), 1.87 (vt, J = 14.4 Hz, PC(CH_3)$_3$), 1.40 (bs, PC(CH_3)$_3$), 0.19 (s, Si(CH_3)$_2$), 0.01 (s, Si(CH_3)$_2$). ^{13}C NMR (150 MHz, C_6D_6): δ 166.7 (vt, J = 9.8 Hz, PCCO), 138.7 (s, PC(Ar)CH), 136.5 (s, SiCCH), 124.6 (vt, J = 20.8 Hz, PC(Ar)), 123.2 (s, SiCCH), 122.9 (vt, J = 4.7 Hz, PCCCH), 39.1 (vt, J = 10.4 Hz, PC(CH$_3$)$_3$), 38.9 (vt, J = 13.8 Hz, PC(CH$_3$)$_3$), 33.4 (vt, J = 5.8 Hz, PC(CH$_3$)$_3$), 29.5 (bs, PC(CH$_3$)$_3$), 0.8 (s, Si(CH$_3$)$_2$), -4.2 (s, Si(CH$_3$)$_2$), HRMS calcd for $C_{30}H_{48}O_3P_2RhSi$ [M-Cl]$^+$ m/z = 649.1898; found = 649.1917.

[Rh(*t*-Bu-thixantphos)Cl(η^2-O$_2$)]

This compound was synthesised as for [Rh(*t*-Bu-sixantphos)Cl(η^2-O$_2$)] using [Rh(*t*-Bu-thixantphos)Cl] (0.050 g).

^{31}P NMR (121 MHz, C_6D_6): δ 39.0 (d, J_{RhP} = 101.5 Hz). ^{1}H NMR (500 MHz, C_6D_6): δ 7.07 (d, J_{PH} = 2.2 Hz, PC(Ar)CH), 6.50 (s, SCCH), 1.83 (vt, J = 14.5 Hz, PC(CH_3)$_3$), 1.79 (s, C(Ar)CH_3), 1.44 (bs, PC(CH_3)$_3$). ^{13}C NMR (125 MHz, C_6D_6): δ 155.9 (vt, J = 12.5 Hz, PCCO), 134.6 (s, PC(Ar)CH), 134.0 (vt, J = 5.3 Hz, C(Ar)CH$_3$), 129.8 (s, SCCH), 125.2 (vt, J = 19.7 Hz, PC(Ar)), 119.9 (vt, J = 7.2 Hz, SCCH), 39.1 (vt, J = 10.6 Hz, PC(CH$_3$)$_3$), 38.9 (vt, J = 13.5 Hz, PC(CH$_3$)$_3$), 33.2 (vt, J = 5.5 Hz, PC(CH$_3$)$_3$), 28.9 (bs, PC(CH$_3$)$_3$), 19.9 (s, C(Ar)CH$_3$). HRMS calcd for $C_{30}H_{46}O_3P_2Rh$ [M-Cl]$^+$ m/z = 651.1692; found = 651.1695.

[Rh(*t*-Bu-xantphos)Cl(η^2-O_2)]

This compound was synthesised as for [Rh(*t*-Bu-sixantphos)Cl(η^2-O_2)] using [Rh(*t*-Bu-xantphos)Cl] (0.050 g).

^{31}P NMR (121 MHz, C_6D_6): δ 40.5 (d, J_{RhP} = 100.7 Hz) ^{1}H NMR (600 MHz, C_6D_6): δ 7.40 (m, PC(Ar)C*H*), 7.08 (d, J = 7.5 Hz, C(bridge)CC*H*), 6.87 (t, J = 7.7 Hz, PCCC*H*), 1.83 (vt, J = 14.4 Hz, PC(C*H*$_3$)$_3$), 1.43 (bs, PC(C*H*$_3$)$_3$), 1.32 (s, C(bridge)(C*H*$_3$)$_2$), 1.00 (s, C(bridge)(C*H*$_3$)$_2$). ^{13}C NMR (150 MHz, C_6D_6): δ 157.3 (vt, J = 11.5 Hz, PC*C*O), 133.9 (s, PC(Ar)*C*H), 133.1 (vt, J = 5.8 Hz, C(bridge)*C*CH), 127.4 (s, C(bridge)CCH), 123.9 (vt, J = 4.7 Hz, PCC*C*H), 123.3 (vt, J = 21.6 Hz, P*C*(Ar)), 38.9 (vt, J = 11.0 Hz, P*C*(CH$_3$)$_3$), 38.7 (vt, J = 14.0 Hz, P*C*(CH$_3$)$_3$), 35.5 (s, C(bridge)(*C*H$_3$)$_2$), 34.7 (s, *C*(bridge)), 33.3 (vt, J = 5.8 Hz, PC(*C*H$_3$)$_3$), 29.0 (bs, PC(*C*H$_3$)$_3$), 24.2 (s, C(bridge)(*C*H$_3$)$_2$). HRMS calcd for $C_{31}H_{48}O_3P_2Rh$ [M-Cl]$^+$ m/z = 633.2128; found = 633.2140.

Reaction of [Rh(*t*-Bu-sixantphos)Cl] with $ONMe_3$

In a glovebox, solid $ONMe_3$ (0.004 g, 0.05 mmol) was added to an NMR tube containing a CD_2Cl_2 solution of [Rh(*t*-Bu-sixantphos)Cl] (0.035 g, 0.05 mmol). The NMR tube was sealed with a J. Young tap. By ^{31}P NMR spectroscopy the mixture contained uncoordinated *t*-Bu-sixantphos (18.6%), *t*-Bu-sixantphos oxide (12.5%) and [Rh(*t*-Bu-sixantphos)Cl(η^2-O_2)] (68.9%). After four days the reaction contained uncoordinated *t*-Bu-sixantphos (6.1%), *t*-Bu-sixantphos oxide (5.3%), [Rh(*t*-Bu-sixantphos)Cl(η^2-O_2)] (36.7%), [Rh(*t*-Bu-sixantphos)Cl] (46.2%) and an unidentified species possibly [Rh(*t*-Bu-sixantphos)Cl$_2$(OH)] (5.8%).

[Rh(*t*-Bu-sixantphos)Cl$_2$(OH)]

^{31}P NMR (121 MHz, CD_2Cl_2): δ 70.5 (d, J_{RhP} = 114.1 Hz)

Reaction of [Rh(*t*-Bu-thixantphos)Cl] with $ONMe_3$

In a glovebox, solid $ONMe_3$ (0.008 g, 0.11 mmol) was added to an NMR tube containing a C_6D_6 solution of [Rh(*t*-Bu-thixantphos)Cl] (0.066 g, 0.10 mmol).

The NMR tube was sealed with a J. Young tap. Solid was evident in the NMR tube so the solvent was removed *in vacuo* and replaced with CD_2Cl_2. By ^{31}P NMR the mixture contained uncoordinated *t*-Bu-thixantphos (22.9%), [Rh(*t*-Bu-thixantphos-κ*P,O,P'*)Cl(η^2-O_2)] (8.6%), [Rh(*t*-Bu-thixantphos-κ*P,O,P'*)Cl] (64.4%) and a new compound proposed as [Rh(*t*-Bu-thixantphos-κ*P,O,P'*)Cl(O)] (7.1%).

[Rh(*t*-Bu-thixantphos-κ*P,O,P'*)Cl(O)]

^{31}P NMR (121 MHz, CD_2Cl_2): δ 40.9 (d, J_{RhP} = 90.4 Hz).

After 10 days no starting material remained and the reaction mixture contained [Rh(*t*-Bu-thixantphos-κ*P,O,P'*)Cl(η^2-O_2)] (66.7%), [(*t*-Bu-thixantphos)H]$^+$ (14.2%), *t*-Bu-thixantphos (5.3%) and a new complex proposed as [Rh(*t*-Bu-thixantphos)-Cl_2(OH)].

[Rh(*t*-Bu-thixantphos)Cl_2(OH)]

^{31}P NMR (121 MHz, CD_2Cl_2): δ 74.1 (d, J_{RhP} = 116.3 Hz).

Reaction of [Rh(*t*-Bu-xantphos)Cl] with $ONMe_3$

Solid $ONMe_3$ (0.007 g, 0.088 mmol) was added to a solution of [Rh(*t*-Bu-xantphos)Cl] (0.056 g, 0.088 mmol) in CD_2Cl_2 at -78 °C. The NMR tube was sealed with a J. Young tap, and immediately transferred to an NMR spectrometer at -80 °C. The reaction contained unreacted [Rh(*t*-Bu-xantphos)Cl] (85.7%) and [Rh(*t*-Bu-xantphos)Cl(η^2-O_2)] (14.3%). Upon warming to room temperature over 24 hours the reaction mixture contained [Rh(*t*-Bu-xantphos)Cl] (25.4%), [Rh(*t*-Bu-xantphos)Cl(η^2-O_2)] (70.5%), and a new set of peaks proposed as [Rh(*t*-Bu-xantphos)Cl(O)] (4.2%).

[Rh(*t*-Bu-xantphos)Cl(O)]

^{31}P NMR (121 MHz, CD_2Cl_2): δ 42.6 (d, J_{RhP} = 90.4 Hz).

After 14 days at room temperature the reaction mixture contained [Rh(*t*-Bu-xantphos)Cl(O)] (42.8%), [Rh(*t*-Bu-xantphos)Cl(η^2-O_2)] (49.9%) and a new complex proposed as [Rh(*t*-Bu-xantphos)Cl_2(OH)] (7.3%).

[Rh(*t*-Bu-xantphos)Cl_2(OH)]

^{31}P NMR (121 MHz, CD_2Cl_2): δ 75.1 (d, J_{RhP} = 116.3 Hz)

8.5 Platinum Complexes

1:1 Reaction of Ph-thixantphos with [Pt(nb)$_3$]

A solution of Ph-thixantphos (0.020 g, 0.035 mmol) in C_6D_6 was added to an NMR tube containing tris(norbornene)platinum (0.017 g, 0.035 mmol). Immediate ^{1}H and ^{31}P NMR spectroscopy showed [Pt(nb)(Ph-thixantphos)] (39.6%) and [Pt(Ph-thixantphos)$_2$] (60.4%). No change was observed in the ratio over 7 days.

[Pt(Ph-thixantphos)(nb)]

^{31}P NMR (121 MHz, C_6D_6): δ 20.0 (s, J_{PtP} = 3470 Hz).

[Pt(Ph-thixantphos)$_2$]

A solution of Ph-thixantphos (0.200 g, 0.35 mmol) in toluene (5 mL) was added to tris(norbornene)platinum (0.084 g, 0.18 mmol) in toluene (5 mL). The reaction was stirred for one hour before removing the solvent under reduced pressure. The yellow powder was purified by recrystallisation from a mixture of toluene and diethyl ether yielding the title compound as a yellow microcrystalline solid (0.066 g, 14%). Single X-ray quality crystals were grown by inwards diffusion of diethyl ether into a dichloromethane solution of the complex over three days.

Data at -80 °C: ^{31}P NMR (121 MHz, CD_2Cl_2): δ -2.4 (t, J = 55.0, J_{PtP} = 3976 Hz,), -6.2 (t, J = 55.0, J_{PtP} = 3864 Hz,). ^{1}H NMR (300 MHz, CD_2Cl_2): δ 5.7-7.4 (m, Ar). HRMS calcd for $C_{72}H_{52}O_2P_4S_2Pt$ $[M]^+$ m/z = 1330.2002; found = 1330.1986.

Reaction of Ph-thixantphos with $[Pt(C_2H_4)_3]$

A solution of Ph-thixantphos (0.017 g, 0.029 mmol) in C_6D_6 was added to an NMR tube containing tris(ethene)platinum (0.008 g, 0.029 mmol). The reaction became orange after 10 minutes. By ^{31}P NMR analysis $[Pt(Ph\text{-}thixantphos)_2]$ was the major product (93 %) with a small amount of $[Pt(C_2H_4)(Ph\text{-}thixantphos)]$ (7%) as a minor component.

$[Pt(C_2H_4)(Ph\text{-}thixantphos)]$

^{31}P NMR (121 MHz, C_6D_6): δ 20.9 (s, J_{PtP} = 3659 Hz). ^{1}H NMR (300 MHz, C_6D_6): δ 2.29 (s, J_{PtH} = 61.0 Hz, C=C−H).

Reaction of *t*-Bu-thixantphos with $[Pt(nb)_3]$

In a glovebox, *t*-Bu-thixantphos (0.057 g, 0.110 mmol) in C_6D_6 (0.5 mL) was added to a J. Young's tap NMR tube containing $[Pt(nb)_3]$ (0.053 g, 0.110 mmol). The NMR tube was closed under a nitrogen atmosphere and the reaction was heated to 60 °C until the reaction was deemed complete by the absence of *t*-Bu-thixantphos from the ^{31}P and ^{1}H NMR spectra (4-6 days). At this stage, ^{1}H, ^{13}C and ^{31}P NMR analysis was carried out to characterise [Pt(*t*-Bu-thixantphos)(nb)] complex (39.2%). The solution was filtered through a plug of diatomaceous earth washing through with toluene (2 x 1 mL). The solvent was removed under reduced pressure for one hour leaving [Pt(*t*-Bu-thixantphos)] as a brown expanded oil (0.073 g, 93%).

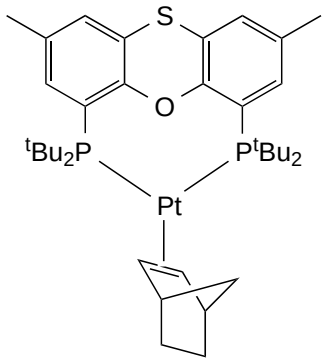

^{31}P NMR (121 MHz, C_6D_6): δ 55.6 (s, J_{PtP} = 3612 Hz) ^{1}H NMR (600 MHz, C_6D_6): δ 7.61 (s, PC(Ar)C*H*), 6.95 (s, SCC*H*), 3.12 (s, nb CH), 2.37 (bs, $^{1}J_{PtH}$ = 67.8 Hz, nb =C*H*), 1.96 (s, C(Ar)C*H*$_3$), 1.93 (obscured, assigned by COSY correlation, 2H, nb C*H*$_2$), 1.42-1.56 (m, PC(C*H*$_3$)$_3$), 1.32 (obscured, assigned by COSY correlation, 3H, nb C*H*$_2$, bridge CH$_2$), 0.62 (d, 15.3 Hz, 1H, nb bridge CH$_2$). ^{13}C NMR (150 MHz, C_6D_6): δ 158.9 (vt, J_{PC} = 9.8 Hz, PC*C*O), 135.4 (s, $^{2}J_{PtC}$ = 26.6 Hz, PC(Ar)*C*H), 130.9 (bs, *C*(Ar)CH$_3$), 130.7 (bs, SC*C*H), 127.6 (vt, J_{PC} = 5.8 Hz, SC*C*H), 125.9 (bs, P*C*(Ar)), 51.9 (bs, $^{1}J_{PtC}$ = 343.9 Hz, nb =*C*H), 44.9 (s, nb *C*H), 38.5 (m, P*C*(CH$_3$)$_3$), 38.0-38.5 (obscured, assigned by HSQC correlation, nb bridge *C*H$_2$), 31.7 (bs, PC(*C*H$_3$)$_3$), 31.4 (bs, $^{3}J_{PtC}$ = 61.4 Hz, nb *C*H$_2$), 20.7 (s, C(Ar)*C*H$_3$).

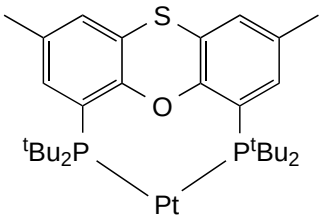

^{31}P NMR (121 MHz, C_6D_6): δ 78.6 (s, J_{PtP} = 4809.5 Hz) ^{1}H NMR (600 MHz, C_6D_6): δ 7.32 (d, J_{PH} = 1.8 Hz, PC(Ar)C*H*), 6.87 (s, SCC*H*), 1.95 (s, C(Ar)C*H*$_3$), 1.52 (vt, J_{PH} = 13.8 Hz, PC(C*H*$_3$)$_3$). ^{13}C NMR (150 MHz, C_6D_6): δ 155.9 (vt, J_{PC} = 10.4 Hz, PC*C*O), 133.3 (s, PC(Ar)*C*H), 132.1 (vt, J_{PC} = 5.2 Hz, *C*(Ar)CH$_3$), 128.8 (s, SC*C*H), 126.6 (vt, J_{PC} = 28.9 Hz, P*C*(Ar)), 126.1 (vt, J_{PC} = 5.8 Hz, SC*C*H), 37.8 (vt, J_{PC} = 15 Hz, P*C*(CH$_3$)$_3$), 31.7 (vt, J_{PC} = 10.4 Hz, PC(*C*H$_3$)$_3$), 20.5 (s, C(Ar)*C*H$_3$). HRMS calcd for $C_{30}H_{47}OP_2PtS$ $[M^+H]^+$ m/z = 711.2438; found = 711.2450.

Reaction of *t*-Bu-sixantphos with [Pt(nb)$_3$]

A solution of *t*-Bu-sixantphos (0.19 g, 0.37 mmol) in C_6D_6 (0.5 mL) was added to [Pt(nb)$_3$] (0.018 g, 0.37 mmol) in a J. Young's tap NMR tube. After 24 hours at 60 °C the ^{31}P NMR spectrum showed a mixture of unreacted *t*-Bu-sixantphos (75.0%), [Pt(*t*-Bu-sixantphos)] (15.8%), and [Pt(*t*-Bu-sixantphos)(nb)] (9.2%). After five days at 60 °C the reaction mixture contained unreacted *t*-Bu-sixantphos (11.1%), [Pt(*t*-Bu-sixantphos)] (32.5%), [Pt(*t*-Bu-sixantphos)(nb)] (24.1%) and an unidentified Pt(II) species (18.2%).

[Pt(*t*-Bu-sixantphos)]

^{31}P NMR (121 MHz, C_6D_6): δ 79.5 (s, J_{PtP} = 4826.6 Hz)

[Pt(*t*-Bu-sixantphos)(nb)]

^{31}P NMR (121 MHz, C_6D_6): δ 59.3 (s, J_{PtP} = 3571.8 Hz)

Pt(II) *t*-Bu-sixantphos species

^{31}P NMR (121 MHz, C_6D_6): δ 34.7 (s, J_{PtP} = 2676.9 Hz)

[Pt(*t*-Bu-xantphos)H]X

A solution of *t*-Bu-xantphos (0.016 g, 0.032 mmol) in C_6D_6 (0.5 mL) was added to tris-(norbornene)-platinum (0.015 g, 0.032 mmol) in an Young's tap NMR tube. The tube was closed under argon and heated to 60 °C overnight. After 24 hours no free ligand remained and the major product is proposed as [Pt(*t*-Bu-xantphos-κ*P,O,P'*)H]X. After 7 days at room temperature small yellow crystals had formed. The solution was decanted and the product was isolated (0.020 g).

^{31}P NMR (121 MHz, C_6D_6): δ 46.7 (s, J_{PtP} = 3246 Hz) ^{1}H NMR (600 MHz, C_6D_6): δ 7.43 (m, PC(Ar)C*H*), 7.11 (d, J = 7.5 Hz, C(bridge)CC*H*), 6.84 (t, J = 7.6 Hz, PCCC*H*), 1.7 (bs, C(bridge)(CH_3)$_2$), 1.5 (bs, PC(CH_3)$_3$), -18.49 (t, 13.1 Hz, $^1J_{PtH}$ = 1107 Hz, Pt−H). ^{13}C NMR (150 MHz, C_6D_6): δ 158.6 (vt, J = 8.0 Hz, PC*C*O), 138.4 (vt, J = 4.1 Hz, C(bridge)*C*CH), 132.1 (s, PC(Ar)*C*H), 124.8 (vtd, J = 39.3, 2.9 Hz, P*C*(Ar)), 125.8 (s, C(bridge)C*C*H), 121.8 (vt, J = 5.7 Hz, PCC*C*H), 38.0 (vt, J = 17.5 Hz, P*C*(CH$_3$)$_3$), 36.7 (s, *C*(bridge)), 30.7 (bs, PC(*C*H$_3$)$_3$). HRMS calcd for $C_{31}H_{49}OP_2Pt$ $[M-X]^+$ m/z = 689.2858; found = 689.2864.

Reaction of *t*-Bu-thixantphos with [Pt(cod)$_2$]

A solution of *t*-Bu-thixantphos (0.026 g, 0.050 mmol) in C_6D_6 (0.3 mL) was added to a solution of bis-(1,5-cyclooctadiene)platinum (0.020 g, 0.050 mmol) in C_6D_6 (0.3 mL). The NMR tube was closed with a septum and the reaction was followed

by ^{1}H and ^{31}P NMR spectroscopy. After 48 hrs at room temperature the reaction had become black and contained 72 % unreacted *t*-Bu-thixantphos with the remainder being [Pt(*t*-Bu-thixantphos)]. The reaction was heated to 40 °C for 24 hours, then 60 °C for 24 hours, but no further reaction was observed.

Reaction of *t*-Bu-sixantphos with [Pt(C_2H_4)$_3$]

C_6D_6 (0.5 mL) which had been previously dried and degassed then stored under Ar, was sparged by bubbling ethene through the liquid for 10 mins, then stirring vigorously under an ethene atmosphere for a further 10 mins. [Pt(cod)$_2$] (0.026 g, 0.063 mmol) was placed under ethene and 0.03 mL of the C_6D_6 was added. The solution was stirred vigorously for 30 mins to ensure complete conversion to [Pt(C_2H_4)$_3$]. *t*-Bu-Sixantphos(0.032 g, 0.063 mmol) was placed in a Young's tap NMR tube under an ethene atmosphere and dissolved in the remaining C_6D_6. The [Pt(C_2H_4)$_3$] solution was added to the NMR tube, which was closed under ethene and shaken to ensure mixing of the solutions. After four hours at room temperature [Pt(*t*-Bu-sixantphos)(C_2H_4)] (11.1%) had been produced. The reaction did not proceed further.

^{31}P NMR (121 MHz, C_6D_6): δ 53.7 (s, J_{PtP} = 3499 Hz).

[Pt(*t*-Bu-thixantphos)(C_2H_4)]

C_6D_6 (0.5 mL) which had been previously dried and degassed then stored under Ar, was sparged by bubbling ethene through the liquid for 10 mins, then stirring vigorously under an ethene atmosphere for a further 10 mins. Bis-(1,5-cyclooctadiene)platinum (0.032 g, 0.078 mmol) was placed under ethene and 0.03 mL of the C_6D_6 was added. The solution was stirred vigorously for 30 mins to ensure complete conversion to [Pt(C_2H_4)$_3$]. *t*-Bu-Thixantphos(0.040 g, 0.077 mmol) was placed in a Young's tap NMR tube under an ethene atmosphere and dissolved in the remaining C_6D_6. The [Pt(C_2H_4)$_3$] solution was added to the NMR tube, which was closed under ethene and shaken to ensure mixing of the solutions. After 48 hours at room temperature the only product was [Pt(*t*-Bu-thixantphos)(C_2H_4)] (100 % by NMR).

^{31}P NMR (121 MHz, C_6D_6): δ 55.7 (s, J_{PtP} = 3899 Hz) ^{1}H NMR (600 MHz, C_6D_6): δ 7.63 (s, PC(Ar)C*H*), 6.96 (s, SCC*H*), 2.50 (bs, $^{2}J_{PtH}$ = 59.5 Hz, C=CH_2), 1.97 (s, C(Ar)CH_3), 1.38-1.40 (m, PC(CH_3)$_3$). ^{13}C NMR (150 MHz, C_6D_6): δ 158.7 (bs, PC*C*O), 135.3 (s, $^{4}J_{PtC}$ = 29.5 Hz, PC(Ar)*C*H), 131.0 (bs, *C*(Ar)CH$_3$), 130.5 (bs, SC*C*H), 128.5 (vt, J_{PC} = 5.8 Hz, S*C*CH), 125.7 (bs, P*C*(Ar)), 38.7 (m, P*C*(CH$_3$)$_3$), 34.2 (bs, $^{1}J_{PtC}$ = 223.2 Hz, C=C) 31.6 (bs, PC(*C*H$_3$)$_3$), 20.7 (s, C(Ar)*C*H$_3$).

Reaction of *t*-Bu-xantphos with [Pt(C_2H_4)$_3$]

C_6D_6 (0.5 mL) which had been previously dried and degassed then stored under Ar, was sparged by bubbling ethene through the liquid for 10 mins, then stirring vigorously under an ethene atmosphere for a further 10 mins. [Pt(cod)$_2$] (0.015 g, 0.036 mmol) was placed under ethene and 0.03 mL of the C_6D_6 was added. The solution was stirred vigorously for 30 mins to ensure complete conversion to [Pt(C_2H_4)$_3$]. *t*-Bu-Xantphos(0.018 g, 0.036 mmol) was placed in a Young's tap NMR tube under an ethene atmosphere and dissolved in the remaining C_6D_6. The [Pt(C_2H_4)$_3$] solution was added to the NMR tube, which was closed under ethene and shaken to ensure mixing of the solutions. Both [Pt(*t*-Bu-xantphos)(C_2H_4)] (41.7%) and [Pt(*t*-Bu-xantphos)H]X (8.6%)) were evident after four hours at room temperature. After five days [Pt(*t*-Bu-xantphos)H]X was the only phosphorus containing compound in solution.

[Pt(*t*-Bu-xantphos)(C_2H_4)]

^{31}P NMR (121 MHz, C_6D_6): δ 53.4 (s, J_{PtP} = 3878 Hz) ^{1}H NMR (600 MHz, C_6D_6): δ 7.79 (d, J = 6.8 Hz, PC(Ar)C*H*), 7.09 (dd, J = 7.6, 1.1 Hz, C(bridge)CC*H*), 6.87 (t, J = 7.7 Hz, PCCC*H*), 2.52 (bs, $^{2}J_{PtH}$ = 58.0 Hz, C=CH_2), 1.43 (s, C(bridge)(CH_3)$_2$), 1.42 (d, J = 13.0 Hz, PC(CH_3)$_3$). ^{13}C NMR (150 MHz, C_6D_6): δ 161.0 (m, PC*C*O), 138.4 (s, C(bridge)*C*CH), 133.6 (s, $^{4}J_{PtC}$ = 28.1 Hz, PC(Ar)*C*H), 124.6 (s, C(bridge)C*C*H), 124.1 (m, P*C*(Ar)), 121.2 (s, PCC*C*H), 38.4 (vt, J = 18.5, $^{2}J_{PtC}$= 34.1 Hz, P*C*(CH$_3$)$_3$), 37.4 (s, *C*(bridge)), 31.6 (vt, J = 8.1, $^{3}J_{PtC}$= 17.3 Hz, PC(*C*H$_3$)$_3$) 25.6 (s, C(bridge)(*C*H$_3$)$_2$).

[Pt(*t*-Bu-thixantphos)(η^2-O_2)]

A solution of *t*-Bu-thixantphos (0.117 g, 0.23 mmol) in toluene (1 mL) was added to a Schlenk tube containing tris-(norbornene)platinum (0.108 g, 0.023 mmol) in toluene (3 mL). The reaction was stirred at 40 °C for 3 days. The solvent was reduced in vacuo and the reaction mixture was placed under air. The title compound was isolated by cooling the reaction mixture for two weeks at -20 °C forming [Pt(*t*-Bu-thixantphos)(η^2-O_2)] as a pale peach solid (0.109 g, 65%). X-ray quality crystals were grown by slow diffusion of air into a C_6D_6 solution of [Pt(*t*-Bu-thixantphos)].

^{31}P NMR (121 MHz, CD_2Cl_2): δ 38.4 (s, J_{PtP} = 4488 Hz) ^{1}H NMR (600 MHz, CD_2Cl_2): δ 7.59 (dd, J = 5.9, 1.0 Hz, a), 7.32 (s, c), 2.34 (s, g), 1.43 (d, J_{PH} = 14.4 Hz, C(Ar)CH_3). ^{13}C NMR (125 MHz, CD_2Cl_2): δ 156.6 (bs, *C*O), 133.8 (s, $^2J_{PtC}$ = 37.9 Hz, PC(Ar)*C*H), 133.1 (d, J_{PC} = 5.3 Hz, *C*(Ar)CH_3), 131.7 (bs, SC*C*C(CH_3)), 128.5 (s, *C*S), 119.3 (d, J_{PC} = 27.8 Hz, P*C*(Ar)), 39.3 (d, J_{PC} = 23.5 Hz, P*C*CH_3), 31.2 (d, J_{PC} = 5.3 Hz, PC*C*H_3), 21.2 (s, C(Ar)*C*H_3). HRMS calcd for $C_{30}H_{47}O_3P_2PtS$ $[M+H]^+$ m/z = 743.2326; found = 743.2291.

Reaction of [Pt(*t*-Bu-thixantphos)(C_2H_4)] with Air

Air was bubbled through a solution of [Pt(*t*-Bu-thixantphos)(C_2H_4)] (0.020 g, 0.027 mmol) in C_6D_6 (0.4 mL) for a total of 10 mins. The sample was sealed under air with a septum and analysed by NMR spectroscopy immediately. [Pt(*t*-Bu-thixantphos)(η^2-O_2)] was produced in quantitative yield by NMR spectroscopy.

Reaction of [Pt(*t*-Bu-thixantphos)(C_2H_4)] with argon

Argon was bubbled through a solution of [Pt(*t*-Bu-thixantphos)(C_2H_4)] (0.020 g, 0.027 mmol) in C_6D_6 (0.4 mL) for 10 mins. The sample was sealed under argon and NMR analysis showed slight conversion to [Pt(*t*-Bu-thixantphos)].

Reaction of [Pt(*t*-Bu-thixantphos)(η^2-O_2)] with CO

Carbon monoxide was bubbled through a solution of [Pt(*t*-Bu-thixantphos)(η^2-O_2)] (0.032 g, 0.043 mmol) in CD_2Cl_2 (0.4 mL) for 10 mins. The reaction was followed by NMR spectroscopy and no further changes were observed after 7 days. The solution was passed through an alumina plug (washing with 3 x 1 mL CH_2Cl_2) and the solvent removed *in vacuo* to give the metallated complex shown below as a brown solid (0.010 g, 32%).

Reaction with ^{13}CO: [Pt(*t*-Bu-thixantphos)(η^2-O_2)] (0.030 g, 0.040 mmol) was dissolved in CD_2Cl_2 and transferred to an NMR tube and sealed with a septum. The sample was frozen in liquid nitrogen and attached by cannula to a solid potassium hydroxide trap, which in turn was attached to a sample vial containing ^{13}C-sodium formate. The system was placed under vacuum, using syringes attached to both the NMR tube and the sample vial. The system was closed under vacuum and the NMR tube was transferred to a dry ice/acetone bath and allowed to melt. The vacuum syringe on the NMR tube was replaced with a gas-tight syringe to collect any excess carbon monoxide that may be produced. Conc. sulfuric acid (1 mL) was added dropwise into the sample vial containing sodium formate producing rapid bubbling. The set-up was left until the bubbling had mostly abated (approx. 10 mins). All syringes and the cannula were removed from the sample vial and the septum was secured with Parafilm. No unexpected differences were observed in the NMR spectra.

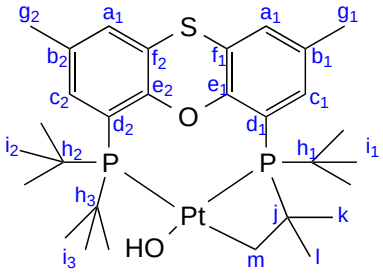

^{31}P NMR (121 MHz, CD_2Cl_2): δ 38.2 (s, J_{PtP} = 1794 Hz, P-^{t}Bu$_2$), −49.6 (s, J_{PtP} = 3943 Hz, PCCPt). ^{1}H NMR (600 MHz, CD_2Cl_2): δ 7.60 (d, J_{PH} = 3.8 Hz, c_2), 7.25 (s, a_1), 7.16 (s, a_2), 6.95 (d, J_{PH} = 6.5 Hz, c_1), 2.34 (s, g_1), 2.32 (s, g_2), 1.71 (d, J_{PH} = 12.9 Hz, i_3), 1.41 (d, J = 15.9 Hz, k), 1.36 (d, J = 14.9 Hz, l), 1.34 (d, J_{PH} = 13.2 Hz, i_2), 1.2-1.5, obscured (m, m), 1.03 (d, J_{PH} = 15.0 Hz, i_1). ^{13}C NMR (150 MHz, CD_2Cl_2): δ, 157.1 (d, J_{PC} = 9.0 Hz, e_2), 153.9 (d, J_{PC} = 4.3 Hz, e_1), 134.2 (d, J_{PC} = 3.2 Hz, c_2), 133.8 (d,

J_{PC} = 6.3 Hz, b_1), 133.4 (d, J_{PC} = 3.2 Hz, b_2), 132.8 (s, c_1), 130.5 (d, J_{PC} = 1.6 Hz, a_1), 129.6 (d, J_{PC} = 1.6 Hz, a_2), 128.5 (dd, J_{PC} = 4.2, 1.6 Hz, f_1), 124.0 (d, J_{PC} = 4.3 Hz, f_2), 121.3 (d, J_{PC} = 13.8 Hz, d_2), 116.6 (dd, J_{PC} = 30.7, 1.6 Hz, d_1), 46.7 (d, J_{PC} = 37.6 Hz, j) 40.8 (d, J_{PC} = 10.1 Hz, h_2), 36.8 (d, J_{PC} = 8.0 Hz, h_3), 36.0 (d, J_{PC} = 22.3 Hz, h_1), 33.2 (d, J_{PC} = 5.8 Hz, i_3), 32.6 (s, l), 32.1 (dd, J_{PC} = 10.1, 3.7 Hz, k), 31.3 (d, J_{PC} = 5.3 Hz, i_2), 28.8 (bs, i_1), 21.3 (s, g_2), 21.0 (s, g_1), 15.7 (dd, J = 81.6, 35.5 Hz, m).

Attempted reaction of [Pt(*t*-Bu-thixantphos)(η^2-O_2)] with CO_2

Carbon dioxide was bubbled through a solution of [Pt(*t*-Bu-thixantphos)(η^2-O_2)] (0.030 g, 0.040 mmol) in CD_2Cl_2 (0.4 mL) for 10 mins. The NMR tube was sealed under carbon dioxide with a septum and the reaction was followed by ^{1}H, ^{13}C and ^{31}P NMR. No reaction was observed after four days at room temperature.

Attempted reaction of [Pt(*t*-Bu-thixantphos)(η^2-O_2)] with CH_4

Methane was bubbled through a solution of [Pt(*t*-Bu-thixantphos)(η^2-O_2)] (0.015 g, 0.020 mmol) in C_6D_6 (0.5 mL) for 10 mins. The NMR tube was sealed under methane with a septum and the reaction was followed by ^{1}H, ^{13}C and ^{31}P NMR. No reaction was observed after 14 days at room temperature.

Attempted reaction of [Pt(*t*-Bu-thixantphos)(η^2-O_2)] with C_2H_2

Ethyne was bubbled through a solution of [Pt(*t*-Bu-thixantphos)(η^2-O_2)] (0.037 g, 0.050 mmol) in C_6D_6 (0.5 mL) for 10 mins. The NMR tube was sealed under ethyne with a septum and the reaction was followed by ^{1}H and ^{31}P NMR spectroscopy. No reaction was observed after 48 hours.

Attempted reaction of [Pt(*t*-Bu-thixantphos)(η^2-O_2)] with C_2H_4

Ethene was bubbled through a solution of [Pt(*t*-Bu-thixantphos)(η^2-O_2)] (0.037 g, 0.050 mmol) in C_6D_6 (0.5 mL) for 10 mins. The NMR tube was sealed under

ethene with a septum and the reaction was followed by ^{1}H and ^{31}P NMR spectroscopy. No reaction was observed after 48 hours.

Attempted reaction of [Pt(*t*-Bu-thixantphos)(η^2-O_2)] with NH_4PF_6

A solution of NH_4PF_6 (0.007 g, 0.043 mmol) in THF (2 mL) was added to a suspension of [Pt(*t*-Bu-thixantphos)(η^2-O_2)] (0.029 g, 0.039 mmol) in THF (3 mL). The reaction was stirred at room temperature for 24 hours. The solvent was removed under reduced pressure and the brown solid was taken up in d_6-acetone for NMR. No reaction was observed so the sample was heated to 40 °C for four days. No evidence of reaction was present.

Attempted reaction of [Pt(*t*-Bu-thixantphos)(η^2-O_2)] with H_2

Hydrogen gas was bubbled through a solution of [Pt(*t*-Bu-thixantphos)(η^2-O_2)] (0.032 g, 0.043 mmol) in C_6D_6 (0.5 mL) for 10 mins. The NMR tube was sealed under hydrogen with a septum and the reaction was followed by ^{1}H and ^{31}P NMR spectroscopy. No reaction was observed after three days.

1:1 reaction of [Pt(*t*-Bu-thixantphos)(η^2-O_2)] with pta

1,3,5-triaza-7-phosphaadamantane (0.003 g, 0.020 mmol) was added to a solution of [Pt(*t*-Bu-thixantphos)(η^2-O_2)] (0.015 g, 0.020 mmol) in $CDCl_3$. The ^{31}P NMR spectrum showed peaks indicative of 75% starting material and uncoordinated *t*-Bu-thixantphos (25 % of the *t*-Bu-thixantphos signals). There was also a complex at -74.1 ppm (J_{PtP}= 3562 Hz) consistent with literature precedence for [Pt(pta)$_4$].[319]

1:4 reaction of [Pt(*t*-Bu-thixantphos)(η^2-O_2)] with pta

1,3,5-triaza-7-phosphaadamantane (0.019 g, 0.120 mmol) was added to a solution of [Pt(*t*-Bu-thixantphos)(η^2-O_2)] (0.022 g, 0.030 mmol) in $CDCl_3$. The ^{31}P NMR spectrum showed the presence of uncoordinated *t*-Bu-thixantphos and [Pt(pta)$_4$].[319]

Reaction of *t*-Bu-thixantphos with $[Pt(C_6H_{10})Cl_2]$ in C_6D_6

$[Pt(C_6H_{10})Cl_2]$ (0.007 g, 0.020 mmol) was weighed into an NMR tube and placed under argon. A solution of *t*-Bu-thixantphos (0.010 g, 0.019 mmol) in C_6D_6 (0.4 mL) was added to the NMR tube and the top was closed with a septum and parafilm. The reaction mixture was gently shaken to promote dissolution of the sparingly soluble $[Pt(C_6H_{10})Cl_2]$. The reaction was kept at room temperature for four hours, after which time no change was observed by NMR spectroscopy. The reaction was then heated for 72 hours at 40 °C, with intermediary monitoring by NMR spectroscopy, during which time the colourless solution became dark red. After 72 hours the reaction showed 75 % conversion (by ^{31}P NMR spectroscopy) to *trans*-[Pt(*t*-Bu-xantphos)Cl_2].

Attempted reaction of *t*-Bu-thixantphos with $[Pt(C_6H_{10})Cl_2]$ in CH_2Cl_2

$[Pt(C_6H_{10})Cl_2]$ (0.136 g, 0.39 mmol) was added to a Schlenk tube containing a solution of *t*-Bu-thixantphos (0.202 g, 0.39 mmol) in CH_2Cl_2 (10 mL). The reaction was stirred overnight generating a yellow solution. The solvent was removed under reduced pressure leaving a yellow solid. NMR analysis of this solid in C_6D_6 showed a mixture of unreacted *t*-Bu-thixantphos (43.5%), *t*-Bu-thixantphosH+ (32.5%) and *trans*-[Pt(*t*-Bu-thixantphos)Cl_2] (24.0%, yields based on ^{31}P NMR spectroscopy).

Attempted reaction of *t*-Bu-thixantphos with $[PtCl_2(SEt_2)_2]$

t-Bu-Thixantphos (0.012 g, 0.023 mmol) in C_6D_6 (0.4 mL) was added to an NMR tube containing $[PtCl_2(SEt_2)_2]$ (0.012 g, 0.025 mmol). The top was sealed with a septum and wrapped with parafilm. The reaction was kept at room temperature for 24 hours then analysed by ^1H and ^{31}P NMR spectroscopy. No change was observed in either spectrum. The reaction was heated to 40 °C for 7 days then analysed again displaying unreacted *t*-Bu-thixantphos (99.6%) and *trans*-[$PtCl_2$(*t*-Bu-thixantphos)] (0.4% based on ^{31}P NMR spectroscopy). The reaction was heated to 60 °C for a further 4 days at which time the reaction had progressed to 3.1 %

trans-[$PtCl_2$(*t*-Bu-thixantphos)]. Heating at 60 °C was continued to give a total of 28 days at this temperature. NMR spectroscopy showed 6.7% *trans*-[$PtCl_2$(*t*-Bu-thixantphos)] with unreacted *t*-Bu-thixantphos accounting for the remaining 92.4%.

Attempted reaction of *t*-Bu-thixantphos with *cis*-[$PtCl_2(NCMe)_2$]

t-Bu-Thixantphos (0.014 g, 0.027 mmol) was dissolved in CD_2Cl_2 (0.2 mL) and added to a solution of *cis*-[$PtCl_2(NCMe)_2$] (0.009, 0.026 mmol) in CD_2Cl_2 (0.2 mL) in an NMR tube. The tube was sealed with a septum wrapped in parafilm. The reaction was followed by ^1H and ^{31}P NMR spectroscopy. After 72 hours the reaction mixture contained unreacted *t*-Bu-thixantphos (83.8 %) and *t*-Bu-thixantphos H^+ (16.2%) by ^{31}P NMR spectroscopy.

Attempted reaction of *t*-Bu-thixantphos with *trans*-[$PtCl_2(NCMe)_2$]

t-Bu-Thixantphos (0.012, 0.023 mmol) was dissolved in $CDCl_3$ (0.2 mL) and added to an NMR tube containing a solution of *trans*-[$PtCl_2(NCMe)_2$] (0.010 g, 0.029 mmol) in $CDCl_3$ (0.2 mL). The tube was sealed with a septum and the reaction was followed by ^1H and ^{31}P NMR spectroscopy. After 24 hours at room temperature no changes were observed in the NMR spectrum. The reaction was heated to 50 °C for 7 days. At this stage the reaction showed unreacted *t*-Bu-thixantphos (66.7%) and *t*-Bu-thixantphosH^+ (33.3%) based on the ^{31}P NMR spectrum. After a total of 21 days heating at 50 °C the reaction contained unreacted *t*-Bu-thixantphos (43.0%), *t*-Bu-thixantphosH^+ (31.7%) and *trans*-[$PtCl_2$(*t*-Bu-thixantphos)] (25.3%).

Attempted reaction of *t*-Bu-thixantphos with *trans*-[$PtCl_2(NCt\text{-}Bu)_2$]

t-Bu-Thixantphos (0.024 g, 0.046 mmol) was dissolved in $CDCl_3$ (0.4 mL) and added to an NMR tube containing a solution of *trans*-[$PtCl_2(NCt\text{-}Bu)_2$] (0.020 g, 0.046 mmol) in $CDCl_3$ (0.4 mL). The reaction was sealed with a septum and followed by ^1H and ^{31}P NMR spectroscopy. After 24 hours at room temperature

the reaction showed unreacted *t*-Bu-thixantphos (91.1%) and *t*-Bu-thixantphosH$^+$ (8.9%). The reaction was heated to 50 °C for 24 hours upon which the amount of *t*-Bu-thixantphosH$^+$ had increased to 24.4%. After 7 days at 50 °C the reaction contained unreacted *t*-Bu-thixantphos (49.3%), *t*-Bu-thixantphosH$^+$ (32.5%) and *trans*-[$PtCl_2$(*t*-Bu-thixantphos)] (18.2%). After 21 days at 50 °C only 7.4% unreacted *t*-Bu-thixantphos remained, with 50.7% *t*-Bu-thixantphosH$^+$ and 41.9% *trans*-[$PtCl_2$(*t*-Bu-thixantphos)].

trans-[Pt(*t*-Bu-thixantphos)Cl_2]

t-Bu-Thixantphos (0.198 g, 0.38 mmol) and [Pt(C_6H_{10})Cl_2] (0.133 g, 0.38 mmol) were dissolved in toluene (10 mL) and heated to 50 °C for three days, resulting in an orange solution. The solvent was removed *in vacuo* and the resulting solid was dissolved in a minimum of dichloromethane. Diethyl ether was added until a small amount of oily residue became evident. The sample was cooled to -14 °C, resulting the title compound as red crystals (0.199 g, 66%).

^{31}P NMR (121 MHz, C_6D_6): δ 32.9 (s, J_{PtP} = 2700 Hz) ^{1}H NMR (500 MHz, C_6D_6): δ 7.11 (s, PC(Ar)C*H*), 6.98 (s, SCC*H*), 1.86 (s, C(Ar)CH_3), 1.71 (vt, J_{PH} = 7.3 Hz, PCCH_3), 1.56 (bs, PCCH_3), ^{13}C NMR (125 MHz, C_6D_6): δ 155.8 (vt, J_{PC} = 6.3 Hz, *C*O), 134.3 (s, PC(Ar)*C*H), 131.0 (vt, J_{PC} = 3.4 Hz, *C*(Ar)CH_3), 129.9 (s, SC*C*C(CH_3)), 124.0 (vt, J = 18.5 Hz, P*C*(Ar)), 124.5 (vt, J = 6.7 Hz, *C*S), 20.3 (s, C(Ar)*C*H_3), 39.7 (vt, J_{PC} = 11.6 Hz, PC*C*H_3), 38.8 (vt, J_{PC} = 11.1 Hz, PC*C*H_3), 32.8 (vt, J_{PC} = 3.9 Hz, P*C*CH_3), 30.2 (bs, P*C*CH_3), HRMS calcd for $C_{30}H_{46}OP_2SClPt$ [M-Cl]$^+$ m/z = 745.2060; found = 745.2052.

trans-[Pt(*t*-Bu-sixantphos)Cl_2]

A solution of *t*-Bu-sixantphos (0.051 g, 0.10 mmol) in toluene (5 mL) was added to a suspension of [Pt(C_6H_{10})Cl_2] (0.035 g, 0.10 mmol) in toluene (5 mL). The reaction mixture was stirred at 50 °C for 72 hours. The solvent was removed under reduced pressure and the solid was taken up in C_6D_6 for NMR analysis. The reaction showed a mixture of unreacted *t*-Bu-sixantphos (53.4%), *t*-Bu-sixantphosH$^+$ (22.8%) and *trans*-[Pt(*t*-Bu-sixantphos)Cl_2] (23.8%). The NMR sample was heated at 50 °C for a further 11 days. At this stage no [Pt(C_6H_{10})Cl_2] was observed in the

^{1}H NMR spectrum and no change in the ratio of the compounds in the ^{31}P NMR spectrum was observed over a period of 24 hours. The final ratio of the compounds was 63.8% *t*-Bu-sixantphosH^{+}, and 36.2% *trans*-[Pt(*t*-Bu-sixantphos)Cl_2]. Attempts to isolate *trans*-[Pt(*t*-Bu-sixantphos)Cl_2] were unsuccessful. Due to the complex nature of the ^{1}H and ^{13}C NMR spectra for this system the product *trans*-[Pt(*t*-Bu-sixantphos)Cl_2] is proposed based on the similarities of the ^{31}P NMR spectrum with those for *trans*-[Pt(*t*-Bu-thixantphos)Cl_2] and *trans*-[Pt(*t*-Bu-xantphos)Cl_2] which were formed *via* the same reaction conditions.

^{31}P NMR (121 MHz, C_6D_6): δ 34.7 (s, J_{PtP} = 2686 Hz). HRMS calcd for $C_{30}H_{48}ClOP_2PtSi$ [M-Cl]$^{+}$ m/z = 739.2237; found = 739.2178.

Reaction of *t*-Bu-xantphos with [Pt(C_6H_{10})Cl_2]

A solution of *t*-Bu-xantphos (0.063 g, 0.126 mmol) in toluene (5 mL) was added to a suspension of [Pt(C_6H_{10})Cl_2] (0.044 g, 0.126) in toluene (5 mL). The reaction mixture was stirred at 50 °C for 72 hours. The solvent was removed *in vacuo* leaving an orange solid. The solid was recrystallised by inwards diffusion of diethyl ether into a dichloromethane solution of the complex, yielding the title complex as a yellow solid (0.027 g, 28%). The complex was analysed by NMR spectroscopy in C_6D_6, $CDCl_3$, CD_2Cl_2 and d_6−acetone. In C_6D_6 the complex is formulated as *trans*-[Pt(*t*-Bu-xantphos)Cl_2] while in $CDCl_3$ and CD_2Cl_2 the complex is thought to lose a chloride ligand resulting in [Pt(*t*-Bu-xantphos-κ*P,O,P'*)Cl]Cl. In d_6−acetone the ^{31}P NMR spectrum appears as a broad singlet at 46 ppm. The full NMR characterisation in the other solvents is given below.

trans-[Pt(*t*-Bu-xantphos)Cl_2]

^{31}P NMR (121 MHz, C_6D_6): δ 32.4 (s, J_{PtP} = 2721.4 Hz). ^{1}H NMR (500 MHz, C_6D_6): δ 7.36 (m, PC(Ar)C*H*), 7.14 (d, *J* = 7.8 Hz, C(bridge)CC*H*), 6.89 (t, *J* = 7.0 Hz, PCCC*H*), 1.67 (bs, PC(C*H*$_3$)$_3$), 1.37 (s, C(bridge)(C*H*$_3$)$_2$), 1.40 (s, C(bridge)(C*H*$_3$)$_2$). ^{13}C NMR (125 MHz, C_6D_6): δ 157.1 (vt, *J* = 6.3 Hz, PC*C*O), 136.0 (vt, *J* = 4.8 Hz, C(bridge)*C*CH), 132.9 (s, PC(Ar)*C*H), 126.0 (s, C(bridge)C*C*H), 122.5 (vt, *J* = 38.9 Hz, P*C*(Ar)), 122.1 (vt, *J* = 6.3 Hz, PCC*C*H), 39.2 (bs, P*C*(CH_3)$_3$), 36.5 (m, C(bridge)(*C*H_3)$_2$), 32.8 (bs, PC(*C*H_3)$_3$), 27.5 (s, C(bridge)(*C*H_3)$_2$).

[Pt(*t*-Bu-xantphos-κ*P,O,P'*)Cl]Cl

^{31}P NMR (121 MHz, $CDCl_3$): δ 47.7 (s, J_{PtP} = 2349.6 Hz) ^{1}H NMR (500 MHz, $CDCl_3$): δ 7.96 (d, J = 7.9 Hz, C(bridge)CC*H*), 7.93 (bs, PC(Ar)C*H*), 7.70 (t, J = 7.3 Hz, PCCC*H*), 1.80 (s, C(bridge)(C*H*$_3$)$_2$), 1.57 (vt, J_{PH} = 15.6 Hz, PC(C*H*$_3$)$_3$). ^{13}C NMR (125 MHz, $CDCl_3$): δ 158.5 (vt, J_{PC} = 11.0 Hz, PC*C*O), 134.7 (s, PC(Ar)*C*H), 133.8 (s, C(bridge)C*C*H), 132.5 (s, C(bridge)*C*CH), 128.6 (vt, J_{PC} = 6.8 Hz, PCC*C*H), 117.2 (vt, J_{PC} = 33.2 Hz, P*C*(Ar)), 39.6 (vt, J_{PC} = 21.1 Hz, P*C*(CH$_3$)$_3$), 34.1 (s, C(bridge)(*C*H$_3$)$_2$), 30.1 (vt, J_{PC} = 4.3 Hz, PC(*C*H$_3$)$_3$), 27.1 (s, *C*(bridge)).

^{31}P NMR (121 MHz, CD_2Cl_2): δ 47.8 (s, J_{PtP} = 2345.3 Hz) ^{1}H NMR (500 MHz, CD_2Cl_2): δ 7.93 (m, PC(Ar)C*H*), 7.78 (dd, J = 7.7, 1.2 Hz, C(bridge)CC*H*), 7.60 (t, J = 7.8 Hz, PCCC*H*), 1.78 (s, C(bridge)(C*H*$_3$)$_2$), 1.57 (vt, J = 16.1 Hz, PC(C*H*$_3$)$_3$). ^{13}C NMR (125 MHz, CD_2Cl_2): δ 158.8 (vt, J = 11.1 Hz, PC*C*O), 135.0 (s, PC(Ar)*C*H), 133.72 (s, C(bridge)C*C*H), 132.7 (s, C(bridge)*C*CH) 128.3 (vt, J = 6.7 Hz, PCC*C*H), 117.8 (vt, J = 33.1 Hz, P*C*(Ar)), 39.8 (vt, J = 21.1 Hz, P*C*(CH$_3$)$_3$), 34.5 (s, *C*(bridge)), 34.1 (s, C(bridge)(*C*H$_3$)$_2$), 30.0 (vt, J = 4.8 Hz, PC(*C*H$_3$)$_3$).

HRMS calcd for $C_{31}H_{48}ClOP_2Pt$ $[M\text{-}Cl]^+$ m/z = 723.2468; found = 723.2455.

[Pt(*t*-Bu-thixantphos-κ*P,O,P'*)Cl]PF_6

Dissolved (*tert*-butyl-Thixantphos)platinum dichloride (0.035 g, 0.045 mmol) in dichloromethane (2 mL) and added ammonium hexafluorophosphate (0.015 g, 0.090 mmol). After 1 hour of stirring the red solution had become yellow with a white precipitate. The solution was filtered through a plug of alumina and the solvent removed *in vacuo* yielding the title compound as a yellow solid (0.030g, 75%).

^{31}P NMR (121 MHz, CD_2Cl_2): δ 46.4 (s, J_{PtP} = 2347 Hz) -144.5 (septet, J_{PF} = 710.5 Hz, *P*F$_6$) ^{1}H NMR (500 MHz, CD_2Cl_2): δ 7.41 (s, PC(Ar)C*H*), 7.11 (s, SCC*H*), 2.38 (s, C(Ar)C*H*$_3$), 1.55 (vt, J_{PH} = 8.0 Hz, PC(C*H*$_3$)$_3$), ^{13}C NMR (125 MHz, C_6D_6): δ 157.4 (m, PC*C*O), 138.9 (s, *C*(Ar)CH$_3$), 134.4 (s, PC(Ar)*C*H), 132.6 (s, SC*C*H), 119.8 (m, P*C*(Ar)), 119.1 (m, S*C*CH), 40.0 (vt, J_{PC} = 10.4 Hz, P*C*(CH$_3$)$_3$), 30.1 (s, PC(*C*H$_3$)$_3$), 20.4 (s, C(Ar)*C*H$_3$), ^{19}F NMR (282 MHz, CD_2Cl_2): δ -73.4 (d, J_{PF} = 710.6 Hz, P*F*$_6$) HRMS calcd for $C_{30}H_{46}ClOP_2PtS$ $[M\text{-}PF_6]^+$ m/z = 741.2032; found = 741.2069.

[Pt(*t*-Bu-xantphos-κ*P,O,P'*)Cl]PF_6

A solution of *t*-Bu-xantphos (0.014 g, 0.018 mmol) in dichloromethane (2.0 mL) was added to solid ammonium hexafluorophosphate (0.006 g, 0.037 mmol) in a Schlenk tube. The reaction mixture was stirred for 1 hour before filtering through a plug of alumina. The solvent was removed *in vacuo* yielding the title compound as a yellow solid (0.008 g, 50%).

^{31}P NMR (121 MHz, CD_2Cl_2): δ 47.8 (s, J_{PtP} = 2350.3 Hz), -144.5 (septet, J_{PF} = 710.4 Hz, PF_6). ^{1}H NMR (600 MHz, CD_2Cl_2): δ 7.92 (m, PC(Ar)C*H*), 7.82 (dd, *J* = 7.7, 1.5 Hz, C(bridge)CC*H*), 7.53 (t, *J* = 7.7 Hz, PCCC*H*), 1.75 (s, C(bridge)(CH_3)$_2$), 1.57 (vt, *J* = 15.9 Hz, PC(CH_3)$_3$). ^{13}C NMR (150 MHz, CD_2Cl_2): δ 158.8 (vt, *J* = 9.4 Hz, PC*C*O), 135.0 (s, PC(Ar)*C*H), 133.4 (s, C(bridge)C*C*H), 132.6 (vt, *J* = 5.8 Hz, C(bridge)*C*CH), 128.1 (vt, *J* = 6.4 Hz, PCC*C*H), 118.0 (vt, *J* = 32.9 Hz, P*C*(Ar)), 39.8 (vt, *J* = 21.4 Hz, P*C*(CH_3)$_3$), 34.5 (s, *C*(bridge)), 33.9 (s, C(bridge)(*C*H_3)$_2$), 30.0 (vt, *J* = 4.6 Hz, PC(*C*H_3)$_3$). HRMS calcd for $C_{31}H_{48}OP_2Pt$ [M-PF_6]$^+$ *m/z* = 723.2468; found = 723.2513.

Attempted reaction of *t*-Bu-thixantphos with [Pt(C_6H_{10})Me_2]

A solution of *t*-Bu-thixantphos (0.020 g, 0.039 mmol) in C_6D_6 (0.5 mL) was added to an NMR tube containing [Pt(C_6H_{10})Me_2]. No reaction was observed after 24 hours at room temperature. The reaction was heated to 60 °C. After 28 days no conversion was evident by ^{31}P or ^{1}H NMR spectroscopy. $CH_2(SO_2CF_3)_2$ (1 eq.) was added, resulting in the immediate formation of [(*t*-Bu-thixantphos)H]$^+$.

[Pt(*t*-Bu-thixantphos-κ*P,O,P'*)Me]Cl

A solution of *t*-Bu-thixantphos (0.043 g, 0.083 mmol) in toluene (1.0 mL) was added to solid [Pt(C_6H_{10})ClMe] (0.027 g, 0.083 mmol) in a Schlenk tube. The reaction mixture was stirred for 24 hours at room temperature, during which, an off-white precipitate formed. The solution was decanted and the solid dried under vacuum, giving [Pt(*t*-Bu-thixantphos)Me]Cl as an off-white powder (0.057 g, 90%).

^{31}P NMR (121 MHz, acetone−d_6): δ 50.5 (s, J_{PtP} = 2793.3 Hz) ^{1}H NMR (600 MHz, acetone−d_6): δ 7.69 (d, J_{PH} = 1.8 Hz, PC(Ar)C*H*), 7.34 (d, J_{PH} = 1.2 Hz, SCC*H*), 2.42 (s, C(Ar)C*H*$_3$), 1.56 (vt, J_{PH} = 15.6 Hz, PC(C*H*$_3$)$_3$), 1.94 (t, J_{PH} = 5.5, $^{2}J_{PtP}$ = 97.4 Hz, Pt-C*H*$_3$), ^{13}C NMR (150 MHz, acetone−d_6): δ 153.8 (vt, J_{PC} = 10.3 Hz, PC*C*O), 137.1 (vt, J_{PC} = 6.3 Hz, *C*(Ar)CH$_3$), 134.4 (s, PC(Ar)*C*H), 131.4 (s, SC*C*H), 120.8 (vt, J_{PC} = 31.8 Hz, P*C*(Ar)), 118.2 (vt, J_{PC} = 7.2 Hz, S*C*CH), 38.8 (vt, J_{PC} = 20.6 Hz, P*C*(CH$_3$)$_3$), 29.6 (obscured, assigned by HSQC correlation, PC(*C*H$_3$)$_3$), 19.2 (s, C(Ar)*C*H$_3$), -23.8 (t, J_{PC} = 5.6, $^{1}J_{PtC}$ = 777.2 Hz, Pt-*C*H$_3$) HRMS calcd for $C_{31}H_{49}OP_2PtS$ [M-Cl]$^+$ m/z = 721.2579; found = 721.2602.

[Pt(*t*-Bu-xantphos)Me]Cl

A solution of *t*-Bu-xantphos (0.024 g, 0.048 mmol) in toluene (0.5 mL) was added to solid [Pt(C_6H_{10})ClMe] (0.016 g, 0.048 mmol) in a Schlenk tube. The reaction mixture was stirred for 24 hours at room temperature, during which, an off-white precipitate formed. The solution was decanted and the solid dried under vacuum, giving the title compound as an off-white powder (0.028 g, 78%).

^{31}P NMR (121 MHz, acetone−d_6): δ 51.0 (s, J_{PtP} = 2788.2 Hz) ^{1}H NMR (500 MHz, acetone−d_6): δ 8.15 (dt, J = 7.5, 3.7 Hz, PC(Ar)C*H*), 8.07 (d, J = 7.8 Hz, C(bridge)CC*H*), 7.63 (t, J = 7.9 Hz, PCCC*H*), 1.92 (t, J_{PH} = 5.4, $^{2}J_{PtP}$ = 97.4 Hz, Pt-C*H*$_3$), 1.78 (s, C(bridge)(C*H*$_3$)$_2$) 1.55 (vt, J_{PH} = 15.4 Hz, PC(C*H*$_3$)$_3$) ^{13}C NMR (125 MHz, acetone−d_6): δ 156.1 (vt, J_{PC} = 10.2 Hz, PC*C*O), 135.9 (s, PC(Ar)*C*H), 133.2 (s, C(bridge)C*C*H), 132.7 (s, C(bridge)*C*CH), 127.4 (vt, J_{PC} = 6.6 Hz, PCC*C*H), 119.7 (vt, J_{PC} = 34.1 Hz, P*C*(Ar)), 39.5 (vt, J_{PC} = 21.4, $^{2}J_{PtC}$ = 43.3 Hz, P*C*(CH$_3$)$_3$), 35.0 (s, *C*(bridge)), 33.7 (s, C(bridge)(*C*H$_3$)$_2$), 30.4 (vt, J_{PC} = 6.1 Hz, PC(*C*H$_3$)$_3$). -23.9 (t, J_{PC} = 5.6, $^{1}J_{PtC}$ = 774.6 Hz, Pt-*C*H$_3$) HRMS calcd for $C_{32}H_{51}OP_2Pt$ [M-Cl]$^+$ m/z = 703.3014; found = 703.2987.

[Pt(*t*-Bu-sixantphos)Me]Cl

A solution of *t*-Bu-sixantphos (0.026 g, 0.051 mmol) in C_6D_6 was added to an NMR tube containing [Pt(C_6H_{10})ClMe] (0.017 g, 0.051 mmol). After 72 hours at room temperature little reaction was observed, so the solution was heated to 50 °C for 24 hours during which time a white precipitate formed. NMR spectroscopy

showed no unreacted *t*-Bu-sixantphos was evident in the ^{1}H or ^{31}P NMR spectra. The solution was decanted and the title compound was dried under vacuum (0.014 g, 36%).

^{31}P NMR (121 MHz, acetone−d_6): δ 48.7 (s, J_{PtP} = 2762.9 Hz) ^{1}H NMR (500 MHz, acetone−d_6): δ 8.39-8.36 (m, PC(Ar)C*H*), 8.11 (dd, 7.1, 1.7 Hz, SiCC*H*), 7.65 (t, J = 7.4 Hz, PCCC*H*), 2.01 (t, J = 5.5 $^{2}J_{PtP}$ = 98.6 Hz, Pt-CH_3), 1.55 (vt, J = 15.2 Hz, PC(C*H*$_3$)$_3$), 0.59 (s, Si(C*H*$_3$)$_2$). ^{13}C NMR (125 MHz, acetone−d_6): δ 167.3 (vt, J_{PC} = 8.2 Hz, PC*C*O), 140.72 (s, PC(Ar)*C*H), 140.67 (s, SiC*C*H), 126.1 (vt, J_{PC} = 6.1 Hz, PCC*C*H), 123.5 (s, Si*C*CH), 121.2 (vt, J_{PC} = 32.4 Hz, P*C*(Ar)), 39.7 (vt, J_{PC} = 21.8 Hz, P*C*(CH$_3$)$_3$), 30.6 (vt, J_{PC} = 5.6 Hz, PC(*C*H$_3$)$_3$), -0.5 (s, Si(*C*H$_3$)$_2$), -22.7 (t, J_{PC} = 5.6, $^{1}J_{PtC}$ = 780.5 Hz, Pt-*C*H$_3$). HRMS calcd for $C_{31}H_{51}OP_2PtSi$ [M-Cl]$^{+}$ m/z = 724.2829; found = 724.2760.

8.6 Palladium Complexes

Reaction of *t*-Bu-thixantphos with [Pd(nb)$_3$]

A solution of *t*-Bu-thixantphos (0.051 g, 0.10 mmol) in C_6D_6 (0.5 mL) was added to an NMR tube containing [Pd(nb)$_3$] (0.038 g, 0.10 mmol) and a small crystal of norbornene. The NMR tube was sealed with a J. Young's tap. After 72 hours at room temperature no *t*-Bu-thixantphos was present by ^{31}P NMR spectroscopy. The mixture contained [Pd(*t*-Bu-thixantphos)] (62.0%) and [Pd(*t*-Bu-thixantphos)(nb)] (38.0%).

[Pd(*t*-Bu-thixantphos)(nb)]

^{31}P NMR (121 MHz, C_6D_6): δ 33.6 (s)

[Pd(*t*-Bu-thixantphos)]

A solution of *t*-Bu-thixantphos (0.056 g, 0.11 mmol) in toluene (1.0 mL) was added to a Schlenk tube containing [Pd(nb)$_3$] (0.042 g, 0.11 mmol) and a small crystal of norbornene (0.012 g). The reaction was stirred overnight. The solvent

was removed *in vacuo* leaving [Pd(*t*-Bu-thixantphos)] as a oily brown solid (0.061 g, 90%).

^{31}P NMR (121 MHz, C_6D_6): δ 42.9 (s) ^{1}H NMR (500 MHz, C_6D_6): δ 7.35 (s, PC(Ar)C*H*), 6.83 (s, SCC*H*), 1.95 (s, C(Ar)C*H*$_3$), 1.46 (vt, J_{PH} = 13.7 Hz, PC(C*H*$_3$)$_3$), ^{13}C NMR (125 MHz, C_6D_6): δ 155.9 (vt, J_{PC} = 14.0 Hz, PC*C*O), 133.6 (s, PC(Ar)*C*H), 131.9 (s, *C*(Ar)CH$_3$), 128.8 (s, SC*C*H) 127.8 (vt, J_{PC} = 8.2 Hz, P*C*(Ar)), 124.6 (vt, J_{PC} = 5.3 Hz, S*C*CH), 35.7 (vt, J_{PC} = 3.8 Hz, P*C*(CH$_3$)$_3$), 31.9 (s, PC(*C*H$_3$)$_3$), 20.4 (s, C(Ar)*C*H$_3$)

Reaction of *t*-Bu-xantphos with [Pd(nb)$_3$]

A solution of *t*-Bu-xantphos (0.046 g, 0.092 mmol) in C_6D_6 (0.5 mL) was added to an NMR tube containing [Pd(nb)$_3$] (0.036 g, 0.092 mmol) and a small crystal of norbornene. The NMR tube was sealed with a J. Young's tap. The NMR after one hour showed a mixture with no uncoordinated *t*-Bu-xantphos and multiplet products. The mixture contained [Pd(*t*-Bu-xantphos)] (73.1%) and [Pd(*t*-Bu-xantphos)(nb)] (12.6%), as well as several other unidentified phosphorus containing compounds.

[Pd(*t*-Bu-xantphos)(nb)]

^{31}P NMR (121 MHz, C_6D_6): δ 32.6 (s)

[Pd(*t*-Bu-xantphos)]

^{31}P NMR (121 MHz, C_6D_6): δ 42.6 (s)

[Pd(*t*-Bu-sixantphos)]

A solution of *t*-Bu-sixantphos (0.040 g, 0.078 mmol) in C_6D_6 (0.5 mL) was added to a J. Young's tap NMR tube containing [Pd(nb))$_3$] (0.030 g, 0.078 mmol) and norbornene (0.010 g). The tube was sealed under argon and the reaction was followed by NMR spectroscopy. After 48 hours at room temperature a mixture

of uncoordination *t*-Bu-sixantphos (56.9%) and [Pd(*t*-Bu-sixantphos)] (43.1%) is present by ^{31}P NMR. After 24 hours no progress was observed. However, after six months, the mixture contained *t*-Bu-sixantphos (32.0%) and [Pd(*t*-Bu-sixantphos)] (68%).

^{31}P NMR (121 MHz, C_6D_6): δ 41.9 (s) ^{1}H NMR (300 MHz, C_6D_6): δ 7.51 (m, PC(Ar)C*H*), 7.30 (dd, J = 7.1, 1.5 Hz, SiC*C*H), 6.92 (t, J = 7.4 Hz, PCC*C*H), 1.63 (bs, PC(C*H*$_3$)$_3$), 0.23 (s, Si(C*H*$_3$)$_2$).

[Pd(*t*-Bu-thixantphos)(η^2-O_2)]

Air was bubbled through a solution of [Pd(*t*-Bu-thixantphos)] (0.058 g, 0.093 mmol) in C_6D_6 (0.5 mL) for 10 minutes. The solution turned green immediately. The sample was filtered through a plug of alumina and reduced to dryness giving the title compound as a green solid (0.052 g, 90%).

^{31}P NMR (121 MHz, $CDCl_3$): δ 52.0 (s) ^{1}H NMR (500 MHz, $CDCl_3$): δ 7.49 (s, 2H, Ar), 7.23 (s, 2H, Ar), 2.32 (s, C(Ar)C*H*$_3$), 1.50 (d, J = 13.7 Hz, PC(C*H*$_3$)$_3$).

trans-[Pd(*t*-Bu-sixantphos)Cl_2]

Combined *t*-Bu-sixantphos (0.015 g, 0.029 mmol) and [Pd(cod)Cl_2] (0.008 g, 0.029 mmol) in an sealed tube and stirred at 60 °C for hours then 35 °C. The solvent was removed *in vacuo* yielding the title compound as a red solid (0.018 g, 89%).

^{31}P NMR (121 MHz, $CDCl_3$): δ 45.7 (s) ^{1}H NMR (500 MHz, $CDCl_3$): δ 7.71 (m, PC(Ar)C*H*), 7.68 (d, 7.1 Hz, SiCC*H*), 7.33 (t, 7.3 Hz, PCCC*H*), 1.60 (vt, J_{PH} = 7.3 Hz, PC(C*H*$_3$)$_3$), 0.52 (s, Si(C*H*$_3$)$_2$). ^{13}C NMR (125 MHz, $CDCl_3$): δ 165.1 (vt, J_{PC} = 6.8 Hz, PC*C*O), 137.6 (s, PC(Ar)*C*H), 136.9 (s, SiC*C*H), 124.9 (s, Si*C*CH), 123.1 (s, PCC*C*H), 121.8 (vt, J_{PC} = 13.4 Hz, P*C*(Ar)), 39.6 (vt, J_{PC} = 6.3 Hz, P*C*(CH$_3$)$_3$), 31.1 (vt, J_{PC} = 2.7 Hz, PC(*C*H$_3$)$_3$), -2.0 (s, Si(*C*H$_3$)$_2$).

^{31}P NMR (121 MHz, CD_2Cl_2): δ 46.7 (s) ^{1}H NMR (600 MHz, CD_2Cl_2): δ 7.72-7.74 (m, 2H, SiCC*H*, PC(Ar)C*H*), 7.35 (t, J = 7.2 Hz, PCCC*H*), 1.59 (vt, J = 15.0 Hz, PC(C*H*$_3$)$_3$), 0.53 (s, Si(C*H*$_3$)$_2$). ^{13}C NMR (150 MHz, CD_2Cl_2): δ 165.4 (bs, PC*C*O), 137.9 (s, PC(Ar)*C*H), 137.2 (s, SiC*C*H), 125.2 (s, Si*C*CH), 123.2 (s, PCC*C*H), 122.0

(vt, *J* = 25.4 Hz, P*C*(Ar)), 39.7 (vt, *J* = 12.8 Hz, P*C*(CH_3)$_3$), 31.1 (bs, PC(*C*H_3)$_3$), -2.2 (s, Si(*C*H_3)$_2$).

^{31}P NMR (121 MHz, C_6D_6): δ 42.0 (s) ^{1}H NMR (500 MHz, C_6D_6): δ 7.51 (dtd, *J* = 7.7, 3.9, 1.8 Hz, PC(Ar)C*H*), 7.30 (dd, *J* = 7.0, 1.6 Hz, SiCC*H*), 6.92 (t, *J* = 7.3 Hz, PCCC*H*), 1.64 (bs, PC(C*H*$_3$)$_3$), 0.23 (s, Si(C*H*$_3$)$_2$). ^{13}C NMR (125 MHz, C_6D_6): δ 164.9 (vt, *J* = 6.2 Hz, PC*C*O), 137.2 (s, PC(Ar)*C*H), 135.5 (s, SiC*C*H), 125.4 (vt, *J* = 3.0 Hz, Si*C*CH), 124.1 (vt, *J* = 26.9 Hz, P*C*(Ar)), 121.9 (vt, *J* = 4.8 Hz, PCC*C*H), 39.4 (vt, *J* = 11.5 Hz, P*C*(CH_3)$_3$), 31.6 (bs, PC(*C*H_3)$_3$), -3.1 (bs, Si(*C*H_3)$_2$).

HRMS calcd for $C_{30}H_{48}OP_2SiPdCl$ [M-Cl]$^+$ *m/z* = 655.1676; found = 655.1663.

trans-[Pd(*t*-Bu-thixantphos)Cl_2]

t-Bu-Thixantphos (0.197 g, 0.38 mmol) and [Pd(cod)Cl_2] (0.108 g, 0.38 mmol) were dissolved in toluene then heated to 40 °C for three days. The solvent was removed *in vacuo* yielding the title compound as an orange solid (0.265 g, 100%).

^{31}P NMR (121 MHz, CD_2Cl_2): δ 40.0 (s) ^{1}H NMR (600 MHz, CD_2Cl_2): δ 7.16 (s, SCC*H*), 7.15 (s, PC(Ar)C*H*), 2.33 (s, C(Ar)C*H*$_3$), 1.59 (vt, *J* = 13.6 Hz, PC(C*H*$_3$)$_3$), ^{13}C NMR (150 MHz, CD_2Cl_2): δ 155.1 (vt, *J* = 8.7 Hz, PC*C*O), 134.4 (s, SC*C*H), 133.1 (vt, *J* = 5.8 Hz, *C*(Ar)CH_3), 130.2 (s, PC(Ar)*C*H), 123.8 (vt, *J* = 26.1 Hz, P*C*(Ar)), 123.3 (vt, *J* = 6.3 Hz, S*C*CH), 39.5 (vt, *J* = 12.1 Hz, P*C*(CH_3)$_3$), 31.3 (bs, PC(*C*H_3)$_3$), 20.7 (s, C(Ar)*C*H_3). HRMS calcd for $C_{30}H_{46}OP_2SPdCl$ [M-Cl]$^+$ *m/z* = 657.1468; found = 657.1446.

trans-[Pd(*t*-Bu-xantphos)Cl_2]

t-Bu-Xantphos (0.021 g, 0.042 mmol) and [Pd(cod)Cl_2] (0.012 g, 0.042 mmol) were dissolved in C_6D_6 in an NMR tube then heated to 40 °C for three days. The solvent was removed *in vacuo* and the residue was washed with pentane yielding the title compound as an orange solid (0.015 g, 53%).

^{31}P NMR (121 MHz, C_6D_6): δ 40.0 (s) ^{1}H NMR (600 MHz, C_6D_6): δ 7.33 (dtd, *J* = 8.1, 3.4, 1.5 Hz, PC(Ar)C*H*), 7.13 (dd, *J* = 7.7, 1.2 Hz, C(bridge)CC*H*), 6.87 (t, *J* = 7.7 Hz, PCCC*H*), 1.65 (bs, PC(C*H*$_3$)$_3$), 1.32 (bs, C(bridge)(C*H*$_3$)$_2$).

^{13}C NMR (150 MHz, C_6D_6): δ 156.9 (vt, J = 8.7 Hz, PC*C*O), 135.4 (vt, J = 4.6 Hz, C(bridge)*C*CH), 132.8 (s, PC(Ar)*C*H), 126.2 (s, C(bridge)C*C*H), 123.0 (vt, J = 27.7 Hz, P*C*(Ar)), 122.2 (vt, J = 5.3 Hz, PCC*C*H), 39.1 (vt, J = 12.1 Hz, P*C*(CH_3)$_3$), 36.2 (s, *C*(bridge)), 31.5 (bs, PC(*C*H_3)$_3$), 24.9 (s, C(bridge)(*C*H_3)$_2$).

^{31}P NMR (121 MHz, CD_2Cl_2): δ 54.1 (s) ^{1}H NMR (600 MHz, CD_2Cl_2): δ 7.87 (d, J = 7.6 Hz, C(bridge)CC*H*), 7.76 (m, PC(Ar)C*H*), 7.52 (t, J = 7.7 Hz, PCCC*H*), 1.75 (s, C(bridge)(*C*H_3)$_2$), 1.59 (vt, J = 15.5 Hz, PC(C*H*$_3$)$_3$), ^{13}C NMR (150 MHz, CD_2Cl_2): δ 156.6 (vt, J = 11.6 Hz, PC*C*O), 134.6 (s, C(bridge)*C*CH) 132.0 (s, PC(Ar)*C*H), 126.5 (s, C(bridge)C*C*H), 118.1 (vt, J = 24.3 Hz, P*C*(Ar)), 117.6 (s, PCC*C*H), 39.8 (vt, J = 13.8 Hz, P*C*(CH_3)$_3$), 32.6 (s, *C*(bridge)), 31.4 (s, C(bridge)(*C*H_3)$_2$), 30.3 (vt, J = 5.8 Hz, PC(*C*H_3)$_3$).

HRMS calcd for $C_{31}H_{48}OP_2PdCl$ $[M\text{-}Cl]^+$ m/z = 635.1925; found = 635.1966.

[Pd(*t*-Bu-thixantphos-κ*P,O,P'*)Cl]PF_6

NH_4PF_6 (0.052 g, 0.32 mmol) and *trans*-[Pd(*t*-Bu-thixantphos)Cl_2] (0.050, 0.061 mmol) were combined in an Schlenk tube and suspended in CH_2Cl_2 (10 mL). The reaction mixture was stirred overnight and the volume was reduced by half. The solution was filtered through a plug of alumina and reduced to dryness giving the title compound as a yellow solid (0.039 g, 68%).

^{31}P NMR (121 MHz, CD_2Cl_2): δ 56.4 (s) -144.5 (septet, J_{PF} = 710.5 Hz, *P*F_6) ^{1}H NMR (500 MHz, CD_2Cl_2): δ 7.36 (d, J_{PH} = 2.0 Hz, PC(Ar)C*H*), 7.15 (s, SCC*H*), 2.38 (s, C(Ar)C*H*$_3$), 1.58 (vt, J_{PH} = 8.2 Hz, PC(C*H*$_3$)$_3$), ^{13}C NMR (125 MHz, C_6D_6): δ 154.86 (vt, J_{PC} = 6.5 Hz, PC*C*O), 138.3 (vt, J_{PC} = 5.8 Hz, *C*(Ar)CH_3), 134.6 (s, PC(Ar)*C*H), 132.6 (s, SC*C*H), 119.1 (s, S*C*CH), 118.7 (vt, J_{PC} = 10.8 Hz, P*C*(Ar)), 40.2 (vt, J_{PC} = 7.2 Hz, P*C*(CH_3)$_3$), 30.1 (s, PC(*C*H_3)$_3$), 20.4 (s, C(Ar)*C*H_3) ^{19}F NMR (282 MHz, CD_2Cl_2): δ -73.4 (d, J_{PF} = 710.6 Hz, P*F*$_6$) HRMS calcd for $C_{30}H_{46}ClOP_2PdS$ $[M\text{-}PF_6]^+$ m/z = 653.1489; found = 653.1527.

[Pd(*t*-Bu-sixantphos-κ*P,O,P'*)Cl]PF_6

This compound was synthesised as for [Pd(*t*-Bu-thixantphos-κ*P,O,P'*)Cl]PF_6 using *trans*-[Pd(*t*-Bu-sixantphos)Cl_2] (0.018 g, 0.026 mmol) and NH_4PF_6 (0.005 g, 0.030 mmol) giving the title compound as a yellow solid (0.020 g, 96%).

^{31}P NMR (121 MHz, CD_2Cl_2): δ 52.4 (s, *t*-Bu-sixantphos) -144.5 (septet, J_{PF} = 710.3 Hz, PF_6) ^{1}H NMR (500 MHz, CD_2Cl_2): δ 8.07 (m, PC(Ar)C*H*), 7.91 (dd, *J* = 7.0, 1/9 Hz, SiCC*H*), 7.56 (t, *J* = 7.4 Hz, PCCC*H*), 1.59 (vt, *J* = 16.1 Hz, PC(C*H*$_3$)$_3$), 0.60 (s, Si(C*H*$_3$)$_2$). ^{13}C NMR (125 MHz, CD_2Cl_2): δ 168.4 (vt, *J* = 10.6 Hz, PC*C*O), 140.9 (s, SiC*C*H), 139.7 (s, PC(Ar)*C*H), 126.1 (vt, *J* = 5.3 Hz, PCC*C*H), 124.1 (s, Si*C*CH) 118.0 (vt, *J* = 22.1 Hz, P*C*(Ar)), 40.2 (vt, *J* = 15.4 Hz, P*C*(CH$_3$)$_3$), 30.2 (vt, *J* = 5.3 Hz, PC(*C*H$_3$)$_3$), -0.4 (s, Si(*C*H$_3$)$_2$). ^{19}F NMR (282 MHz, CD_2Cl_2): δ -73.4 (d, *J* = -706.6 Hz, PF_6) HRMS calcd for $C_{30}H_{48}ClOP_2PdSi$ [M-PF_6]$^+$ m/z = 651.1694; found = 651.1717.

[Pd(*t*-Bu-xantphos-κ*P,O,P'*)Cl]PF_6

This compound was synthesised as for [Pd(*t*-Bu-thixantphos-κ*P,O,P'*)Cl]PF_6 using *trans*-[Pd(*t*-Bu-xantphos)Cl_2] (0.020 g, 0.030 mmol) and NH_4PF_6 (0.005 g, 0.030 mmol) giving the title compound as a yellow solid (0.020 g, 86%).

^{31}P NMR (121 MHz, CD_2Cl_2): δ 58.3 (s, *t*-Bu-xantphos), -144.5 (septet, J_{PF} = 710.4 Hz, PF_6) ^{1}H NMR (500 MHz, CD_2Cl_2): δ 7.87 (dd, *J* = 7.7, 1.6 Hz, PC(Ar)C*H*), 7.84 (m, C(bridge)CC*H*), 7.53 (t, *J* = 7.9 Hz, PCCC*H*), 1.76 (s, C(bridge)(C*H*$_3$)$_2$), 1.59 (vt, *J* = 16.1 Hz, C(bridge)(C*H*$_3$)$_2$) ^{13}C NMR (125 MHz, CD_2Cl_2): δ 156.7 (vt, *J* = 11.6 Hz, PC*C*O), 135.1 (s, PC(Ar)*C*H), 133.4 (s, C(bridge)C*C*H), 132.7 (bs, C(bridge)*C*CH), 127.4 (vt, *J* = 6.6 Hz, PCC*C*H), 117.1 (vt, *J* = 24.0 Hz, P*C*(Ar)), 40.1 (vt, *J* = 14.9 Hz, P*C*(CH$_3$)$_3$), 34.5 (s, *C*(bridge)), 34.0 (s, C(bridge)(*C*H$_3$)$_2$), 30.0 (vt, *J* = 7.3 Hz, PC(*C*H$_3$)$_3$). ^{19}F NMR (282 MHz, CD_2Cl_2): δ -73.5 (d, *J* = -709.6 Hz, PF_6) HRMS calcd for $C_{31}H_{48}ClOP_2Pd$ [M-PF_6]$^+$ m/z = 635.1925; found = 635.1959.

Bibliography

[1] Lamansky, S.; Djurovich, P.; Murphy, D.; Abdel-Razzaq, F.; Lee, H.-E.; Adachi, C.; Burrows, P. E.; Forrest, S. R.; Thompson, M. E. *J. Am. Chem. Soc.* **2001**, *123*, 4304–4312.

[2] Rosenberg, B.; VanCamp, L.; Trosko, J. E.; Mansour, V. H. *Nature* **1969**, *222*, 385–386.

[3] Wilson, J. J.; Lippard, S. J. *Chem. Rev.* **2013**, *114*, 4470–4495.

[4] Orpen, A. G.; Connelly, N. G. *Organometallics* **2001**, *9*, 1206–1210.

[5] Noyori, R. *Angew. Chem. Int. Ed. Engl.* **2002**, *41*, 2008–2022.

[6] Nicolaou, K. C.; Bulger, P. G.; Sarlah, D. *Angew. Chem. Int. Ed.* **2005**, *44*, 4442–4489.

[7] Knowles, W. S. *Angew. Chem. Int. Ed.* **2002**, *41*, 1998–2007.

[8] Tolman, C. A. *Chem. Rev.* **1977**, *77*, 313–348.

[9] Banger, K. K.; Brisdon, A. K.; Herbert, C. J.; Ghaba, H. A.; Tidmarsh, I. S. *J Fluorine Chem* **2009**, *130*, 1117–1129.

[10] Dunne, B. J.; Morris, R. B.; Orpen, A. G. *J. Chem. Soc., Dalton Trans.* **1991**, 653–661.

[11] Roodt, A.; Otto, S.; Steyl, G. *Coord. Chem. Rev.* **2003**, *245*, 121–137.

[12] Mann, B. E.; Musco, A. *J. Chem. Soc., Dalton Trans.* **1980**, 776–785.

[13] Tiburcio, J.; Bernès, S.; Torrens, H. *Polyhedron* **2006**, *25*, 1549–1554.

[14] Tolman, C. A. *J. Am. Chem. Soc.* **1970**, *92*, 2953–2956.

[15] Connelly, N. G.; Damhus, T.; Hartshorn, R. M.; Hutton, A. T. *Nomenclature of Inorganic Chemistry - IUPAC Recommendations 2005*; The Royal Society of Chemistry: Cambridge, 2005.

[16] Pregosin, P. S. *NMR in Organometallic Chemistry*; Wiley VCH GmbH & Co. KGaA: Weinheim, 2012.

[17] Beckmann, U.; Süslüyan, D.; Kunz, P. C. *Phosphorus, Sulfur Silicon Relat Elem* **2011**, *186*, 2061–2070.

[18] Allman, T.; Goel, R. G. *Can. J. Chem.* **1982**, *60*, 716–722.

[19] Hillier, A. C.; Sommer, W. J.; Yong, B. S.; Petersen, J. L.; Cavallo, L.; Nolan, S. P. *Organometallics* **2003**, *22*, 4322–4326.

[20] Clavier, H.; Nolan, S. P. *Chem. Commun.* **2010**, *46*, 841.

[21] Agbossou, F.; Carpentier, J.-F.; Mortreux, A. *Chem. Rev.* **2001**, *95*, 2485–2506.

[22] Shimizu, H.; Nagasaki, I.; Matsumura, K.; Sayo, N.; Saito, T. *Acc. Chem. Res.* **2007**, *40*, 1385–1393.

[23] Housecroft, C. E.; Sharpe, A. G. *Inorganic Chemistry*, 2nd ed.; Pearson Education Limited: Madrid, 2005.

[24] Casey, C. P.; Whiteker, G. T. *Israel J. Chem.* **1990**, *30*, 299–304.

[25] Dierkes, P.; van Leeuwen, P. *J. Chem. Soc., Dalton Trans.* **1999**, 1519–1529.

[26] Lai, T. W.; Sen, A. *Organometallics* **2001**, *3*, 866–870.

[27] Drent, E.; Van Broekhoven, J.; Doyle, M. J. *J. Organomet. Chem.* **2014**, *417*, 235–251.

[28] van Leeuwen, P. W. N. M., Claver, C., Eds. *Rhodium Catalyzed Hydroformylation*; Kluwer Academic Publishers: Dordrecht, 2000.

[29] Eastham, G. R.; Tooze, R. P.; Heaton, B. T.; Iggo, J. A.; Whyman, R.; Zacchini, S. *Chem. Commun.* **2000**, 609–610.

[30] Kranenburg, M.; Vanderburgt, Y.; Kamer, P.; van Leeuwen, P.; Goubitz, K.; Frannje, J. *Organometallics* **1995**, *14*, 3081–3089.

[31] Tsuji, J. *Palladium Reagents and Catalysts - Innovations in Organic Synthesis*; John Wiley & Sons, Ltd.: Chichester, 1995.

[32] Freixa, Z.; van Leeuwen, P. *Dalton Trans.* **2003**, 1890–1901.

[33] Freixa, Z.; Beentjes, M. S.; Batema, G. D.; Dieleman, C. B.; van Strijdonck, G. P. F.; Reek, J. N. H.; Kamer, P. C. J.; Fraanje, J.; Goubitz, K.; van Leeuwen, P. W. N. M. *Angew. Chem. Int. Ed.* **2003**, *42*, 1284–1287.

[34] Kamer, P.; van Leeuwen, P.; Reek, J. *Acc. Chem. Res.* **2001**, *34*, 895–904.

[35] Serrano-Becerra, J. M.; Morales-Morales, D. *Curr. Org. Synth.* **2009**, *6*, 169–192.

[36] Choi, J.; MacArthur, A. H. R.; Brookhart, M.; Goldman, A. S. *Chem. Rev.* **2011**, *111*, 1761–1779.

[37] van der Vlugt, J. I.; Reek, J. N. H. *Angew. Chem. Int. Ed.* **2009**, *48*, 8832–8846.

[38] Kataoka, Y.; Tsuji, Y.; Matsumoto, O.; Ohashi, M.; Yamagata, T.; Tani, K. *J. Chem. Soc., Chem. Commun.* **1995**, 2099–2100.

[39] Singleton, J. T. *Tetrahedron* **2003**, *59*, 1837–1857.

[40] Takenaka, K.; Minakawa, M.; Uozumi, Y. *J. Am. Chem. Soc.* **2005**, *127*, 12273–12281.

[41] Zim, D.; Gruber, A. S.; Ebeling, G.; Dupont, J.; Monteiro, A. L. *Org. Lett.* **2000**, *2*, 2881–2884.

[42] Hahn, F. E.; Jahnke, M. C.; Pape, T. *Organometallics* **2007**, *26*, 150–154.

[43] Moulton, C. J.; Shaw, B. L. *J. Chem. Soc., Dalton Trans.* **1976**, 1020–1024.

[44] Alcock, N. W.; Brown, J. M.; Jeffery, J. C. *J. Chem. Soc., Dalton Trans.* **1976**, 583–588.

[45] Zhu, H. J.; Ziegler, T. *Organometallics* **2008**, *27*, 1743–1749.

[46] Albrecht, M.; Gossage, R. A.; Lutz, M.; Spek, A. L.; van Koten, G. *Chem. Eur. J.* **2000**, *6*, 1431–1445.

[47] Albrecht, M.; Lutz, M.; Spek, A. L.; van Koten, G. *Nature* **2000**, *406*, 970–974.

[48] Albrecht, M.; van Koten, G. *Angew. Chem. Int. Ed.* **2001**, *40*, 3750–3781.

[49] Bedford, R. B.; Draper, S. M.; Noelle Scully, P.; Welch, S. L. *New J. Chem.* **2000**, *24*, 745–747.

[50] Kimura, T.; Uozumi, Y. *Organometallics* **2006**, *25*, 4883–4887.

[51] Obora, Y.; Kimura, M.; Ohtake, T.; Tokunaga, M.; Tsuji, Y. *Organometallics* **2006**, *25*, 2097–2100.

[52] Sandhya, K. S.; Suresh, C. H. *Organometallics* **2011**, *30*, 3888–3891.

[53] Holscher, M.; Prechtl, M. H. G.; Leitner, W. *Chem. Eur. J.* **2007**, *13*, 6636–6643.

[54] Crabtree, R. H. *J. Chem. Soc., Dalton Trans.* **2001**, 2951–2951.

[55] van der Veen, L. A.; Keeven, P. K.; Kamer, P. C. J.; van Leeuwen, P. W. N. M. *J. Chem. Soc., Dalton Trans.* **2000**, 2105–2112.

[56] Malaise, G.; Sortais, J.-B.; Barloy, L.; Pfeffer, M.; Kyritsakas, N. *Polyhedron* **2006**, *25*, 3349–3365.

[57] Goertz, W.; Keim, W.; Vogt, D.; Englert, U.; Boele, M. D. K.; van der Veen, L. A.; Kamer, P. C. J.; van Leeuwen, P. W. N. M. *J. Chem. Soc., Dalton Trans.* **1998**, 2981–2988.

[58] van Haaren, R. J.; Keeven, P. H.; van der Veen, L. A.; Goubitz, K.; van Strijdonck, G. P. F.; Oevering, H.; Reek, J. N. H.; Kamer, P. C. J.; van Leeuwen, P. W. N. M. *Inorg. Chim. Acta* **2002**, *327*, 108–115.

[59] Goedheijt, M. S.; Kamer, P.; van Leeuwen, P. *J. Mol. Catal. A-Chem.* **1998**, *134*, 243–249.

[60] Goedheijt, M. S.; Reek, J. N. H.; Kamer, P. C. J.; van Leeuwen, P. W. N. M. *Chem. Commun.* **1998**, 2431–2432.

[61] van der Veen, L. A.; Kamer, P. C. J.; van Leeuwen, P. W. N. M. *Organometallics* **1999**, *18*, 4765–4777.

[62] van der Veen, L. A.; Keeven, P. H.; Schoemaker, G. C.; Reek, J.; Kamer, P.; van Leeuwen, P.; Lutz, M.; Spek, A. L. *Organometallics* **2000**, *19*, 872–883.

[63] van der Veen, L. A.; Boele, M. D. K.; Bregman, F. R.; Kamer, P. C. J.; van Leeuwen, P. W. N. M.; Goubitz, K.; Fraanje, J.; Schenk, H.; Bo, C. *J. Am. Chem. Soc.* **1998**, *120*, 11616–11626.

[64] van Leeuwen, P. W. N. M.; Kamer, P. C. J.; Reek, J. N. H.; Dierkes, P. *Chem. Rev.* **2000**, *100*, 2741–2770.

[65] van der Slot, S. C.; Duran, J.; Luten, J.; Kamer, P. C. J.; van Leeuwen, P. W. N. M. *Organometallics* **2002**, *21*, 3873–3883.

[66] Kranenburg, M.; Kamer, P.; van Leeuwen, P.; Vogt, D.; Keim, W. *J. Chem. Soc., Chem. Commun.* **1995**, 2177–2178.

[67] Birkholz née Gensow, M.-N.; Freixa, Z.; van Leeuwen, P. W. N. M. *Chem. Soc. Rev.* **2009**, *38*, 1099–1118.

[68] Allen, F. H. *Acta Crystall. B-Stru.* **2002**, *58*, 380–388.

[69] Escalle, A.; Mora, G.; Gagosz, F.; Mezailles, N.; Le Goff, X. F.; Jean, Y.; Le Floch, P. *Inorg. Chem.* **2009**, *48*, 8415–8422.

[70] Moxham, G. L.; Randell-Sly, H. E.; Brayshaw, S. K.; Woodward, R. L.; Weller, A. S.; Willis, M. C. *Angew. Chem. Int. Ed.* **2006**, *45*, 7618–7622.

[71] Moxham, G. L.; Randell-Sly, H.; Brayshaw, S. K.; Weller, A. S.; Willis, M. C. *Chem. Eur. J.* **2008**, *14*, 8383–8397.

[72] Pawley, R. J.; Moxham, G. L.; Dallanegra, R.; Chaplin, A. B.; Brayshaw, S. K.; Weller, A. S.; Willis, M. C. *Organometallics* **2010**, *29*, 1717–1728.

[73] Zuideveld, M. A.; Swennenhuis, B. H. G.; Boele, M. D. K.; Guari, Y.; van Strijdonck, G. P. F.; Reek, J. N. H.; Kamer, P. C. J.; Goubitz, K.; Fraanje, J.; Lutz, M.; Spek, A. L.; van Leeuwen, P. W. N. M. *J. Chem. Soc., Dalton Trans.* **2002**, 2308–2317.

[74] Miedaner, A.; Raebiger, J. W.; Curtis, C. J.; Miller, S. M.; DuBois, D. L. *Organometallics* **2004**, *23*, 2670–2679.

[75] Raebiger, J. W.; Miedaner, A.; Curtis, C. J.; Miller, S. M.; Anderson, O. P.; DuBois, D. L. *J. Am. Chem. Soc.* **2004**, *126*, 5502–5514.

[76] Asensio, G.; Cuenca, A. B.; Esteruelas, M. A.; Medio-Simón, M.; Oliván, M.; Valencia, M. *Inorg. Chem.* **2010**, *49*, 8665–8667.

[77] Alós, J.; Bolaño, T.; Esteruelas, M. A.; Oliván, M.; Oñate, E.; Valencia, M. *Inorg. Chem.* **2013**, *52*, 6199–6213.

[78] Alós, J.; Bolaño, T.; Esteruelas, M. A.; Oliván, M.; Oñate, E.; Valencia, M. *Inorg. Chem.* **2014**, *53*, 1195–1209.

[79] Bakhmutov, V. I.; Bozoglian, F.; Gómez, K.; González, G.; Grushin, V. V.; Macgregor, S. A.; Martin, E.; Miloserdov, F. M.; Novikov, M. A.; Panetier, J. A.; Romashov, L. V. *Organometallics* **2012**, *31*, 1315–1328.

[80] Jover, J.; Miloserdov, F. M.; Benet-Buchholz, J.; Grushin, V. V.; Maseras, F. *Organometallics* **2014**, *33*, 6531–6543.

[81] Esteruelas, M. A.; Oliván, M.; Vélez, A. *Inorg. Chem.* **2013**, *52*, 5339–5349.

[82] Haibach, M. C.; Wang, D. Y.; Emge, T. J.; Krogh-Jespersen, K.; Goldman, A. S. *Chem. Sci.* **2013**, *4*, 3683–3692.

[83] Esteruelas, M. A.; Oliván, M.; Vélez, A. *Inorg. Chem.* **2013**, *52*, 12108–12119.

[84] Mispelaere-Canivet, C.; Spindler, J. F.; Perrio, S.; Beslin, P. *Tetrahedron* **2005**, *61*, 5253–5259.

[85] Dongol, K. G.; Koh, H.; Sau, M.; Chai, C. L. L. *Adv. Synth. Catal.* **2007**, *349*, 1015–1018.

[86] Ohshima, T.; Miyamoto, Y.; Ipposhi, J.; Nakahara, Y.; Utsunomiya, M.; Mashima, K. *J. Am. Chem. Soc.* **2009**, *131*, 14317–14328.

[87] Cabello-Sanchez, N.; Jean, L.; Maddaluno, J.; Lasne, M. C.; Rouden, J. *J. Org. Chem.* **2007**, *72*, 2030–2039.

[88] Partyka, D. V.; Updegraff, J. B.; Zeller, M.; Hunter, A. D.; Gray, T. G. *Dalton Trans.* **2010**, *39*, 5388–5397.

[89] Pintado-Alba, A.; de la Riva, H. c.; Nieuwhuyzen, M.; Bautista, D.; Raithby, P. R.; Sparkes, H. A.; Teat, S. J.; L pez-de Luzuriaga, J. M.; Lagunas, M. C. *Dalton Trans.* **2004**, 3459–3467.

[90] Zhan, J.-H.; Lv, H.; Yu, Y.; Zhang, J.-L. *Adv. Synth. Catal.* **2012**, *354*, 1529–1541.

[91] Miyata, K.; Nakagawa, T.; Kawakami, R.; Kita, Y.; Sugimoto, K.; Nakashima, T.; Harada, T.; Kawai, T.; Hasegawa, Y. *Chem. Eur. J.* **2011**, *17*, 521–528.

[92] Miyata, K.; Nakanishi, T.; Fushimi, K.; Hasegawa, Y. *J Photoch. Photobio. A* **2012**, *235*, 35–39.

[93] Friis, S. D.; Skrydstrup, T.; Buchwald, S. L. *Org. Lett.* **2014**, *16*, 4296–4299.

[94] Dang, T. T.; Ramalingam, B.; Shan, S. P.; Seayad, A. M. *ACS Catal.* **2013**, *3*, 2536–2540.

[95] Liu, Y.-Y.; Yang, X.-H.; Huang, X.-C.; Wei, W.-T.; Song, R.-J.; Li, J.-H. *J. Org. Chem.* **2013**, *78*, 10421–10426.

[96] Raoufmoghaddam, S.; Drent, E.; Bouwman, E. *Adv. Synth. Catal.* **2013**, *355*, 717–733.

[97] Ashcroft, C. P.; Fussell, S. J.; Wilford, K. *Tetrahedron Lett.* **2013**, *54*, 4529–4532.

[98] Behr, A.; Vorholt, A. J.; Rentmeister, N. *Chem. Eng. Sci.* **2013**, *99*, 38–43.

[99] Raoufmoghaddam, S.; Drent, E.; Bouwman, E. *ChemSusChem* **2013**, *6*, 1759–1773.

[100] Shang, R.; Xu, Q.; Fu, Y.; Guo, Q.; Liu, L. *Method for Preparing 2-Benzylpyridine Compound in the Presence of Palladium Catalyst and Phosphine Ligand*; CN 101863826, 2010.

[101] Shang, R.; Fu, Y.; Liu, L. *Process for Preparation of Naproxen from 2-halo-6-methoxynaphthalenes*; CN 102001933, 2011.

[102] Shang, R.; Huang, Z.; Fu, Y.; Guo, Q.; Liu, L. *Method for Synthesizing 2,2'-(5-methyl-1,3-phenylene)di(2-methylpriopionitrile) as Intermediate for Preparing Anastrozole*; CN 101973911, 2011.

[103] Shang, R.; Huang, Z.; Fu, Y.; Liu, L. *Process for Preparation of Flurbiprofen*; CN 101973869, 2011.

[104] Shang, R.; Ji, D.; Fu, Y.; Guo, Q.; Liu, L. *Method for Preparing Arylactonitrile Compounds*; CN 102452867, 2012.

[105] Brandstadt, K.; Cook, S.; Nguyen, B. T.; Surgenor, A.; Taylor, R.; Tzou, M.-s. *Cobalt Containing Hydrosilylation Catalysts and Compositions Containing the Catalysts*; PCT Int. Appl. WO 2013/043783 A2, 2013.

[106] Brandstadt, K.; Cook, S.; Nguyen, B. T.; Surgenor, A.; Taylor, R.; Tzou, M.-s. *Nickel Containing Hydrosilylation Catalysts and Compositions Containing the Catalysts*; PCT Int. Appl. WO 2013043785 A2 20130328, 2013.

[107] Brandstadt, K.; Cook, S.; Nguyen, B. T.; Surgenor, A.; Taylor, R.; Tzou, M.-s. *Iron-Containing Hydrosilylation Catalysts and Compositions Containing the Catalysts*; PCT Int. Appl. WO 2013043912 A2 20130328, 2013.

[108] Brandstadt, K.; Cook, S.; Nguyen, B. T.; Surgenor, A.; Taylor, R.; Tzou, M.-s. *Ruthenium Containing Hydrosilylation Catalysts and Compositions Containing the Catalysts*; PCT Int. Appl. WO 2013043787 A2 20130328, 2013.

[109] Surgenor, A.; Brandstadt, K.; Nguyen, B. T.; Cook, S.; Tzou, M.-s.; Taylor, R. *Vanadium Containing Hydrosilylation Catalysts and Compositions Containing the Catalysts*; PCT Int. Appl. WO 2013043825 A2 20130328, 2013.

[110] Kranenburg, M.; Kamer, P. C. J.; van Leeuwen, P. W. N. M. *Eur. J. Inorg. Chem.* **1998**, 25–27.

[111] Meijboom, R.; Bowen, R. J.; Berners-Price, S. J. *Coord. Chem. Rev.* **2009**, *253*, 325–342.

[112] van der Veen, L. A.; Kamer, P. C. J.; van Leeuwen, P. W. N. M. *Angew. Chem. Int. Ed.* **1999**, *38*, 336–338.

[113] van der Veen, L. A.; Kamer, P. C. J.; van Leeuwen, P. W. N. M. *CATTECH* **2002**, *6*, 116–120.

[114] Zuidema, E.; Escorihuela, L.; Eichelsheim, T.; Carbo, J. J.; Bo, C.; Kamer, P. C. J.; van Leeuwen, P. W. N. M. *Chem. Eur. J.* **2008**, *14*, 1843–1853.

[115] Petocz, G.; Berente, Z.; Kegl, T.; Kollar, L. *J. Organomet. Chem.* **2004**, *689*, 1188–1193.

[116] Bronger, R. P. J.; Kamer, P. C. J.; van Leeuwen, P. W. N. M. *Organometallics* **2003**, *22*, 5358–5369.

[117] Marimuthu, T.; Friedrich, H. B. *ChemCatChem* **2012**, *4*, 2090–2095.

[118] Vivekananda Bhatt, M.; Kulkarni, S. U. *Synthesis* **1983**, *1983*, 249–282.

[119] Gilman, H.; Haubein, A. H.; Hartzfeld, H. *J. Org. Chem.* **1954**, *19*, 1034–1040.

[120] Gilman, H.; Bebb, R. L. *J. Am. Chem. Soc.* **1939**, *61*, 109–112.

[121] Wittig, G.; Fuhrman, B. *Chem. Ber.* **1940**, *73*, 1197.

[122] Wakefield, B. J. Organolithium Methods. 1988.

[123] Turck, A.; Ple, N.; Pollet, P.; Mojovic, L.; Duflos, J.; Queguiner, G. *J. Heterocyclic Chem.* **1997**, *34*, 621–627.

[124] Harris, R. K. *Can. J. Chem.* **1964**, *42*, 2275–2281.

[125] Abraham, R. J.; Bernstein, H. J. *Can. J. Chem.* **1961**, *39*, 216–230.

[126] Hierso, J.-C. *Chem. Rev.* **2014**, *114*, 4838–4867.

[127] van Haaren, R. J.; van Strijdonck, G. P. F.; Oevering, H.; Reek, J. N. H.; Kamer, P. C. J.; van Leeuwen, P. W. N. M. *Eur. J. Inorg. Chem.* **2001**, 837–843.

[128] Dudle, B.; Rajesh, K.; Blacque, O.; Berke, H. *J. Am. Chem. Soc.* **2011**, *133*, 8168–8178.

[129] Fanjul, T.; Eastham, G.; Floure, J.; Forrest, S. J. K.; Haddow, M. F.; Hamilton, A.; Pringle, P. G.; Orpen, A. G.; Waugh, M. *Dalton Trans.* **2012**, *42*, 100.

[130] Aguilà, D.; Escribano, E.; Speed, S.; Talancón, D.; Yermán, L.; Alvarez, S. *Dalton Trans.* **2009**, 6610.

[131] Becke, A. D. *J. Chem. Phys.* **1993**, *98*, 5648–5652.

[132] Lee, C,; Yang, W.; Parr, R. G. *Phys. Rev. B* **1988**, 785–789.

[133] Vosko, S. H.; Wilk, L.; Nusair, M. *Can. J. Chem.* **1980**, 1200–1211.

[134] Stephens, P. J.; Devlin, F. J.; Chabalowski, C. F.; J, F. M. *The Journal of Physical Chemistry* **1994**, *98*, 11623–11627.

[135] Andrae, D.; Haeussermann, U.; Dolg, M.; Stoll, H.; Preuss, H. *Theoretica Chimica Acta* **1990**, *77*, 123–141.

[136] Weigend, F.; Ahlrichs, R. *Phys. Chem. Chem. Phys.* **2005**, *7*, 3297.

[137] Freixa, Z.; van Leeuwen, P. W. N. M. *Coord. Chem. Rev.* **2008**, *252*, 1755–1786.

[138] Yano, T. *B. Chem. Soc. JPN* **2006**, *50*, 1272–1277.

[139] Netherton, M. R.; Fu, G. C. *Org. Lett.* **2001**, *3*, 4295–4298.

[140] Koppel, I. A.; Koppel, J.; Pihl, V.; Leito, I.; Mishima, M.; Vlasov, V. M.; Yagupolskii, L. M.; Taft, t. l. R. W. *J. Chem. Soc., Perkin Trans. 2* **2000**, 1125–1133.

[141] Muller, A.; Otto, S.; Roodt, A. *Dalton Trans.* **2008**, 650–657.

[142] Andersen, N. G.; Keay, B. A. *Chem. Rev.* **2001**, *101*, 997–1030.

[143] Bungu, P. N.; Otto, S. *J. Organomet. Chem.* **2007**, *692*, 3370–3379.

[144] Bent, H. A. *Chem. Rev.* **2001**, *61*, 275–311.

[145] Jahromi, B. T.; Kharat, A. N.; Zamanian, S.; Bakhoda, A.; Mashayekh, K.; Khazaeli, S. *Appl. Catal. A-Gen.* **2012**, *433-434*, 188–196.

[146] Enghag, P. *Encylcopedia of the Elements*; Wiley VCH GmbH & Co. KGaA, 2004.

[147] Berners-Price, S. J.; Johnson, R. K.; Giovenella, A. J.; Faucette, L. F.; Mirabelli, C. K.; Sadler, P. J. *J. Inorg. Biochem.* **1988**, *33*, 285–295.

[148] Liu, J. J.; Galettis, P.; Farr, A.; Maharaj, L.; Samarasinha, H.; McGechan, A. C.; Baguley, B. C.; Bowen, R. J.; Berners-Price, S. J.; McKeage, M. J. *J. Inorg. Biochem.* **2008**, *102*, 303–310.

[149] Suzuki, A. *J. Organomet. Chem.* **1999**, *576*, 147–168.

[150] Iglesias, M. J.; Nicasio, M. C.; Caballero, A.; Pérez, P. J. *Dalton Trans.* **2012**, *42*, 1191–1195.

[151] Sawamura, M.; Hamashima, H.; Ito, Y. *J. Org. Chem.* **1990**, *55*, 5935–5936.

[152] Yanagisawa, A.; Kageyama, H.; Nakatsuka, Y.; Asakawa, K.; Matsumoto, Y.; Yamamoto, H. *Angew. Chem. Int. Ed.* **1999**, *38*, 3701–3703.

[153] Balakrishna, M. S.; Venkateswaran, R.; Mobin, S. M. *Polyhedron* **2008**, *27*, 899–904.

[154] Kobayashi, N.; Higashimura, H.; Suenobu, K. *Luminescent Silver Complexes*; PCT Int. Appl. WO 2010064601 A1 20100610, 2010.

[155] Kobayashi, N.; Higashimura, H. *Preparation of Triphenylphosphine-Silver Complexes and Luminescent Membrane Containing Silver Complexes*; PCT Int. Appl. WO2011152358 A1 20111208, 2011.

[156] Kobayashi, N.; Higashimura, H. *Preparation of Amine-Containing Phosphine Compound and its Metal Complex*; PCT Int. Appl. WO 2012056966 A1 20120503, 2012.

[157] Kaltzoglou, A.; Cox, P. J.; Aslanidis, P. *Polyhedron* **2007**, *26*, 1634–1642.

[158] Pingen, D.; Lebl, T.; Lutz, M.; Nichol, G. S.; Kamer, P. C. J.; Vogt, D. *Organometallics* **2014**, *33*, 2798–2805.

[159] Ainscough, E. W.; Bowmaker, G. A.; Brodie, A. M.; Freeman, G. H.; Hanna, J. V.; Jameson, G. B.; Otter, C. A. *Polyhedron* **2011**, *30*, 638–646.

[160] Bayler, A.; Schier, A.; Bowmaker, G. A.; Schmidbaur, H. *J. Am. Chem. Soc.* **1997**, *118*, 7006–7007.

[161] van der Vlugt, J. I.; Siegler, M. A.; Janssen, M.; Vogt, D.; Spek, A. L. *Organometallics* **2009**, *28*, 7025–7032.

[162] Heuer, B.; Pope, S. J.; Reid, G. *Polyhedron* **2000**, *19*, 743–749.

[163] Joshi, B. *Unpublished Work*.

[164] Yam, V. W.-W.; Fung, W. K.-M.; Cheung, K.-K. *Organometallics* **1997**, *16*, 2032–2037.

[165] Wing-Wah Yam, V.; Kam-Wing Lo, K.; Kit-Mai Fung, W.; Wang, C.-R. *Coordination Chemistry Reviews* **2003**, *171*, 17–41.

[166] Xu, L.-J.; Wang, J.-Y.; Zhang, L.-Y.; Shi, L.-X.; Chen, Z.-N. *Organometallics* **2013**, *32*, 5402–5408.

[167] Enghag, P. *Encyclopedia of the Elements*; Wiley VCH GmbH & Co. KGaA: Weinheim, 2004.

[168] Heck, R. M.; Farrauto, R. J. *Applied Catalysis A: General* **2001**, *221*, 443–457.

[169] Cui, X. H.; Burgess, K. *Chem. Rev.* **2005**, *105*, 3272–3296.

[170] Pospech, J.; Fleischer, I.; Franke, R.; Buchholz, S.; Beller, M. *Angew. Chem. Int. Ed.* **2013**, *52*, 2852–2872.

[171] Osborn, J. A.; Jardine, F. H.; Young, J. F.; Wilkinson, G. *J. Chem. Soc. A* **1966**, 1711–1732.

[172] Evans, D. A.; Fu, G. C.; Hoveyda, A. H. *J. Am. Chem. Soc.* **2001**, *110*, 6917–6918.

[173] Ojima, I.; Kogure, T. *Organometallics* **2001**, *1*, 1390–1399.

[174] Sharpless, K. B. *Angew. Chem. Int. Ed.* **2002**, *41*, 2024–2032.

[175] Knowles, W. S.; Sabacky, M. J. *Chem. Commun. (London)* **1968**, 1445–1446.

[176] Knowles, W. S.; Noyori, R. *Acc. Chem. Res.* **2007**, *40*, 1238–1239.

[177] Dallanegra, R.; Chaplin, A. B.; Weller, A. S. *Organometallics* **2012**, *31*, 2720–2728.

[178] Pawley, R. J.; Huertos, M. A.; Lloyd-Jones, G. C.; Weller, A. S.; Willis, M. C. *Organometallics* **2012**, *31*, 5650–5659.

[179] Canepa, G.; Brandt, C. D.; Ilg, K.; Wolf, J.; Werner, H. *Chem. Eur. J.* **2003**, *9*, 2502–2515.

[180] Bleeke, J. R.; Donaldson, A. J. *Organometallics* **1986**, *5*, 2401–2405.

[181] Fryzuk, M. D.; Piers, W. E.; Rettig, S. J.; Einstein, F. W.; Jones, T.; Albright, T. A. *J. Am. Chem. Soc.* **1989**, *111*, 5709–5721.

[182] Hashimoto, H.; Suzuki, T.; Tobita, H. *Dalton Trans.* **2010**, *39*, 9386–9400.

[183] Khan, M. M.; Khan, B. T.; Begum, S.; Aali, S. M. *Journal of Molecular Catalysis* **1988**, *49*, 43–58.

[184] Hermann, D.; Gandelman, M.; Rozenberg, H.; Shimon, L. J. W.; Milstein, D. *Organometallics* **2002**, *21*, 812–818.

[185] van der Boom, M. E.; Liou, S.-Y.; Ben-David, Y.; Shimon, L. J.; Milstein, D. *J. Am. Chem. Soc.* **1998**, *120*, 6531–6541.

[186] Winter, A. M.; Eichele, K.; Mack, H.-G.; Potuznik, S.; Mayer, H. A.; Kaska, W. C. *J. Organomet. Chem.* **2003**, *682*, 149–154.

[187] Salem, H.; Shimon, L. J. W.; Leitus, G.; Weiner, L.; Milstein, D. *Organometallics* **2008**, *27*, 2293–2299.

[188] Fryzuk, M. D.; MacNeil, P. A.; Rettig, S. J. *Organometallics* **1986**, *5*, 2469–2476.

[189] Hanson, S. K.; Heinekey, D. M.; Goldberg, K. I. *Organometallics* **2008**, *27*, 1454–1463.

[190] Bronger, R. P. J.; Silva, S. M.; Kamer, P. C. J.; van Leeuwen, P. W. N. M. *Chem. Commun.* **2002**, 3044–3045.

[191] Bronger, R. P. J.; Bermon, J. P.; Herwig, J.; Kamer, P. C. J.; van Leeuwen, P. W. N. M. *Adv. Synth. Catal.* **2004**, *346*, 789–799.

[192] Bronger, R. P. J.; Bermon, J. P.; Reek, J. N. H.; Kamer, P. C. J.; van Leeuwen, P. W. N. M.; Carter, D. N.; Licence, P.; Poliakoff, M. *J. Mol. Catal. A-Chem.* **2004**, *224*, 145–152.

[193] Bronger, R. P. J.; Silva, S. M.; Kamer, P. C. J.; van Leeuwen, P. W. N. M. *Dalton Trans.* **2004**, 1590–1596.

[194] Buhling, A.; Kamer, P.; van Leeuwen, P.; Elgersma, J. W.; Goubitz, K.; Fraanje, J. *Organometallics* **1997**, *16*, 3027–3037.

[195] Buhling, A.; Kamer, P.; vanLeeuwen, P.; Elgersma, J. W. *J. Mol. Catal. A-Chem.* **1997**, *116*, 297–308.

[196] Dieleman, C. B.; Kamer, P. C. J.; Reek, J. N. H.; van Leeuwen, P. W. N. M. *Helv. Chim. Acta* **2001**, *84*, 3269–3280.

[197] Leclercq, L.; Hapiot, F.; Tilloy, S.; Ramkisoensing, K.; Reek, J. N. H.; van Leeuwen, P. W. N. M.; Monflier, E. *Organometallics* **2005**, *24*, 2070–2075.

[198] van Leeuwen, P. W. N. M.; Kamer, P. C. J.; Reek, J. N. H. *Pure Appl. Chem.* **1999**, *71*, 1443–1452.

[199] Mora, G.; Deschamps, B.; van Zutphen, S.; Le Goff, X. F.; Ricard, L.; Le Floch, P. *Organometallics* **2007**, *26*, 1846–1855.

[200] Sandee, A. J.; van der Veen, L. A.; Reek, J. N. H.; Kamer, P. C. J.; Lutz, M.; Spek, A. L.; van Leeuwen, P. W. N. M. *Angew. Chem. Int. Ed.* **1999**, *38*, 3231–3235.

[201] Silva, S. M.; Bronger, R. P. J.; Freixa, Z.; Dupont, J.; van Leeuwen, P. W. N. M. *New J. Chem.* **2003**, *27*, 1294–1296.

[202] van der Vlugt, J. I.; Sablong, R.; Magusin, P. C. M. M.,; Mills, A. M.; Spek, A. L.; Vogt, D. *Organometallics* **2004**, *23*, 3177–3183.

[203] Zuidema, E.; Daura-Oller, E.; Carbo, J. J.; Bo, C.; van Leeuwen, P. W. N. M. *Organometallics* **2007**, *26*, 2234–2242.

[204] Zuidema, E.; Goudriaan, P. E.; Swennenhuis, B. H. G.; Kamer, P. C. J.; van Leeuwen, P. W. N. M.; Lutz, M.; Spek, A. L. *Organometallics* **2010**, *29*, 1210–1221.

[205] Johnson, H. C.; McMullin, C. L.; Pike, S. D.; Macgregor, S. A.; Weller, A. S. *Angew. Chem. Int. Ed.* **2013**, *52*, 9776–9780.

[206] Guiu, E.; Caporali, M.; Munoz, B.; Muller, C.; Lutz, M.; Spek, A. L.; Claver, C.; van Leeuwen, P. W. N. M. *Organometallics* **2006**, *25*, 3102–3104.

[207] Bertoux, F.; Tilloy, S.; Monflier, E.; Castanet, Y.; Mortreux, A. *J. Mol. Catal. A-Chem.* **1999**, *138*, 53–57.

[208] Kjonaas, R. A.; Williams, P. E.; Counce, D. A.; Crawley, L. R. *J. Chem. Educ.* **2011**, *88*, 825–828.

[209] Franke, R.; Selent, D.; Börner, A. *Chem. Rev.* **2012**, *112*, 5675–5732.

[210] Henderson, W.; Nickleson, B. K.; McCaffrey, L. J. *Polyhedron* **1998**, *17*, 4291–4313.

[211] Sanger, A. R. *Canadian Journal of Chemistry* **1984**, *62*, 2168–2169.

[212] Sanger, A. R. *Canadian Journal of Chemistry* **1985**, *63*, 571–575.

[213] Deb, B.; Dutta, D. K. *J. Mol. Catal. A-Chem.* **2010**, *326*, 21–28.

[214] Williams, G. L.; Parks, C. M.; Smith, C. R.; Adams, H.; Haynes, A.; Meijer, A. J.; Sunley, G. J.; Gaemers, S. *Organometallics* **2011**, *30*, 6166–6179.

[215] Valentine, J. S. *Chem. Rev.* **1973**, *73*, 235–245.

[216] Choy, V. J.; J O'Connor, C. *Coordination Chemistry Reviews* **1972**, *9*, 145–170.

[217] Baird, M. C.; Lawson, D. N.; Mague, J. T.; Osborn, J. A.; Wilkinson, G. *Chem. Commun. (London)* **1966**, 129–130.

[218] Atlay, M. T.; Gahan, L. R.; Kite, K.; Moss, K.; Read, G. *J. Mol. Catal.* **1980**, *7*, 31–42.

[219] Atlay, M. T.; Carlton, L.; Read, G. *Journal of Molecular Catalysis* **2001**, *19*, 57–68.

[220] Carlton, L.; Read, G.; Urgelles, M. *J. Chem. Soc., Chem. Commun.* **1983**, 586–588.

[221] Read, G.; Urgelles, M. *J. Chem. Soc., Dalton Trans.* **1985**, 1591–1596.

[222] Ahijado, M.; Braun, T.; Noveski, D.; Kocher, N.; Neumann, B.; Stalke, D.; Stammler, H.-G. *Angew. Chem. Int. Ed.* **2005**, *44*, 6947–6951.

[223] Aresta, M.; Quaranta, E.; Ciccarese, A. *Journal of Molecular Catalysis* **1987**, *41*, 355–359.

[224] Bennett, M. J.; Donaldson, P. B. *Inorg. Chem.* **1977**, *16*, 1581–1585.

[225] Busetto, C.; D'Alfonso, A.; Maspero, F.; Perego, G.; Zazzetta, A. *J. Chem. Soc., Dalton Trans.* **1977**, 1828–1834.

[226] Van Gaal, H.; van den Bekerom, F. A. *J. Organomet. Chem.* **1977**, *134*, 237–248.

[227] Richter, B.; Spek, A. L.; van Koten, G.; Deelman, B.-J. *J. Am. Chem. Soc.* **2000**, *122*, 3945–3951.

[228] Selke, M.; Foote, C. S.; Karney, W. L. *Inorg. Chem.* **1993**, *32*, 5425–5426.

[229] Selke, M.; Karney, W. L.; Khan, S. I.; Foote, C. S. *Inorg. Chem.* **2001**, *34*, 5715–5720.

[230] Teets, T. S.; Nocera, D. G. *Inorg. Chem.* **2012**, *51*, 7192–7201.

[231] Wakatsuki, Y.; Maniwa, M.; Yamazaki, H. *Inorg. Chem.* **1990**, *29*, 4208–4214.

[232] Banwell, M. G.; Coster, M. J.; Edwards, A. J.; Karunaratne, O. P.; Smith, J. A.; Welling, L. L.; Willis, A. C. *Aust. J. Chem.* **2003**, *56*, 585.

[233] James, B. R.; Mahajan, D. *Canadian Journal of Chemistry* **1980**, *58*, 996–1004.

[234] Mague, J. T.; Davis, E. J. *Inorg. Chem.* **1977**, *16*, 131–137.

[235] McGinnety, J. A.; Payne, N. C.; Ibers, J. A. *J. Am. Chem. Soc.* **1969**, *91*, 6301–6310.

[236] Miller, J. S.; Caulton, K. G. *J. Am. Chem. Soc.* **1975**, *97*, 1067–1073.

[237] Morvillo, A.; Bressan, M. *Inorganica Chimica Acta* **1986**, *121*, 219–222.

[238] Pettinari, C.; Marchetti, F.; Cingolani, A.; Bianchini, G.; Drozdov, A.; Vertlib, V.; Troyanov, S. *... of organometallic ...* **2002**,

[239] Slack, D. A.; Greveling, I.; Baird, M. C. *Inorg. Chem.* **1979**, *18*, 3125–3132.

[240] Kashiwabara, K.; Morikawa, A.; Suzuki, T.; Isobe, K.; Tatsumi, K. *J. Chem. Soc., Dalton Trans.* **1997**, 1075–1082.

[241] Lindner, E.; Wang, Q.; Mayer, H. A.; Bader, A.; Kuehbauch, H.; Wegner, P. *Organometallics* **1993**, *12*, 3291–3296.

[242] Perera, S. D.; Shaw, B. L. *J. Chem. Soc., Dalton Trans.* **1995**, 633–639.

[243] Yu, X.-Y.; Patrick, B. O.; James, B. R. *Organometallics* **2006**, *25*, 4870–4877.

[244] Doux, M.; Mézailles, N.; Ricard, L.; Le Floch, P. *Organometallics* **2003**, *22*, 4624–4626.

[245] Frech, C. M.; Shimon, L. J.; Milstein, D. *Helv. Chim. Acta* **2006**, *89*, 1730–1739.

[246] Hayashi, Y.; Szalda, D. J.; Grills, D. C.; Hanson, J. C.; Huang, K.-W.; Muckerman, J. T.; Fujita, E. *Polyhedron* **2013**, *58*, 106–114.

[247] Lanci, M. P.; Roth, J. P. *J. Am. Chem. Soc.* **2006**, *128*, 16006–16007.

[248] Vasapollo, G.; Giannoccaro, P.; Nobile, C. F.; Sacco, A. *Inorganica Chimica Acta* **2000**, *48*, 125–128.

[249] Verat, A. Y.; Fan, H.; Pink, M.; Chen, Y. S.; Caulton, K. G. *Chem. Eur. J.* **2008**, *14*, 7680–7686.

[250] Vigalok, A.; Shimon, L. J. W.; Milstein, D. *Chem. Commun.* **1996**, 1673–1674.

[251] Aylward, T.; Findlay, G. *SI Chemical Data*; Wiley, 2002.

[252] Appleton, T. G.; Bennett, M. A. *Inorg. Chem.* **2001**, *17*, 738–747.

[253] Rigamonti, L.; Rusconi, M.; Manassero, C.; Manassero, M.; Pasini, A. *Inorg. Chim. Acta* **2010**, *363*, 3498–3505.

[254] Lindner, E.; Wang, Q.; Mayer, H. A.; Fawzi, R. *J. Organomet. Chem.* **1993**, *453*, 289–293.

[255] Penner, A.; Braun, T. *Eur. J. Inorg. Chem.* **2011**, *2011*, 2579–2587.

[256] Cipot-Wechsler, J.; Covelli, D.; Praetorius, J. M.; Hearns, N.; Zenkina, O. V.; Keske, E. C.; Wang, R.; Kennepohl, P.; Crudden, C. M. *Organometallics* **2012**, *31*, 7306–7315.

[257] Ledger, A. E. W.; Moreno, A.; Ellul, C. E.; Mahon, M. F.; Pregosin, P. S.; Whittlesey, M. K.; Williams, J. M. J. *Inorg. Chem.* **2010**, *49*, 7244–7256.

[258] Gangopadhyay, S.; Basak, P.; Drew, M.; Gangopadhyay, P. K. *Chem. Commun.* **2010**, *46*, 7436–7438.

[259] Lipscomb, J. D. *Annu. Rev. Microbiol.* **1994**, *48*, 371–399.

[260] Merkx, M.; Kopp, D. A.; Sazinsky, M. H.; Blazyk, J. L.; Muller, J.; Lippard, S. J. *Angew. Chem. Int. Ed.* **2001**, *40*, 2782–2807.

[261] Tinberg, C. E.; Lippard, S. J. *Acc. Chem. Res.* **2011**, *44*, 280–288.

[262] de Montellano, P. R. O. *Chem. Rev.* **2010**, *110*, 932–948.

[263] Balcells, D.; Clot, E.; Eisenstein, O. *Chem. Rev.* **2010**, *110*, 749–823.

[264] Borovik, A. S. *Chem. Soc. Rev.* **2011**, *40*, 1870–1874.

[265] Holm, R. H. *Chem. Rev.* **1987**, *87*, 1401–1449.

[266] Poverenov, E.; Efremenko, I.; Frenkel, A. I.; Ben-David, Y.; Shimon, L. J. W.; Leitus, G.; Konstantinovski, L.; Martin, J. M. L.; Milstein, D. *Nature* **2008**, *455*, 1093–1096.

[267] Anderson, T. M.; Neiwert, W. A.; Kirk, M. L.; Piccoli, P. M. B.; Schultz, A. J.; Koetzle, T. F.; Musaev, D. G.; Morokuma, K.; Cao, R.; Hill, C. L. *Science* **2004**, *306*, 2074–2077.

[268] Winkler, J. R.; Gray, H. B. *Electronic Structures of Oxo-Metal Ions*; Springer Berlin Heidelberg: Berlin, Heidelberg, 2011; pp 17–28.

[269] Betley, T. A.; Wu, Q.; Van Voorhis, T.; Nocera, D. G. *Inorg. Chem.* **2008**, *47*, 1849–1861.

[270] Hay-Motherwell, R. S.; Wilkinson, G.; Hussain-Bates, B.; Hursthouse, M. B. *Polyhedron* **1993**, *12*, 2009–2012.

[271] Tsvetkov, N. P.; Andino, J. G.; Fan, H.; Verat, A. Y.; Caulton, K. G. *Dalton Trans.* **2013**, *42*, 6745–6755.

[272] Di Pasqua, A. J.; Goodisman, J.; Kerwood, D. J.; Toms, B. B.; Dubowy, R. L.; Dabrowiak, J. C. *Chem. Res. Toxicol.* **2007**, *20*, 896–904.

[273] Dierkes, P.; Ramdeehul, S.; Barloy, L.; De Cian, A.; Fischer, J.; Kamer, P. C. J.; van Leeuwen, P. W. N. M.; Osborn, J. A. *Angew. Chem. Int. Ed.* **1998**, *37*, 3116–3118.

[274] Peris, E.; Crabtree, R. H. *Coord. Chem. Rev.* **2004**, *248*, 2239–2246.

[275] Shen, Q.; Ogata, T.; Hartwig, J. F. *J. Am. Chem. Soc.* **2008**, *130*, 6586–6596.

[276] Wu, X.-F.; Neumann, H.; Beller, M. *Chem. Rev.* **2013**, *113*, 1–35.

[277] Simeone, J. P.; Braun, M. P.; Liu, L.; Natarajan, S. R. *J. Labelled Compd. Radiopharm.* **2010**, *53*, 511–516.

[278] Trost, B. M.; Thaisrivongs, D. A.; Donckele, E. J. *Angew. Chem. Int. Ed.* **2012**, *52*, 1523–1526.

[279] Wagaw, S.; Yang, B. H.; Buchwald, S. L. *J. Am. Chem. Soc.* **1999**, *121*, 10251–10263.

[280] Chianese, A. R.; Lee, S. J.; Gagne, M. R. *Angew. Chem. Int. Ed.* **2007**, *46*, 4042–4059.

[281] Johns, A. M.; Utsunomiya, M.; Incarvito, C. D.; Hartwig, J. F. *J. Am. Chem. Soc.* **2006**, *128*, 1828–1839.

[282] Klingensmith, L. M.; Strieter, E. R.; Barder, T. E.; Buchwald, S. L. *Organometallics* **2006**, *25*, 82–91.

[283] Yin, J. J.; Buchwald, S. L. *J. Am. Chem. Soc.* **2002**, *124*, 6043–6048.

[284] Carr, N.; Dunne, B. J.; Mole, L.; Orpen, A. G.; Spencer, J. L. *J. Chem. Soc., Dalton Trans.* **1991**, 863–871.

[285] Grushin, V. V.; Marshall, W. J. *J. Am. Chem. Soc.* **2006**, *128*, 12644–12645.

[286] Harrison, N. C.; Murray, M.; Spencer, J. L.; Stone, F. G. A. *J. Chem. Soc., Dalton Trans.* **1978**, 1337–1342.

[287] Howard, J. A.; L, S. J.; Mason, S. A. *Proceedings of the Royal Society of London. A. Mathematical and Physical Sciences* **1983**, *386*, 145–161.

[288] Yoneda, N.; Kusano, S.; Yasui, M.; Pujado, P.; Wilcher, S. *Applied Catalysis A: General* **2001**, *221*, 253–265.

[289] Degnan, T. F., Jr; Smith, C. M.; Venkat, C. R. *Applied Catalysis A: General* **2001**, *221*, 283–294.

[290] Ugo, R.; Cariati, F.; La Monica, G. *Chem. Commun. (London)* **1966**, 868–869.

[291] Green, M.; Howard, J. A.; Spencer, J. L.; Stone, F. G. A. *J. Chem. Soc., Chem. Commun.* **1975**, 3–4.

[292] Otsuka, S.; Yoshida, T.; Matsumoto, M.; Nakatsu, K. *J. Am. Chem. Soc.* **1976**, *98*, 5850–5858.

[293] Clark, H. C.; Smith, M. H. *J. Am. Chem. Soc.* **2001**, *108*, 3829–3830.

[294] Hackett, M.; Whitesides, G. M. *J. Am. Chem. Soc.* **2001**, *110*, 1449–1462.

[295] Nicolas, E.; le Goff, X.-F.; Bouchonnet, S.; Mézailles, N. *Chem. Commun.* **2012**, *48*, 8350–8352.

[296] Williams, D. B. G.; Lawton, M. *J. Org. Chem.* **2010**, *75*, 8351–8354.

[297] Allan, K. M. *Hybrid P,E Ligands. Synthesis, Coordination Chemistry and Catalysis*; Ph.D thesis, Victoria University of Wellington, 2014.

[298] Somerville, R. Unpublished Work.

[299] Green, M.; Grove, D. M.; Spencer, J. L.; Stone, F. G. A. *J. Chem. Soc., Dalton Trans.* **1977**, 2228–2234.

[300] Fulmer, G. R.; Miller, A. J. M.; Sherden, N. H.; Gottlieb, H. E.; Nudelman, A.; Stoltz, B. M.; Bercaw, J. E.; Goldberg, K. I. *Organometallics* **2010**, *29*, 2176–2179.

[301] Tolman, C. A. *J. Am. Chem. Soc.* **2001**, *96*, 2780–2789.

[302] Goel, A. B.; Goel, Sarla, *Inorg. Chim. Acta* **1983**, *77*, L5–L6.

[303] Yoshida, T.; Otsuka, S. *J. Am. Chem. Soc.* **1977**, *99*, 2134–2140.

[304] Kashiwagi, T.; Yasuoka, N.; Kasai, N.; Kakudo, M.; Takahashi, S.; Hagihara, N. *J. Chem. Soc. D* **1969**, 743.

[305] Cheng, P. T.; Cook, C. D.; Nyburg, S. C.; Wan, K. Y. *Canadian Journal of Chemistry* **1971**, *49*, 3772–3777.

[306] Cook, C. D.; Cheng, P.-T.; Nyburg, S. C. *J. Am. Chem. Soc.* **2001**, *91*, 2123–2123.

[307] Yoshida, T.; Tatsumi, K.; Matsumoto, M.; Nakatsu, K.; Nakamura, A.; Fueno, T.; Otsuka, S. *Nouveau Journal De Chimie* **1979**, *3*, 761–774.

[308] Cramer, C. J.; Tolman, W. B.; Theopold, K. H.; Rheingold, A. L. *Proc. Natl. Acad. Sci. U.S.A.* **2003**, *100*, 3635–3640.

[309] Clark, H. C.; Goel, A. B.; Wong, C. S. *J. Am. Chem. Soc.* **1978**, *100*, 6241–6243.

[310] Mimoun, H. *Journal of Molecular Catalysis* **1980**, *7*, 1–29.

[311] Qu, F.; Khusnutdinova, J. R.; Rath, N. P.; Mirica, L. M. *Chem. Commun.* **2014**, *50*, 3036–3039.

[312] Sugimoto, R.; Suzuki, H.; Moro-Oka, Y.; Ikawa, T. *Chem. Lett.* **1982**, 1863–1866.

[313] Sergeev, A. G.; Neumann, H.; Spannenberg, A.; Beller, M. *Organometallics* **2010**, *29*, 3368–3373.

[314] Garrou, P. E. *Chem. Rev.* **1981**, *81*, 229–266.

[315] Zayya, A. I.; Spencer, J. L. *Organometallics* **2012**, *31*, 2841–2853.

[316] Zayya, A. I.; Vagana, R.; Nelson, M. R. M.; Spencer, J. L. *Tetrahedron Lett.* **2012**, *53*, 923–926.

[317] Hoyte, S. A. *Platinum Complexes of Bicyclopropylidene and Related Ligands*; Ph.D thesis, Victoria University of Wellington, 2014.

[318] Phillips, A. D.; Gonsalvi, L.; Rornerosa, A.; Vizza, F.; Peruzzini, M. *Coord. Chem. Rev.* **2004**, *248*, 955–993.

[319] Darensbourg, D. J.; Decuir, T. J.; Stafford, N. W.; Robertson, J. B.; Draper, J. D.; Reibenspies, J. H.; Kathó, A.; Joó, F. *Inorg. Chem.* **1997**, *36*, 4218–4226.

[320] Spencer, J. L. *Inorg. Synth.* **1979**, *19*, 213–218.

[321] Green, M.; Howard, J. A.; Spencer, J. L.; Stone, F. G. A. *J. Chem. Soc., Dalton Trans.* **1977**, 271–277.

[322] Pregosin, P. S.; Favez, R.; Roulet, R.; Boschi, T.; Michelin, R. A.; Ros, R. *Inorg. Chim. Acta* **1980**, *45*, L7–L9.

[323] Addison, A. W.; Rao, T. N.; Reedijk, J.; van Rijn, J.; Verschoor, G. C. *J. Chem. Soc., Dalton Trans.* **1984**, 1349.

[324] Yang, L.; Powell, D. R.; Houser, R. P. *Dalton Trans.* **2007**, 955.

[325] Bachechi, F.; Zambonelli, L. *Acta Crystallogr., Sect. C: Cryst. Struct.* **1992**, 1–5.

[326] Engeldinger, E.; Armspach, D.; Matt, D.; Jones, P. G. *Chem. Eur. J.* **2003**, *9*, 3091–3105.

[327] Newman, P. D.; Cavell, K. J.; Kariuki, B. M. *Dalton Trans.* **2012**, *41*, 12395–12407.

[328] Owens, S. B., Jr.; Smith, D. C., Jr.; Lake, C. H.; Gray, G. M. *Eur. J. Inorg. Chem.* **2008**, *2008*, 4710–4718.

[329] van den Beuken, E. K.; Meetsma, A.; Kooijman, H.; Spek, A. L.; Feringa, B. L. *Inorg. Chim. Acta* **1997**, *264*, 171–183.

[330] Ruhland, K.; Brück, A.; Herdtweck, E. *Eur. J. Inorg. Chem.* **2007**, *2007*, 944–964.

[331] van der Vlugt, J. I.; Sablong, R.; Mills, A. M.; Kooijman, H.; Spek, A. L.; Meetsma, A.; Vogt, D. *Dalton Trans.* **2003**, 4690–4699.

[332] Mora, G.; Piechaczyk, O.; Houdard, R.; Mézailles, N.; le Goff, X.-F.; Le Floch, P. *Chem. Eur. J.* **2008**, *14*, 10047–10057.

[333] van Duren, R.; Cornelissen, L. L.; van der Vlugt, J. I.; Huijbers, J. P.; Mills, A. M.; Spek, A. L.; Müller, C.; Vogt, D. *Helvetica chimica acta* **2006**, *89*, 1547–1558.

[334] van Duren, R.; van der Vlugt, J. I.; Kooijman, H.; Spek, A. L.; Vogt, D. *Dalton Trans.* **2007**, 1053–1059.

[335] Niksch, T.; Görls, H.; Friedrich, M.; Oilunkaniemi, R.; Laitinen, R.; Weigand, W. *Eur. J. Inorg. Chem.* **2010**, *2010*, 74–94.

[336] Armarego, W. L. F.; Chai, C. L. L. *Purification of Laboratory Chemicals*, 5th ed.; Butterworth-Heinemann: Burlington MA, 2003.

[337] Kranenburg, M.; Kamer, P. C. J.; van Leeuwen, P. W. N. M. *Eur. J. Inorg. Chem.* **1998**, 155–157.

[338] Doherty, S.; Eastham, G. R.; Tooze, R. P.; Scanlan, T. H.; Williams, D.; Elsegood, M. R. J.; Clegg, W. *Organometallics* **1999**, *18*, 3558–3560.

[339] Moss, J. R. *Journal of Molecular Catalysis A: Chemical* **2003**, *107*, 169–174.

[340] Bernskoetter, W. H.; Schauer, C. K.; Goldberg, K. I.; Brookhart, M. *Science* **2009**, *326*, 553–556.

[341] Silverstein, R. M.; Webster, F. X.; Kiemle, D. J. *Spectrometric Identification of Organic Compounds*, 7th ed.; John Wiley & Sons, Ltd., 2005.

[342] Scollard, J. D.; Day, M.; Labinger, J. A.; Bercaw, J. E. *Helvetica chimica acta* **2001**, *84*, 3247–3268.

[343] Ingleson, M. J.; Mahon, M. F.; Weller, A. S. *Chem. Commun.* **2004**, 2398–2399.

[344] Walter, M. D.; White, P. S.; Brookhart, M. *New J. Chem.* **2013**, *37*, 1128–1133.

[345] Daigle, D. J.; Decuir, T. J.; Robertson, J. B.; Darensbourg, D. J. *Inorg. Synth.* **1998**, *32*, 40–45.

[346] Dieter, R. K.; Topping, C. M.; Nice, L. E. *J. Org. Chem.* **2001**, *66*, 2302–2311.

[347] Suter, C. M.; Maxwell, C. E. *Org. Synth.* **1938**, *18*, 64–65.

[348] Koshar, R. J.; Mitsch, R. A. *The Journal of Organic Chemistry* **2001**, *38*, 3358–3363.

[349] Vaughan, T. F.; Koedyk, D. J.; Spencer, J. L. *Organometallics* **2011**, *30*, 5170–5180.

[350] Giordano, G.; Crabtree, R. H.; Heintz, R. M.; Forster, D.; Morris, D. E. *Inorg. Synth.* **1979**, *19*, 218–220.

[351] Hartley, F. R.; Murray, S. G.; McAuliffe, C. A. *Inorg. Chem.* **1979**, *18*, 1394–1397.

[352] Crascall, L. E.; Spencer, J. L.; Doyle, R. A.; Angelici, R. J. *Inorg. Synth.* **1990**, *28*, 126–132.

[353] Jensen, C. M. *Acta Chem. Scand.* **1953**, *7*, 866–868.

[354] Cramer, R. D.; Jones, F. N. US Pat., US3356748. 1967.

[355] Anderson, B. G. *Late transition metal complexes of pentafluorophenylphosphino-pincer ligands.*; Ph.D thesis, Victoria University of Wellington, 2012.

[356] Palatinus, L.; Chapuis, G. *J. Appl. Crystallogr.* **2009**, *50*, 834–835.

[357] Sheldrick, G. M. *Acta Crystallogr., Sect. A: Found. Crystallogr.* **2008**, *64*, 112–122.

[358] Dolomanov, O. V.; Bourhis, L. J.; Gildea, R. J.; Howard, J. A. K.; Puschmann, H. J. *J. Appl. Crystallogr.* **2009**, *42*, 339–341.

[359] Frisch, M. J.; al, e. Gaussian 09 Revision B.01. Wallingford CT, 2009.

[360] Glendening, E. D.; Reed, A. E.; Carpenter, J. E.; Weinhold, F. NBO Version 3.1 E. D.